



Les rechargements sédimentaires d'avant-côte : une nouvelle méthode de lutte contre l'érosion côtière Shoreface nourishment: a new method for fighting against coastal erosion

Programme LITEAU II Rapport de fin de contrat

Annexe : Texte des publications

IMAGES (Institut de Modélisation et d'Analyse en Géo-Environnements et Santé)
E.A. 4218
Raphaël CERTAIN, MCF,
Université de Perpignan Via Domitia, 52 av. Paul Alduy
66860 Perpignan
Tel : 04.68.66.20.57
Fax : 04.68.66.17.47
Email : certain@univ-perp.fr

Date : 27/07/2009

N° de contrat : CV05000192

Date du contrat : 27/01/2006

Geomorphic coastal vulnerability to storms in microtidal fetch-limited environments: application to NW Mediterranean & N Adriatic Seas

J.A. Jiménez†, P. Ciavola‡, Y. Balouin§, C. Armaroli‡, E. Bosom† and M. Gervais§

† Laboratori d'Enginyeria Marítima,
Universitat Politècnica de Catalunya,
Barcelona 08034, Spain
jose.jimenez@upc.edu

‡ Dipartimento di Scienze della
Terra, Università di Ferrara, Ferrara
44100, Italy, cvp@unife.it

§ BRGM – Geological Survey of
Languedoc-Roussillon, Montpellier
34000, France, y.balouin@brgm.fr



ABSTRACT

JIMÉNEZ, J.A., CIAVOLA, P., BALOUIN, Y., ARMAROLI, C., BOSOM, E. and GERVAIS, M., 2009. Geomorphic coastal vulnerability to storms in microtidal fetch-limited environments: Application to NW Mediterranean & N Adriatic Seas. *Journal of Coastal Research*, SI 56 (Proceedings of the 10th International Coastal Symposium), 1641 – 1645. Lisbon, Portugal, ISSN 0749-0258.

A methodology to compare in relative terms the coastal vulnerability to storm impacts is presented and applied to three sites in the Mediterranean Sea. The analysis separately evaluates the vulnerability to storm-induced processes (inundation and erosion) and, it quantifies the contribution of the forcing (storm properties) and receptor (beach geomorphology) to the overall vulnerability. Beach geomorphology affects calculated vulnerability by influencing process intensity and the ability of the beach to cope with the impacts (resilience). Results showed that regarding wave-induced inundation, the highest vulnerable area is the Ebro delta (Catalan coast) due to a combination of storm properties and the existence of a very low-lying profile. On the other hand, when considering the storm-induced erosion, Lido di Dante (Italy) is the highest vulnerable area because despite the fact that the estimated erosion is not the largest one, the beach width is narrower than in the other sites. In any case, actual beach width at the three sites exceeds the estimated shoreline retreat. According to the obtained results the main induced process affecting coastal vulnerability is inundation.

ADDITIONAL INDEX WORDS:

Inundation, erosion, runup

INTRODUCTION

Coastal vulnerability to storms can be simply defined as the potential of a coastal stretch to be harmed by the impact of a storm. In spite of this simple definition, there is not a single way of evaluation, with existing methods ranging from simple indices including basic geomorphic characteristics to detailed quantifications of the coastal response. In many cases, these methods have been developed for specific cases that make them hardly exportable to other sites. When referring to the geomorphic component, this vulnerability accounts for the modification of the coastal substrate (morphodynamic response to the storm) supporting socio-economic and environmental values. This will serve to managers to assess the expected magnitude of damages along the coast due to storm hazards to take (informed) decisions on mitigation/adaptation strategies.

As the magnitude of the coastal response to storms depends on both the magnitude of the forcing (storm properties) and characteristics of the receptor (coastal geomorphology), we assume vulnerability as being composed by two components associated to each factor (forcing and receptor). This approach permits to discriminate for any coastal site which is the main contribution to the overall vulnerability and, in consequence, to provide managers with information on which should be the main factor to be modified if coastal vulnerability has to be managed.

Within this context, the main aim of this work, we comparatively assess the vulnerability to storm impacts of three coastal areas representative of microtidal and fetch-restricted environments located in the NW Mediterranean and N Adriatic Sea. Here we evaluate the coastal vulnerability to storms by

separately considering two induced processes: inundation and erosion (see e.g. MENDOZA and JIMÉNEZ, 2008).

AREA OF STUDY

The coastal vulnerability assessment is performed in three sites representative of microtidal and fetch restricted environments: the Ebro Delta (Catalan coast, Spain), the Lido de Sète beach (Sète, France) in the NW Mediterranean and the Lido di Dante beach (Emilia Romagna coast, Italy) in the N Adriatic (figure 1).

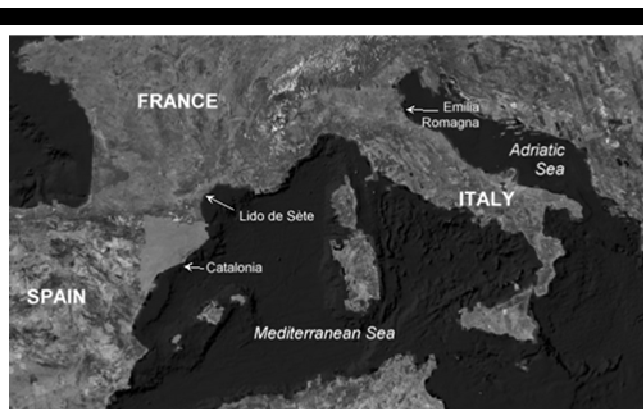


Figure 1. Area of study (Photo courtesy of Google Earth™).

These sites are characterized by the existence of dissipative beaches composed by fine sands (a common grain size could be used to represent local sediments, with $d_{50} = 0.250$ mm). Averaged beach slopes range from 0.028 in the Italian case to 0.042 and 0.048 in the Catalan and French coasts respectively. Surf zone slopes are typical of dissipative beaches and they are around 0.02. Beach heights are relatively low, being the Ebro delta the lowest due to the absence of any dune on the back of the beach. The average height of the selected area is 1.2, with a maximum value of 1.7 m. Along the French and Italian sites there is a dune ridge on the back of the beach with average heights of 3 m and 2.6 m respectively.

Figure 2 shows the wave height extreme probability function obtained for the three sites by using local wave data. Used wave time series are of different length and obtained wave climate can be considered as representative of the local values up to a return period, T_R , of 50 years in the French and Italian cases (due to the length of the used time series) whereas for the Spanish case they are valid up to 150 years. As it can be seen, wave heights associated to any T_R are almost equal in the Spanish and Italian case, whereas the corresponding value in the French coast is significantly higher.

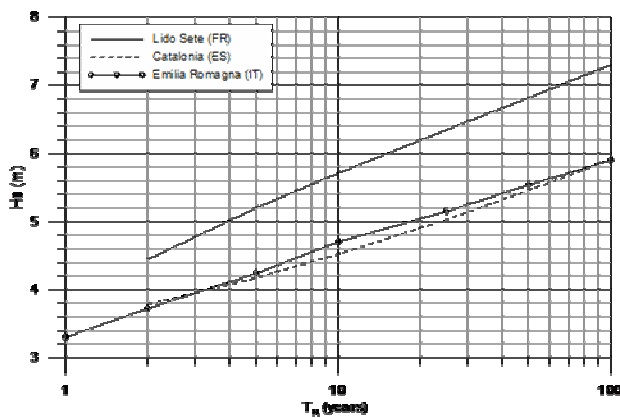


Figure 2. Wave height extreme distributions at the study areas.

In addition to this, we obtained the relationship between the remaining parameters characterizing storm properties (wave peak period, T_p , and storm duration, τ) with H_s . With these relationships we can reconstruct the full characteristics of a storm associated to any return period.

A description on study site characteristics including wave climate can be found in CERTAIN and BARUSSEAU (2005), JIMÉNEZ *et al.* (1997) and ARMAROLI *et al.* (2005) among others.

COASTAL VULNERABILITY ASSESSMENT

Generalities

To comparatively assess the geomorphic vulnerability of the three sites we have analyzed separately the component of the vulnerability associated to the forcing (the storm) and to the receptor (the coast). Finally, they have been integrated into a vulnerability index to assess the overall vulnerability at each site.

One of the main questions regarding vulnerability assessments to storms is to decide which will be the event to be used in the analysis. This selection will severely control the results since the longer the T_R is, the larger the response will be and, consequently, (potentially) also the vulnerability will be. In this work we have

Table 1: Probability of occurrence of a 50 year T_R event for different time periods.

Time period (years)	Probability (%)
2	3.96
5	9.61
10	18.29
25	39.65

(arbitrarily) selected a $T_R = 50$ years as the base event to calculate the coastal vulnerability. To get a guess of the relevance of the selected T_R , table 1 shows the probability of exceedence of such event to be equalled or exceeded during some time periods.

As it was mentioned above, the vulnerability is separately calculated for the two storm-induced processes: inundation and erosion. In this paper, we consider that storm-induced inundation is mainly driven by wave action, i.e. it is defined by the run-up at the peak of the storm. Here we calculate it by using the $Ru_{2\%}$ formula proposed by STOCKDON *et al* (2006). To calculate the storm-induced erosion we follow the approach proposed by MENDOZA AND JIMÉNEZ (2006) where beach profile erosion is calculated by using both the *Sbeach* model (LARSON and KRAUS, 1989; WISE *et al.* 1996) and a parametric way in function of storm and beach profile parameters (H_s , T_p , τ , $w_f \tan\beta$).

Vulnerability component associated to the forcing

To calculate the component of the vulnerability associated to the forcing, we have used two intermediate parameters only accounting the wave induced contribution to each process.

Taking into account the dependence of $Ru_{2\%}$ with wave variables, the used parameter to characterize inundability, IN , is given by

$$IN \propto \sqrt{(H_s L_o)} \quad (1)$$

Following MENDOZA and JIMÉNEZ (2006), beach profile erodibility due to storm impact, ER , is proportional to an excess of the Dean's parameter, $D (= H / w_f T)$, above an equilibrium value,

$$ER \propto \left(|D - D_{eq}|^{0.5} \tan\beta \right) \tau \quad (2)$$

To only account differences associated to wave climate, ER is evaluated assuming that the beach profile at the three sites is the same, being characterized by a $d_{50} = 0.25$ mm and a $\tan\beta = 0.05$.

Figure 3 shows the comparison of the vulnerability to inundation for the three sites associated to storm properties. Curves are presented in relative terms with respect to the maximum calculated IN value associated to the reference T_R (50 years). As it can be seen, the highest vulnerability in terms of inundation corresponds to the Catalan coast whereas storms in the Adriatic present the lowest associated potential values. This is due to the fact that recorded T_p during storms off Catalonia are the longest ones and, this variable dominates over H_s in wave runup calculations (see equation 1).

To illustrate the differences found between the three sites, table 2 shows the T_R associated to a given storm inducing the same potential vulnerability at each site. Thus, for instance, to induce the same vulnerability to inundation associated to the impact of a storm with a T_R of 27 years in the Catalan coast, a storm with a T_R of 50 years should be required in Lido de Sète and with a T_R longer than 100 years in the Italian case.

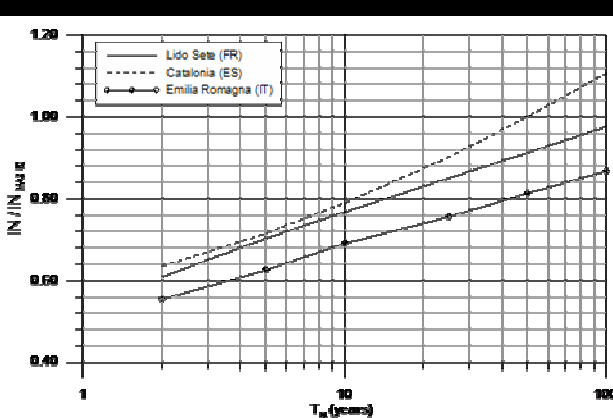


Figure 3. Ratio of the vulnerability to inundation associated to storm properties at each site with respect to the maximum value at the reference T_R (50 years).

These values clearly indicate that unless the coastal geomorphology at each site will modulate/modify the induced vulnerability, the Catalan coast should be the most vulnerable coast to storm-induced inundation. In addition to this, it has to be considered that differences in storm surge regimes at the three sites could alter this result because the obtained assessment only includes the wave induced part.

Figure 4 shows the comparison of the vulnerability to erosion for the three sites associated to storm properties. As in the previous case, curves are presented in relative terms with respect to the maximum calculated ER value associated to the reference T_R (50 years). In this case, the highest vulnerability in terms of beach erosion corresponds to the French coast whereas storms in the Catalan coast present the lowest associated potential values although very similar to the obtained for the Italian coast. In any case, the estimated difference in the response between sites is smaller than the obtained for inundation. This is clearly seen in Table 2 where the comparison of required storms to induce the same vulnerability along the three sites is presented.

Thus, to induce the same vulnerability to erosion associated to the impact of a storm with a T_R of 50 years in the French coast, a storm with a T_R of 67 and 65 years should be required at the Spanish and Italian cases.

Table 2: Storms defined in terms of T_R required to induce the same vulnerability to inundation and erosion at each site.

process	Catalonia (ES)	Lido de Sète (FR)	Emil.- Romag. (IT)
Inundat.	50	> 100	>> 100
	27	50	> 100
	12	17	50
erosion	50	35	46
	67	50	65
	53	38	50

Vulnerability component associated to the receptor

Once the component of the vulnerability associated to the wave climate was evaluated, a similar analysis to account for the contribution of the receptor's characteristics (coastal

geomorphology) to the overall vulnerability was performed. The modulation of calculated vulnerability due to beach characteristics is done at two levels: first, the profile shape and sediment grain size will condition the magnitude of the response (smaller erosion

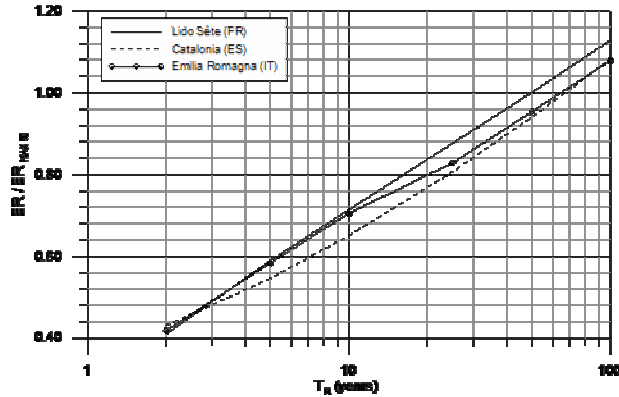


Figure 4. Ratio of the vulnerability to erosion associated to storm properties at each site with respect to the maximum value at the reference T_R (50 years).

and smaller runup for more dissipative profiles) and, second, the dimensions of the profile will determine their "resilience" (e.g. higher profiles will have a lower probability to be inundated). Due to this, the introduction of the effect of the receptor's characteristics will be done in two consecutive phases: first by estimating the effects on the magnitude of the induced process and, second, by estimating the effects on the overall response.

As in the previous case, the analysis is separately done for inundation and erosion and, again, results are presented in relative terms with respect to the maximum calculated for $T_R = 50$ years.

Figure 5 shows the vulnerability calculated for inundation when beach properties are also accounted for. In this case, instead of using equation (1) that only includes the wave-related part of the runup model, we used the full predictive runup formula which in practical terms means to assess the additional effect of the beach slope in the before mentioned calculations.

As it can be seen, when including local beach characteristics, the estimated vulnerability to inundation of the three sites differ from the previously presented one (figure 3). Thus, although the Italian site is again the lowest vulnerable to inundation, the estimated difference with respect to the other sites is larger. This is because it presents the mildest beach slopes and, in consequence, the wave induced runup will be the smallest. To put these results in the adequate context, it has to be considered that we are only accounting for the wave contribution to inundation and, the local storm surge regime (marginal and/or jointly with waves) could significantly modify this vulnerability.

The estimated vulnerabilities for the Spanish and French sites have the same magnitude (figure 5). This is because beach slopes in Lido de Sète are steeper than in the coastal stretch analyzed in the Ebro delta (Catalan coast). Thus, the above calculated difference in inundability for these sites just based on wave climates (figure 3) is strongly modified by the local coastal geomorphology. Just to put in context these results, it has to be considered that along the Catalan coast beach profiles range from dissipative to reflective ones. Of course, when estimating the vulnerability to inundation for reflective beaches, the calculated value drastically increases as the beach slope does.

The vulnerabilities to erosion assessed for each site in relative terms when beach properties are also accounted can be seen in figure 6. In this case, equation (2) is fully employed by including a representative (averaged) value of beach (surf zone) slope of each site. As occurred with inundation, these results significantly differ from those obtained by only using storm properties (figure 4).

Although the French site is again the highest vulnerable to erosion, the difference in magnitude with respect to the other sites is much larger. This is because this area is characterized by the largest inner surf zone slope (in average) and, in consequence,

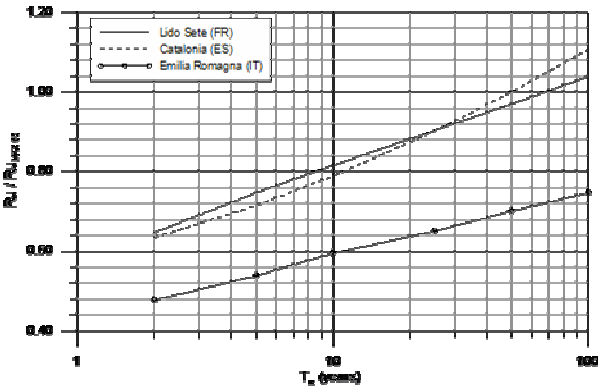


Figure 5. Ratio of the vulnerability to inundation associated to storm properties and beach morphology at each site with respect to the maximum value at the reference T_R (50 years).

erosion will be much larger. The lowest calculated vulnerability for the Catalan case is due to the fact that beach profiles of the analyzed coastal stretch (Ebro delta) are very dissipative and, although wave climate should potentially be able to induce significant erosion, a large part of wave energy will be efficiently dissipated in the surf zone. As it was previously mentioned, if

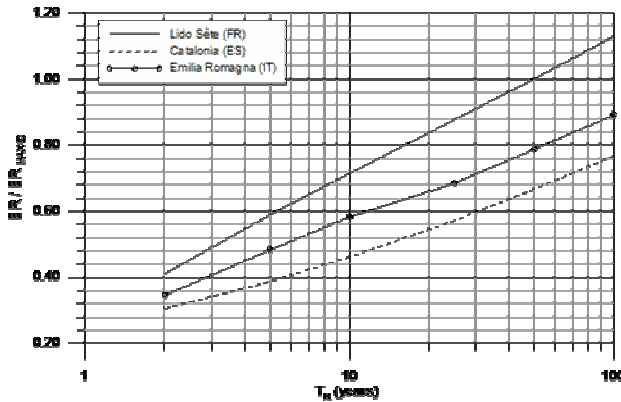


Figure 6. Ratio of the vulnerability to erosion associated to storm properties and beach morphology at each site with respect to the maximum value at the reference T_R (50 years).

reflective beaches should be selected to make the analysis in the Catalan coast (they dominate in some parts of the coast), results will be significantly different and, the largest induced erosion should be expected.

Finally, to estimate the total vulnerability to each process at each site, an index including the variable of the beach

characterizing the ability to cope with each process (an indicator of the beach resilience) was calculated. To compare the results in simple terms, this indicator is a simplified version of the used ones by MENDOZA and JIMÉNEZ (2008) and they are given for inundation, V_I , and erosion, V_E , respectively by

$$V_I = Ru/Z \quad (3)$$

$$V_E = \Delta x/W \quad (4)$$

where Z is the beach/dune height, Δx is the induced shoreline erosion and W is beach width.

In the case of inundation, the index V_I represents a measure of the relative dimension of the maximum water level at the beach (which in this case is just given by the wave-induced runup, Ru) with respect to the maximum elevation of the beach. Thus, for coasts characterized by a high inundability (determined both by wave climate and beach slope), the presence of a dune or a dike will significantly reduce its vulnerability. Figure 7 shows the calculated values for this vulnerability index at the three sites in relative terms. Values are normalized with respect to the maximum value associated to the reference storm ($T_R = 50$ years).

As it can be clearly seen, the introduction of the geomorphological variable characterizing the ability to cope with inundation fully conditions and changes the previous estimated comparisons (figures 3 and 5). Obtained results show that the highest vulnerable area to inundability due to storm impacts is the Catalan coast (the Ebro delta in this case). This huge difference with respect to the other two sites is because this area can be classified as a very low-lying environment, whereas the French and the Italian sites are characterized by the presence of a dune row along the back of the beach. In fact, whereas Ru/Z values for

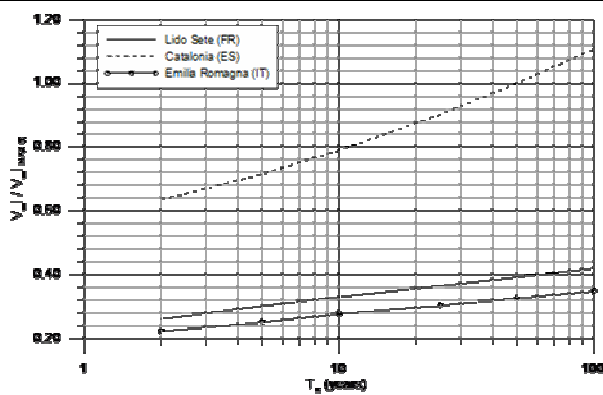


Figure 7. Ratio of the vulnerability to inundation at each site with respect to the maximum value at the reference T_R (50 years).

any storm are larger than 1 in the case of the Catalan coast (all induced runups exceed the beach height and the coast should be potentially inundated), in the case of the French and Italian cases, Ru/Z values are ever below unity, indicating that reached water level is lower than dune elevation (in average along the beach, although there are some few locations along each coast where local values can exceed the beach height).

In the case of erosion, the index V_E represents a measure of the relative dimension of the storm-induced shoreline retreat with respect to the actual beach width. Thus, for coasts characterized by a high erodibility (determined both by wave climate and beach characteristics), the existence of a wide beach will significantly

reduce its vulnerability. In some cases, this vulnerability can be even zero if existing uses and resources are not affected by the storm. To incorporate the effect of the beach width, instead of characterizing the erosion potential (equation 2), we directly evaluate the storm-induced erosion in each profile by using the Sbeach model. Figure 8 shows an example of the obtained results for one representative profile of Lido de Sète (France) under the impact of different storms.

Figure 9 shows the calculated erosion vulnerability, V_E , values at the three sites normalized with respect to the maximum value associated to the reference storm ($T_R = 50$ y). In this case, the introduction of the beach width as characteristic variable of the ability to cope with erosion also modifies the previous estimated comparisons (figures 4 and 6). Results show that the highest vulnerable area is the Ebro delta (Catalan coast) due to a combination of storm properties and the existence of a very low-

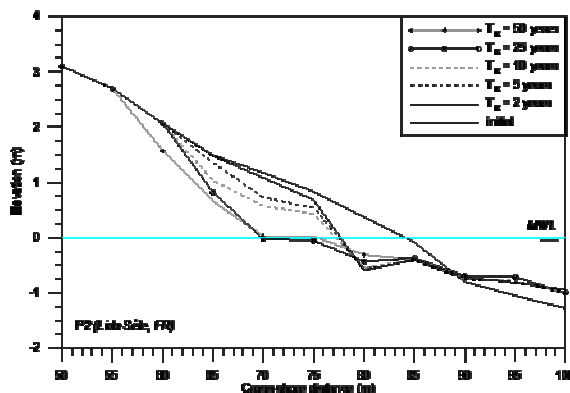


Figure 8. Example of simulated beach profile erosion due to the impact of storms associated to different T_R at the French site (only a zoom of the inner part of the beach is showed).

each site, all the calculated $\Delta x/W$ values for any storm are smaller than 1. This means that under ideal conditions (beach width not affected by other processes), beach configurations will be able to cope with storm-induced erosion (in average terms). The lowest values calculated for the Catalan case are due to the fact that the potential vulnerability is the lowest (due to the combination of storm properties and beach characteristics) and that the local beach is very wide. In any case, the vulnerability to erosion has been calculated for average widths and, it is possible to find coastal stretches with smaller local values. As an example, values obtained for the French site only comprise the northern part where the beach is the narrowest. If overall width values along the barrier were used, the relative vulnerability should decrease because the beach width in the southern part increases between 4 to 7 times.

CONCLUSIONS

A comparative vulnerability assessment to storms in three sites of the Mediterranean has been done. The analysis separately evaluates the vulnerability to storm-induced processes (inundation and erosion) and, quantifies the contribution to the estimated vulnerability of the forcing (storm properties) and receptor (beach geomorphology). This last one accounts for geomorphologic influence on the process's intensity and on the beach resilience. Results showed that regarding wave-induced inundation, the

highest vulnerable area is the Ebro delta (Catalan coast) due to a combination of storm properties and the existence of a very low-

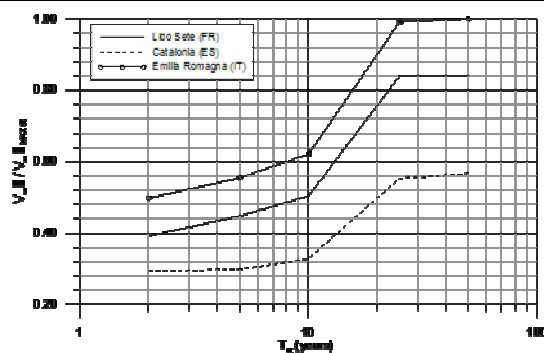


Figure 9. Ratio of the vulnerability to erosion at each site with respect to the maximum value at the reference T_R (50 y).

lying profile. On the other hand, when considering the storm-induced erosion, Lido di Dante (Italy) is the highest vulnerable area because although the estimated erosion is not the largest one the beach width is narrower than in the other sites. In any case, actual beach width at the three sites exceeds the estimated shoreline retreat due to storm impacts.

ACKNOWLEDGEMENTS

This work was partially funded by VuCoMa and Micore projects, funded by the Spanish Ministry of Education (CTM2008-05597/MAR) and the EU (202798) respectively. The first author was supported by a University Research Promotion Award for Young Researchers from Generalitat de Catalunya. Last author was supported by the Languedoc-Roussillon Region. We thank authorities providing used data (Generalitat de Catalunya and DRE-LR, Regional Direction of Ministry of Equipment).

LITERATURE CITED

- ARMAROLI C., BALOUIN Y., CIAVOLA P. and CAPATTI D. 2005. Nearshore bars as a natural protection of beaches, field evidences from Lido di Dante beach, Adriatic Sea. *Proc ICCCM'05*, University of Porto, 295–303.
- CERTAIN, R. and BARUSSEAU, JP. 2005. Conceptual modelling of sandbar morphodynamics fo a microtidal beach (Sète, France). *Bull. Soc. Geol. Fr.* 176(4), 343–354.
- JIMÉNEZ, J.A., SÁNCHEZ-ARCILLA, A., VALDEMORO, H.I., GRACIA, V. and NIETO, F. 1997. Processes reshaping the Ebro delta. *Marine Geology*, 144, 59–79.
- LARSON, M. and KRAUS, N.C., 1989. *SBEACH: Numerical Model for Simulating Storm-Induced Beach Change*. CERC-89-9, US Army Corps of Engineers, Vicksburg.
- MENDOZA, E.T. and JIMÉNEZ, J.A. 2006. Storm-Induced Beach Erosion Potential on the Catalonian Coast. *Journal of Coastal Research*, SI 48, 81–88.
- MENDOZA, E.T. and JIMÉNEZ, J.A. 2008. Vulnerability assessment to coastal storms at a regional scale. *Proc. 31st Int. Conf. on Coastal Engineering*, ASCE, Hamburg, (in press).
- STOCKDON, H.F., HOLMAN, R.A., HOWD, P.A. and SALLINGER, A.H. 2006. Empirical parameterization of setup, swash, and runup. *Coastal Engineering*, 53, 573–588.
- WISE, R.S., SMITH, S.J. and LARSON, M. 1996. *SBEACH: Numerical model for simulating storm-induced beach change*, CERC, US Army Corps of Engineers, Vicksburg.

Turbulent measurements in the surf zone suspension

D. Hurther, H. Michallet and X. Gondran

Laboratoire des Ecoulements Géophysiques et Industriels
(CNRS – UJF – INPG)
BP 53, 38041 Grenoble cedex 9, France
[david.hurter@hmg.inpg.fr](mailto:david.hurther@hmg.inpg.fr)



ABSTRACT

HURTER, D., MICHALLET, H. and GONDRA, X., 2007. Turbulent measurements in the surf zone suspension. *Journal of Coastal Research*, SI 50 (Proceedings of the 9th International Coastal Symposium), 297 – 301. Gold Coast, Australia, ISSN 0749.0208

An irregular wave field experiment over a mobile bed is performed in a laboratory channel. The surf zone measurements are collected at the average breaking point after the formation of a stable, non-progressing beach profile (Michallet *et al.* 2007). The use of a wave averaging technique allows the decomposition of the velocity into mean, orbital and turbulent components for the representation of all ensemble averaged quantities as a function of wave period normalised time. As a result, we present fields of wave velocity, TKE, TKE production, TKE dissipation rate and sediment concentration (only two points in the outer region), below the trough of the waves. Nearbed and outer region processes are both seen in the TKE production and dissipation fields. In particular, the cross-shore velocity lead due to bed friction effects shown in SHIN and COX (2006) is observed in the wave velocity and TKE fields. Although the phase lead zone is seen in the velocity and TKE fields, no corresponding production or dissipation zones could be observed. Furthermore, the zone of high TKE is much more uniformly distributed over the water column than the zones of TKE production and dissipation that are clearly separated between the nearbed and the outer regions. In the outer region, the sediment concentration (orbital component) is seen to be well correlated to the TKE and TKE dissipation zones. Finally, we detect a low frequency correlation at 0.025Hz between the velocity and sediment concentration. This frequency corresponds well to the first mode of the infra-gravity wave released at the average breaking point (MICHALLET *et al.* 2007).

ADDITIONAL INDEX WORDS: *Irregular waves, Equilibrium beach profile, ADVP, surfzone suspension, surfzone turbulence*

INTRODUCTION

The present wave channel experiment is devoted to the study of surf zone hydrodynamics and coupled suspension processes under the forcing by an irregular wave field in equilibrium with the formed beach profile. Compared to the rigid bottom and regular wave forcing conditions of most of the documented laboratory studies (TING and KIRBY 1994, COX and KOBAYASHI, 2000, TING 2001, SCOTT *et al.* 2004, SHIN and COX 2006), the tests herein are conducted over a well established mean beach profile with negligible bed evolution velocity. A similar type of beach profile was obtained in a wave basin experiment by WANG *et al.* (2002) for their case of spilling breakers. They performed velocity and concentration measurements over a beach that was formed by irregular breaking waves. They focussed on the estimation of wave induced currents but did not resolve turbulent scales.

The objective herein consists in (a) analysing the fine scale turbulent and suspension processes in the surf zone occurring at the scale of the gravity wave forcing, (b) examine the coupling between the infragravity wave released at the average breaking point and the surf zone suspension. For point (a) the measurements will be compared to recent laboratory results (SHIN and COX 2006) showing the effects of rough bed turbulence and bore generated turbulence on the cross-shore velocity and Turbulent Kinetic Energy (TKE). Furthermore we will present novel TKE production and dissipation rate estimations in order to examine whether one of the turbulent process (bed or bore

generated) is leading the correlation with the surf zone suspension events.

EXPERIMENTAL, WAVE AND BEACH CONDITIONS

The experiment is carried out in a 36m long by 0.55m wide flume with a piston wave maker producing a JONSWAP type potential energy spectrum. The deep water wave conditions are 0.33Hz and 11cm for the wave peak frequency and H_{rms} . The bed of the wave tank is composed of loose non-cohesive sediments for which the density and diameter allow representative sheet-flow and suspension flow regimes. The particles have a density of 1.19 g L⁻¹ and a median diameter of 0.6 mm. Starting from a strongly disrupted initial condition, the beach profile is formed by the breaking waves in about 15 hours. During the following 150 hours of experiment duration the beach profile did not change in mean confirming an equilibrium state between the bed morphology and its wave forcing. The form of the obtained profile (see Figure 1) is at the transition between a barred and a terraced beach, similar to the one obtained in a wave basin for spilling waves by WANG *et al.* (2002). The same experiment has been repeated several times with the same wave field but with very different initial beach profiles. All tests converged towards the same stationary beach profile.

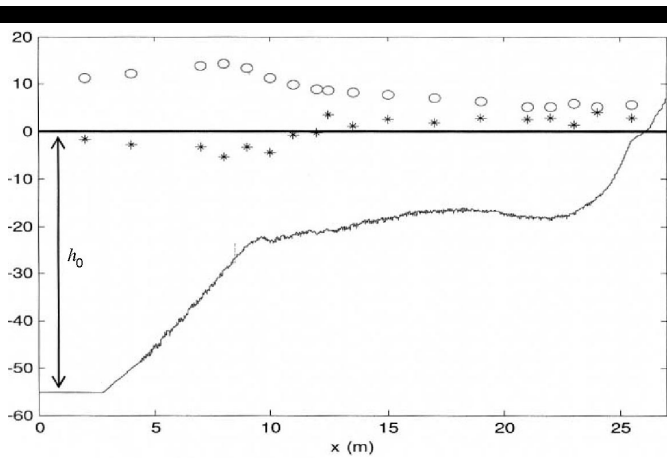


Figure 1. Cross-shore profile of bottom elevation at equilibrium, mean free-surface elevation $\bar{\eta}$ in mm (set-down and setup: *) and H_{rms} in cm (o) for $h_0=55.3$ cm.

Also shown in Figure 1 are the cross-shore distributions of the measured mean water level and H_{rms} represented by crosses and circles, respectively. The regions of setdown and setup can be seen in the mean level profile. The location of the average breaking point is found at $x=12$ m which corresponds well to the region of maximum undertow (not shown here). This is also in good agreement with the region of maximal potential energy loss due to wave breaking in the external surf zone. A distinct bed slope rupture is observed in the beach profile at $x=9$ m corresponding to the start of the surf zone. Finally the mean momentum is found to be well conserved locally at each cross-shore position between wave and mean level (setup / setdown) contributions such as:

$$\frac{\partial \bar{\eta}}{\partial x} = \frac{3\alpha}{2} \frac{1}{h} \frac{\partial H_{rms}^2}{\partial x} \quad (1)$$

where α is 1/8 and 1/12 when the waves are symmetric and skewed, respectively.

Although measured at 8 different locations across the surf zone, Figure 2 only shows a typical data sample obtained at $x=12$ m (average breaking point) where the mean water depth is equal to 20cm. It shows the synchronised timeseries at 20 Hz of normalised surface elevations noted z^* (*i.e.* relative to the mean local water depth), suspended sediment concentration at $z^*=0.23$ and $z^*=0.45$, and cross-shore orbital velocity at $z^*=0.23$. The wave heights are measured with calibrated capacitive gauges. A 2D-ADV Profiler is used to perform u-w velocity measurements at the average breaking point and calibrated OBS provide the sediment concentration data at two points in the water column ($z^*=0.23$ and $z^*=0.45$). All measurements are sampled simultaneously at a frequency above 20 Hz over long data samples to allow the analysis of infragravity and gravity waves as well as the production and inertial scales of the turbulent processes. Please note that the piezo-electrical transducers of the ADVP are always immersed and therefore located below the lowest wave trough. Moreover, the velocity measurements in the first 7cm from the emitter cannot be exploited due to near field limitations. As a result the study addresses nearbed processes since the measurement depth is limited to 60% of the water depth at $x=12$ m.

In order to decompose the instantaneous velocity profiles into mean, orbital and turbulent components we apply an ensemble average over 32 identical sequences of irregular waves with a peak frequency at 0.33 Hz. A time-length of 20 minutes (roughly 380

waves) is sufficient to obtain well established setup, setdown, and undertow processes under our irregular wave field forcing. The residual bias error for the ensemble averaged first and second order velocity moments over 32 sequences is less than 5%.

Figure 3 shows the results of the velocity decomposition on the spectra of orbital and turbulent cross-shore velocity components at $x=12$ m. The typical $-5/3$ slope can be seen in the turbulent signals supporting the validity of the decomposition method.

Qualitatively, the timeseries in Figure 2 reveal that sediment and velocity processes occur at two very different scales. The wave scale and a much larger scale being approximately twelve times superior. In the following we address these processes separately.

FINE-SCALE PROCESSES AT THE GRAVITY WAVE SCALE

The wave averaging procedure for the case of irregular waves requires special attention. The first step of the procedure consists in selecting a reference wave in one of the 32 sequences composed of 380 waves. In a second step we look for very similar waves by cross-correlating the surface elevation of the reference wave with the complete timeseries of surface elevation. The wave selection criteria is a correlation coefficient above 90% with a maximum of the cross-correlation function at time lag zero. Furthermore we check that each selected wave is well correlated with the reference wave in terms of orbital velocity. It is seen that very few of the waves selected after the first step are rejected based on the velocity correlation criteria. Typically 80 waves per sequence are selected. Three types of reference waves have been tested for small, moderate and high amplitude levels. Only the results corresponding to the moderate amplitude wave are presented herein but negligible differences are found with the high amplitude wave case. Fig. 4a shows the reference wave (of moderate amplitude) represented by the dotted curve and the surface elevation averaged over roughly 80×32 selected waves. Good resemblance is seen between the two wave profiles except at the crest corresponding to the well developed breaking region. Both wave fronts are in phase with very similar slopes. Fig. 4b shows the ensemble averaged wave velocity field in cross-shore direction. Very good agreement is found with the result shown in SHIN and COX (2006) for their regular wave forcing with a plunging type breakers (at their point E before the impinging point). The leading phase wave velocity due to bed friction effects in the benthic boundary layer is clearly seen. We show here that similar effects are found for mobile bed conditions at the bed interface for irregular waves with spilling type breaking. Fig. 4c emphasises this phase-lag effect by representing the normalised wave velocity at three different depths in the nearbed region. Over the time interval 0.4-0.8, we find a maximal phase shift of nearly 7% between the velocity at $z^*=-0.095$ and $z^*=0.055$.

Figure 4d to 4f represents the ensemble averaged turbulent fields below the wave trough. The TKE, TKE production, TKE dissipation rate are estimated as follows:

$$\langle k \rangle = 1.33 \left(\langle u' \rangle^2 + \langle w' \rangle^2 \right) \quad (2)$$

$$\langle P \rangle = -\langle u' w' \rangle \frac{\partial \langle u \rangle}{\partial z} \quad (3)$$

$$\langle D \rangle = -15\nu \left\langle \left(\frac{\partial w'}{\partial z} \right)^2 \right\rangle \quad (4)$$

where the approximation by SHIN and COX (2006) is taken for the TKE.

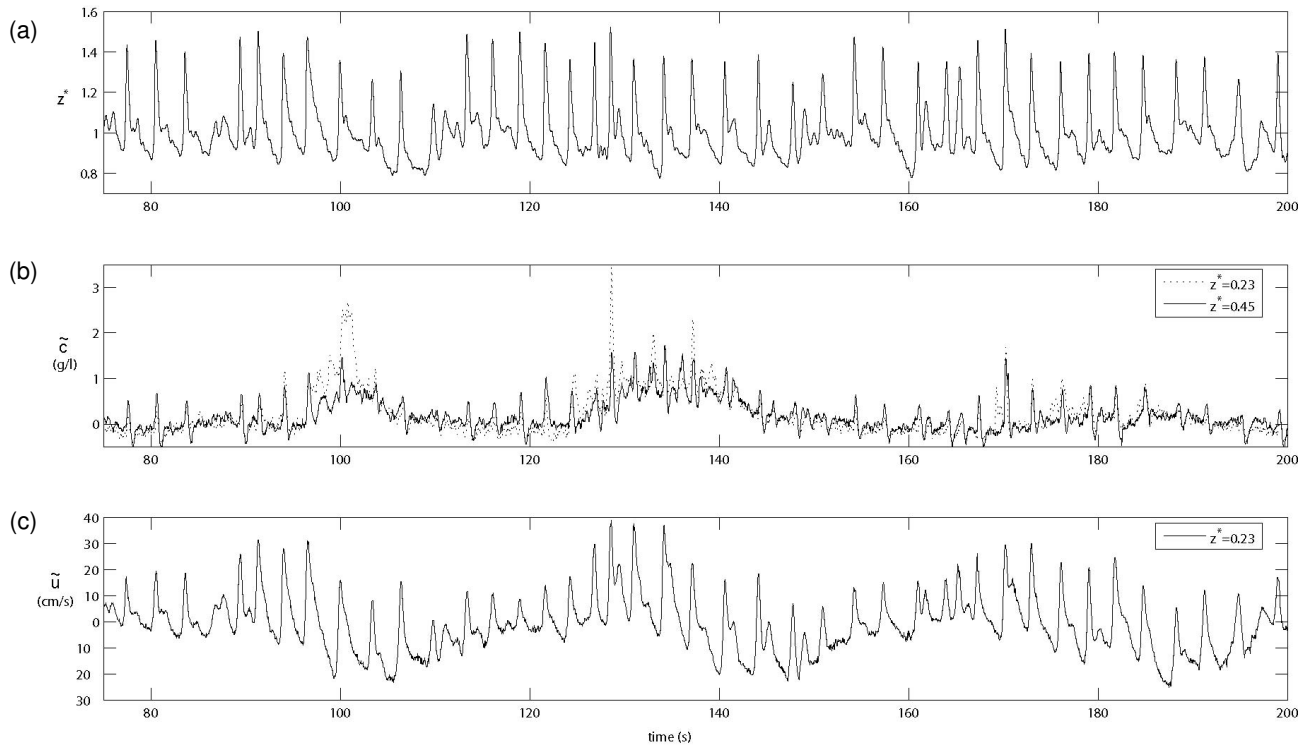


Figure 2. Timeseries at $x=12\text{m}$ (average breaking point) of surface elevation (calibrated capacitive gauges), sediment concentration (OBS) at $z^*=0.23$ and $z^*=0.45$ and orbital velocity (2D-ADVP) in cross-shore direction

The observed TKE field in Figure 4d is in good agreement with the results shown in SHIN and Cox (2006) for regular plunging breakers over rough rigid bottom. It is clearly seen that in our nearbed region, the first TKE region is correlated to the region of phase leading cross-shore wave velocity. A larger region of high TKE is seen above with a centre located at $t/T=0.57$ and $z^*=0.25$. It is in phase with the wave crest. Different from SHIN and COX (2006) we observe another TKE region close to the bed with a lower amplitude than the phase leading one but clearly detached from it (centre at $t/T=0.59$, $z^*=0$).

Figure 4e and 4f represent the TKE production and dissipation rate fields, respectively. The TKE production in the nearbed region covers the two regions seen before in the nearbed region of the TKE field. The TKE production in the outer region is not in phase with the TKE core seen in the outer region. Its centre is located above, phase leading and well detached from the bed region compared to the TKE core in the outer region. The ensemble averaged TKE dissipation field in Figure 4f is closer to the field of TKE production than the TKE, especially in the outer region. However we do not see the effect of the phase leading wave velocity in the nearbed region. Only the phase delayed TKE region is seen to be in better agreement with the nearbed dissipation region at $t/T=0.61$, $z^*=0.1$. Although this result is quite unexpected, its repeatability is very good for other reference waves with moderate and high amplitude levels. Whether turbulent transport processes such as turbulent diffusion can explain the differences between the observed turbulent fields will be investigated in the future.

Finally, the ensemble averaged sediment concentration (corresponding to the wave component) at $z^*=0.23$ and $z^*=0.45$ (far outside the near bed region) is seen to be more correlated to

the TKE and TKE dissipation field in the outer region. New experiments will be undertaken providing concentration profiles by acoustic inversion of the backscattered ADVP intensity.

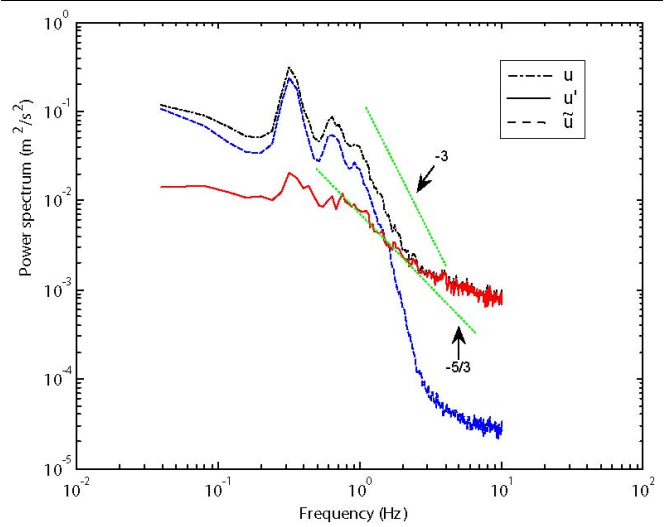


Figure 3. Velocity spectra of the decomposed cross-shore velocity into wave and turbulent components at $x=12\text{m}$.

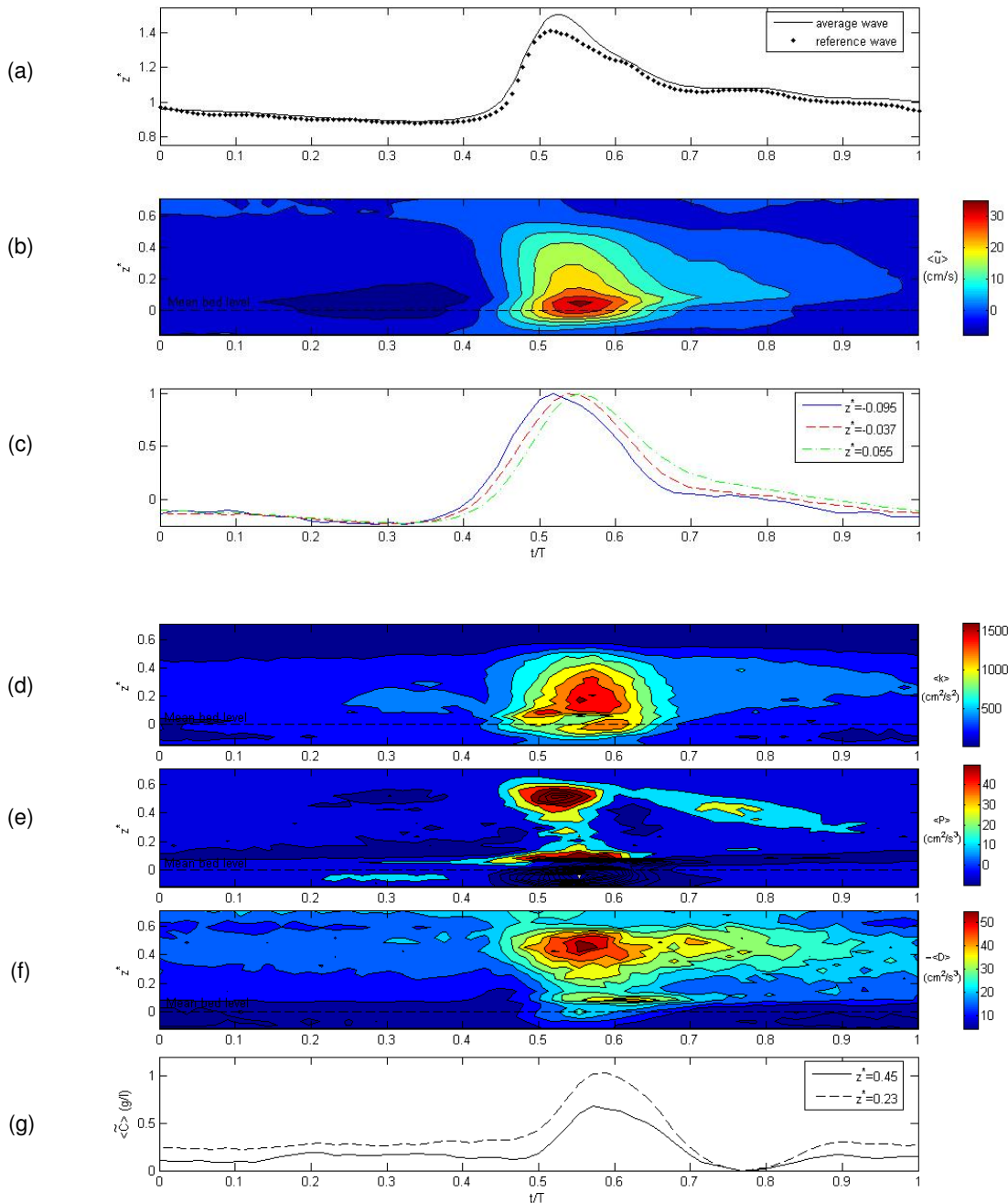


Figure 4. Measurements at $x=12\text{m}$ of (a) surface elevation (b) cross-shore wave velocity field, (c) normalised cross-shore wave velocity at three depths, (d) TKE field, (e) TKE production field, (f) TKE dissipation rate field, (g) sediment concentration (wave component) at two depths.

LARGE-SCALE VELOCITY / SEDIMENT PROCESSES

As observed previously, a large scale effect is seen to contribute to suspended sediment fluctuations (see Figure 2). In order to examine this process, Figure 5 represents the normalised correlation function between the cross-shore wave velocity and

sediment concentration (wave component) at $z^*=0.23$. It can be seen that the suspension is correlated to a low frequency velocity signal of period equal to 40s and to the wave velocity of frequency corresponding to the wave peak frequency at 0.33Hz (see the periodicity of the correlation function in the zoomed area of Figure 5b).

In order to check for the origin of the low frequency correlation, the spectra of the wave velocity is calculated in Figure 6. The

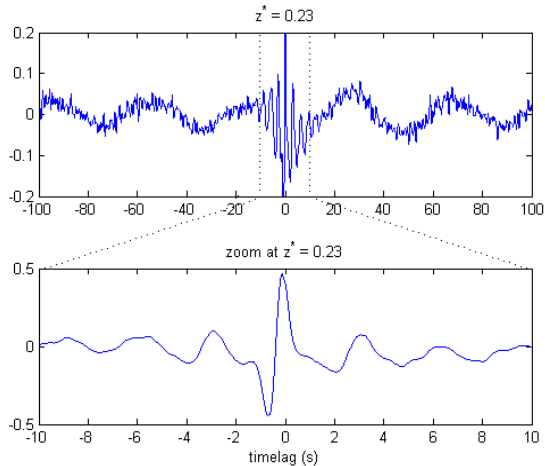


Figure 5. Temporal cross-correlation function between cross-shore wave velocity and sediment concentration at $x=12$ (average wave breaking point) for $z^*=0.23$.

lower spectral range reveal the presence of a peak at frequency $1/40s=0.025Hz$. MICHALLET *et al.* (2007) has shown that this peak corresponds to the first mode of the infra-gravity wave released at the average breaking point. The energy of this infra-gravity wave is lower at $z^*=0.45$ which is in good agreement with the lower degree of correlation between the suspension and the velocity at $z^*=0.45$ (not shown here).

CONCLUSION

Surface elevation, 2D-velocity profiles and sediment concentration measurements have been performed in the surf zone of an irregular wave field in equilibrium with its formed beach profile (mobile sediment bed). Following results are found.

-The phase lead of the cross-shore wave velocity in the nearbed region is clearly observed. This confirms the recent result by SHIN and COX (2006). The validity of this nearbed friction process is shown here for the case of irregular wave breaking over a mobile bed.

-The TKE field shows good similarity with the TKE field measured by SHIN and COX (2006) in the outer region. The effect of the velocity phase lead can be seen in the TKE field but we detect another nearbed process. It is clearly separated and phase delayed from the first one.

-The TKE production and dissipation fields show much clearer separations between nearbed and outer region processes than the velocity and TKE fields do.

-The turbulent process in the outer region is well identified in the TKE production and dissipation fields.

-In the nearbed region the TKE production and dissipation fields reveal a much lower correlation with the phase lead effect than with the second phase delayed process.

-We detect a low frequency correlation at $0.025Hz$ between the velocity and sediment concentration. This frequency corresponds to the first mode of the infra-gravity wave released at the average breaking point as addressed by (MICHALLET *et al.* 2007). Its contribution to cross-shore sediment flux merits further investigation.

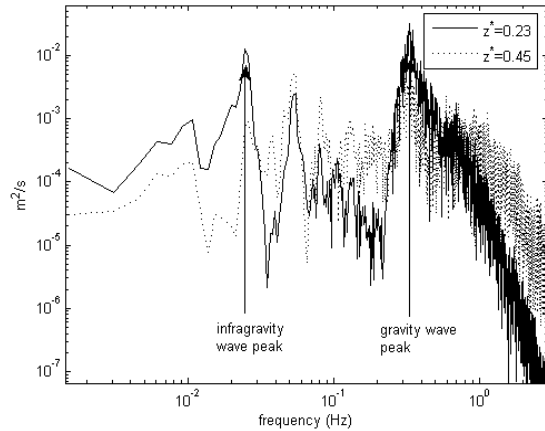


Figure 6 Velocity spectra of cross-shore wave velocity at average wave breaking point ($x=12m$)

Based on these results we intend: (a) to verify whether transport processes can explain the more widely distributed field of TKE, especially the link between nearbed and outer region processes below irregular breaking waves. (b) to perform new measurements from the bed towards the free-surface in order to determine the origin of the outer region turbulence (most likely due to wave breaking). (c) to measure high resolution profiles of nearbed sediment concentration and sediment fluxes.

LITERATURE CITED

- Cox, D.T. and KOBAYASHI, N. 2000. Identification of intense, intermittent coherent motions under shoaling and breaking waves, *J. Geophys. Res.*, 105 (C6), 14223-14236.
 MICHALLET, H., GRASSO, F. and BARTHÉLEMY, E., 2007. Long waves and beach profiles evolutions. *Journal of Coastal Research*, SI 50 (Proceedings of the 9th International Coastal Symposium), 221 – 225. Gold Coast, Australia.
 SCOTT, C.P., D.T. COX, S. SHIN, AND N. CLAYTON. 2004. Estimates of surf zone turbulence in a large-scale laboratory flume, *Proc. 29th Int. Conf. Coastal Eng.*
 SHIN, S. AND COX, D., 2006. Laboratory observations of inner surf and swash-zone hydrodynamics on a steep slope, *Cont. Shelf Res.*, 26, 561-573.
 TING, F.C.K., AND J.T. KIRBY. 1994. Observation of undertow and turbulence in a laboratory surf zone, *Coastal Eng.*, 24, 51-80.
 TING, F.C.K. 2001. Laboratory study of wave and turbulence velocities in a broad-banded irregular wave surf zone, *Coastal Eng.*, 43, 183-208.
 WANG, P.; EBERSOLE, B.A.; SMITH, E.R. and JOHNSON, B.D., 2002. Temporal and spatial variations of surf zone currents and suspended sediment concentration, *Coastal Eng.*, 46, 175-211.

ACKNOWLEDGEMENTS

This work has been partially funded by the French research program CNRS-LEFE-IDAO and the European Hydraulab III-SANDS project. The technical support of J.-M. Barnoud is gratefully acknowledged.

Long Waves and Beach Profile Evolutions

H. Michallet, F. Grasso and E. Barthélemy

Laboratoire des Ecoulements Géophysiques et Industriels
(CNRS – UJF – INPG)
BP 53, 38041 Grenoble cedex 9, France
herve.michallet@hmg.inpg.fr



ABSTRACT

MICHALLET, H., GRASSO, F. and BARTHÉLEMY, E., 2007. Long waves and beach profiles evolutions. *Journal of Coastal Research*, SI 50 (Proceedings of the 9th International Coastal Symposium), 221 – 225. Gold Coast, Australia, ISSN 0749.0208

Experiments were carried out in a flume 36 m long and 55 cm wide equipped with a piston wave generator. The sloping bottom consists of a loose material of low density (1190 kg m^{-3}) with a median diameter $d_{50}=0.6 \text{ mm}$ in order that Shields and Rouse numbers are of the same magnitude as those of natural environments. Time and length scales ratios are roughly 1/3 and 1/10. Irregular waves were generated according to a JONSWAP spectrum. The waves were measured along the flume and bottom profiles were recorded in between repeated wave sequences. A wave climate (characterized by its peak frequency and root mean square wave height) was run for several tens of hours, so as to reach bottom equilibrium conditions. H_{rms} and infragravity mode amplitudes along the flume were obtained for transient and equilibrium bottom profiles. The long waves node positions and structure conform to model solutions of the linearized Saint-Venant equations. On the equilibrium bottom profile they are more energetic and the correlation between infragravity waves and the incident short wave envelope clearly indicate that they conform on both breaking point and bound long wave release mechanisms.

ADDITIONAL INDEX WORDS: *Irregular waves, Equilibrium beach profile, Infragravity waves*

INTRODUCTION

Field measurements indicate that waves in the infragravity range play an important role on beach morphology. The generation of such long period waves can be explained by two different mechanisms. On one hand the breaking is thought to release bound long waves due to wave grouping (LONGUET-HIGGINS and STEWART, 1962). On the other hand wave grouping produces a break point and set-up oscillation that acts as a piston at the wave group period (SYMONDS et al., 1982). In both cases these incident long period waves reflect on the beach face, interfering with the incident waves to produce long period standing waves known as surf-beats. The strong correspondence in field experiments between long wave and morphological features length scales (AAGAARD and BRYAN, 2003), has suggested that long waves may generate off-shore bars. While strongly depending on the incident wave conditions (CERTAIN et al., 2005), these infragravity waves also play an important role on the swash process (MASSELINK et al., 2005). Nevertheless, descriptions of these long waves on real beaches are difficult due to the need of high spatial and temporal resolutions and tri-dimensional effects. Besides, wave climates and beach topographies are continuously changing in the real environment.

In a wave basin, WANG et al. (2002) performed velocity and concentration measurements over a beach that was formed by breaking irregular waves. A similar topography was obtained in a wave flume and included turbulent measurements in the surf zone suspension by HURTHER et al. (2007). Such laboratory experiments in wave tanks with beaches made of loose material are rare (DETTE et al., 2002). Most experimental studies were performed with a rigid bottom topography. JANSSEN et al. (2003) evaluated the long waves generation for a mild slope topography

moulded in sand with a smooth concrete surface. They concluded on a dominant mechanism of bound wave release. BALDOCK and HUNTLEY (2002) and BALDOCK et al. (2004) observed breaking forced waves for steeper uniform slopes and a barred beach profile.

The aim of the present paper is to investigate the characteristics of such surf-beats in small-scale mobile bed experiments and evaluate their relation to the bottom profile under controlled conditions.

EXPERIMENTAL SET-UP

Experiments were carried out in a flume 36 m long and 55 cm wide equipped with a piston wave generator. The still water depth was 55.3 cm. The mean overall slope is approximately 1/40. The sloping bottom consists of a loose material (PolyMethyl MethAcrylate particles) of low density (1190 kg m^{-3}) with a median diameter $d_{50}=0.6 \text{ mm}$. In the experiments, the Froude number, the Shields number in the shoaling part and the Rouse number in the breaking zone (ratio of turbulent agitation to the settling velocity of the sediment) were of the same magnitude as those in natural environments. Time and length scales were roughly 1/3 and 1/10. Irregular waves were generated according to a JONSWAP spectrum (peak enhancement factor $\gamma=3.3$). For each simulation, it is ensured that these waves conform to the expected spectrum and that they follow a Rayleigh distribution at 2 m downstream of the wave maker. Twelve wave gauges mounted on trolleys measured instantaneous water elevations over at least 30 minutes durations to obtain statistical convergence. Bottom profiles are recorded between wave series.

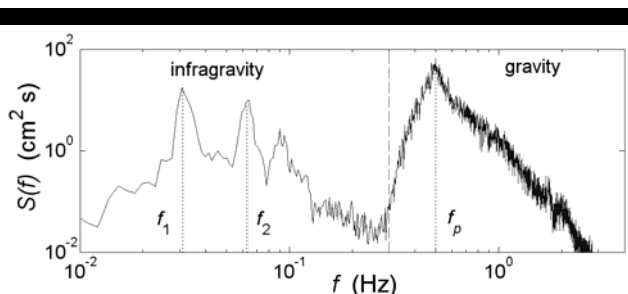


Figure 1. Surface elevation energy spectrum at $x=2$ m in the flume on the equilibrium beach plotted in fig. 2d (—). On the right: “gravity” domain, corresponding to the generated JONSWAP spectrum. On the left: “infragravity” domain, generated by wave breaking. Wave parameters: $H_{\text{rms}0}=7.5$ cm, $f_p=0.5$ Hz, $h_0=55.3$ cm. Two first modes infragravity frequency peaks $f_1=0.031$ Hz and $f_2=0.063$ Hz.

Spectral estimates $S(f)$ were obtained from Fourier transforms of five 50 overlapping data segments, each comprising 32768 points sampled at 50 Hz. A wave spectrum measured at $x = 2$ m has been plotted in Figure 1. Frequencies above $3/5 \times f_p$, correspond to the generated JONSWAP spectrum, representing the “gravity” domain. The generation of low frequency waves was clearly

visible in the power spectral density below $3/5 \times f_p$ (this is the “infragravity” domain). A closer inspection of the low frequency range showed a broad peak at a frequency f_1 around 0.03 Hz. Harmonics of this peak were also visible. The amplitude of the long wave motion was estimated within finite frequency bands of 0.02 Hz centered on peak frequencies as the square root of twice the sum of $S(f)$. The energy contained at various locations along the flume was estimated.

LONG WAVES STRUCTURE

A wave climate characterized by its peak frequency ($f_p=0.5$ Hz) and the root mean square wave height at 2 m downstream of the wave maker ($H_{\text{rms}0}=7.5$ cm) was run for several tens of hours. Evolutions of H_{rms} and infragravity mode amplitudes along the flume are plotted in Figure 2 for two different bottom profiles. These (plotted in Figure 2d) correspond to two different stages. One is a transient stage characterized by a bar that travels onshore at about 1 m/h. This profile shows interesting similarity to the rigid bottom profile in the experiments of BALDOCK et al. (2004). The other profile is at equilibrium in the sense that there is no additional change (at plotting precision) over several hours. Note that the barred profile data is more scattered than the equilibrium profile data. The bottom changes between two sets of measurements are not entirely negligible in this case.

The infragravity wave energy is plotted in terms of significant amplitude in Figures 2b-c. The first mode amplitude is maximum

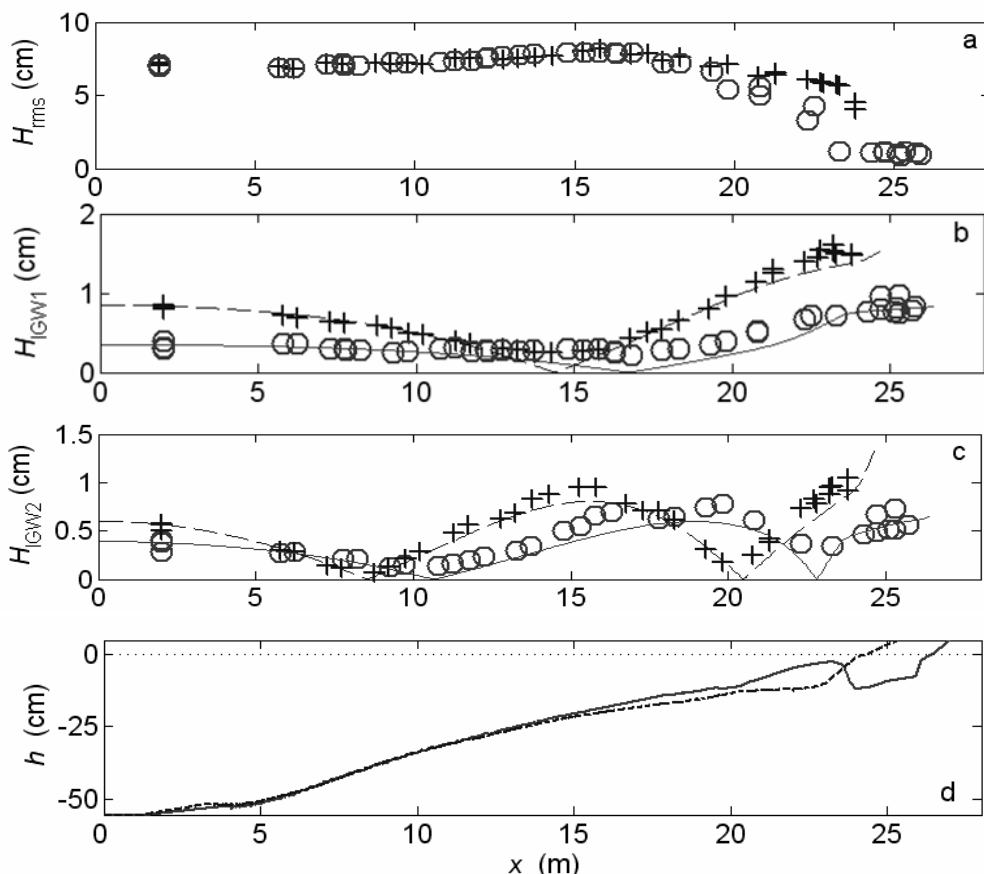


Figure 2. Wave and bottom characteristics along the flume axis for equilibrium profile (+) and transient profile (o): a) root mean square wave height, b) 1st mode infragravity rms wave height, c) 2nd mode infragravity rms wave height and d) equilibrium bottom profile (--) and transient bottom profile (—).

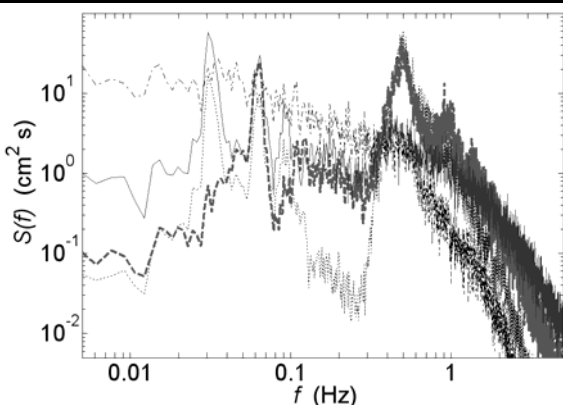


Figure 3. Total wave energy spectra at $x = 2$ m (...), $x = 15.3$ m (---), $x = 23.3$ m (—) and spectrum of the short wave envelope at $x = 2$ m (- -); equilibrium bottom profile.

at the berm, minimum close to $x=15$ m and large again close to the wave maker. This indicates that a low frequency standing wave with a node somewhere around $x=15$ m is generated in the flume. Despite the fact that the equilibrium profile is far from being a plane beach, the Wilson formula for a uninodal seiche in a rectangular flume with a uniform beach reported by DEAN and DALRYMPLE (1984, p.149) gives a very good estimate of f_1 (i.e. 0.03 Hz). In addition, the data was compared with an analytical solution for a small amplitude free standing long wave of the linearized Saint-Venant equations (plotted in Figures 2b-c as a solid line for equilibrium profile and a dashed line for the transient profile). The solution yields with the modes frequencies, the nodal structure and the relative amplitudes as the amplitudes are fitted to the data at $x=2$ m. The overall agreement of the nodal structure is good and the peak frequencies are remarkably well predicted (i.e. $f_1=0.031$ Hz and $f_2=0.063$ Hz for the equilibrium profile and $f_1=0.024$ Hz and $f_2=0.047$ Hz for the transient profile). The infragravity standing waves are always present whatever shape the bottom profiles have.

Our results in the barred case exhibit the same features, in terms of long wave amplitudes and node positions, as the results of BALDOCK et al. (2004). They concluded that a maximum long wave radiation occurs when the mean breakpoint closely coincides with the nodal point for the long wave on the barred beach. In our experiments, the long waves are more energetic on the equilibrium bottom profile for which the breaking point and first mode node position are several meters apart. Experiments performed for other wave conditions show that the long wave structure mainly depends on the beach morphology rather on the generated wave characteristics.

WAVE SPECTRA

Surface elevation energy spectra for the two different topographies are plotted in Figures 3 and 4. They are presented for three positions along the flume that correspond to the deep region, the breaking region and close to shoreline. The location of the breaking region (maximum of H_{rms} in Figure 2a) is close to the node of the first mode (Figure 2b) and the anti-node of the second mode (Figure 2c). The spectra confirm that the energy in the infragravity domain is larger and the peaks more clearly defined in the case of the equilibrium profile. In the case of the transient profile, we may note that the energy in the gravity domain is very

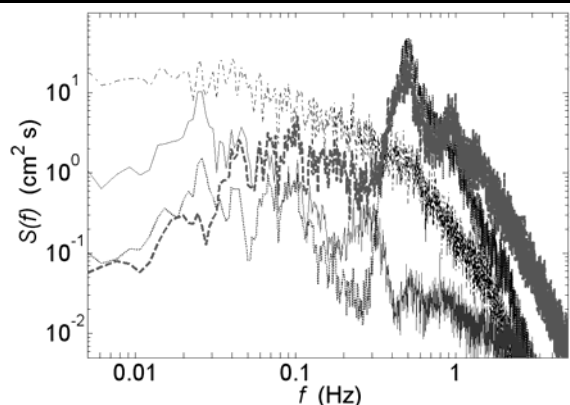


Figure 4. Total wave energy spectra at $x = 2$ m (...), $x = 16.8$ m (---), $x = 25.8$ m (—) and spectrum of the short wave envelope at $x = 2$ m (- -); transient bottom profile.

low close to the shoreline. Indeed, the short waves have dissipated almost all their energy passing the bar, as indicated by the estimate of H_{rms} for $x>23$ m in Figure 2a.

In addition, the spectrum of the short wave envelope, obtained via a Hilbert transform of the measured surface elevation data, is plotted in dashed-dotted line in Figures 3 and 4. This does not account for real energy in surface elevation but as energy possibly contained in the wave packets that could be released in the breaking region. It is important to emphasize that there is no dominant frequency in the wave grouping. This confirms that the frequency peaks of the infragravity waves depend on the beach profile only.

CORRELATION WITH SHORT WAVE ENVELOPE

Figure 5 shows the cross-correlation between the short wave envelope in the constant depth region of the flume ($x=2$ m) and the total low pass filtered surface motion ($f<0.3$ Hz) at $x=2$ m, in the breaking region and close to shoreline. There is a negative correlation for lags close to zero at $x=2$ m. This corresponds to the locally forced incident bound long wave, which is out of phase with the short wave envelope (LONGUET-HIGGINS and STEWART, 1962). The lag is increasing and the correlation becomes stronger further shoreward as the bound wave shoals and represents a larger proportion of the total long wave energy (at $\tau\approx10$ s and $x=15.3$ m). This bound wave is released in the shoaling and breaking and still negatively correlated to the wave envelope at lags $\tau\approx18$ s at $x=2$ m and $\tau\approx20$ s at $x=23.3$ m. On the other hand, a positive correlation is seen for $\tau\approx7$ s at $x=15.3$ m. This corresponds to a dynamic setup generated by the breaking of the wave packets. The correlation becomes very strong at the shoreline ($\tau\approx13$ s). The long wave is reflected and propagates offshore as seen on the correlation signature for $\tau\approx21$ s at $x=15.3$ m and $\tau\approx28$ s at $x=2$ m. At larger lags, both negative and positive correlation peaks are still present but damped. This indicates that the long waves reflect on both ends of the flume but are not amplified. JANSSEN et al. (2003) concluded on a dominant mechanism of bound wave release, in their mild slopes laboratory experiments, while BALDOCK et al. (2004) observed breaking forced waves for stronger slopes. Both mechanisms are clearly observed in our case of an equilibrium beach profile.

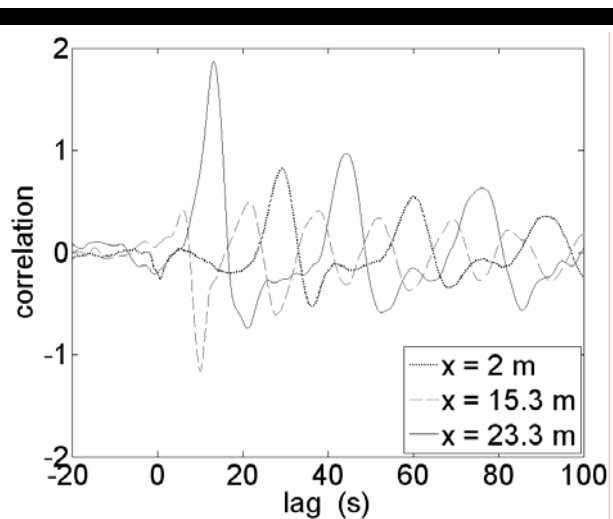


Figure 5. Cross-correlation between the infragravity waves and the short wave envelope at $x=2$ m, equilibrium bottom profile.

To further understand the process, a large wave packet is considered. The first large waves travelling at the phase velocity produce an increase of the setup. The bound long wave propagates slower, at the group velocity. Once released, the free wave propagates at the phase velocity in both directions, onshore and offshore. The time travel of the free long wave from breaking region to shoreline and back is about the same as the one to the wave-maker and back (*i.e.* approximately 16 s). This lowers the mean water level and may enhance the breaking of the short waves at that time and thus maintains the process. This justifies the good agreement between first mode node and second mode anti-node positions (Figures 2b-c) in this very special equilibrium configuration.

For the transient bottom profile, the correlation picture shown in Figure 6 is in marked contrast. The correlation peaks at weaker values compared to the equilibrium case. The bound long wave signature is seen for $\tau \approx 0$ s and $\tau \approx 22$ s in the deep region and for $\tau \approx 12$ s in the breaking region ($x=16.8$ m) but not really at the shoreline ($x=25.8$ m). More clearly the dynamic setup induces a stronger positive correlation for $\tau \approx 8$ s at $x=16.8$ m and $\tau \approx 18$ s at $x=25.8$ m. The break point mechanism is apparently dominant for this topography that is closer to BALDOCK et al. (2004) experiments. We also note that the long wave is partially reflected by the bar and the berm as indicated by the double peak for $\tau \approx 27$ s and $\tau \approx 38$ s at $x=2$ m. This probably leads to the weak correlation for larger time lags ($\tau > 60$ s). Bound wave release and breakpoint forcing do not reinforce the generation of the infragravity waves as for the equilibrium beach profile.

BEGINNING OF THE WAVE SEQUENCE

The significant spectral peaks at the shoreline do not necessarily imply resonant amplification, since the incident short wave groups do not have a dominant frequency (as shown by the short waves envelope spectra in Figures 3 and 4). The generated wave packets are not necessarily in phase with the radiated long waves. In that sense, seiching is not really stationary in the flume. To illustrate this point, the beginning of the wave sequence is plotted in Figure 7. In Figure 7a, the short wave packets in the deep region are visible. They induce a modulation of the mean level close to shoreline. Resulting low frequency motions are shown in

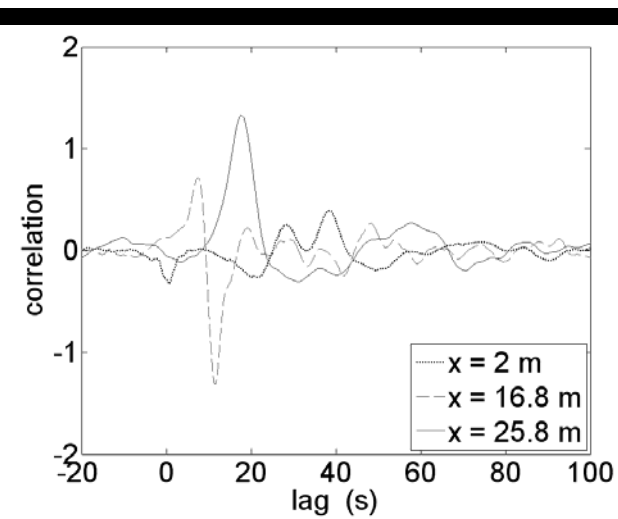


Figure 6. Cross-correlation between the infragravity waves and the short wave envelope at $x=2$ m, transient bottom profile.

Figure 7b. The main period of about 32 s, corresponding to f_l , is sometimes observed. For instance, at $x=23.8$ m, the peak for $\tau \approx 34$ s is enhanced for $\tau \approx 66$ s. In that case, a large wave packet has arrived in the breaking region in phase with the return of the generated long wave. This is not a general feature. The signature of a long wave is generally not seen after a couple of flume travel lengths. The main period of 32 s is not visible in the infragravity wave signal corresponding to the deep region for $\tau > 130$ s in Figure 7b. In that sense, amplification in the long wave generation process is not noted.

CONCLUSIONS

The experiments show that the long wave structure strongly depends on the beach morphology rather than on the generated short wave characteristics. In particular, the infragravity waves are more energetic on the equilibrium bottom profile compared to the transient barred profile. The nodal structure of the infragravity waves is determined by the beach shape that is, mainly the distance between the breaking point and the shoreline.

The correlation between the infragravity waves and the incident short wave envelope indicate that the infragravity waves generation conform to both breaking point and bound long wave release mechanisms.

It is suggested that the beach topography evolves as to reinforce both the bound long wave release and the dynamic setup generation. At equilibrium, the distance between breaking and shoreline is such that the return of the free wave lowers the water level and energizes the breaking of wave packets. These experiments yield new results for a deeper understanding of the link between infragravity waves and beach dynamics.

LITERATURE CITED

- AAGAARD, T. and BRYAN, K.R., 2003. Observations of infragravity wave frequency selection, *Cont. Shelf Res.*, 23, 1019-1034.
- BALDOCK, T.E.; O'HARE, T.J. and HUNTLEY, D.A., 2004. Long wave forcing on a barred beach, *J. Fluid Mech.*, 503, 321-343.
- BALDOCK, T.E. and HUNTLEY, D.A., 2002. Long wave forcing by the breaking of random gravity waves on a beach, *Proc. R. Soc. Lond.*, A 458, 2177-2201.

- CERTAIN, R.; MEULÉ, S.; REY, V. and PINAZO, C., 2005. Wave transformation on a microtidal barred beach (Sète, France), *J. Marine Systems*, 38, 19-34.
- DEAN, R.G. and DALRYMPLE, R.A., 1984. *Water Wave Mechanics for Engineers and Scientists*, World Scientific.
- DETTE, H.H.; LARSON, M.; MURPHY, J.; NEWE, J.; PETERS, K.; RENIERS, A. and STEETZEL, H., 2002. Application of prototype flume tests for beach nourishment. *Coastal Eng.*, 47, 137-177.
- HURTHE, D.; MICHALLET, H. and GONDRA, X., 2007. Turbulent measurements in the surf zone suspension. *Journal of Coastal Research*, SI50.
- JANSSEN, T.T.; BATTJES, J.A. and VAN DONGEREN, A.R., 2003. Observation of long waves induced by short wave groups, *J. Geophys. Res.*, 108, 3252-3264.
- LONGUET-HIGGINS, M.S. and STEWART, R.W., 1962. Radiation stress and mass transport in gravity waves, with application to 'surf-beats', *J. Fluid Mech.*, 13, 481-504.
- MASSELINK, G.; EVANS, D.; HUGHES, M.G. and RUSSEL, P., 2005. Suspended sediment transport in the swash zone of a dissipative beach, *Marine Geol.*, 216, 169-189.
- SYMONDS, G.; HUNTLEY, D.A. and BOWEN, A.J., 1982. Two dimensional surf beat: long wave generation by a time-varying break point, *J. Geophys. Res.*, 87(C1), 492-498.
- WANG, P.; EBERSOLE, B.A.; SMITH, E.R. and JOHNSON, B.D., 2002. Temporal and spatial variations of surf-zone currents and suspended sediment concentration, *Coastal Eng.*, 46, 175-211.

ACKNOWLEDGEMENT

This work has been partially funded by the CNRS-INSU PATOM. The technical support of J.-M. Barnoud is gratefully acknowledged.

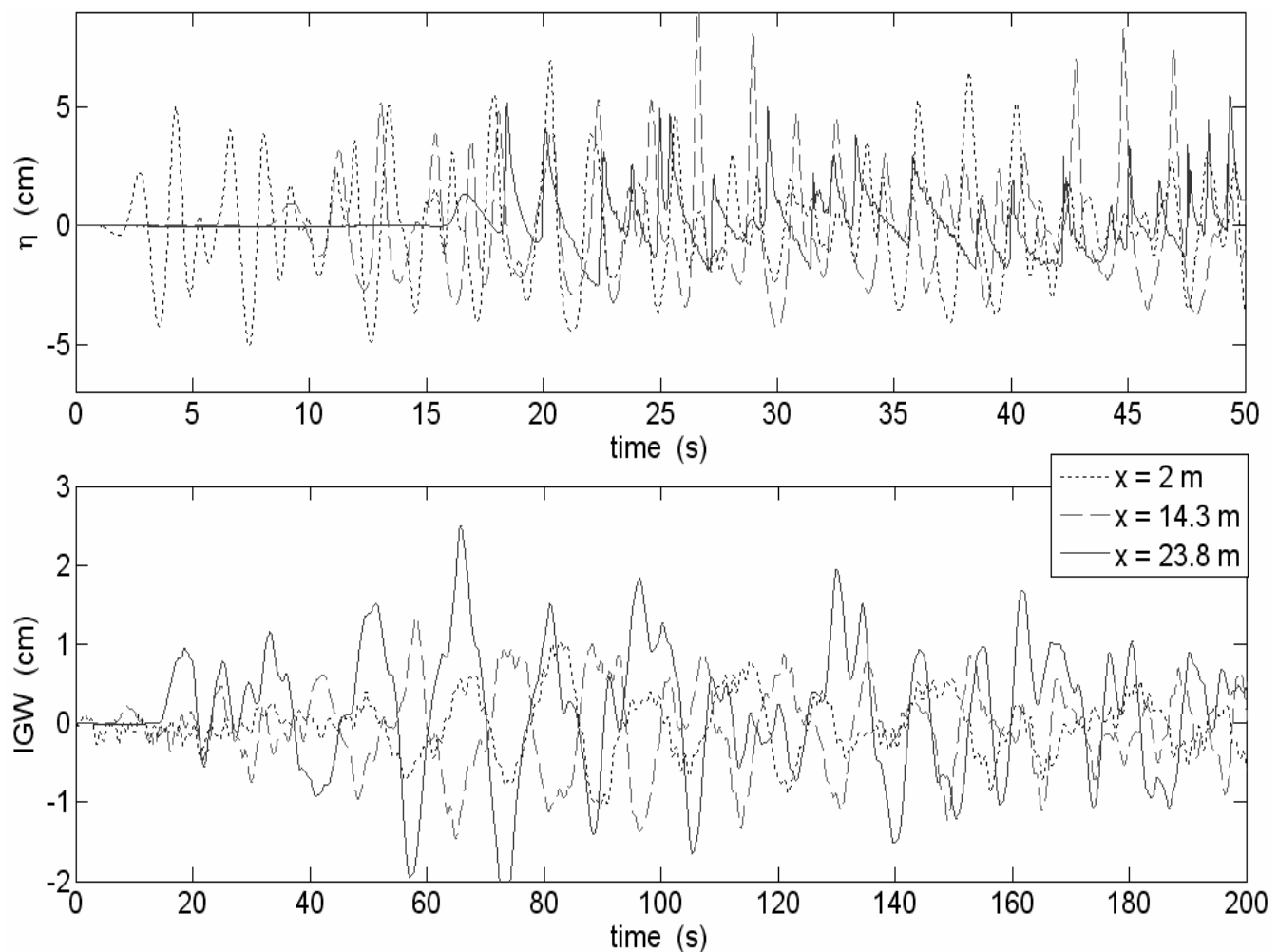


Figure 7. Surface elevations (a) and infragravity waves (b) in the deep, breaking and shoreline regions for the equilibrium bottom profile.

THE LATE HOLOCENE SEDIMENT INFILLING AND BEACH BARRIER DYNAMICS OF THE THAU
LAGOON (GULF OF LIONS, MEDITERRANEAN SEA, SE FRANCE).

Pierre Ferrer¹, Massinissa Benabdellouahed², Raphaël Certain¹, Bernadette Tessier², Jean-Paul Barusseau¹, Frédéric Bouchette³

¹ Université de Perpignan, IMAGES, 52 avenue Paul Alduy, 66860 Perpignan Cedex, France.

² Université de Caen, UMR CNRS 6143 M2C, 24 rue des tilleuls, 14000 Caen, France.

³ Université de Montpellier 2, Géosciences marines, UMR 5573, Laboratoire GTS, cc60, 34095 Montpellier Cedex 05, France.

Abstract

A study combining very high resolution seismic and sediment core data has been carried out on the Thau lagoon (Mediterranean coast, microtidal setting, SE France) in order to understand more clearly the dynamics and Holocene chronology of its closure through the different stages of its filling. One main seismic unit (U2) has been defined into the infill, above the rocky basement (U0) and a composite unit U1 which is interpreted as remnants of Pleistocene fluvial terraces or/and to early marine Holocene deposits. U2 constitutes the main part of the infill, reaching locally 9 m in thickness. U2 is mainly conformable (in the center part of the lagoon) and discordant showing an onlap surface on the substratum close to the edge of the lagoon, consisting in alternate high amplitude and continuous parallel reflectors and low amplitude, poorly continuous ones. It can be divided in two sub-units, U2-1 and U2-2. U2-2 lies paraconformably on U2-1 in the center of the lagoon where the infill is the thickest, while a marked erosional unconformity is observed between U2-1 and U2-2 on topographic highs of the basement and on the seaward edge of the lagoon. 7 elementary sequences have been observed in U2-1 and U2-2.

According to the core data, U2 consists in a series of mud-dominated sequences, with shell fragments dispersed at the base. The vertical distribution of the fauna into U2-1 and U2-2 reveals a lagoonal environment. However in U2-1, marine species are more abundant in the south of the lagoon. ¹⁴C AMS dating provides three ages: ~ 6000 cal y. BP in the lower part of U2-1 on CAL1, ~ 5400 y. BP just above the boundary between U2-1 and U2-2 on CAL4, ~ 3000 cal y. BP in the middle of U2-2 on CAL4.

A scenario to explain the lagoon infill stratigraphy and geometry is proposed. The beginning of the lagoon infill occurred with the initiation of the barrier construction, as soon as the sea-level rise slowed down significantly, i.e. between 7000-6000 BP. Infill began into the back-barrier system, with a high rate of sedimentation for U2-1, according to the radiocarbon data. At 5400 y. BP, the barrier is assumed to be totally closed leading to the deposition of the fully lagoonal U2-2 succession. The unconformity between U2-1 and U2-2 is interpreted as the result of a rapid landward retreat of the barrier. This severe retreat could be related to climate forcing and/or brutal change in sediment discharge driven by the Rhone River which is the main sediment source of the longshore drift. In this scenario, the last sub-unit, U2-2, represents most of the late Holocene infill. In this framework, the repetitive sequences observed in U2-2 through sedimentary and seismic facies, could be related to high frequency climate changes of about 1000-1500 y periodicity according ¹⁴C dates.

REMPISSAGE SEDIMENTAIRE TARDI-HOLOCENE ET DYNAMIQUE DU LIDO DE LA LAGUNE DE THAU (GOLFE DU LION, MER MEDITERRANEE, SE FRANCE).

Résumé

Une étude combinant des données de sismique très haute résolution et de carottes sédimentaires a été menée sur la lagune de Thau (SE France) dans le but de clarifier la dynamique et la chronologie Holocène de sa fermeture grâce au remplissage sédimentaire. Une unité sédimentaire principale (U2) a été définie dans le remplissage de la lagune qui repose sur le substratum rocheux (U0) et sur une unité composite U1 qui correspond à des remaniements de terrasses fluviatiles Pléistocène et/ou à des dépôts marin pré-Holocène. L'unité U2 constitue la majeure partie du remplissage sédimentaire pouvant atteindre une épaisseur de 9 m. U2 repose principalement en concordance au centre de la lagune et en discordance présentant une surface en onlap sur le substratum en bordure de la lagune. Elle consiste en une alternance de réflecteurs parallèles continus de haute amplitude et de réflecteurs peu continus de faible amplitude. Cette unité peut être divisée en deux sous-unités U2-1 et U2-2. U2-2 repose en concordance sur U2-1 au centre de la lagune où le remplissage sédimentaire est maximal pendant qu'une discordance est marquée entre ces deux sous-unités sur les remontées du substratum et sur la bordure orientale de la lagune. 7 séquences élémentaires ont été décrites dans U2-1 et U2-2.

D'après l'interprétation des données sédimentologiques des carottes, U2 est constituée de séries à dominante argileuse avec des fragments de coquilles à sa base. La distribution verticale de la faune dans U2-1 et U2-2 révèle un environnement de dépôt lagunaire. Cependant, dans U2-1, des espèces marines sont plus abondantes dans la partie sud de la lagune. Des datations AMS au ^{14}C ont été réalisées et trois âges ont été obtenus : ~ 6000 cal ans BP dans la partie inférieure de U2-1, ~ 5400 ans BP juste au dessus de la limite entre U2-1 and U2-2, ~ 3000 cal ans BP au milieu de U2-2.

Un scénario est proposé afin d'expliquer la stratigraphie et la géométrie du remplissage sédimentaire. Le début du remplissage sédimentaire a commencé avec l'initiation de la construction du lido dès que le niveau marin s'est stabilisé, i.e. 7-6000 ans BP. Le remplissage commença dans la lagune par un dépôt rapide de U2-1 suite aux datations. A 5400 ans BP, la lagune est totalement isolée par le lido, permettant le dépôt de U2-2. La discordance entre U2-1 et U2-2 est interprétée comme le résultat d'une migration rapide du lido vers le continent. Ce recul brutal peut être relié aux variations climatiques et/ou à un changement brutal des apports sédimentaires du Rhône, principale source sédimentaire alimentant la dérive littorale. Dans ce scénario, la sous-unité U2-2 représente la majeure partie du remplissage tardi-Holocène. Dans cette idée, les séquences répétitives, observées dans U2-2 à travers les faciès sismiques et sédimentaires, peuvent être corrélées à des changements climatiques de haute fréquence avec une périodicité comprise entre 1000 et 1500 ans en accord avec les datations ^{14}C .

1. Introduction

Along wave-dominated coastal systems, as soon as coastal barriers begin to be created, lagoons could isolate progressively [Zecchin *et al.*, 2008]. These lagoons can be considered as closed or partially closed wave-dominated estuaries [Reinson, 1992] described by Dalrymple *et al.* [1992]. Lagoonal systems are appropriate fields to understand the influence of the sea-level rise [Sorrel *et al.*, 2009], sediment availability FitzGerald *et al.*, 2000, hydrodynamic forcing and the inherited bedrock morphology [Bertin *et al.*, 2004] on coastal sediment body construction [Ricci-Lucchi *et al.*, 2006, Allard *et al.*, 2009]. We proposed here to study the different stages of the barrier construction and evolution by analyzing the sedimentary record preserved into the lagoon.

In the Gulf of Lions, where the Languedoc-Roussillon coast is characterized by many coastal lagoons, the Holocene evolution has been controlled by a rapid sea-level rise reaching

10.6 mm/year before 7000 years B.P. [Aloisi *et al.*, 1978], followed by a much slower rise, i.e. 1 mm/year [Vella and Provansal, 2000]. Each lagoon is separated from the sea by an emerged beach barrier which is the result of the combined activity of waves and currents, longshore littoral drift, transport and sand accumulation [Barusseau *et al.*, 1996; Certain *et al.*, 2005b]. As is generally the case, lagoonal sediments are characterized by mixed silty clay and organic matter, locally interbedded with marine sand layers (wash-over fans) preserved close to the sand barrier [Hesp and Short, 1999]. The accumulation rates are relatively high, about 2.5 mm/year in the Thau lagoon on the last century timescale [Schmidt *et al.*, 2007], up to 4 mm/year in the Pierre Blanche lagoon located East to the Thau lagoon [Sabatier *et al.*, 2008]. The Languedoc-Roussillon lagoons have been the subject of various studies such as life conditions and shellfish production [Gangnery *et al.*, 2001, Soletchnik *et al.*, 2002], biogeochemistry and heavy metal distribution or pollution [Schmidt *et al.*, 2007]. Geological studies focused mainly on the sedimentary infill and the paleogeographical evolution [Certain *et al.*, 2004, Tesson *et al.*, 2005]. In other Mediterranean areas, stratigraphic and paleontological approaches have revealed that sedimentary sequences contained in the lagoon infill are correlated with Holocene climate changes [Massari *et al.*, 2004, Ricci-Lucchi *et al.*, 2006]. Some studies focused specifically on lagoon closure in relation to sand spit evolution [Simeoni *et al.*, 2007], and more generally on the evolution of adjacent systems such as alluvial plain [Amorosi *et al.*, 2004], delta [Bellotti *et al.*, 1994] and embayment [Suursaar *et al.*, 2008].

The aim of the present work, based on a combination of new data of very high resolution seismic, sediment core and radiocarbon data, is to reconstruct the history of the sedimentary infill of the Thau lagoon in order to define the role of factors that have controlled the sand barrier dynamics and associated closure of the lagoon. This study shows the influence of the Rhône river on the sandy barrier dynamics along the Languedoc-Roussillon coast in adding to other similar works performed on other regional lagoons [Planchais *et al.*, 1984, Canet-St Nazaire lagoon; Certain *et al.*, 2004, Leucate lagoon; Raynal *et al.*, this volume; Sabatier *et al.*, submitted, Palavasian lagoons]. This allows comparing regional responses and thus deciphering the role of global from specifically local factors.

2. The study area

The study area is the Thau lagoon, located on the French Mediterranean coast (fig. 1) and more precisely in the gulf of Lion where the general hydrodynamic circulation on the continental shelf is westward [Millot, 1990]. This circulation shows the sedimentary influence of the rivers located eastward like the Rhône [Ulses *et al.*, 2008], nowadays essentially for the fine sediments. This littoral is under the influence of a westward longshore drift during the Holocene [Akouango, 1997, Raynal, 2008]. The Thau lagoon is the largest lagoon along the Languedoc-Roussillon coast. It covers an area of 75 km² with a maximum length of 19 km and maximum width of 1.3 km. The average water depth is 4 m; 35 % of the lagoon have more than 5.5 m depth of water, with a local maximum of 10 m.

The lagoon catchment area (280 km²) consists of Jurassic karstified limestones and Miocene and Eocene marly limestones (fig. 1). It is limited by the Quaternary volcanic mountain of Agde in the south, the Upper Jurassic limestone of the Moure Mountains in the west, and the Jurassic (Callovian and Sequanian) limestone of the Gardiole Mountains in the north. Along the northern coast of the lagoon, Pliocene lacustrine limestone outcrops are found. Between the Quaternary volcanic mountain and the Moure Mountains, the alluvial plain of the Hérault river is constituted by quaternary marls. The catchment is drained by small intermittent rivers characterised by a long dry period between May and September, and flush flash floods during the wet season in autumn. All the rivers are located in the Moure

Mountains. The hydrological regime is dominated by two main rivers, the Vène River (67 km²), fed by karstic springs, and the Pallas River (52 km²).

Previous works on the Thau lagoon sediment infilling performed by Chassefière [1968] have shown that during the Early Holocene transgression, the lagoon area formed a wide embayment. During the transgression, small shelly shoals formed in the embayment before the definitive closure by the beach barrier. These shoals were then isolated to form the “cadoules”, a local name that designates mounds (circular bioherms and/or shelly shoal), a few hundred metres in diameter, scattered in the northern part of the lagoon [Chassefière, 1968]. Today, the lagoon is connected to the sea by three inlets. Two of them, the Pissoyaumes and Quilles inlets, crossing through the sandy barrier (fig. 1), are almost closed. The main connection is provided by an artificial inlet, the Sète harbour inlet. No active washover dynamics occurs at present, although the sandy barrier is subject to severe erosion on its marine edge in the northern part, near Sete [Certain *et al.*, 2005b].

The prevailing winds blow from the north-west (the Tramontane wind, 23%) and west (18%) [Certain, 2002; Certain *et al.*, 2005a]. The hydrodynamic circulation in the Thau lagoon is not well known but modelling under different wind conditions shows vortex occurrence around the oyster beds [Millet, 1989]. In the northern part of the lagoon, the Vise spring, close to Balaruc, surges after a complex circulation within the Jurassic karst [Aquilina *et al.*, 2003; Pinault *et al.*, 2004]. Most sea waves in the area have mean significant height (H_s) < 2 m, 30% of the values being < 1 m, predominantly in summer. The directions are 140–220°N associated with sea breeze. Only 2% of waves have H_s > 4 m with periods from 5 to 10 s and a SE to E direction. These storms typically last only 24 h. Tidal range does not exceed 0.30 cm [Akouango, 1997 and S.H.O.M., 2003]. Nevertheless, higher water level variations are observed in response to set-ups and set-downs under the influence of wind and atmospheric pressure fluctuations. In extreme cases, set-ups can reach 0.50 m in the shoaling zone during storms [Akouango, 1997] and 1 m on the beach under the action of breaking waves [Certain, 2002]. The Thau lagoon is an important shellfish breeding area [Soletchnik *et al.*, 2002] leading to a strong biological production. About 15,000 tons of oysters per year are produced in the lagoon, i.e. roughly 10% of the French total production [Gangnery *et al.*, 2001].

3. Methods

The seismic device used for the study is a boomer IKB-Seistec, specifically conceived for shallow water investigations [Simpkin and Davis, 1993]. It is characterized by a line-in-cone receiver located close to the boomer plate (70 cm). Its frequency band is 1–10 kHz. During the survey, performed in June 2003 on board of a small open boat (5 m), a SIG Energos power supply was used with a power of 100 J and a shooting rate of 2 shots/s. The seismic data and DGPS positioning were simultaneously recorded on a PC with Delph-Erics. Post-survey processing was made by using Delph-Erics and Seismic Unix software, including frequency bandpass filtering, trace stacking, and swell filtering when necessary. The available seismic data almost cover the total area of the Thau lagoon. 46 profiles were shot, representing a total length of 57 km [Benabdellouahed, 2005]. The profiles are oriented both longshore (NE-SW) and cross-shore (NW-SE) (fig. 1).

In order to ground-truth part of the seismic data, four gravity cores, from 1 to 2 m long, have been collected in the Thau lagoon during the CALAMAR2 campaign in November 2005 (fig. 1). The cores were simply analysed for sedimentary facies interpretation and macrofauna determination. In addition, three samples (organic matter in bulk sediment) were collected along the cores for radiocarbon dating (performed by Beta Analytics). Ages have been calibrated using IntCal04 [Reimer *et al.*, 2004].

4. Results

Seismic units

The seismic profiles have been analyzed on the basis of the conventional principles of seismic stratigraphy [Mitchum *et al.*, 1977]. Above the substrate (named U0) two main seismic units, named U1 and U2, have been recognized in the sedimentary infilling according to their geometry, upper and lower boundaries (onlap, toplap, downlap, conformable and unconformable) and acoustic facies (amplitude, continuity, frequency and configuration of the internal reflectors). Seven acoustic facies have been distinguished. Their characteristics are listed in the Table I. Since the infill is mainly made of soft muds, a P-wave velocity of 1600 m/s was chosen for time-to-depth conversion [Hamilton, 1972, Billeaud *et al.*, 2005].

The unit U0 (fig. 2) represents the rocky substrate and its upper boundary, a truncated surface, corresponds to the bottom of the lagoon basin. Depending on the substrate nature, acoustic facies in U0 are variable but they mainly show a parallel configuration, the dip of which (SE) conforms to the regional geological strata of the bedrock [Denizot *et al.*, 1967; Barrière et Berger, 1978; Berger *et al.*, 1981].

The unit U1 rests on U0 (fig. 2). Its lower limit is in angular unconformity. Its upper limit is conformable. Its general shape almost mimics the underlying bedrock morphology. U1 has a maximum thickness of about 5 m. U1 is not present everywhere. It is characterized by a transparent facies (T1) sometimes masked by gas (C) showing a chaotic facies [e.g. Garcia-Gil *et al.*, 2002, Bertin and Chaumillon, 2005]. It disappears toward the inner edge of the lagoon and locally on the substrate highs (fig. 2, 4, 7). On the barrier edge, the seismic interpretation is more difficult and does not allow concluding on the presence of U1.

The unit U2 is the main unit of the lagoon sedimentary infill (fig. 2). It is present everywhere. It rests on U1 or directly on U0 (fig. 3). It is conformable on U1 or on onlap on the U0. It comprises two major acoustic facies: P2 and P3 associated to minor acoustic facies (S1, S2 and C) and shows an overall aggradational configuration in the center of the lagoon. The thickness of U2 varies from 1.5 to 9 m. On the basis of acoustic facies and internal surface geometry, U2 can be divided into two sub-units, named U2-1 and U2-2. In most of the lagoon, the boundary between U2-1 and U2-2 is a conformable surface. However, on the seaward edge of the lagoon, the basal surface of U2-2 corresponds to a geometric onlap surface or, close to the sandy barrier, a downlap surface (fig. 6).

U2-1, 0 to 4.5 m thick, shows parallel configuration reflectors and generally a lower amplitude facies than U2-2. In the north of the lagoon, U2-1 displays higher amplitude reflectors than in the south. Locally on some substrate highs, U2-1 displays oblique reflectors and numerous acoustic hyperboles, indicating probably very coarse materiel (fig. 2). On the basis of internal reflector characteristics, U2-1 can be subdivided into three elementary acoustic sequences (named s1, s2, s3) made of a succession of low amplitude/low continuity reflectors and high continuity/high amplitude reflectors (fig. 2). The elementary sequences of U2-1 present an aggradational configuration (conformable surface) in the center part of the lagoon and geometric onlap surfaces (fig. 3A) on the substratum (discordant surface) northwestward and in front of the substrate highs on U1 (tabl. II). U2-2 is 1.5 to 4.5 m thick. On the basis of the same facies variations than those defined in U2-1, U2-2 comprises four elementary acoustic sequences, from s4 to s7. The limits between these elementary sequences are draping surfaces. Each seismic reflector of the elementary sequence describes geometric

onlap surfaces on the substratum close to the lagoonal edges. However, around substrate highs, the top of s5, characterized by oblique to sigmoid reflectors, is locally truncated (toplal surface) by s6 (fig. 3B, tabl. II). Close to the sandy barrier, the aggradational sequences of U2-2 display a body with sigmoid configuration with downlap surface on the limit of U2-1/U2-2 (fig. 7).

In the northern part of the lagoon, the sedimentary infilling cannot be clearly divided into seismic units and subunits. Acoustic facies are mostly made of wavy parallel reflectors defining more or less regularly spaced mounds (tabl. I), corresponding to the so-called “Cadoules” defined by Chassefière [1968]. The origin of these bodies, which is still a matter of debate (bioherm development or hydrothermal circulation?) will not be discussed in the present paper.

Acoustic masks appear on most of the profiles. On the landward edges of the lagoon, acoustic mask is due to the presence of dense grass (or seaweed?) beds. In the center of the lagoon, acoustic masks correspond to thick sedimentary infilling and are interpreted to be due to the presence of gas (biomethane) generated by the degradation of the organic matter contained in the lagoonal deposits.

In addition to the detailed analysis of the lagoon infill, seismic data allowed us to reconstruct a bathymetric map of the lagoon, the isopach map of the infill, and an isohyps map of the rocky substrate top (fig. 5). The deepest part of the lagoon is in the centre (fig. 5a) with a water depth close to 12 m. The top of the substrate (fig. 5b) is characterized by two heights in the north of the lagoon, and one height in the south. In the centre of the lagoon, a paleovalley is evidenced, reaching up to 22 m deep. The sedimentary infill is the thickest in the palaeovalley, close to 12 m (fig. 5c).

Sedimentological data and chronology

In order to determine the lithology and the age of the different seismic units, four cores, 1 to 2 m long (fig. 6), have been collected in the lagoon - three along the northern (inland) edge and one close to the barrier (fig. 1). The cores allow imaging mainly U2-2, the base of CAL1 reaching however U2-1 (fig. 4). They demonstrate that the main lagoon infill unit, U2, is essentially made of clay-rich muds. Fine sand layers appear in the core CAL2, collected close to the sandy barrier (fig. 4). In all cores, shell-rich intervals alternate with organic clay-rich intervals containing few shell debris (fig. 6). This alternation of sedimentary facies seems to fit the seismic facies alternation that allows defining elementary seismic sequences in U2-1 and U2-2. In CAL2 core, fine sand layers are intercalated in the clay-rich succession (fig. 6) at the proximity of the beach barrier.

Two macrofauna assemblages are present in the core CAL4: a marine assemblage, dominated by *Bittium reticulatum* (gastropod), and a lagoonal assemblage, with *Hydrobia ulvae* (gastropod) as the dominant species [Sabatier *et al.*, 2008]. The lagoonal assemblage is prevalent all along the cores but at the base of CAL4, located in the south part of the lagoon and reaching the base of U2-2, the marine assemblage is dominant.

Three radiocarbon ages have been obtained along the cores. At the base of CAL1, the sample D1, located in the basal part of U2-1 (in the seismic elementary sequence s2), provides an age of 6290-6010 cal. y BP. (fig. 6). In the CAL4 core, the sample D2, located at the limit between U2-1 and U2-2, provides an age of 5600-5320 cal. y BP. D3, located in the middle of U2-2 (at the limit between s5 and s6), gives an age of 3230-2850 cal. y BP.

5. Interpretation of seismic and core data

Seismic data collected into the Thau lagoon allow two main stages of construction to be distinguished: 1) the first stage is marked by the basal draping unit U1. U1 rests on the substratum (U0) and smoothes the irregularities of the latter; 2) the second stage is materialized by a fine-grained, aggradational unit (U2), constituting the sedimentary infill.

The substratum U0 of the lagoon is mainly Pliocene in age according to the available data on the regional geology [Denizot *et al.*, 1967; Barrière et Berger, 1978; Berger *et al.*, 1981; Tessier *et al.*, 2000; Tesson *et al.*, 2005; Raynal *et al.*, this volume], and the strata dip angle observed on the seismic profiles. Its very irregular top is the result of incision that occurred during the successive Pleistocene sea-level drops (fig. 8A).

No radiocarbon age and sedimentological data are available in the “draping” unit U1, and thus its origin and depositional chronology remain speculative. According to its transparent acoustic facies, geometry and location, U1 must be considered as a composite unit, constituted mainly by continental weathered formations originating from the underlying substrate or by coarse sediments corresponding to remnants of Pleistocene fluvial terraces [Zecchin *et al.*, 2009] topping substratum highs (fig. 8A). These formations could have been reworked during the transgression. In the troughs, the transparent acoustic facies of U1 could correspond locally with a transgressive sand sheet [e.g. Cattaneo and Steel, 2003]. Sand layers have been cored in the bottom of others lagoons along the Gulf of Lions coastal zone [Raynal *et al.*, this volume; Martin *et al.*, 1981]. They have been interpreted as shoreface sands that were deposited during the first stage of the transgression, prior to the forthcoming closure of the lagoons (fig. 8B, C) which prevent marine hydrodynamic processes on the deposits. This configuration could explain that no wave-cut surface is observed in the languedocien lagoons [Raynal *et al.*, this volume; Martin *et al.*, 1981]. Locally, some substrate highs could have been reworked under wave induced by wind forcing into the lagoon (fig. 3B).

The main part of the lagoon sedimentary infill is clearly identified on the seismic data. It corresponds to the unit U2. The aggradational character of U2 (in the center part of the lagoon) and the nicely draping reflector configuration (geometric onlap surface on the edge of the lagoon), evoke an infilling with a constant sea-level close to nowadays. It indicates a globally low energy lagoonal depositional environment using the sedimentological data which could show some similarities with estuaries (Reinson, 1992). This means that U2 represented the infill of the area as soon as a barrier started to be created, isolating the lagoon. The elementary sequences can be interpreted as a change in sedimentation linked to a stop in the sedimentation or a high productivity shells period [Sabatier *et al.*, in press]. However the geometric onlap shows a sedimentary infill made by compensation during a constant sea-level closed to the actual. Radiocarbon dating clearly indicates that U2 is Holocene in age and more precisely post-6500 cal. y BP.

According to the internal surfaces into U2, two sub-units are distinguished (U2-1, U2-2). More transparent seismic facies demonstrate that energy was higher during U2-1 deposition in the south than in the north. Moreover, macrofauna analysis indicates more marine influence in the south. Thus it is assumed that the sandy barrier already existed and was rapidly formed at the time of U2-1 deposition in an offshore location, since U2-1 is preserved below the present beach barrier (fig. 4B) and is identified with cores on the shoreface [Akouango, 1997; Tessier *et al.*, 2000]. The lagoon was still largely open in the south through wide inlets. This partial closure allows the fast deposition of U2-1 up to 5600-5320 cal y. BP (fig. 8D).

An important change occurred between the deposition of U2-1 and U2-2 sub-units. On the seismic data, U2-2 clearly shows in the seaward edge of the lagoon, landward dipping strata interpreted as washover fans. No washover fans have been observed in U2-1. Similar geometries have been recently imaged in a gravel barrier [Bennett *et al.*, 2009]. This configuration of U2-2 indicates that an important landward migration of the sandy barrier occurred after the deposition of U2-1 (fig. 8E). If the migration of the barrier and past washover fans are observed on the seismic data, no active washover fans exist today maybe due to the large size of the barrier in contrast to the barrier of palavasian lagoons [Sabatier *et al.*, 2008].

Around 5600-5320 cal y. BP. U2-2 deposited unconformably on U2-1 in the central part of the lagoon, testifying a continuity in the infilling. As described previously, in the thickest aggradational part of the infill, U2-1 and U2-2 comprise elementary seismic sequences, 0.5 to 1 m in thickness. We believe that the shell-rich interval that forms the base of each sequence, reflects a period of high vitality of lagoonal fauna that could result from marine incursion in the lagoon or high development periods of lagoonal species.

The age of 5600-5320 cal y. BP. for the U2-1/U2-2 boundary indicates an average sedimentation rate for U2-2 of 0.37 mm/y at the scale of the late Holocene. Based on this sedimentation rate, the time of deposition of the elementary sequences comprised in U2-2, varies from about 1080 to 1620 years. In addition, the datation at the limit of s5 and s6, 3230-2850 cal. y BP, is in accord to this mean sedimentation rate. However these values are only indicative of a mean depositional rate, covering up disparities between the different sequences.

6. Discussion

The different data and results obtained on the Thau lagoon allow discussion of the main factors that have controlled its sedimentary infilling, such as the basement morphology, sediment supply and climate variations.

The inherited bedrock morphology

The substrate was deeply carved before and during the last glacial maximum regression, acting as sediment traps for early to mid-Holocene deposits in the incised valleys of the inner shelf [Tesson *et al.*, 2005] and in some sheltered areas in the lagoon (i.e. CAL 1 core). This substrate is supposed to be Pliocene. The reflector dip of the substrate is coherent with the Pliocene outcrops dip onshore and, in the western part, Pliocene passes through the bank from the emerged domain to the lagoon. Such a pattern is found in other Languedocian lagoons as the Vic lagoon [Raynal *et al.*, this volume] where the sedimentary infill tops the underlying Pliocene strata. On the shoreface, such deposits were reworked between 7530 and 6000 y BP [Barusseau *et al.*, 1996; Akouango, 1997].

In the Thau lagoon area, the unit U1 covering the Pliocene substratum, formed before this episode and then reworked, was however insufficient to erase the inherited bedrock morphology. Consequently the maximum thickness of the sedimentary infill is found in the trough, located between the two topographic highs of the substrate (fig. 5b). At the beginning of the deposition of U2-1, the lagoon was quickly isolated from the sea by a south-westward oriented sand spit, which constitutes today the barrier, using the Saint-Clair mount as an anchor point [Fitzgerald *et al.*, 2000]. The position of the outcrops of the Saint-Clair mount and Agde volcanic mount have some consequences on the position of the barrier. Some authors have demonstrated that the bedrock has an influence on the dynamic of the barrier [Belknap and Kraft, 1985; Riggs *et al.*, 1995; Heap and Krantz, 1997; Fitzgerald *et al.*, 2000;

Browder and McNinch, 2006; Burningham, 2008]. The link between the dynamic of the barrier and the underlying inherited bedrock will be discussed in a future work about the continuum from the onshore outcrops to the inner shelf.

The incident local wave conditions are under the influence of the inherited bedrock. Hydrodynamics is one of the control factors of the dynamic of the barrier [Cooper, 2001; Bertin *et al.*, 2004; Regnault *et al.*, 2004]. Here, the barrier closes the bay quickly isolating the lagoon from the marine hydrodynamical control. So there is no evidence of the inherited bedrock control on the marine hydrodynamics in the sediment record of the lagoon. However, the lagoon is under the influence of local hydrodynamical control induced by offshore winds. This control can explain the erosion surface around the substrate highs which exercise a local control factor considering its low depth.

Sediment supply

Thanks to a general westward littoral drift, the Rhône delta, located at about 100 km to the east of the Thau lagoon, is the main provider of sediment, since the late Holocene, to the shoreface and adjacent coastal zones in the northern part of the Gulf of Lions. Relative sea-level rise and fluvial sediment discharge are assumed to be the main controlling factors of the delta evolution [L'Homer *et al.*, 1981; Oomkens, 1970; Pons *et al.*, 1979; Provansal *et al.*, 2003]. The edification of the Rhône delta started in 7200 y. BP using the Saint Ferréol channel located in the central western part of the present-day deltaic system. Between 7200 and 6000 y. BP, a first deltaic lobe developed thanks to large sediment supply. Without this sediment supply source, the construction of the barrier could not start. However, the relative sea level rise is often proposed as the responsible factor of a barrier construction [Hesp and short, 1999, Davis and FitzGerald, 2004]. The early construction of the sandy barrier of the Thau lagoon could be linked to this first stage of construction of the Rhône delta. The relationship between a sediment source and a barrier has been demonstrated on the Atlantic coast [Chaumillon and Weber, 2006, Fitzgerald *et al.*, 2000 and 2005], in Mediterranean Sea [Certain *et al.*, 2005] and in Africa [Anthony *et al.*, 1999]. The construction of the western lobe of the delta occurred between 6000 and 5350 y. BP, corresponding to the main construction of the Thau sandy barrier and the coeval deposition of U2-1. Shortly after, the delta plain developed a multilobate shape and the construction of the Ulmet lobe in the east of the delta started [L'Homer, 1975]. According to Vella *et al.* [2005], this phase could have been initiated as soon as 5780 ± 40 y. BP. From that time, the sediment supply in the western part of the delta decreased drastically. As a consequence, sandy barriers located to the west of the delta, including the Thau lagoon barrier, probably started to retreat rapidly because of low sediment supply. From the period during which the retreat occurred, U2-2 started its deposition in the lagoon and continuing until the present day.

Climate variations

Around 6000 y. BP, the sea had almost reached its present-day level [Labeyrie *et al.*, 1976; Aloïsi *et al.*, 1978; Dubar and Anthony, 1995]. From that time of sea-level highstand or very slow sea-level rise, climate fluctuations appear to be major forcing factors of coastal geomorphology evolution [Dabrio *et al.*, 2000, Zazo *et al.*, 2008, Allard *et al.*, 2009]. North-Atlantic millennial-scale climate-change signal, including Dansgaard/Oeschger oscillations, Heinrich events and Bond cycles are generally evoked to describe these fluctuations, and generated numerous cyclic rapid climate changes (RCC) [Bond *et al.*, 1997; deMenocal *et al.*, 2000; Zic *et al.*, 2002; Timmermann *et al.*, 2003; Mayewski *et al.*, 2004; Debret *et al.*, 2007]. In the Mediterranean area, along the southern coasts of Spain, Zazo *et al.* [2008] demonstrated how changes in coastal morphology evolution have been controlled by centennial climate crisis occurring, with a millennial periodicity in relation to the Bond

events. Two major RCC are generally mentioned, one at 6000-5000 cal. y. BP, a second at 3500-2500 cal. y. BP; two minor RCC appear at 4200-3800 cal. y. BP, another at 1200-1000 cal. y. BP. Prokopenko *et al.* [2001] showed how Heinrich events and Bond cycles entailed also strong changes in atmospheric precipitation regime far from the North Atlantic. This explanation might be valuable also in the case of the Gulf of Lions coastal zone. The 6000-5000 cal. y. BP RCC is coeval with the first main Rhone avulsion, which is assumed to have an impact on the sandy barrier construction and migration rate. In the absence of an accurate chronological control, it is however not possible to discuss further about the potential impact of late Holocene climatic fluctuations on the Thau lagoon infilling and associated barrier evolution. However, it is worth noting that the lagoon infill has lasted about 6500 years, and is composed of 7 elementary sequences. Hence, these sequences have a millennial time-scale fitting that of late Holocene climate changes as observed in other preserved environments [Amorosi *et al.*, 2005, Billeaud *et al.*, 2007, Sorrel *et al.*, 2009]. A future work will develop this topic.

Conclusion

The present study highlights the Holocene sedimentary infilling of the Thau lagoon, the largest lagoon of the Languedoc-Roussillon coast (SE France). The infilling is made up of one main sedimentary unit composed principally of lagoonal muds. This unit rests on a relatively thin basal formation that represents the first stage of the lagoon infilling above the eroded rocky basement. The nature of these basal deposits is unknown. We believe they correspond to remnants of Pleistocene terraces or (and) early Holocene sand sheets that were laid down during the first stages of the transgression. In the main sedimentary unit, the deposition of which began around 6500 y. BP, two major construction steps have been distinguished: (1) around 6500 y. BP, the barrier is partly developed and the lagoon is semi-enclosed. The large amount of sediments delivered at that time by the Rhone River and the relative sea level rise are believed to have started the construction of the barrier. A first step of lagoon infilling occurred; (2) from 5400 y. BP, a new stage of infill began. The lagoon is believed to be totally closed, but the barrier has retreated severely, probably in response to a decrease in sediment supplied by the Rhone river, the main deltaic lobe of which has shifted eastward. These major steps are directly related to the evolution of the sandy barrier that has isolated the lagoon.

Our study points out finally that three main factors have controlled the evolution of the Thau lagoon area (1) the diminution of the relative sea level rise is responsible of the major barrier construction during this period (2) the bedrock morphology that controls directly the local hydrodynamic, the infill thickness and the location of the lagoon depocentres. In addition, bedrock highs into the lagoon have induced differentiated infill geometries. Also, changes in bedrock dip and altitude are assumed to have favoured the settlement of the sandy barrier that led to the lagoon formation; (3) sediment supply that controls the barrier development and dynamics. Sediment is provided in the area by the Rhone Delta. We believe that the lagoon sedimentary infill had recorded the first steps of the delta construction during the late Holocene, since these steps have a direct impact on the sandy barrier behaviour. The causes of these major stages are probably related to climate changes. However, our data does not allow us to reach a firm conclusion that climate fluctuations, such as the late Holocene millennial climate cycles, are recorded in the lagoonal mud succession.

References

- AKOUANGO E. (1997). - Morphodynamique et dynamique sédimentaire dans le golfe du Lion. Contribution à l'étude de la zone côtière dans l'Actuel et le Quaternaire récent. - *Unpublished PhD thesis*, Université de Perpignan, 191 p.
- ALLARD J., CHAUMILLON E. & FÉNIÈS H. (2009). - A synthesis of morphological evolutions and Holocene stratigraphy of a wave-dominated estuary: The Arcachon lagoon, SW France. - *Continental Shelf Research*, **29**, 8, 957-969.
- ALOÏSI J., MONACO A., PLANCHAS N., THOMMERET J. & THOMMERET Y. (1978). - The Holocene 282 transgression in the Golfe du Lion, southeastern France: paleogeographic and paleobotanical evolution. - *Geogr. Phys. Quat.*, **15**, 145-162.
- AMOROSI A., CENTINEO M.C., COLALONGO M.L. & FIORINI F. (2005). - Millennial-scale depositional cycles from the Holocene of the Po Plain, Italy. - *Marine Geology*, **222-223**, 7-18.
- AMOROSI A., COLALONGO M.L., FIORINI F., FUSCO F., PASINI G., VAIANI S.C. & SARTI, G. (2004). - Palaeogeographic and palaeoclimatic evolution of the Po Plain from 150-ky core records. - *Global and Planetary Change*, **40**, 1-2, 55-78.
- ANTHONY E.J. & BLIVI A.B. (1999). - Morphosedimentary evolution of a delta-sourced, drift-aligned sand barrier-lagoon complex, western Bight of Benin. - *Marine Geology*, **158**, 1-4, 161-176.
- AQUILINA L., LADOUCHE B., DOERFLIGER N. & BAKALOWICZ M. (2003). - Deep water circulation, residence time, and chemistry in a karst complex, *Ground Water*, **41**, 790-805.
- BARD E., HAMELIN B., FAIRBANKS R.G. & ZINDLER A. (1990). - Calibration of the "C timescale over the past 30.000 years using mass spectrometric U-Th ages from Barbados corals. - *Nature*, **345**, 405-410.
- BARRIERE J. & BERGER G. (1978). - Carte géologique de la France à 1/50000, feuille 1040. - 1ère édition. - 1 feuille en couleur, et notice explicative par BERGER G. *et al.*, 31 p., BRGM éditions.
- BARUSSEAU J.P., AKOUANGO E., BÂ M., DESCAMPS C. & GOLF A. (1996). - Evidence for short term retreat of the barrier shorelines. - *Quaternary Science Reviews*, **15**, 763-771.
- BELLOTTI P., CARBONI M.G., DI BELLA L., PALAGI I. & VALERI P. (1994). - Benthic foraminiferal assemblages in the depositional sequence of the Tiber Delta. - *Boll. Soc. Paleontol. Ital.*, **Spec. vol. 2**, 29-40.
- BELKNAP D.F. & KRAFT J.C. (1985). - Influence of antecedent geology on stratigraphic preservation potential and evolution of Delaware's barrier systems. - *Marine Geology*, **63**, 1-4, 235-262.
- BENABDELOUAHED M. (2005). - Etude du remplissage Holocène de l'étang de Thau, Golfe du lion (Analyse par prospection sismique THR). - *Rapport de Master 2 Recherche*, Université de Caen, 76 p.
- BENNETT M.R., CASSIDY N.J. & PILE J. (2009). - Internal structure of a barrier beach as revealed by ground penetrating radar (GPR): Chesil beach, UK. - *Geomorphology*, **109**, 3-4, 218-229.
- BERGER G., FEIST R. & FREYTET P. (1981). - Carte géologique de la France à 1/50000, feuille 1015. - 1ère édition. - 1 flle en coul., et notice explicative 42 p. BRGM éditions.
- BERTIN X., CHAUMILLON E., WEBER N. & TESSON M. (2004). - Morphological evolution and time-varying bedrock control of main channel at a mixed energy tidal inlet: Maumusson Inlet, France. - *Marine Geology*, **204**, 1-2, 187-202.
- BERTIN X. & CHAUMILLON E. (2005). - New insights in shallow gas generation thank to VHR seismic and bathymetric data in the Marennes-Oléron bay, France. - *Marine geophysical research*, **245**, 65-88.

- BILLEAUD I., CHAUMILLON E. & WEBER O. (2005). - Evidence of a major environmental change recorded in a macrotidal bay (Marennes-Oléron Bay, France) by correlation between VHR seismic profiles and cores. - *Geo-Marine Letters*, **25**, 1, 1-10.
- BILLEAUD I., TESSIER B., LESUEUR P. & CALINE B. (2007). - Preservation potential of highstand coastal sedimentary bodies in a macrotidal basin: Example from the Bay of Mont-Saint-Michel, NW France. - *Sedimentary Geology*, **202**, 4, 754-775.
- BOND G., SHOWER W., CHESEB M., LOTTI R., ALMASI P., DEMENOCAL P., PRIORE P., CULLEN H., HAJDAS I. & BONANI G. (1997). - A Pervasive Millennial-Scale Cycle in North Atlantic Holocene and Glacial Climates. - *Science*, **278**, 5341, 1257-1266.
- BROWDER A.G. & McNINCH J.E. (2006). - Linking framework geology and nearshore morphology: Correlation of paleo-channels with shore-oblique sandbars and gravel outcrops. - *Marine Geology*, **231**, 1-4, 141-162.
- BURNINGHAM H. (2008). - Contrasting geomorphic response to structural control: The Loughros estuaries, northwest Ireland. - *Geomorphology*, **97**, 3-4, 300-320.
- CATTANEO A. & STEEL R.J. (2003). - Transgressive depositis: a review of their variability. - *Earth-Science Reviews*, **62**, 187-228.
- CERTAIN R. (2002). - Morphodynamique d'une côte sableuse microtidale à barres : le golfe du Lion (Languedoc - Roussillon). - *Unpublished PhD thesis*, Université de Perpignan, 209 p.
- CERTAIN R., MEULÉ S., REY V. & PINAZO C. (2005a). - Wave transformation on a microtidal barred beach (Sète, France). - *Journal of Marine Systems*, **38**, 19-34.
- CERTAIN R., TESSIER B., BARUSSEAU J., COURP T. & PAUC H. (2005b). - Sedimentary balance and sand stock availability along a littoral system. The case of the western Gulf of Lions littoral prism (France) investigated by very high resolution seismic. - *Marine and Petroleum Geology*, **22**, 889-900.
- CERTAIN R., TESSIER B., COURP T., BARUSSEAU J.P. & PAUC H. (2004). - Reconnaissance par sismique très haute résolution du remplissage sédimentaire de la lagune de Leucate (Aude et Pyrénées-Orientales - SE France). *Bull. Soc. Geol. Fr.*, **175**, 35-48.
- CHASSEFIERE B. (1968). - Sur la sédimentologie et quelques aspect de hydrologie de l'étang de Thau (Hérault). *Unpublished PhD thesis*, Université de Montpellier, 135 p.
- CHAUMILLON E. & WEBER N. (2006). - Spatial variability of modern incised valleys on the French Atlantic coast : Comparison between the Charente (Pertuis d'Antioche) and the Lay-Sèvre (Pertuis Breton) incised-valleys. In: R. W. Dalrymple, D. A. Leckie and R. W. Tillman, Ed., Incised Valleys in Time and Space. - *SEPM Special publication*, **85**, 57-85.
- COOPER J.A.G. (2001). - Geomorphological variability among microtidal estuaries from the wave-dominated South African coast. - *Geomorphology*, **40**, 1-2, 99-122.
- DABRIO C.J., ZAZO C., GOY J.L., SIERRO F.J., BORJA F., LARIO J., GONZÁLEZ J.A. & FLORES J.A. (2000). - Depositional history of estuarine infill during the last postglacial transgression (Gulf of Cadiz, Southern Spain). - *Marine Geology*, **162**, 2-4, 381-404.
- DALRYMPLE R.W., ZAITLIN B.A. & BOYD R. (1992). - Estuarine facies models; conceptual basis and stratigraphic implications. - *Journal of Sedimentary Research*, **62**, 6, 1130-1146.
- DAVIS R.A. & FITZGERALD D.M. (2004). - Beaches and Coasts. - Blackwell Publishing, Malden, 419 p.
- DEBRET M., BOUT-ROUMAZEILLES V., GROUSSET F., DESMET M., McMANUS J.F., MASSEI N., SEBAG D., PETIT J.-R., COPARD Y. & TRENTESAUX A. (2007). - The origin of the 1500-year climate cycles in Holocene North-Atlantic records. - *Clim. Past Discussions*, **3**, 679-692.

- DE MENOCAL P., ORTIZ J., GUILDERSON T. & SARNTHEIN M. (2000). - Coherent High- and Low-Latitude Climate Variability During the Holocene Warm Period. - *Science*, **288**, 5474, 2198-2202.
- DENIZOT G., COMBES P.-J., BERTRAND J., SEGURET M., MAGNE G., MAGNE J., RAGOT M. & GOTTSIS M. (1967). - Carte géologique de la France à 1/50000, feuille 1016. - 1ère édition. - 1 flle en coul., et notice explicative 10 p. BRGM éditions.
- DUBAR M. & ANTHONY E.J. (1995) - Holocene environmental change and river-mouth sedimentation in the Baie des Anges, French Riviera. - *Quaternary Research*, **43**, 329-343.
- FAIRBANKS R.G. (1989). - A 17,000-year glacio-eustatic sea-level record: influence of glacial melting rates on the Younger Dryas event and deep-ocean circulation. - *Nature*, **342**, 637-642.
- FITZGERALD D.M., BUYNEVICH I.V., FENSTER M.S., KELLEY J.T. & BELKNAP D.F. (2005). - Coarse-grained sediment transport in northern New England estuaries: a synthesis. In: D. M. FitzGerald and J. Knight, Ed., High Resolution Morphodynamics and Sedimentary Evolution of Estuaries. - *Coastal Systems and Continental Margins*, Springer, **8**, 195-214.
- FITZGERALD D.M., BUYNEVICH I.V., FENSTER M.S. & MCKINLAY P.A. (2000). - Sand dynamics at the mouth of a rock-bound, tide-dominated estuary. - *Sedimentary Geology*, **131**, 25-49.
- GANGNERY A., BACHER C. & BUESTEL D. (2001). - Assessing the production and the impact of the cultivated oysters in the Thau lagoon (Mediterranean, France) with a population dynamics model. - *Can. J. Fish. Aquat. Sci.*, **58**, 1012-1020.
- GARCÍA-GIL S., VILAS F. & GARCÍA-GARCÍA A. (2002). - Shallow gas features in incised-valley fills (Vigo ria, NW Spain). - *Cont. Shelf Res.*, **22**, 2303-2315.
- HAMILTON E.L. (1972). - Compressional-wave attenuation in marine sediments. - *Geophysics*, **37**, 620-646.
- HANNEBUTH T.J.J., STATTEGER K. & GROOTES P.M., (2000). - Rapid flooding of the Sunda Shelf - a late-glacial sea-level record. - *Science*, **288**, 1033-1035.
- HEAP A.D. & NICHOL S.L. (1997). - The influence of limited accommodation space on the stratigraphy of an incised-valley succession: Weiti River estuary, New Zealand. - *Marine Geology*, **144**, 1-3, 229-252.
- HESP P.A. & SHORT A.D. (1999). - Barrier Morphodynamics. In: A. D. Short, Ed., Handbook of Beach and Shoreface Morphodynamics. - John Wiley & Sons Ltd, New York, 307-333.
- L'HOMER A. (1975). - Notice de la Carte géologique des Saintes- Maries-de-la-Mer au 1/50,000; Feuille 1018, 33 p., BRGM Editions.
- L'HOMER A., BAZILE A., THOMMERET J. & THOMMERET Y., (1981). - Principales étapes de l'édification du delta du Rhône de 7000BP à nos jours. Variations du niveau marin. - *Oceanis*, **7**, 4, 389- 408.
- LABEYRIE J., LALOU C., MONACO A. & THOMMERET J. (1976). - Chronologie des niveaux eustatiques sur la côte de Roussillon de -33000 ans PB à nos jours. Chronology of eustatic levels on the Roussillon coast from 33000 years ago to the present. - *Comptes Rendus Hebdomadaires des Séances de l'Académie des Sciences, Série D: Sciences Naturelles*, **282**, 349-352.
- MARTIN R.T., GADEL F.Y. & BARUSSEAU J.P. (1981). - Holocene evolution of the Canet St Nazaire lagoon (Golfe du Lion, France) as determined from a study of sedimentological properties. - *Sedimentology*, **28**, 823-836.

- MASSARI F., RIO D., SERANDREI BARBERO R., ASIOLI A., CAPRARO L., FORNACIARI E. & VERGERIO P.P. (2004). - The environment of Venice area in the past two million years. - *Palaeogeogr. Palaeoclimatol. Palaeoecol.* **202**, 273-308.
- MAYEWSKI P.A., ROHLING E.E., CURT STAGER, J., KARLÉN W., MAASCH K.A., DAVID MEEKER L., MEYERSON E.A., GASSE F., VAN KREVELD S., HOLMGREN K., LEE-THORP J., ROSQVIST G., RACK F., STAUBWASSER M., SCHNEIDER R.R., & STEIG E.J. (2004). - Holocene climate variability. - *Quaternary Research*, **62**, 3, 243-255.
- MILLET B. (1989). - Fonctionnement hydrodynamique du Bassin de Thau. Validation écologique d'un modèle numérique de circulation. - *Oceanologica Acta*, **12**, 1, 37-46.
- MILLOT C. (1990). - The Gulf of Lions' hydrodynamics. - *Continental Shelf Research*, **10**, 885-894.
- MITCHUM R.M.J. & VAIL P.R. (1977). - Seismic stratigraphy and global changes of sea-level, part 7. Stratigraphic interpretation of seismic reflection patterns in depositional sequences. In: Payton C.E., Ed., *Seismic Stratigraphy - Applications to Hydrocarbon Exploration*. - Memoir of the American Association of Petroleum Geologists, Tulsa, **26**, 135-144.
- OOMKENS E., (1970). - Depositional sequences and sand distribution in the postglacial Rhône delta complex. In: Morgan, J.P., Ed., *Deltaic Sedimentation Modern and Ancient*, 198-211.
- PINAULT J.-L., DOERFLIGER N., LADOUCHE B. & BAKALOWICZ M. (2004). - Characterizing a coastal karst aquifer using an inverse modeling approach: The saline springs of Thau, southern France. - *Water Resour. Res.*, **40**, W08501, doi:10.1029/2003WR002553.
- PLANCHAS N., GADEL F., BARUSSEAU J.P. & BUSCAIL R. (1984). - Palynologie et sédimentologie d'un dépôt vaso-tourbeux daté de 7 000 ans B.P., situé à Saint Cyprien (Pyrénées Orientales). - *C. R. Acad. Sci., Paris*, **298**, 321-329.
- PONS A., TONI CL. & TRIAT H. (1979). - Edification de la Camargue et histoire Holocène de sa végétation. - *Terre et vie, Rev. Ecol.*, **suppl. 2**, 14-29.
- PROKOPENKO A.A., KARABANOV E.B., WILLIAMS D.F., KUZMIN M.I., KHURSEVICH G.K. & GVOZDKOV A.A. (2001). - The detailed record of climatic events during the past 75,000 yrs BP from the Lake Baikal drill core BDP-93-2. - *Quaternary International*, **80-81**, 59-68.
- PROVANSAL M., VELLA C., ARNAUD-FASSETTA G., SABATIER F. & MAILLET G. (2003). - Role of fluvial sediment inputs in the mobility of the Rhône delta Coast (France). - *Geomorphol.: Relief, Process., Environ.*, **4**, 271-282.
- RAYNAL O. (2008). - Architectures de dépôts et facteurs de contrôle d'un système côtier à faibles apports sédimentaires - le littoral languedocien (Golfe du Lion, Sud de la France). - *Unpublished PhD thesis*, Université de Montpellier II, 153 p.
- RAYNAL O., BOUCHETTE F., CERTAIN R., SÉRANNE M., DEZILEAU L., SABATIER P., LOFI J., BUI XUAN HY A., BRIQUEU L., PEZARD P. & TESSIER B. (accepted). - Control of alongshore-oriented sand spits on the dynamic of a wave-dominated coastal system (Holocene deposits, northern Gulf of Lions, France). - *Marine Geology*.
- RAYNAL O., BOUCHETTE F., CERTAIN R., SÉRANNE M., SABATIER P., LOFI J., DEZILEAU L., BRIQUEU L., FERRER P., COURP T. & TESSIER B. (submitted). - Holocene evolution of languedocien lagoonal environment controlled by inehritied coastal morphology (Northern Gulf of Lions, France). - *Bulletin de la Société Géologique de France*.
- REGNAULD H., PIRAZZOLI P.A., MORVAN G. & RUZ M. (2004). - Impacts of storms and evolution of the coastline in western France. - *Marine Geology*, **210**, 1-4, 325-337.
- REIMER P.J., BAILLIE M.G.L., BARD E., BAYLISS A., BECK J. W., BERTRAND C.J.H., BLACKWELL P.G., BUCK C.E., BURR G.S., CUTLER K.B., DAMON P.E., EDWARDS R.L., FAIRBANKS R.G., FRIEDRICH M., GUILDERSON T.P., HOGG A.G., HUGHEN K.A., KROMER

- B., MCCORMAC G., MANNING S., RAMSEY C.B., REIMER R.W., REMMELE S., SOUTHON J.R., STUIVER M., TALAMO S., TAYLOR F.W., VAN DER PLICHT J. & WEYHENMEYER C.E., (2004). - IntCal04 terrestrial radiocarbon age calibration, 0-26 cal kyr BP. - *Radiocarbon*, **46**, 3, 1029-1058.
- REINSON G.E. (1992). - Transgressive barrier island and estuarine systems. In: R. G. Walker and N. P. James, Ed., Facies Models: Response to Sea Level change. - Geological Association of Canada, Waterloo, 179-194.
- RICCI LUCCHI M., FIORINI F., LUISA COLALONGO M. & VITTORIO CURZI P. (2006). - Late-Quaternary paleoenvironmental evolution of Lesina lagoon (southern Italy) from subsurface data. - *Sedimentary Geology*, **183**, 1-2, 1-13.
- RIGGS S.R., CLEARY W.J. & SNYDER S.W. (1995). - Influence of inherited geologic framework on barrier shoreface morphology and dynamics. - *Marine Geology*, **126**, 1-4, 213-234.
- SABATIER P., DEZILEAU L., BARBIER M., RAYNAL O., LOFI J., BRIQUEU L., CONDOMINES M., BOUCHETTE F., CERTAIN R., VAN GRAFENSTEIN U., JORDA C. & BLANCHEMANCHE P. (in press). - Late-Holocene evolution of a coastal lagoon in the Gulf of Lions (South of France). - *Bulletin de la Société Géologique de France*.
- SABATIER P., DEZILEAU L., CONDOMINES M., BRIQUEU L., COLIN C., BOUCHETTE F., LE DUFF M. & BLANCHEMANCHE P. (2008). - Reconstruction of paleostorm events in a coastal lagoon (Hérault, South of France). - *Marine Geology*, **251**, 224-232.
- SCHMIDT S., JOUANNEAU J.-M., WEBER O., LECROART P., RADAKOVITCH O., GILBERT F. & JÉZÉQUEL D. (2007). - Sedimentary processes in the Thau Lagoon (France): From seasonal to century time scales, *Estuarine, Coastal and Shelf Science*, **72** (3), 534-542.
- SIMEONI U., FONTOLAN G., TESSARI U. & CORBAU C. (2007). - Domains of spit evolution in the Goro area, Po Delta, Italy. - *Geomorphology*, **86**, 3-4, 332-348.
- SIMPKIN P.G. & DAVIS A. (1993). - For Seismic profiling in very shallow water, a novel receiver. - *Sea Technology*, **34**, 9.
- S.H.O.M. (2003). - Tide Tables, Tome1, French Harbors. Edition 2003.
- SOLETCHNIK P., HUVET A., LE MOINE O., RAZET D., GEAIRON P., FAURY N., GOULLETQUER P. & BOUDRY P. (2002). - A comparative field study of growth, survival and reproduction of *Crassostrea gigas*, *C. angulata* and their hybrids. - *Aquatic Living Resources*, **15**, 243-250.
- SORREL P., TESSIER B., DEMORY F., DELSINNE N. & MOUAZÉ D. (2009). - Evidence for millennial-scale climatic events in the sedimentary infilling of a macrotidal estuarine system, the Seine estuary (NW France). - *Quaternary Science Reviews*, **28**, 499-516.
- SUURSAAR Ü., JAAGUS J., KONT A., RIVIS R. & TÖNISON H. (2008). - Field observations on hydrodynamic and coastal geomorphic processes off Harilaid Peninsula (Baltic Sea) in winter and spring 2006-2007. - *Estuarine, Coastal and Shelf Science*, **80**, 1, 31-41.
- TESSIER B., CERTAIN R., BARUSSEAU J.P. & HENRIET J.P. (2000). - Evolution historique du prisme littoral du lido de l'étang de Thau (Sète, Sud-Est de la France). Mise en évidence par sismique réflexion très haute résolution. - *C. R. Acad. Sci. Paris*, **331**, 709-716.
- TESSON M., LABAUNE C. & GENSOUS B. (2005). - Small rivers contribution to the Quaternary evolution of a Mediterranean littoral system: The western gulf of Lion, France. - *Marine Geology*, **222-223**, 313-334.
- TIMMERMANN A., GILDOR H., SCHULZ M. & TZIPERMAN E. (2003). - Coherent Resonant Millennial-Scale Climate Oscillations Triggered by Massive Meltwater Pulses. - *Journal of Climate*, **16**, 15, 2569-2585.
- ULSES C., ESTOURNEL C., DURRIEUF MADRON X. & PALANQUES A. (2008). - Suspended sediment transport in the Gulf of Lions (NW Mediterranean): Impact of extreme storms and floods. - *Continental Shelf Research*, **28**, 2048-2070.

- VELLA C., FLEURY T.-J., RACCASI G., PROVANSAL M., SABATIER F. & BOURCIER M. (2005). - Evolution of the Rhône delta plain in the Holocene. - *Marine Geology*, **222-223**: 235-265.
- VELLA C., & PROVANSAL M. (2000). - Relative sea-level rise and neotectonic events during the last 6500 yr on the southern eastern Rhône delta, France. - *Marine Geology*, **170**, 27-39.
- ZAZO C., DABRIO C.J., GOY J.L., LARIO J., CABERO A., SILVA P.G., BARDAJÍ T., MERCIER N., BORJA F. & ROQUERO E. (2008). - The coastal archives of the last 15 ka in the Atlantic-Mediterranean Spanish linkage area: Sea level and climate changes. - *Quaternary International*, **181**, 1, 72-87.
- ZECCHIN M., BARADELLO L., BRANCOLINI G., DONDA F., RIZZETTO F. & TOSI L. (2008). - Sequence stratigraphy based on high-resolution seismic profiles in the late Pleistocene and Holocene deposits of the Venice area. - *Marine Geology*, **253**, 185-198.
- ZECCHIN M., CIVILE D., CAFFAU M. & RODA C. (2009). - Facies and cycle architecture of a Pleistocene marine terrace (Crotone, southern Italy): A sedimentary response to late Quaternary, high-frequency glacio-eustatic changes. - *Sedimentary Geology*, **216**, 3-4, 138-157.
- ZIC M., NEGRINI R.M. & WIGAND P.E. (2002). - Evidence of synchronous climate change across the Northern Hemisphere between the North Atlantic and the northwestern Great Basin, United States. - *Geology*, **30**, 7, 635-638.

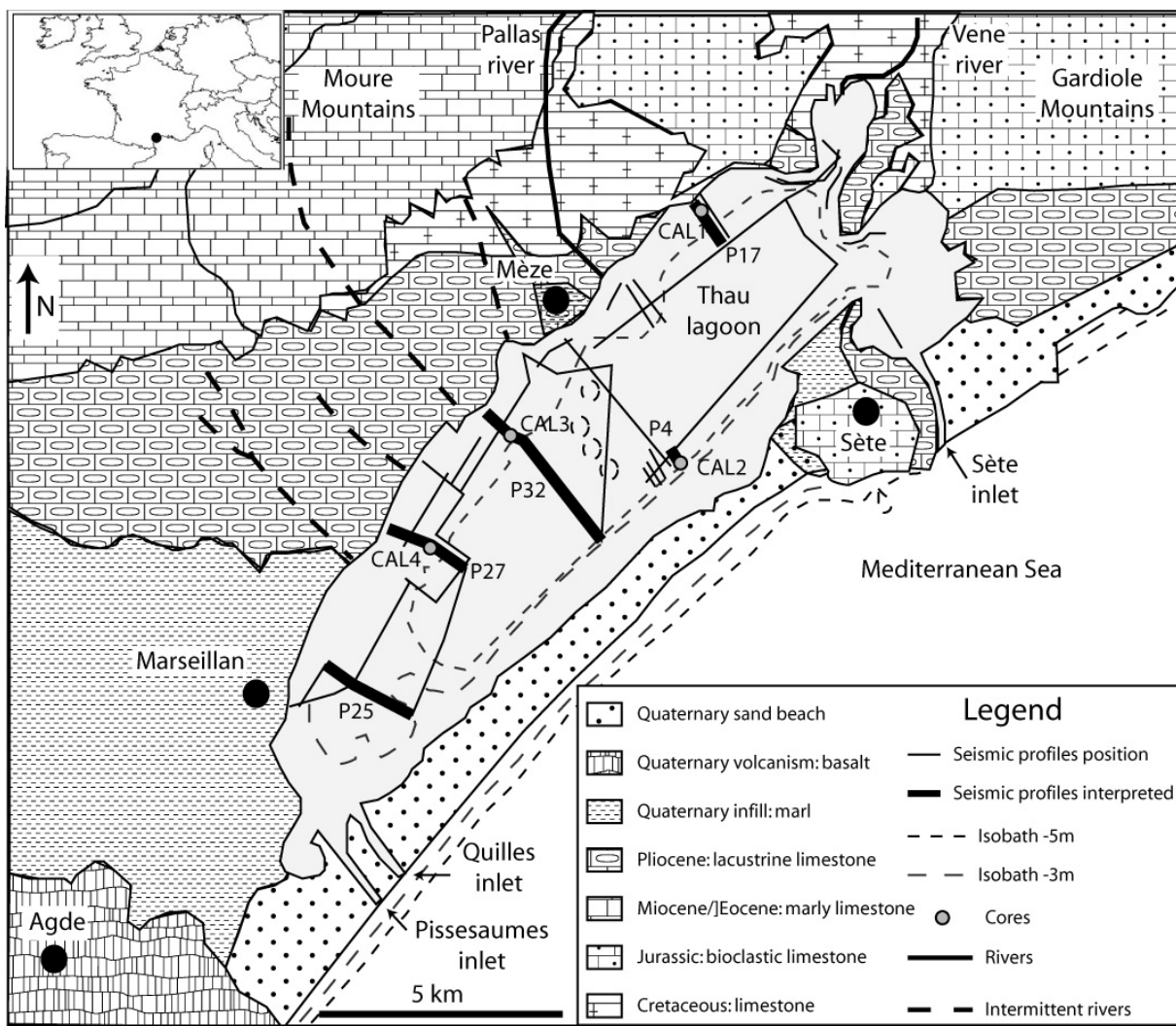
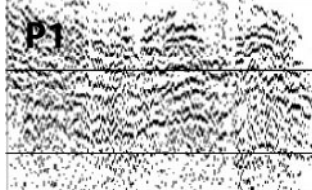
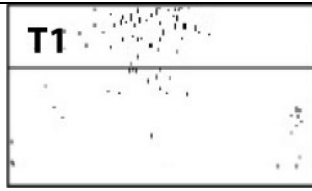
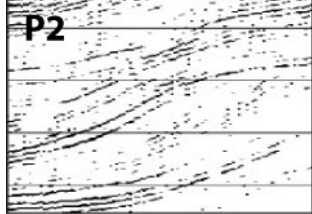
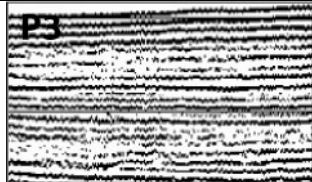


fig. 1. – Geologic map of the Thau lagoon area including its catchment (modified from Barrière et Berger (1978), Berger *et al.* (1981), Denizot *et al.* (1967)). The position of cores (CAL1, 2, 3, 4) and seismic profiles are indicated. Seismic profile shown on the figures (2, 3, 4 and 6) are in thick lines (P4, P17, P25, P27, P32).

fig. 2. – Carte géologique de la lagune de Thau incluant son bassin versant (modifié d'après Barrière et Berger (1978), Berger *et al.* (1981), Denizot *et al.* (1967)). Les positions des carottes sédimentaires (CAL1, 2, 3, 4) et le plan de position des profils sismiques sont indiqués. Les profils sismiques illustrés dans les figures (2, 3, 4 and 6) sont soulignés (P4, P17, P25, P27, P32).

Acoustic facies	Amplitude	Continuity	Frequency	Configuration	Units	Interpretation
	High	Low to medium	High	Parallel to sub parallel	U0	Rocky substrate
	null	Transparent	Transparent	Transparent	U1	Fluvial terraces, colluvions, transgressive sands
	Low to null	Low to medium	Low to medium	Oblique sigmoid	U0	Rocky substrate
					U2-1, U2-2	sand, silt
						Fine grained sediments (clay)

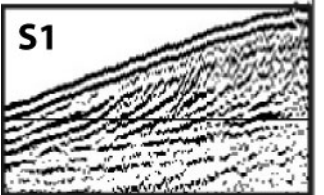
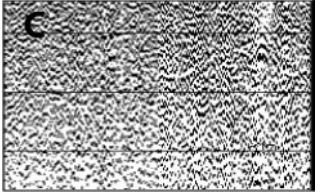
	High	Medium	High	Oblique sigmoid	U2-1, U2-2	Washover fan
	Medium to High	Low to medium	High	Symetric sigmoid	U2-1, U2-2	“Cadoules” (bioclastic mounds)
	High	Weak	High	Chaotic	U1, U2-1, U2-2	Gas, seaweeds

TABLE I. – Characteristics of the acoustic facies observed on the seismic profiles shot in the Thau lagoon.

TABLE I. – Caractéristiques des facies acoustiques observés sur les profils sismiques de la lagune de Thau..

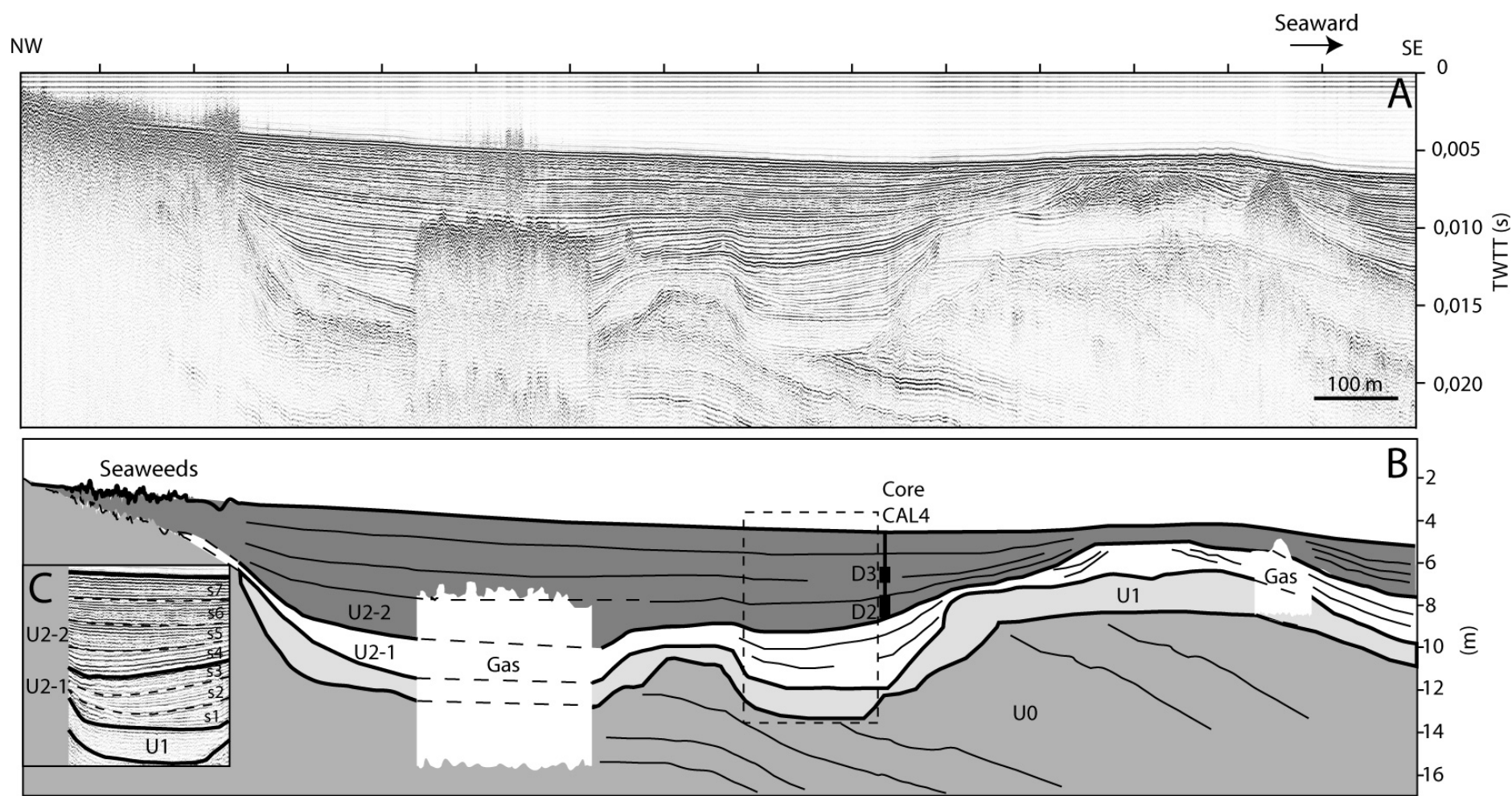


fig. 2. – (A) Seismic profile P27 (cf. fig. 1 for location) and (B) interpretation. The main unit of the lagoon infill is the unit U2 divided into two sub-units U2-1 and U2-2. (C) On the basis of acoustic facies, elementary seismic sequences (from s1 to s7) can be distinguished into U2-1 and U2-2. The vertical thick line in U2-2

indicates the position of the core CAL4. D2 and D3 give the location of dated samples (vertical uncertainty is due to compaction during the coring). TWTT: two way travel time.

fig. 2. – (A) Profil sismique P27 (cf. fig. 1 pour la position) et (B) son interprétation. L’unité principale du remplissage lagunaire est l’unité U2 qui se divise en deux sous-unités U2-1 et U2-2. (C) en se basant sur les faciès acoustiques, des séquences élémentaires (de s1 à s7) peuvent être distinguées dans U2-1 et U2-2. La ligne verticale dans U2-2 montre la position de la carotte sédimentaire CAL4. D2 et D3 indiquent la position des échantillons datés (l’incertitude verticale est liée à la compaction du sédiment durant le prélèvement). TWTT : two way time travel.

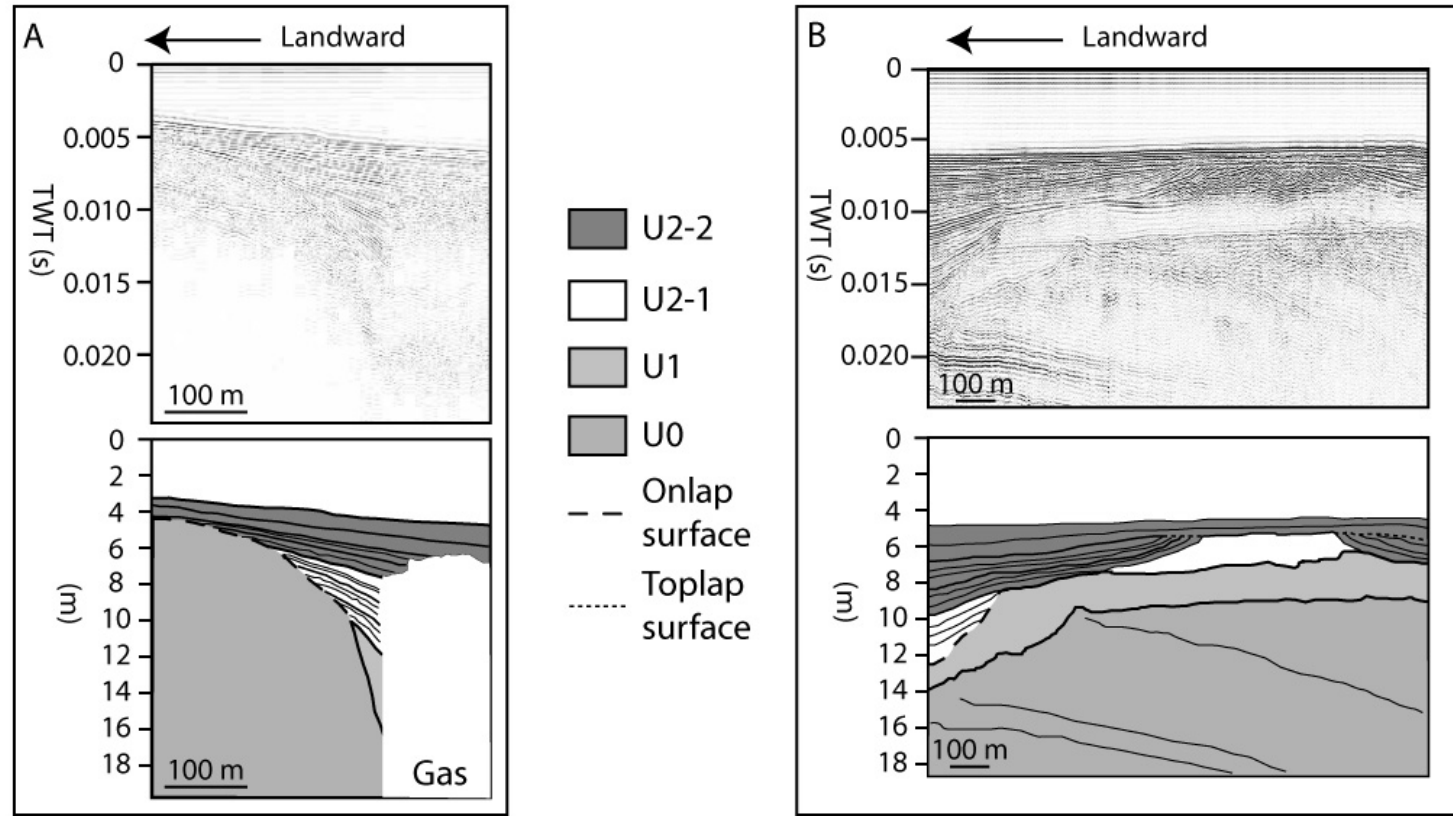


fig. 3. – (A) Extract from seismic profile P32 (cf. fig. 1 for location) and its interpretation. (B) Extract from seismic profile P27 (cf. fig. 1 for location) and its interpretation. The seismic terminations of elementary sequences reflectors present an onlap surface on the substratum at the edge of the lagoon (A). U2-1 reflectors finish on an onlap surface on U1 around the substrate highs (B) while the reflectors of s4 and s5 form a toplap surface truncated by s6.

fig. 3. – (A) Profil sismique extrait de P32 (cf. fig. 1 pour la position) et son interpretation. (B) Profil sismique extrait de P27 (cf. fig. 1 pour la position) et son interpretation. Les terminaisons des réflecteurs sismiques des séquences élémentaires forment des onlap sur le substratum au niveau des bordures de la lagune (A). Les réflecteurs de U2-1 se biseautent en onlap sur U1 autour des points hauts du substratum (B) pendant que les réflecteurs de s4 et s5 sont tronqués en toplap par s6.

Internal configuration of reflectors			
Elementary sequence name	Lagoon centre	Lagoon edges	Substrate highs
s1	Parallel	Onlap on U0	Onlap on U0
s2	Parallel	Onlap on U0 and on the limit of s1/s2	Onlap on U0
s3	Parallel	Onlap on U0 and on the limit of s2/s3	Onlap on U0
s4	Parallel	Onlap on U0 and on the limit of U2-1/U2-2	Onlap on the limit of U2-1/U2-2
s5	Parallel	Onlap on U0 and on the limit of s4/s5	Toplap on s6
s6	Parallel	Onlap on U0 and the limit of s5/s6	Parallel, draping the sedimentary infill
s7	Parallel	Onlap on U0 and the limit of s6/s7	Parallel, draping the sedimentary infill

TABLE II. – Internal configuration of the reflectors of the elementary sequences observed on the seismic profiles shot in the Thau lagoon.

TABLE II. – Configuration interne des réflecteurs des séquences élémentaires observées sur les profils sismiques de la lagune de Thau.

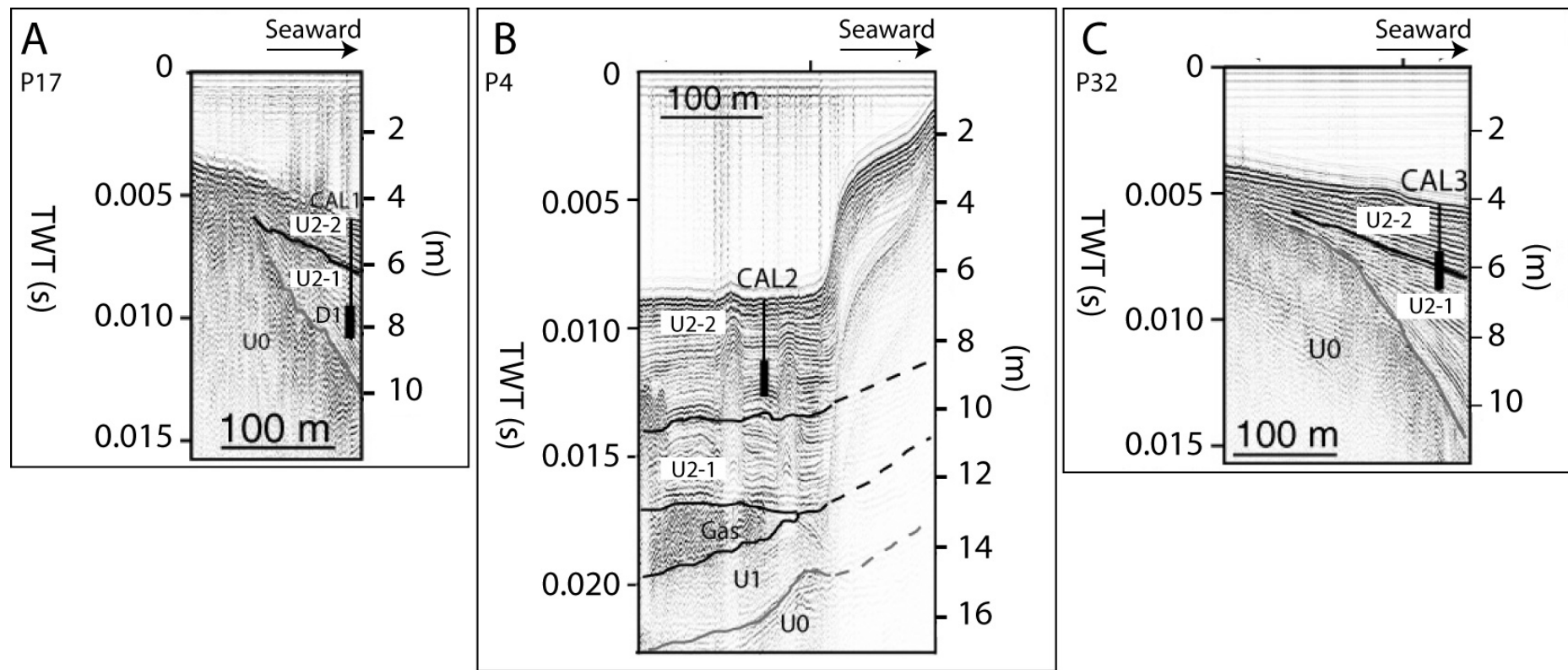


fig. 4. – Location of the cores CAL1, CAL2, CAL3 on the seismic profiles 17 (A), 04 (B), 32 (C) respectively. At the base of CAL1, D1 indicates the sample which has been dated . At the base of CAL1, CAL2 and CAL3, the vertical thick black line indicate core length uncertainty due to compaction.

fig. 4. – Position des carottes sédimentaires CAL1, CAL2, CAL3 sur leurs profils sismiques respectifs 17 (A), 04 (B), 32 (C). A la base de CAL1, D1 indique l'échantillon daté . A la base de CAL1, CAL2 et CAL3, la ligne vertical épaisse indique l'incertitude verticale de la position de la carotte lié à la compaction lors du prélèvement.

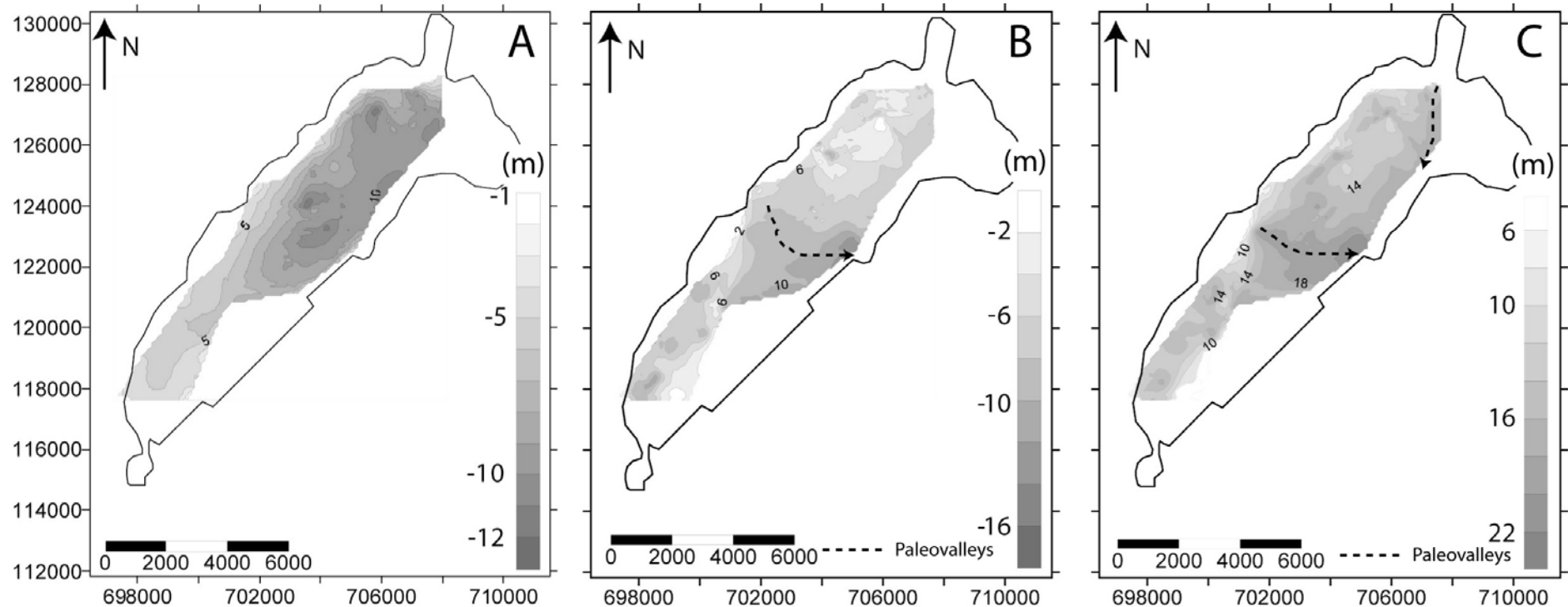


fig. 5. – The Thau lagoon (A) Bathymetric map, (B) Isohypses map of the substrate top (U0) and (C) Isopach map of the sedimentary infill (U1 + U2), reconstructed from the seismic data.

fig. 5. – Cartes de la lagune de Thau représentant (A) la bathymétrie, (B) les isohypses du toit du substratum (U0) et (C) les isopaques du remplissage sédimentaire (U1 + U2), reconstruites à partir des données de sismique réflexion.

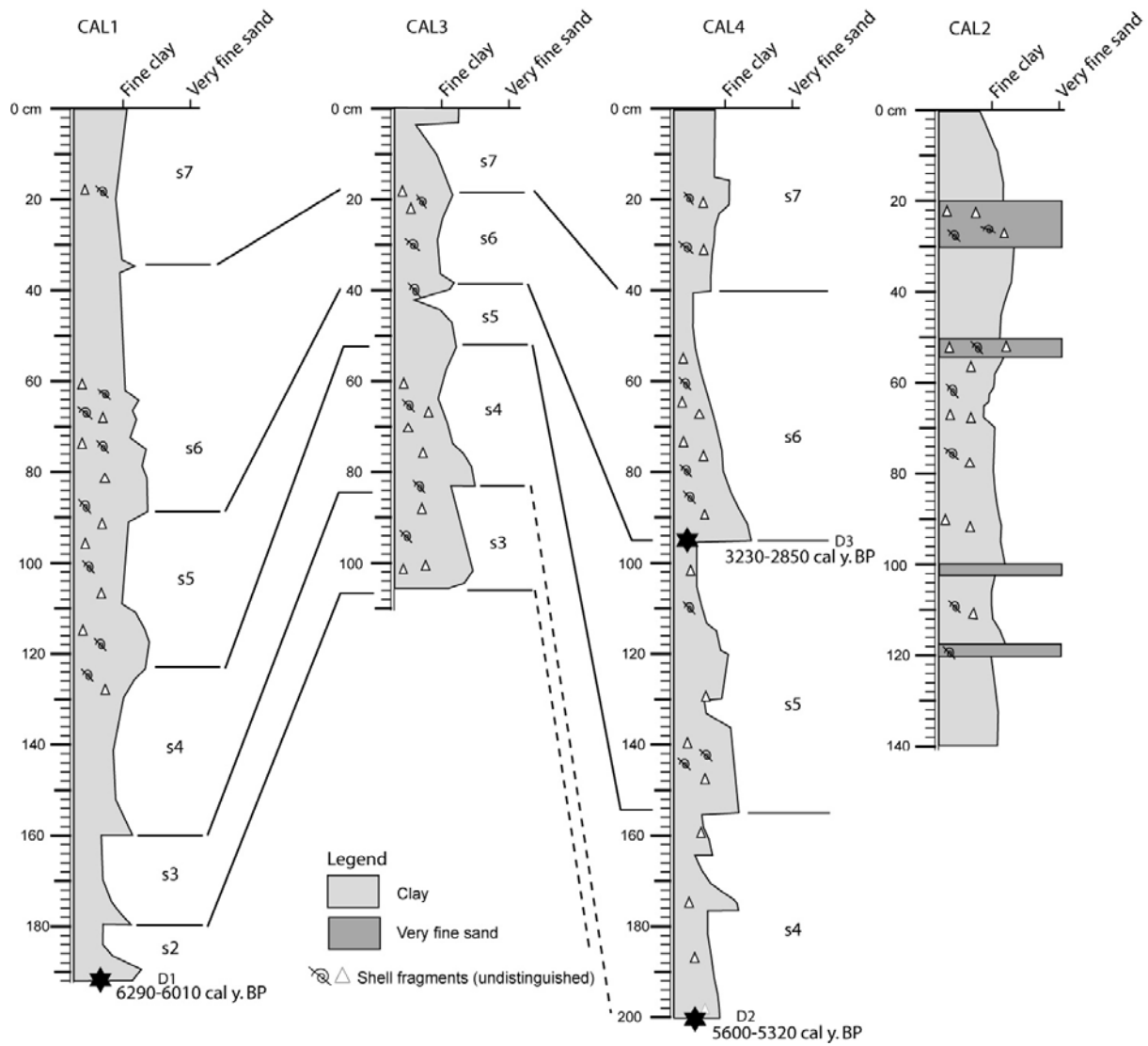


fig. 6. – sedimentological log of the CALAMAR cores. CAL1, CAL3 and CAL4 can be well correlated since they are located inside the lagoon. CAL2 is closer to the sandy barrier. It exhibits a homogenous distribution of sediment with some sandy layers. Dated samples are indicated. s2 to s7 : elementary sequences defined on the seismic profiles.

fig. 6. – Logs sédimentologiques des carottes sédimentaires CALAMAR. CAL1, CAL3 et CAL4 peuvent être corrélées de manière satisfaisante car elles sont positionnées dans la lagune. CAL2 est plus proche du lido. Elle montre une distribution plus homogène du sédiment avec quelques lits sableux intercalés. Les échantillons dates sont indiqués. Les sequences élémentaires de s2 à s7 décrisées sur les profiles sismiques sont indiquées.

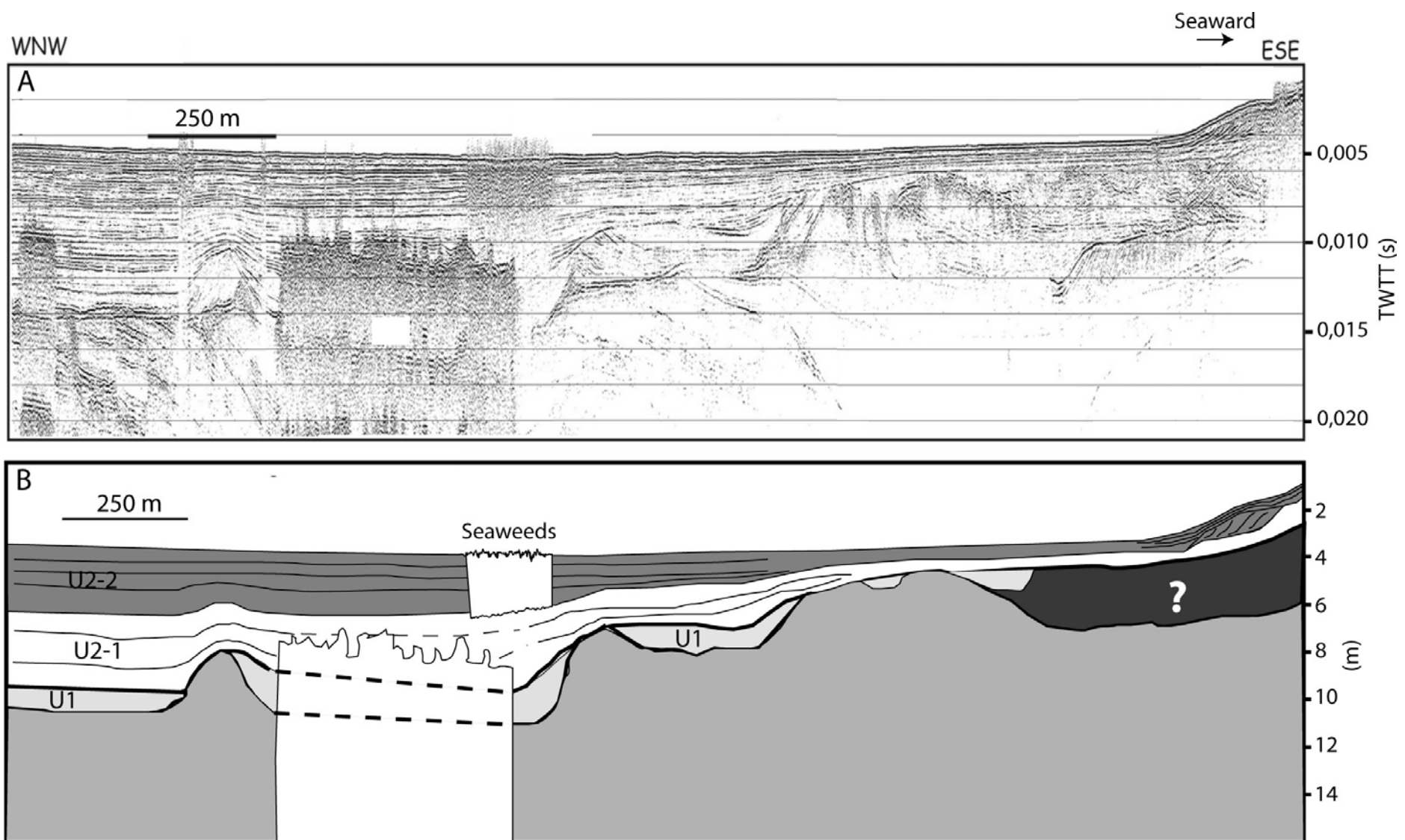


fig. 7. – (A) seismic profile P25 (cf. fig. 1 for location) and (B) interpretation. This profile allows imaging the seaward edge of the lagoon, i.e. the landward side of the sandy barrier, where the upper unit U2-2 is made of a landward migrating body interpreted as a series of washover fans.

fig. 7. – (A) Profil sismique P25 (cf. fig. 1 pour la position) et (B) son interprétation. Ce profil image la bordure orientale de la lagune proche de la mer, i.e. le côté interne du lido, où la sous-unité U2-2 présente des corps sédimentaires progradants vers le continent interprétés comme des cônes de débordement.

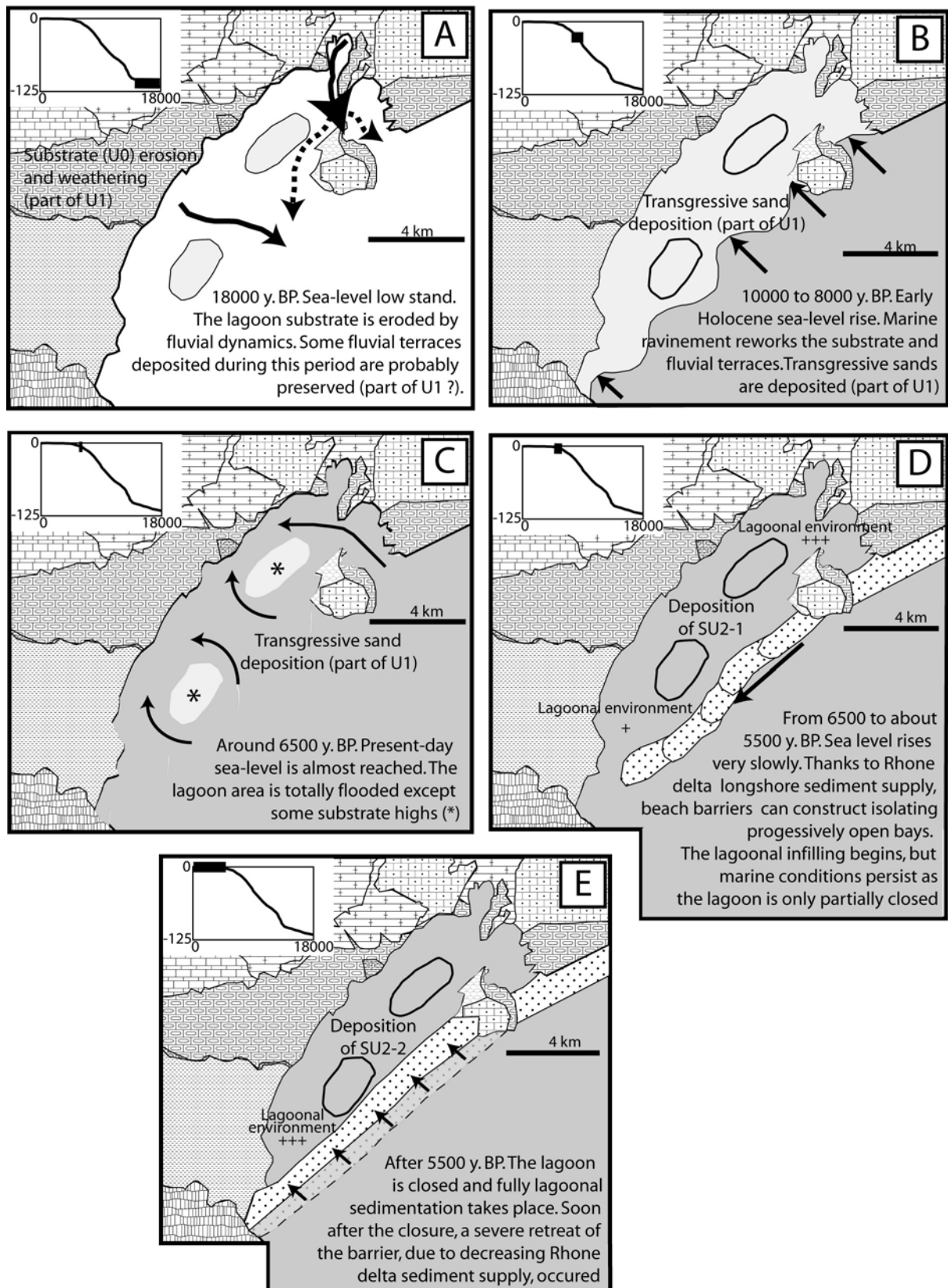


fig. 8. – Palaeogeographic reconstruction of the Thau lagoon formation and occurred sedimentary infilling. In the upper left corner, location of the step during post-glacial sea level fluctuations (based on Fairbanks, 1989; Bard *et al.*, 1990; Hanebuth *et al.*, 2000; Dubar & Anthony, 1995).

fig. 8. – Reconstruction paléogéographique de la formation de la lagune de Thau. Dans le coin supérieur gauche, position chronologique de l'étape durant les variations du niveau marin post-glaciaire (basé sur Fairbanks, 1989; Bard *et al.*, 1990; Hanebuth *et al.*, 2000; Dubar & Anthony, 1995).

Mesures de houles partiellement stationnaires en zones côtière et littorale

VINCENT REY^{1,a}, RAPHAËL CERTAIN², DÉBORAH DREVARD¹, ANNE MEURET¹
ET JACQUES PIAZZOLA¹

¹ Université du Sud Toulon-Var, LSEET-LEPI, BP 56, 83162 La Valette du Var Cedex, France

² Université de Perpignan, LEGEM, 52 Av. P. Alduy, 66860 Perpignan, France

Reçu le 17 décembre 2004, accepté le 13 octobre 2005

Résumé – Les instruments de mesures des courants en mer permettent d'obtenir un nombre d'informations de plus en plus important grâce à des techniques de mesures de plus en plus sophistiquées. En particulier, les mesures ponctuelles de vitesses et de pression permettent d'obtenir des informations sur l'énergie de la houle et sa direction de propagation. Nous avons montré dans ce travail que le caractère partiellement stationnaire des houles réelles peut être mesuré de façon quantitative à partir de données synchrones de vitesse et/ou de pression. Ces capacités sont illustrées par des exemples de mesures à partir de différents appareils immergés en zone littorale (S4, ADV, ligne de capteurs de pression).

Mots clés : Houle / réflexion / littoral / mesures

Abstract – Partially standing wave measurement in the nearshore. Instrumentation for field flow measurements is more and more sophisticated. In particular, local velocity and pressure measurements give informations on the wave energy and its propagation. In the present work, it is demonstrated that the use of coincident velocity and/or pressure data may give quantitative informations on the rate of standing waves. Examples from various instruments displayed in the nearshore are then given (S4, ADV, series of pressure sensors).

Key words: Water wave / reflection / nearshore / measurements

1 Introduction

Les données de houle à partir d'instruments en mer consistent généralement à recueillir des informations sur l'énergie transportée. Au large, l'énergie est répartie sur une gamme de fréquence plus ou moins large selon que la houle est formée ou confondue avec la mer de vent, et se propage autour d'une direction moyenne avec un angle d'ouverture qui dépend aussi de l'état de mer. De façon classique, la répartition énergétique obéit à des lois statistiques qui permettent de définir des paramètres caractéristiques qui sont la hauteur significative H_s , la période significative T_s et la direction de propagation θ .

À l'approche de la côte, la houle a tendance à « tourner » par effets bathymétriques, et une dispersion apparaît dans la direction de propagation en fonction de la fréquence de chacune des composantes spectrales de la houle. De plus, pour des bathymétries abruptes, des

plages de forte pente, ou en présence de structures côtières (digues, épis...), une partie de l'énergie de la houle peut être réfléchie.

Si les caractéristiques de la houle au large sont maintenant bien connues et tout à fait utiles pour la navigation et le dimensionnement des ouvrages en mer, leur caractérisation au niveau du littoral reste plus difficile notamment d'une part pour des côtes accidentées aux bathymétries complexes et d'autre part pour les plages de sable où les facteurs morphologiques « transforment » de façon importante les conditions des houles incidentes du large jusqu'à leur déferlement.

Le but de ce travail est d'étudier les possibilités de mesure de houles multi-directionnelles et partiellement stationnaires à partir d'instruments donnant des informations sur les vitesses et/ou pression à profondeur donnée.

Après une description des modèles de houles puis les techniques d'analyses pour des houles uni- et multi-directionnelles, des applications in situ sont présentées et discutées.

^a Auteur correspondant : rey@univ-tln.fr

Liste des paramètres

C_φ	vitesse de phase de l'onde, en m.s^{-1}
C_g	vitesse de groupe de l'onde, en m.s^{-1}
D	répartition angulaire de l'énergie de l'onde, sans unité (rad^{-1})
E	énergie de l'onde, $E/\rho g$ en $\text{m}^2.\text{Hz}^{-1}$
E_d	énergie par unité de fréquence et d'angle de l'onde, en $\text{m}^2.\text{Hz}^{-1}$
H	hauteur crête à creux de l'onde, en m
R	coefficient de réflexion de l'onde, sans unité
S	énergie par unité de fréquence de l'onde, en $\text{m}^2.\text{Hz}^{-1}$
T	période de l'onde, en s
a	amplitude de l'onde incidente, en m
b	amplitude de l'onde réfléchie, en m
f	fréquence de l'onde, en Hz
g	accélération due à la gravité, en m.s^{-2}
h	profondeur d'eau, en m
k	vecteur d'onde de l'onde, en m^{-1}
p	pression, en Pa
u	amplitude de la vitesse horizontale suivant l'axe Ox , en m.s^{-1}
u_h	amplitude de la vitesse horizontale, en m.s^{-1}
v	amplitude de la vitesse horizontale suivant l'axe Oy , en m.s^{-1}
w	amplitude de la vitesse verticale suivant l'axe Oz , en m.s^{-1}
x, y	distances suivant les axes horizontaux Ox et Oy , en m
z	distance suivant l'axe vertical Oz orienté vers le haut, en m
Δ	différence de phase entre les sondes, sans unité
η	déformée de la surface libre, en m
η_i	déformée de la surface libre pour l'onde incidente, en m
η_r	déformée de la surface libre pour l'onde réfléchie, en m
φ	phase de l'onde, sans unité
ϕ	potentiel des vitesses, en $\text{m}^2.\text{s}^{-1}$
λ	longueur d'onde de l'onde, en m
ρ	masse volumique du fluide, en kg.m^{-3}
θ	angle d'incidence de l'onde, sans unité (rad)
ω	fréquence angulaire de l'onde, en rad.s^{-1}

2 Théorie des ondes monochromatiques linéaires

On se limite dans cette partie au cas bidimensionnel dans le plan xOz , où Ox représente l'axe horizontal, direction de propagation, et Oz , orienté vers le haut, l'axe vertical. Pour une houle ayant pour angle d'incidence θ par rapport à la direction Ox dans le plan horizontal xOy , il suffit de faire une rotation pour revenir au cas bidimensionnel. On peut noter que pour l'analyse des données de vitesses et de pression, l'hypothèse « onde plane » sera requise pour l'analyse des champs de vitesses et de pressions, ce qui signifie que les variations bathymétriques doivent être faibles dans la zone de mesure. On suppose que la houle est monochromatique, de fréquence f et de période $T = 1/f$.

2.1 Onde progressive

Dans l'hypothèse d'ondes de faible amplitude de fréquence angulaire ω , la dépendance vis-à-vis du temps du potentiel des vitesses et de la déformée de la surface libre peut s'écrire sous la forme complexe $e^{i\omega t}$. Les

solutions pour une onde propagative (dans cette section, dans la direction Ox pour simplifier) par profondeur constante h , satisfaisant l'équation de Laplace, les conditions limites au fond et les conditions linéarisées à la surface libre sont données par

$$\phi(x, z, t) = \frac{a C(z)}{k} e^{i(\omega t - kx)} \quad (1)$$

où $C(z) = \omega \frac{\cosh[k(z+h)]}{\sinh(kh)}$. Ceci correspond à une déformée de la surface libre

$$\eta(x, t) = -ia e^{i(\omega t - kx)} \quad (2)$$

où $H = 2a$ est la hauteur crête à creux. Le vecteur d'onde k vérifie la relation de dispersion $\omega^2 = gk \tanh(kh)$ où g est l'accélération due à la gravité. L'onde se propage à la vitesse $C_\varphi = \omega/k$ et sa longueur d'onde $\lambda = ((2\pi)/k) = C_\varphi T$ diminue quand la profondeur d'eau diminue. Les champs de vitesses sont donnés par :

$$u = \frac{\partial \Phi}{\partial x} = -ia C(z) e^{i(\omega t - kx)} = C(z) \eta \quad (3)$$

$$w = \frac{\partial \Phi}{\partial z} = a S(z) e^{i(\omega t - kx)} = iS(z) \eta \quad (4)$$

avec $S(z) = \omega \frac{\sinh[k(z+h)]}{\sinh(kh)}$. Le champ de pression est donné par :

$$p + \rho g z = -\rho \frac{\partial \Phi}{\partial t} = \frac{\rho \omega}{k} C(z) \eta \quad (5)$$

L'énergie moyenne par unité de surface $dxdy$ est $E = \rho g a^2 / 2$, le flux moyen d'énergie E_t à travers le plan xOy est donné par $E_t = EC_g$ où $C_g = \partial \omega / \partial k$ est la vitesse de groupe. En supposant que l'on dispose des mesures $u^{(m)} = |u| e^{i\varphi_u}$, $w^{(m)} = |w| e^{i\varphi_w}$ à la profondeur z , et $p^{(m)} = |p| e^{i\varphi_p}$ à la profondeur z_p , pour une abscisse x fixée, l'amplitude a peut donc être calculée avec l'une de ces trois données :

$$a = \frac{|u|}{C(z)} = \frac{|w|}{S(z)} = \frac{k}{\rho \omega} \frac{|p|}{C(z_p)} \quad (6)$$

Si la pression mesurée est donnée en mètres par l'appareil, alors $p^{(m)} = |p| / \rho g$ et $|p| = \rho g |p^{(m)}|$. Un seul des trois paramètres suffit pour déterminer l'amplitude a .

2.2 Onde partiellement stationnaire

Pour une houle partiellement stationnaire, la déformée de la surface libre peut s'écrire

$$\begin{aligned} \eta(x, t) &= -ia e^{i(\omega t - kx)} - ib e^{i(\omega t + kx + \varphi)} \\ &= \eta_i(x, t) + \eta_r(x, t) \end{aligned} \quad (7)$$

où η_i et η_r correspondent respectivement aux ondes incidente et réfléchie. Dans ce cas, les composantes $u(x, z, t)$ et $w(x, z, t)$ de la vitesse et la pression $p(x, z, t)$, à une profondeur z sont données par (en notation complexe)

$$u = C(z) [\eta_i - \eta_r] \quad (8)$$

$$w = iS(z) [\eta_i + \eta_r] \quad (9)$$

$$p + \rho g z = \frac{\rho \omega}{k} C(z) [\eta_i + \eta_r] \quad (10)$$

2.2.1 Mesures synchrones de vitesses et de pression en un point donné d'abscisse x

Des instruments permettant les mesures simultanées de vitesse horizontale et de pression [1] ou de la vitesse verticale (vélocimètre 3D, [2]) peuvent être utilisés pour la mesure de la réflexion. On remarque cependant que les équations (9) et (10) sont redondantes pour le calcul de a et b . En utilisant $u^{(m)} = |u| e^{i\varphi_u}$ et $w^{(m)} = |w| e^{i\varphi_w}$, on peut écrire :

$$|u| e^{i\varphi_u} = C(z) [-ia e^{i(\omega t - kx)} + ib e^{i(\omega t + kx + \varphi)}] \quad (11)$$

$$|w| e^{i\varphi_w} = iS(z) [-ia e^{i(\omega t - kx)} - ib e^{i(\omega t + kx + \varphi)}] \quad (12)$$

En prenant le module de l'expression obtenue en ajoutant l'équation (11) multipliée par $S(z)$ et l'équation (12) multipliée par $-iC(z)$, on obtient

$$a = \frac{1}{2} \left[\frac{|u|^2}{C^2(z)} + \frac{|w|^2}{S^2(z)} + \frac{2|u||w|}{C(z)S(z)} \sin(\varphi_w - \varphi_u) \right]^{\frac{1}{2}} \quad (13)$$

en multipliant cette fois l'équation (12) par $iC(z)$, on obtient

$$b = \frac{1}{2} \left[\frac{|u|^2}{C^2(z)} + \frac{|w|^2}{S^2(z)} - \frac{2|u||w|}{C(z)S(z)} \sin(\varphi_w - \varphi_u) \right]^{\frac{1}{2}} \quad (14)$$

En utilisant $u^{(m)} = |u| e^{i\varphi_u}$ (profondeur z) et $p^{(m)} = |p| e^{i\varphi_p}$ (profondeur z_p), on obtient par un calcul similaire

$$\begin{aligned} a &= \frac{1}{2} \left[\frac{|u|^2}{C^2(z)} + \frac{k^2}{\rho^2 \omega^2} \frac{|p|^2}{C^2(z_p)} \right. \\ &\quad \left. + \frac{2|u||p|}{C(z)C(z_p)} \frac{k}{\rho \omega} \sin(\varphi_p - \varphi_u) \right]^{\frac{1}{2}} \end{aligned} \quad (15)$$

$$\begin{aligned} b &= \frac{1}{2} \left[\frac{|u|^2}{C^2(z)} + \frac{k^2}{\rho^2 \omega^2} \frac{|p|^2}{C^2(z_p)} \right. \\ &\quad \left. - \frac{2|u||p|}{C(z)C(z_p)} \frac{k}{\rho \omega} \sin(\varphi_p - \varphi_u) \right]^{\frac{1}{2}} \end{aligned} \quad (16)$$

On peut noter que pour des ondes d'incidence oblique, une hypothèse doit être faite sur la direction de l'onde incidence et/ou sur l'angle entre ondes incidente et réfléchie (voir par exemple [1-3]).

2.2.2 Mesures synchrones de pressions en des points donnés d'abscisses différentes

Après transformée de Fourier des données de pression mesurées aux positions x_n , et à la profondeur z , l'amplitude « mesurée » pour la fréquence $f = 2\pi\omega$ peut être écrite en fonction de la pression mesurée $p^{(m)}$ à cette même abscisse selon

$$\eta_n^{(m)} = \frac{k}{\rho \omega C(z_p)} p^{(m)} = A_n e^{i\varphi_n} \quad (17)$$

Si on considère 2 sondes respectivement en x_1 et x_2 , la différence de phase entre les sondes est donnée par $\Delta = k(x_2 - x_1)$ avec k le vecteur d'onde dans cette direction. Si on écrit $\varphi_2 = \varphi_1 + \delta$, et $\eta = \eta_1^{(m)}$ pour $x = x_1$, $\eta = \eta_2^{(m)}$ pour $x = x_2$, on obtient les coefficients des ondes incidente et réfléchie

$$a = \frac{1}{2|\sin \Delta|} [A_1^2 + A_2^2 - 2A_1 A_2 \cos(\delta + \Delta)]^{\frac{1}{2}} \quad (18)$$

$$b = \frac{1}{2|\sin \Delta|} [A_1^2 + A_2^2 - 2A_1 A_2 \cos(\delta - \Delta)]^{\frac{1}{2}} \quad (19)$$

Si on considère 3 sondes respectivement en x_1 , x_2 et x_3 , on définit $\Delta_n = k(x_n - x_1)$, et $\varphi_n = \varphi_1 + \delta_n$, $n = 1, 2, 3$, les modules des amplitudes a et b sont données par Goda et al. (1976) [4], Rey et al. (2002) [5] :

$$|a| = \left| \frac{s_2 s_3 - 3s_4}{s_5} \right|, \quad |b| = \left| \frac{s_1 s_4 - 3s_3}{s_5} \right| \quad (20)$$

où

$$\begin{aligned} s_1 &= \sum_{n=1}^3 e^{-2i\Delta_n}, & s_2 &= \sum_{n=1}^3 e^{2i\Delta_n}, & s_3 &= \sum_{n=1}^3 e^{-i(\Delta_n + \varphi_n)}, \\ s_4 &= \sum_{n=1}^3 e^{i(\Delta_n + \varphi_n)}, & s_5 &= s_1 s_2 - 9 \end{aligned} \quad (21)$$

Le coefficient de réflexion est alors défini par $R = |b/a|$.

2.3 Houles réelles

Les états de mer réels sont souvent considérés comme des états aléatoires et les quantités utilisées pour décrire ces états de mer sont par exemple la hauteur moyenne des vagues, les hauteurs et périodes significatives, etc. Ces paramètres sont calculés à partir d'analyses statistiques de périodogrammes ou de spectres respectivement pour les domaines temporel et fréquentiel. Nous utilisons ici la méthode couramment utilisée basée sur l'analyse de Fourier du signal (analyse spectrale), elle suppose une représentation des houles réelles par une superposition de houles d'Airy (approximation linéaire). Les vitesses pour chacune des composantes spectrales sont $u^{(m)} = |u| e^{i\varphi_u}$, $v^{(m)} = |v| e^{i\varphi_v}$, $w^{(m)} = |w| e^{i\varphi_w}$. Elles sont calculées par transformée de Fourier rapide (FFT). Pour chaque composante spectrale de fréquence f , on calcule la direction de l'onde et l'intensité de la vitesse horizontale u_h

$$\theta(f) = \arctan \left(\frac{|v|}{|u|} \right) \text{ si } |u| \neq 0 \text{ et } \theta = \frac{\pi}{2} \text{ si } |u| = 0 \quad (22)$$

$$|u_h|^2 = |u|^2 + |v|^2 \quad (23)$$

Le spectre directionnel $E_d(f, \theta) = S(f)D(\theta, f)$ dépend de la fréquence en particulier par profondeur finie. Nous nous limitons à la direction de propagation moyenne $\theta(f)$ pour estimer $D(\theta, f)$. En supposant que la pente du fond est faible, l'approximation onde plane peut être appliquée. Le spectre énergétique basé sur une onde propagative ou partiellement réfléchie peut être calculé en utilisant les formules présentées dans les sections 2.1 et 2.2. Les spectres énergétiques montrés dans la section suivante ont été lissés par une moyenne sur les fréquences.

3 Applications

L'instrumentation classique donne des informations soit sur les déplacements de la surface libre (déformation

de la surface libre et accélérations horizontales pour les bouées en pilonnement-roulis), soit sur le mouvement dans le fluide (vitesses et pression). Les instruments peuvent être utilisés de façon indépendante ou synchrone, selon la quantité d'informations requises et les contraintes expérimentales. Les bouées multi-directionnelles sont équipées d'accéléromètres tri-dimensionnels. Après double intégration des signaux, le spectre énergétique peut être déduit de la composante verticale, tandis que les composantes horizontales permettent de déterminer la direction principale de la houle (à π près) et sa répartition angulaire. En eau peu profonde, on utilise plutôt des capteurs de pression. Des instruments plus récents, comme l'ADV (vélocimètre acoustique doppler) ou l'ADCP (profileur acoustique doppler), ou le S4 (de principe basé sur la mesure des vitesses à partir de la déformation d'un champ magnétique) sont utilisés en zones côtière et littorale pour les mesures de vitesses (et de pression). Pour les houles multi-directionnelles, souvent observées en zone littorale, on peut donc s'attendre à des données plus précises concernant les répartitions angulaires, à partir des instruments de mesures des vitesses horizontales. En eau peu profonde ou pour les expériences en laboratoire, les calculs de directions peuvent être facilités par l'utilisation de réseaux de capteurs (sondes à houle, capteurs de pression). Les deux exemples présentés ici ont pour but d'illustrer la capacité d'ADV et S4, et des capteurs de pression à mesurer des houles partiellement stationnaires in situ.

3.1 Campagnes expérimentales de Carqueiranne

Ces campagnes de mesures ont été effectuées avec l'entreprise Thetis en juin 2001 et mai 2002 [6]. Elles ont montré un bon accord pour les données significatives de houle basées sur des ondes progressives [6]. L'ADV, disposé sur un support immergé par 9,65 m de fond, mesurerait les vitesses horizontales à une profondeur $z = 8,70$ m et la pression à la profondeur $z_p = 9,20$ m de fond. La fréquence d'acquisition était de 8 Hz. On a représenté sur la figure 1 le spectre énergétique obtenu à partir des mesures soit de la vitesse horizontale, soit de la vitesse verticale, soit de la pression. On observe que les résultats sont très similaires pour la vitesse horizontale et la pression. Le résultat calculé à partir de la vitesse verticale est très bruité.

Ceci est dû au fait que l'appareil est quasiment au fond, ce qui correspond à une vitesse verticale très faible d'après la condition d'imperméabilité, vitesse en outre très bruitée à cause des perturbations apportées par la présence de l'appareil et de son support. On a ensuite séparé à partir des données combinées de la vitesse horizontale et de la pression les composantes incidente et réfléchie de la houle. On observe sur la figure 2 que la houle est quasiment progressive (réflexion inférieure à 5 %), et on retrouve par conséquent la répartition énergétique présentée sur la figure 1 pour les calculs basés respectivement sur les données de vitesses horizontale et de pression. La figure 3 montre la direction de propagation

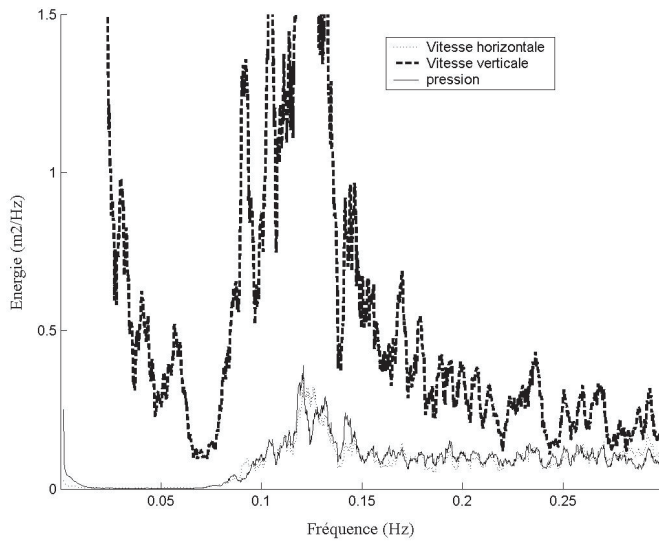


Fig. 1. Spectre d'énergie, calcul dans l'hypothèse d'une houle progressive.

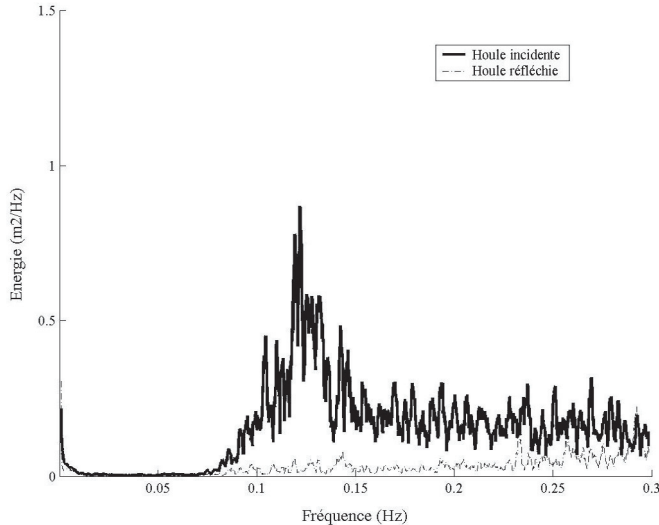


Fig. 2. Spectre d'énergie, calcul dans l'hypothèse d'une houle partiellement stationnaire.

en fonction de la fréquence, elle correspond à une houle de direction ouest sud-ouest. Notons que l'algorithme de calcul basé sur une houle partiellement stationnaire permet de lever l'indétermination d'un angle π sur le sens de propagation. Cette information peut s'avérer utile pour des zones où ni les données climatiques de vent, ni la configuration du site ne permettent d'éliminer un des deux sens de propagation.

3.2 Campagne expérimentale de Sète

Des expériences ont été menées sur la plage à barres de Sète durant un mois en novembre 2000 dans le but d'étudier les effets de la houle sur la formation et la migration des barres sédimentaires sous-marines [7]. Trois instruments S4 étaient disposés respectivement au niveau

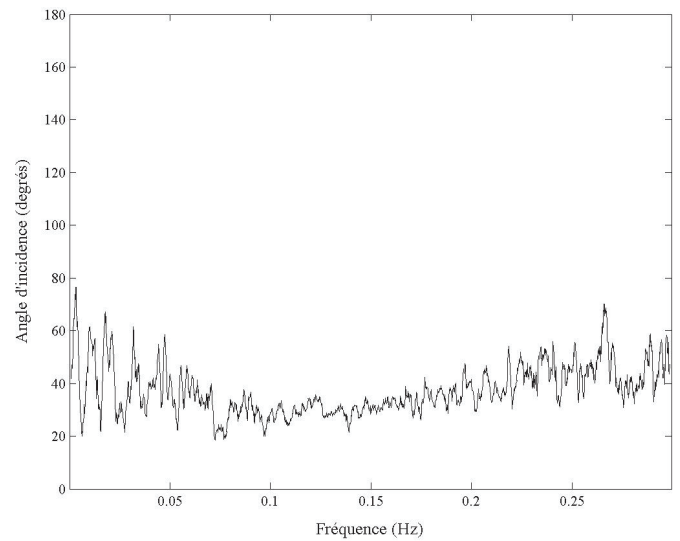


Fig. 3. Direction de propagation de la houle incidente en fonction de la fréquence.

de la fosse interne, de la fosse externe, et au large de la deuxième barre. Par ailleurs, une série de cinq capteurs de pression, distants d'environ 10 m les uns des autres, était alignée dans la direction perpendiculaire à la côte, au niveau du sommet de la barre interne. Les détails d'expériences sont présentés dans [8]. Nous nous limitons ici à des résultats significatifs des possibilités des instruments à mesurer des houles partiellement réfléchies.

Lors d'épisodes de tempêtes, on a pu observer [3] que la plage est dissipative et que la houle est progressive. À titre d'exemple, on a représenté sur les figures 4 et 5 les spectres d'énergies à partir des données de vitesse horizontale et de pression du S4 situé le plus au large par 6 m de fond. On observe sur la figure 4 des données de répartition d'énergie à partir des calculs basés sur des ondes progressives similaires, que ce soit à partir des données de vitesse ou de pression. Le calcul basé sur une onde partiellement stationnaire et présenté sur la figure 5 confirme la répartition spectrale de la figure 4, toute l'énergie étant transportée par l'onde incidente.

Nous avons ensuite étudié les spectres pour un épisode de calme relatif, caractérisé par la présence d'ondes assez longues de faible amplitude. Les données des trois S4 s'accordent à montrer une composante réfléchie notable, et à peu près identique pour les trois S4, et qui est attribuée à une réflexion par le haut de plage [3]. À titre d'exemple, on a représenté sur les figures 6 et 7 les résultats basés sur des ondes partiellement stationnaires, respectivement pour le S4 le plus au large et pour les trois capteurs de pression les plus près de la plage, distants respectivement de 8,5 et 10,5 m.

On observe une réflexion de l'ordre de 30 %, ce qui est assez conséquent pour le S4, celle mesurée à partir des capteurs de pression est cependant plus faible, de l'ordre de 15 %, mais non négligeable. Ceci peut s'expliquer par des mesures en des zones différentes du site d'étude, dont la bathymétrie présente un aspect tridimensionnel.

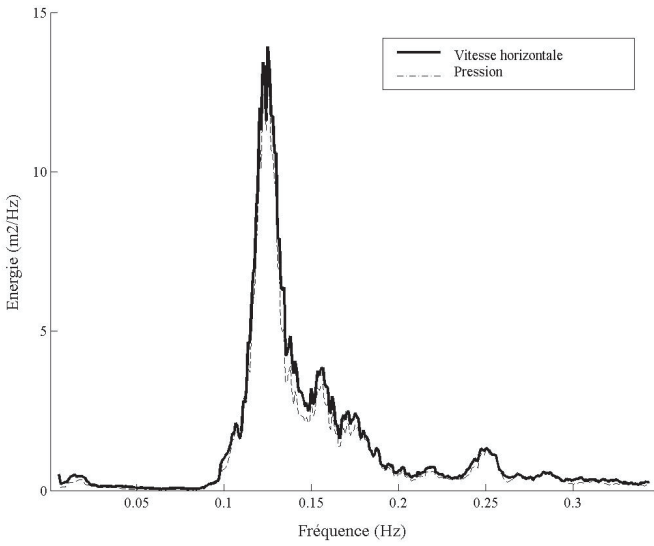


Fig. 4. Spectre d'énergie, épisode de tempête, houle progressive.

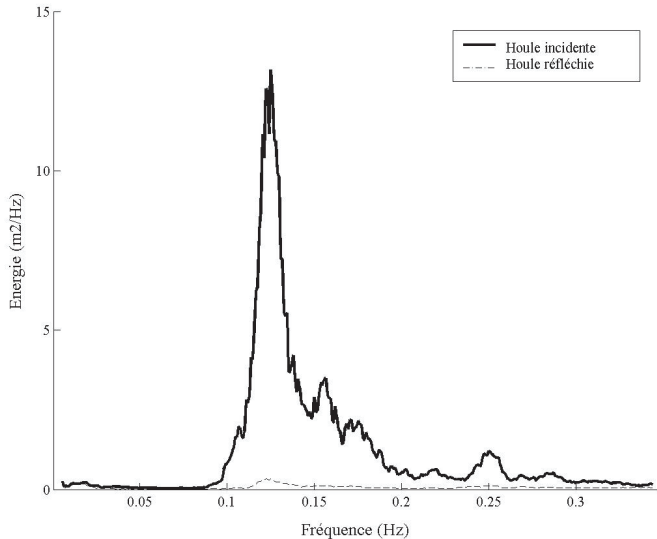


Fig. 5. Spectre d'énergie, épisode de tempête, houle partiellement stationnaire.

4 Conclusions

Les études des houles en zone littorale présentent un intérêt important pour la compréhension de la dynamique littorale, avec en particulier les problèmes d'érosion des plages. De façon plus appliquée, la connaissance de l'hydrodynamique est indispensable pour un dimensionnement adéquat des structures côtières, et les études d'impact d'ouvrage sur l'équilibre dynamique du littoral. Les données de houles sont primordiales, tant pour leur action directe sur les ouvrages ou le fond que pour les courants et le transport sédimentaire associé qu'elles induisent.

À l'heure actuelle, et en complément des modèles numériques développés, les mesures sont toujours autant nécessaires et les nouvelles techniques instrumentales permettent d'obtenir un nombre d'informations de

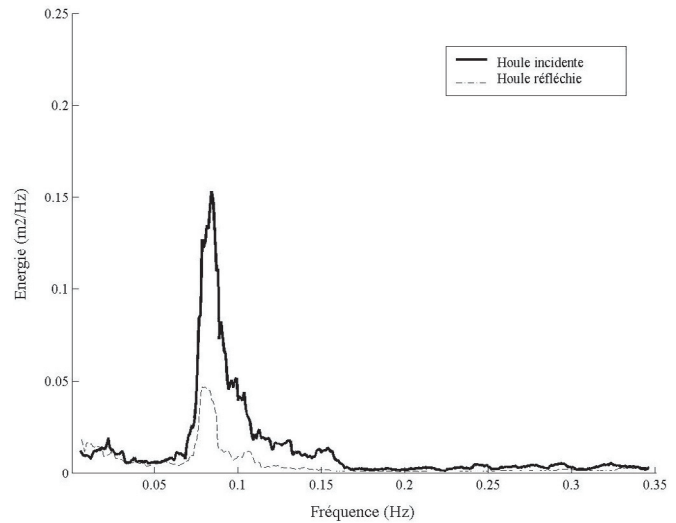


Fig. 6. Spectre d'énergie (S4), épisode de calme relatif, houle partiellement stationnaire.

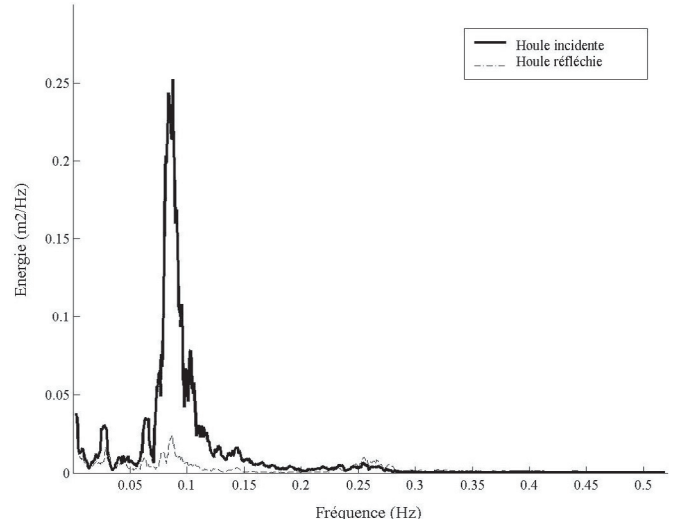


Fig. 7. Spectre d'énergie (capteurs de pression), épisode de calme relatif, houle partiellement stationnaire.

plus en plus important. Nous avons montré dans ce travail que le caractère partiellement stationnaire des houles réelles peut être quantifié, ce qui présente un intérêt particulier pour l'étude de plages réflectives ou d'agitation au voisinage de structures. L'utilisation d'appareils de mesures profileurs de vitesses pour des données plus complètes de courants, de houles ainsi que de turbulence sont envisagées à court terme en complément des appareils présentés.

Remerciements. Les auteurs remercient la Société Thétis SA pour les expériences menées à Carqueiranne dans le cadre du travail de thèse de Anne Meuret (co-financement Région PACA – Société Thétis). La campagne expérimentale de Sète a été menée dans le cadre du Programme National PNEC ART 7. Les auteurs remercient son support financier et les participants à la campagne.

Références

- [1] T.L. Walton Jr, Wave reflection from natural beaches, *Ocean Engineering* 19 (1992) 239–258
- [2] D. Drevard, A. Meuret, V. Rey, J. Piazzola, A. Dolle, Partially reflected waves measurements using Acoustic Doppler Velocimeter (ADV), Thirteenth International Offshore and Polar Engineering Conference ISOPE'03, Honolulu, Hawaii, 25–31 May 2003
- [3] R. Certain, S. Meulé, V. Rey, C. Pinazo, Swell transformation on a microtidal barred beach (Sète, France), 2004, soumis à *J. Marine Systems*
- [4] Y. Goda, Y. Suzuki, Estimation of incident and reflected waves in random wave experiments, *Proceedings of the 15th Coastal Engineering Conference* 1 (1976) 828–845
- [5] V. Rey, R. Capobianco, C. Dulou, Wave scattering by a submerged plate in presence of a steady uniform current, *Coastal Engineering* 47 (2002) 27–34
- [6] A. Meuret, Étude d'un système PUVW pour les mesures de houle et de turbulence en milieu littoral et côtier, Thèse de Doctorat, Univ. du Sud Toulon-Var, 2004, p. 170
- [7] R. Certain, J.P. Barusseau, R. Capobianco, A. Meuret, V. Rey, C. Dulou, A. Stepanian, F. Levoy, H. Howa, Bottom and shoreline evolutions under wave actions at a french Mediterranean site: The beach of Sète, MEDCOAST 2001, Hammamet, Tunisie, October 2001.
- [8] R. Certain, Morphodynamique d'une côte sableuse microtidale à barres : le golfe du Lion (Languedoc-Roussillon), Thèse de Doctorat, Univ. Perpignan, 209 p., 2002

Experiments on cross-shore equilibrium beach profiles and beach morphology

Eric BARTHELEMY¹, Raphaël CERTAIN², Florent GRASSO¹, Hervé MICHALLET¹

Cross-shore morphology and morphological evolutions of sandy beaches is paramount to nourishment techniques, even though cross-shore sediment fluxes are usually an order of magnitude smaller than longshore fluxes. Moreover cross-shore fluxes can be in parts of the profile directed on-shore and others off-shore which tremendously complicates the analysis and the predictive capacity of engineering tools. The direction of the cross-shore fluxes is a key point for predictive tools and is closely related to the non-linear characteristics of the incoming waves such as asymmetry and skewness (Silva et al., 2006). This complexity is very difficult to reproduce with models and physical modelling becomes then an interesting alternative (Dette et al., 2002; Wang et al., 2002; Hurther et al., 2007; Michallet et al., 2007).

Our experiments were carried out in a flume 36 m long and 55 cm wide equipped with a piston wave generator. Our aim was to mimic a beach such as that of the Lido beach in Sète (Certain et al., 2005). The beach profile (BT166700, see Figure 1) yields a closure depth at roughly -5m which locates it at 400 m from the shoreline. A geometrical downscaling of 1/10 will enable to reproduce such beach profile in a flume. The still water depth is then 55.3 cm. The mean overall slope is approximately 1:40. The sloping bottom consists of a loose material of low density (1.19 g cm^{-3}) with a median diameter $d_{50}=0.6 \text{ mm}$. In the experiments, the Froude number, the Shields number in the shoaling part and the Rouse number in the breaking zone (ratio of turbulent agitation to the settling velocity of the sediment) are of the same magnitude as on the beach of Sète. Time scale is then roughly 1/3.

Irregular waves are generated according to a JONSWAP spectrum (peak enhancement factor $\gamma=3.3$). For each simulation, we check that these waves conform to the expected spectrum and that they follow a Rayleigh distribution at 2 m downstream of the wave maker. Twelve wave gages mounted on trolleys measure instantaneous water elevations. Records are at least 30 minutes long in order to achieve statistical convergence. Bottom profiles are recorded in between wave series.

Our experiments clearly show that equilibrium beach profiles are obtained by imposing a given wave climate for a sufficient time lapse (dashed line in Figure 2). These profiles are doubly convex (Black et al., 2002; Wang et al., 2002) with the upper convex part close to a Dean type equilibrium profile.

Erosion and accretion experimental scenarios are also observed. Accretional sequences correspond to onshore migrating asymmetric bars (steep shore facing front; see Figure 2). In these sequences the undertow is deemed to be very weak allowing on-shore sand transport to dominate.

¹ LEGI, BP53, 38041 Grenoble cedex 9, France; email: eric.barthelemy@hmg.inpg.fr, florent.grasso@hmg.inpg.fr, herve.michallet@hmg.inpg.fr; fax: 33 4 76 82 52 71

² IMAGES EA4218, University of Perpignan, 52 av. Alduy 66000 Perpignan Cedex, France; email: certain@univ-perp.fr; fax: 33 4 68 66 17 47

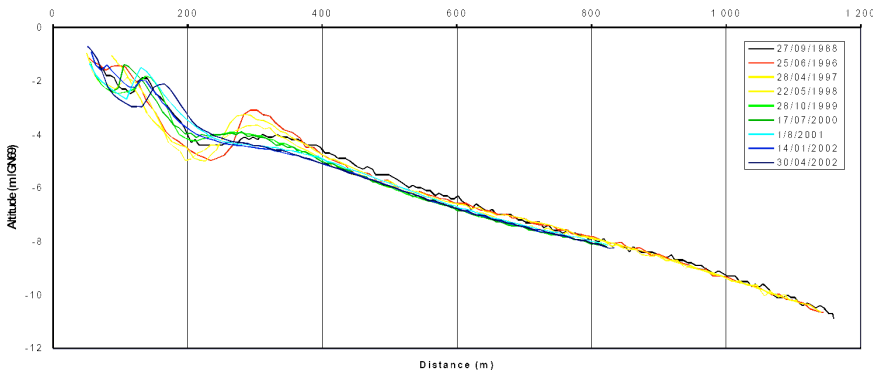


Figure 1 – BT166700 beach profile (Sète) and 6 years evolutions. The shoreline is located at (0, 0).

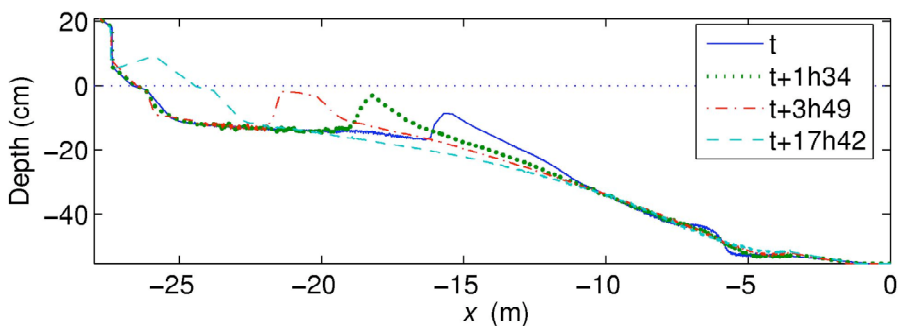


Figure 2 – Transient bottom profiles with a 2s period, 11 cm significant wave height and the resulting final equilibrium bottom profile (--).

Acknowledgements

This work was financially supported by the French program LITEAU-II and the European program INTERREGIIc-Beachmed-e (GESA). The technical support of J.-M. Barnoud is gratefully acknowledged.

References

- BLACK, K.P., GORMAN, R.M., BRYAN, K.R., 2002. Bars formed by horizontal diffusion of suspended sediment. *Coastal Engineering*, 47(1), 53-75.
- CERTAIN, R.; MEULÉ, S.; REY, V. AND PINAZO, C., 2005. Wave transformation on a microtidal barred beach (Sète, France), *J. Marine Systems*, 38, 19-34.
- DETTE, H.H.; LARSON, M.; MURPHY, J.; NEWE, J.; PETERS, K.; RENIERS, A. AND STEETZEL, H., 2002. Application of prototype flume tests for beach nourishment. *Coastal Eng.*, 47, 137–177.
- HURTHER, D.; MICHALLET, H. AND GONDRA, X., 2007. Turbulent measurements in the surf zone suspension. *J. Coastal Res.*, in press.
- MICHALLET H., GRASSO F. & BARTHELEMY E. (2007) Long waves and beach evolution profiles. *J. Coastal Res.*, in press.
- SILVA, P. A., TEMPERVILLE, A. & SEABRA SANTOS, F., 2006. Sand transport under combined current and wave conditions: a semi-unsteady, practical model. *Coastal Engineering*, 53, 897 – 913.
- WANG, P.; EBERSOLE, B.A.; SMITH, E.R. and JOHNSON, B.D., 2002. Temporal and spatial variations of surf-zone currents and suspended sediment concentration, *Coastal Eng.*, 46, 175-211.

CONCEPTUAL MODELLING OF STRAIGHT SAND BARS MORPHODYNAMICS FOR A MICROTIDAL BEACH (GULF OF LIONS, FRANCE)

Raphaël Certain¹ and Jean-Paul Barusseau¹

The sandy microtidal wave-dominated littoral of Sète, with its barred shoreface, shows that the morphological evolution of the sedimentary bars can be synthesized according to two conceptual models, in reaction to hydrodynamic variability. (1) The model of "oscillation around a position of equilibrium" (O.P.E) defines the usual mode of behaviour of the bars, with an alternation of shoreward and seaward movements. (2) The model of "Net Offshore Migration" (N.O.M) points to the tendency to a retreat of the bars under the effect of paroxysmal events (storms with a 20 to 50 yrs return time) being a prelude to their degeneration. A few years after, the standard pattern is restored. These results are compared with those described in the literature.

INTRODUCTION

Nearshore bars are usual features along the shore. Current convergence in the surf zone causes sedimentary accumulations, which result in bar formation. Observations and results for bar dynamics and mobility studies are abundant for conventional bathymetric measurements (Davis and Ethington 1976 ; Hayes 1972 ; Winant et al. 1975 ; Short 1979 ; Sallenger et al. 1985 ; Lippman et al. 1993 ; Kroon 1994 ; Thornton 1998) or, more recently, for time exposure video imagery (Konicki and Holman 2000 ; Ruessink et al. 2000 ; Kingston et al. 2000 ; Van Enckevort and Ruessink 2003 ; Shand and Bailey 1999 ; Shand et al. 1999, 2001), in microtidal or mesotidal environments. New technologies and long time series data from 1963 in the Netherlands allow a better understanding of nearshore bar morphodynamics and lead to the formulation of conceptual models of sedimentary bar morphological evolution (Lippman et al. 1993 ; Ruessink and Kroon 1994 ; Wijnberg 1995).

Are these models valid in other sites, in particular when data sets are shorter? To answer this question, the study of the site of Sète (France) on the lido of the Thau lagoon, started in 1988, is described in this article. We describe here the main results obtained for this microtidal site (S.H.O.M. 2003), in a wave coast dominated environment.

Straight bars are the most studied (Goldsmith et al. 1982). They can be found on shorefaces with a grain size between 0.1 and 0.6 mm and a bottom slope of 0.5 % to 6%. Bar are about 1 or 2 meters high and their volumes around one or several hundred cubic meters per meter alongshore (m^3/m). Sand bars

¹ Université de Perpignan, Laboratoire d'Etude des Géo-Environnements Marins, 52 av Paul Alduy, 66860 Perpignan, France (certain@univ-perp.fr)

volumes are generally equal for inner and outer bar, sometimes higher for the outer bar. Usually, the nearshore bar dynamics depend on hydrodynamic conditions and bars are normally shifting shoreward during low waves periods and seaward during storm events (Ostrowski et al. 1990). A strong correlation exists between inner bar evolution and shoreline migration (Birkemeier 1984). The bar could aggregate to the shore, which consequently migrates seaward. Bar mean speed migration is about 0.5 m/day but maximum "instantaneous" values may be considerably larger, e.g. 20 m/day in Duck (USA) after extreme storms ($H_s > 4$ m) (Larson and Kraus 1992, 1994 ; Birkemeier 1984 ; Mason et al. 1984). Multi-bar systems are therefore more complicated (Sunamura 1988). A dependence exists between bars according to their position and incident energy. For example the outer bar could be inactive during long periods of low wave conditions (months to years) whereas the inner bar keeps moving (Lippmann et al. 1993 ; Southgate and Moller 1998 ; Pruszack et al. 1997). After these stable periods, the outer bar could quickly move offshore during an extreme storm event. So that bars can degenerate and disappear (Lippman et al. 1993). After this disappearance, the inner bar, exposed to the swell, moves quickly seaward nourished by the sediment of the old outer bar (Wijnberg 1995) and gradually becomes a new outer bar. Cycle repeat itself. This behaviour is also described in mesotidal environments, called « *Net Offshore Migration* » (NOM) (Wijnberg 1995 ; Ruessink and Kroon 1994). To sum up, the bar system in microtidal wave coast dominated environment is mainly influenced by extreme storm events.

The purpose of this article is to study the nearshore bar morphological response to hydrodynamic forcing in the site of Sète. This work presents enough data to define morphological models and to compare them to those described in the literature. The field experiment and the methodology are described here below.

STUDY AREA

The whole study area is the Thau lagoon barrier in the Gulf of Lions in the south of France in the Mediterranean Sea near Sète (Fig. 1). The major part of the lido between Agde and Sète (Fig. 2) is affected by a strong to very strong erosion (C.E.P.R.E.L 1995). We focus then on the site of Sète is in the northern and the most eroded part of the Thau lagoon barrier. This studied site is five hundred meters wide and extends seven hundred meters offshore until the closure depth.

The backshore consists in an erosive dune, partially destroyed by a road. The beach is narrow (20 to 50 meters). The nearshore has a slope of one percent and the sandy sediment grain size decreases from 320 micrometer onshore to one 130 micrometer offshore. The shoreface is composed of a system of two straight bars and troughs. The distance between the inner bar crest and the shore is from about 50 m. to 150 m. and 170 m. to 270 m. for the outer bar. Bars are linear and the wave-dominated beach may be classified between intermediate

barred and dissipative barred (Ω value around 6) in conformity with the conceptual beach model of Masselink and Short (1993) (see also Short and Aagard 1993; Gourlay 1968).

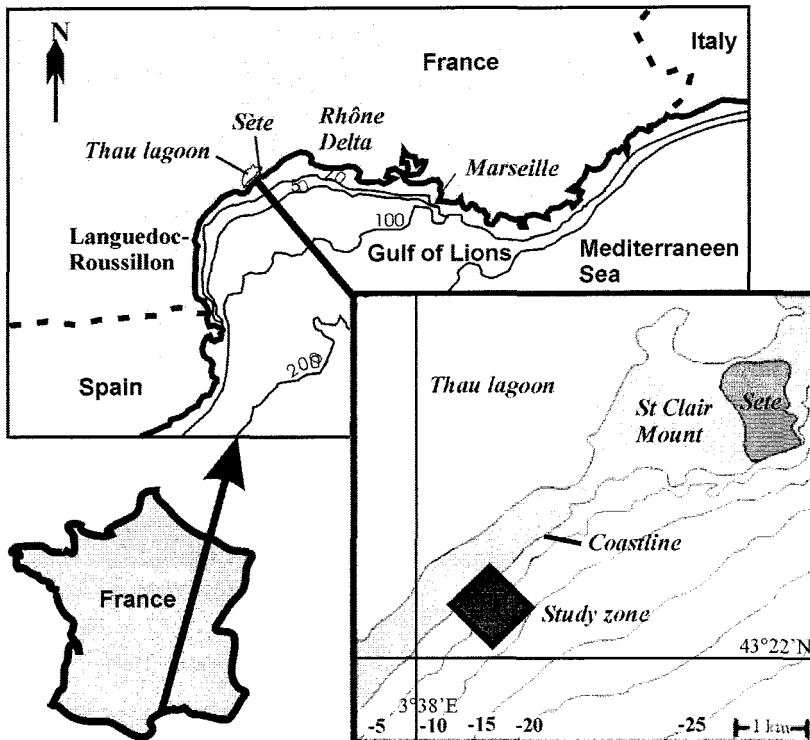


Figure 1. Location of the study zone, Sète, Mediterranean Sea, Gulf of Lions, France.

The most frequent wind on the area is offshore but strong onshore winds (NE to SE) can generate in winter storms from E to SE directions. The strongest waves approach the coast from E inducing a dominant littoral drift towards the SW, evaluate between 20 to 40000 meters cubic by year. Indeed, if the majority of the swells in the area has a mean significant height inferior to 1 m, there remain events of significant height higher than 4 m. We can note twelve of these events between 1989 and 2001, with an exceptional peak in December 1997 when the significant height reaches almost 7 m.

METHODOLOGY

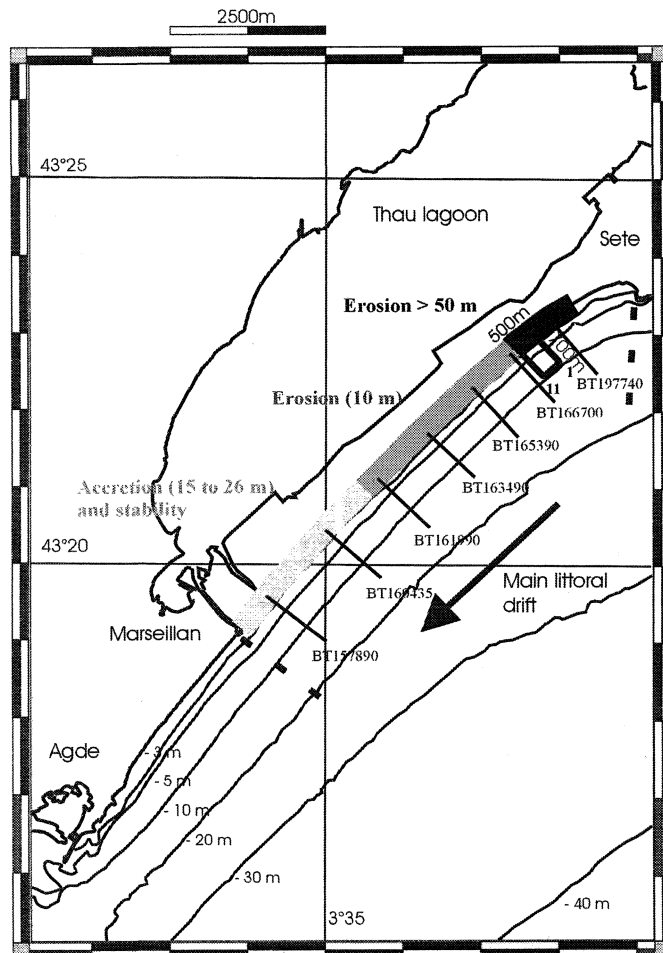


Figure 2 : Tendency of the Thau lagoon coastline evolution. Localization of the studied zone (delimited by the dotted lines), of the site of Sète and the topobathymetric profiles (noted BT) carried out by the SMNLR on the whole lido.

The morphological study of the shoreface of the Thau lagoon is based on seven bathymetric profiles carried out along the 16 km of coast from Sète to the Cap d'Agde by the "Service Maritime et de Navigation du Languedoc-Roussillon" (SMNLR) since mid 1980 (Fig. 2). The study focuses then on a reduced area north of the lido (called "site of Sète" in this article), where erosion is the strongest (Fig. 1 and 2). This site, smaller and only studied since 1989, has a stronger profile density with 11 crossshore profiles spaced out every 50 m. Observations from this site are easy to correlate with the SMNLR data base as

the northern SMNLR profiles frame the site (Fig. 2). The studied site is 500m wide and extends 700m offshore ; the area is covered by crossshore profiles characterizing the double-nearshore bar system resulting in 30 field numerical models.

Repeated bathymetric surveys were carried out with a Tritech 500 echo sounder connected to a computer, aboard a pneumatic boat. This type of sounder gives +/- 5 cm in vertical precision. Positioning was made by DGPS (Sercel), with 1m horizontal precision. The storage frequency measures one point every 1.25 m, at the operational speed of five nodes. The bathymetric survey before 1999 was done using a Fuso graphic sounder (same vertical precision) and an electromagnetic theodolite Geodimeter to carry out the horizontal positioning of the boat. The horizontal precision was ± 5 m with this equipment.

RESULTS

The evolutions observed on a large temporal and spatial scale (on the lido) and those more significant on the site of Sète lead to the definition of two successive evolutionary models which illustrate the bar morphodynamics during the measurement period.

The OPE model (Oscillation around a Position of Equilibrium)

This first model represents a mode of oscillation, well documented for the site of Sète (Certain and Barusseau 2005), which shows a retreat of the bars during storms and a shoreward movement during lower agitation. This model is also demonstrated at several rhythms. On one hand, the alternating response to the great phases of hydrodynamic forcing on a decadal behaviour and, on the other hand, onshore and offshore bar movements on a seasonal scale, particularly well illustrated for the inner bar.

The decadal behaviour of the system presents an equilibrium position. The bars take around it various configurations characterized by a stable geometry during long time periods (Fig. 3). The transition between each period results from storms with significant height higher than 4 meters. Thus, the outer bar oscillates slightly around an average position of balance to approximately 250 m of the shore, passing from a rectilinear to oblique or more sinuous configuration. Important volumes of sediment about several tens of thousands of m^3 are affected by these morphological changes (Certain 2002). We can see that during lower agitation conditions for a long time period (for example, during all of 1993) the outer bar moves slowly towards the shore, infilling the outer trough. However this episode did not involve any change in the global functioning of the nearshore zone: the outer bar, moving towards more exposed depths, returns to its initial position at the end of this event when the first big storm with significant height higher than four meters occurs.

We can also see a seasonal oscillation, well illustrated for the inner bar, the outer bar being poorly affected on this time scale (Fig. 4). Globally, during the weak energy seasons, i.e. in summer, the beach is enlarged and the inner bar approaches the shore because small waves generate onshore wave currents, bringing sediment shoreward. The bed-return flows ('undertow') are weak and don't take material offshore. The inner trough is filled and the coastline moves seaward. In autumn when conditions are more dynamic, the bed-return flows become active again and the inner trough grows after each storm. The offshore sediment exportation leads to a well developed inner bar construction. The winter equilibrium is thus established but the return to summer conditions creates the opposite effect.

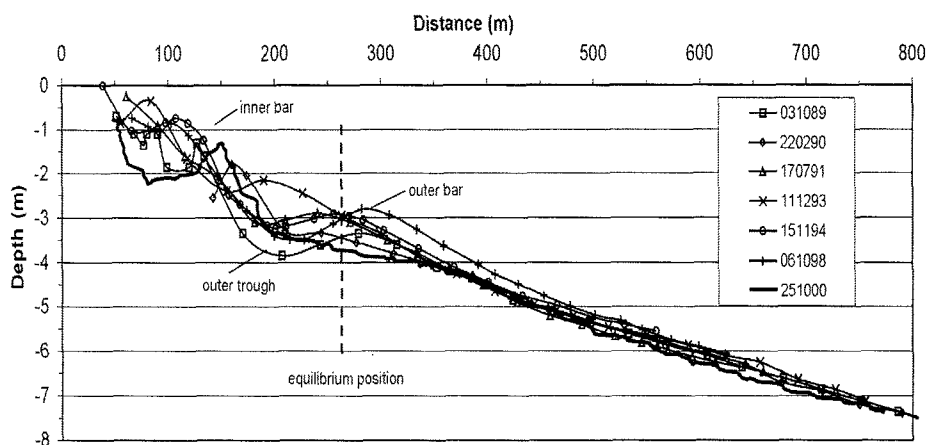


Figure 3. Bathymetric evolution of one profile from 1989 to 2000. Each phase of evolution is illustrated by a date.

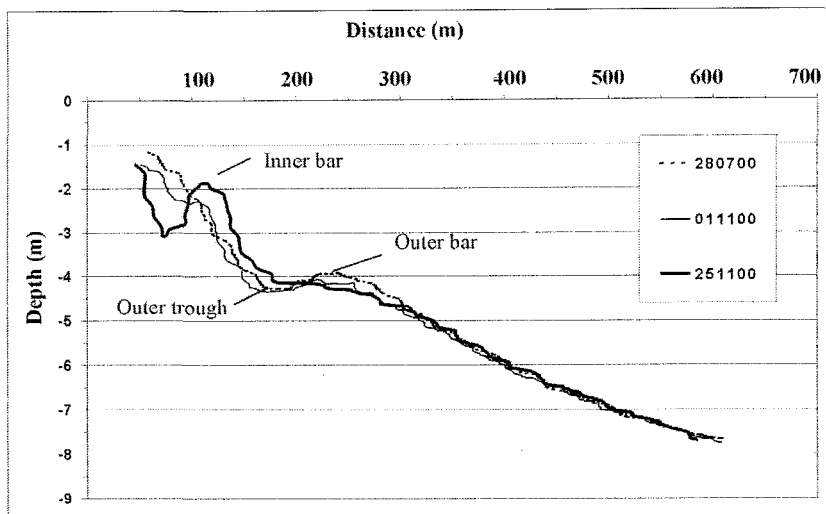


Figure 4. Evolution of the inner bar from a summer situation (28/07/2000), when the bar came to be joined with the shore, to a winter situation by digging of the inner trough and growing-up of the inner bar under the influence of the fall storms (25/11/2000).

The Net Offshore Migration model

The model O.P.E described previously can be strongly disturbed by exceptional storm events. This happened in Sète, during a singular event series in the 1995-96 winter period and during the December 1997 storm, with significant height that exceeded 7 m. The evolution model for the lido is called Net Offshore Migration (N.O.M) and implies an offshore movement and the disappearance of the outer bars (Ruessink and Kroon 1994; Winjberg 1995; Lippman et al. 1993; Shand 2003). From the initial equilibrium position and because of these exceptional storms, the outer bar strongly moves offshore (the retreat ranges between 70 and 90 meters on all the Sète data set) and decreases here between 0,3 and 1 m (Fig. 5). Then, instead of coming back shoreward (O.P.E model), the outer bar, under the lower wave action, loses sediment. This material goes to the inner bar under the wave asymmetry effect and the outer bar degenerates while dropping gradually (Wijnberg 1995). Its disappearance is observed within a few years (3 to 5, for example, between 1995 and 2000). After its gradual offshore disappearance, the inner bar replaced it, nourished by the recovered material (Wijnberg 1995). The inner bar, more exposed to storm effects, moves offshore and gradually reverts to the old outer bar position whereas a new inner bar is created near the shore. This complete replacement was however not yet apparent in Sète in 2000.

In a few years after the event release, the most usual configuration is restored and a second episode of oscillating of the bars around their position of balance (O.P.E. model) starts.

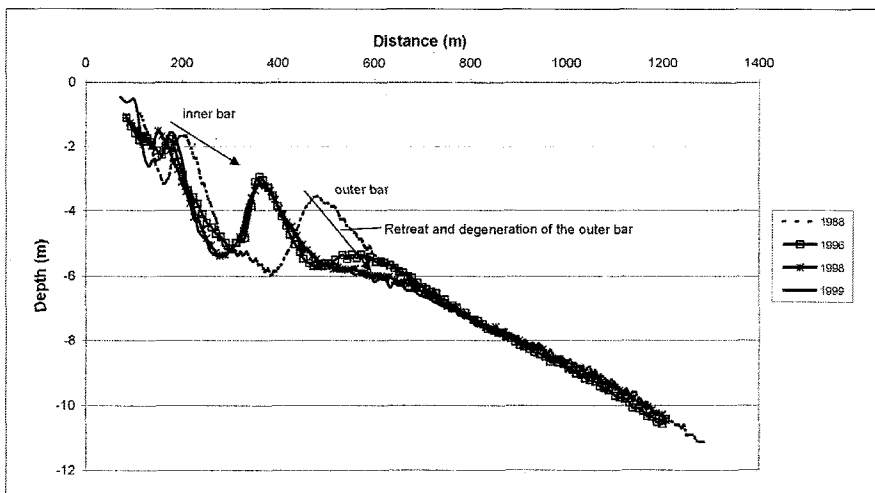


Figure 5. Synthesis of the bathymetric profile evolution in the south of the Thau lagoon.

DISCUSSION

The association of two successive evolution modes, highlighted in Sète, seems to justify the distinction of two original morphological models since they are not observed everywhere or they were not identified so clearly. Indeed, in a mesotidal environment, the study of the Holland coast (Wijnberg 1995; Ruessink and Kroon 1994) and of Wanganui in New-Zealand (Shand and Bailey 1999; Shand et al. 1999, 2001) seem to show the absence of the O.P.E model and a regular sequence of the N.O.M cycles over decades, over a longer period than recorded in Sète for this model. The bar offshore migration takes ten years then its degeneration a few years, without any causal hydrodynamic event and without an interruption in this pattern able to show any oscillation around a position of balance. On the other hand, on the North Atlantic American coast, in Duck, the two models are expressed but it seems that the authors didn't distinguish them clearly. Indeed, the beginning of the N.O.M model functioning corresponds well to a major hydrodynamic event (Larson and Kraus 1992, 1994 ; Birkemeier 1984 ; Mason et al. 1984), but the seasonal oscillation of the inner bar is expressed with a mobility much more important (Lippman et al. 1993 ; Southgate and Moller 1998). A second difference lies in the relative duration of

the successive phases of the models. We have seen that the N.O.M. model is active in Sète during some years, cut in a very short period of imbalance (a storm or a storm series) and a longer period of return to balance after disappearance of the outer bar. The O.P.E. functioning seems to correspond to a more important duration. So, in Sète, a cycle N.O.M+O.P.E from 20 to 25 years on the basis of the actual offshore speed of the inner bar (as at the end of 14 years of survey, the length of the process is not yet known) from the initial position post-N.O.M until the position of external balance. If we compare the speeds of each model and their succession, to what appears to be their equivalents on the American microtidal site of Duck, we see that the stability period of the outer bar is reduced (O.P.E), to 2 to 3 years, and its disappearance and its replacement by the inner bar (N.O.M) are very short, approximately one year (Larson and Kraus 1992, 1994; Birkemeier 1984; Mason et al. 1984). This more important mobility and the quick succession of the two models definitely result from the more dynamic conditions of agitation in the Atlantic than in the Mediterranean Sea.

It is clear that in the future, a better analysis of the hydrodynamic forcing will have to be undertaken to determine the precise effect of the major storms and the asymmetry of the waves in the outer bar migration and degeneration processes (Wijnberg 1995; Ruessink and Kroon 1994), as well as the possible role of the incidence of the swell and the inherited morphology. Perhaps the absence of release event for the N.O.M. model on the Dutch sites is explained, like underlined in Ruessink and Kroon (1994), by data that are not well adapted to the study of hydrodynamic forcing.

Transport and sedimentary dynamics, in particular during the outer bar degeneration deserve also a further study. The two models N.O.M-O.P.E were described as if all displacements were crossshore. However it is expected that the reality of a littoral drift component, which is not well illustrated for the processes described in this article, should also be taken into account.

It will also be necessary in the future to validate the existence of these models to other French coasts and in particular to try to identify them and explain the possible divergences in macrotidal environments, where they haven't yet been described (Stépanian 2002; Stépanian and Levoy 2002).

Lastly, within a more general long term scale framework, we can consider the influence of these models N.O.M-O.P.E, here defined as a decadal behaviour, on the overall evolution of littoral sandy prisms. The bar systems seem fixed at a definite distance from the shore during the phases of destruction and retreat of the prism (Barusseau et al. 1996 ; Tessier et al. 2000). Thus we can now logically question if this position of the bars is maintained by a simple translation of the bars during the O.P.E phases of oscillations or during the return in balance that follows the N.O.M.

CONCLUSION

The main results for the microtidal site of Sète show that the bar morphologic evolution can be synthesized according to two conceptual models in relation to hydrodynamic variability. The "oscillation around a position of equilibrium" model (O.P.E) traduces the usual behaviour of the bars, with retreat and successive shoreward displacement. Punctually this dynamic equilibrium can be strongly destabilized by one or more exceptional storms. A new episode starts then, called "Net Offshore Migration" (N.O.M), with the fast offshore migration of the outer bar, and its degeneration and replacement. A few years after the event release, the standard disposition is restored.

ACKNOWLEDGMENTS

We thank the PNEC program, and the researcher community of the ART 7 for their support. We have also to thank the divers, and in particular Michel Salvat, of the ARESMAR for their human and logistic help. The SMNLR and Météo-France to give us some data.

REFERENCES

- Barusseau, J.P., Akouango, E ., BA, M., Descamps, C. and Golf, A. 1996. Evidence for short-term retreat of the barrier shorelines. *Quaternary Science Reviews*, 15, 763-771.
- Birkemeier, W.A., 1984. Time scales of nearshore profiles changes, p. 1507-1521. *19th ICCE*, Houston, USA.
- CEPREL 1995. Schéma d'orientation pour la protection, la restauration et la gestion des plages du Languedoc-Roussillon. Région Languedoc-Roussillon Ceprel, 162 p.
- Certain, R. 2002. *Morphodynamique d'une côte sableuse microtidale à barres : le golfe du Lion (Languedoc – Roussillon)*. Unpublished thesis, Univ. Perpignan, 209 p., ann.
- Certain, R., and Barusseau, J.P. 2005. Conceptual modelling of sand bars morphodynamics for a microtidal beach (Sète, France). *Bull. Soc. géol. Fr.*, 2005, t. 176, n° 4, 343-354.
- Davis, R.A. and Ethington, R.L. 1976. Eds Beach and nearshore sedimentation. *Soc. Econ. Paleontologists Mineralogists Spec. Publ.*, 24, 187 p.
- Goldsmith, V., Bowman, D. and Kiley, K. 1982. Morphology and dynamics of crescentic bars. *18th ICCE*, Cape Town, South Africa, 941-953.
- Gourlay, M.R. 1968. *Beach and dune erosion tests*. Delft Hydraulics Laboratory, report n°M935/M936.
- Hayes, M.O. 1972. Forms of sediment accumulation in the beach zone in: waves on beaches and resulting sediment transport, Meyer, R.E., eds. *Academic Press.*, New York, 297-356.

- Kingston, K.S., Ruessink, B.G., Van Enckevort, I.M.G., and Davidson, M.A. 2000. Artificial neural network correction of remotely sensed sandbar location. *Marine Geology*, 169, 137-160.
- Konocki, K.M., and Holman, R.A. 2000. The statistics and kinematics of transverse sand bars on a open coast. *Marine Geology*, 169, 69-101.
- Kroon, A. 1994. Sediment transport and morphodynamics of the beach and neashore zone near Egmond, the Netherlands. *PhD thesis*. 273 p.
- Larson, M., and Kraus, N.C. 1992. Dynamics of longshore bars, p. 2219-2232. *23rd ICCE*, Venice, Italy.
- Larson, M., and Kraus, N.C. 1994. Temporal and spatial scales of beach profile change, Duck, North Carolina, USA. *Marine Geology*, 117, p. 75-94.
- Lippman, T.C., Holman, R.A., and Hataway, K.K. 1993. Episodic, nonstationary behaviour of double bar system at Duck, N.C., U.S.A., 1986-1991. *Journal of Coastal Research*, 15(SI), 49-75.
- Mason, C. et al, 1984. Duck82- a coastal storm processes experiment, p. 1913-1927, *19th ICCE*, Houston, USA.
- Masselink, G. and A. D. Short, 1993. The effect of tide range on beach morphodynamics: a conceptual model. *Journal of Coastal Research* 9: 785-800.
- Ostrowski, R., Pruszak, Z., and Zeidler, R.B. 1990. Multi-scale nearshore and beach changes, *22nd ICCE*, Delft, Netherlands, 2101-2116.
- Pruszak, Z., Rozynski, G. and Zeidler, R.B. 1997. Statistical properties of multiplebars, *Coastal Engineering*, 31, 263-280.
- Ruessink, B.G., and Kroon, A. 1994. The behaviour of a multiple bar system in the nearshore zone of Therschelling, The Netherlands 1965-1993. *Marine Geology*, vol. 121, p. 187-197.
- Ruessink, B.G., Van Enckevort, I.M.G, Kingston, K.S, and Davidson, M.A. 2000. Analysis of observed two and three -dimensional nearshore bar behaviour. *Marine Geology*, 169, 161-183.
- Sallenger, A.H., Holman, R.A. and Birkemeyer, W.A. 1985. Storm-induced response of a nearshore bar system. *Mar. Geol.*, 51, 63-76.
- Shand, R.D. and Bailey, D.G. 1999. A review of Net Offshore Migration with Photographic illustrations from Wanganui, New Zealand. *Journal of Coastal Research*, 15 (2), 365-378.
- Shand, R.D., Bailey, D.G. and Sheperd, M.J. 1999. An inter-site comparison of net offshore bar migration characteristics and environmental conditions. *Journal of coastal Research*, 15 (2), 365-378.
- Shand, R.D., Bailey, D.G. and Sheperd, M.J. 2001. Longshore realignment of shore parallel sand-bars at Wanganui, New Zealand. *Marine Geology*, 179, 147-161.
- S.H.O.M., 2003. *Tide Tables*, tome1, French harbors. Edition 2003.
- Short, A.D., 1979. Three dimensional beach stage model. *J. Geophys. Res.*, 80, 3838-3840.

- Short, A.D. and Aagaard, T. 1993. Single and multi-bar beach change models. *Journal of Coastal Research*, Special Issue 15, 141-157.
- Southgate, H.N., and Moller, I. 2000. Fractal properties of coastal profile evolution at Duck, NC, *Journal of Geophysical Research*, 115, 11489.
- Stépanian A. 2002. *Evolution morphodynamique d'une plage macrotidale à barres : Omaha Beach (Normandie)*. Unpublished thesis, Univ. De Caen, 231 p.
- Stépanian A. and Levoy F. 2003. Séquences d'évolution morphodynamique des barres intertidales d'une plage macrotidale : l'exemple d'Omaha Beach (Normandie, France). *Oceanologica Acta*, 26, 167-177.
- Sunamura, T., 1988. Beach morphologies and their change. In Horikawa, K. (ed.) *Nearshore Dynamics and Coastal Processes*, University of Tokyo Press, Tokyo, 136-166.
- Tessier B., Certain R., Barusseau J.P. et Henriet J.P. 2000. Historical evolution of the littoral prism of the Thau lagoon barrier (Sète, South-Est of France). Very high-resolution seismic investigation. – *C. R. Acad. Sci/ Earth and Planetary Sciences.*, Paris, 331, 709-716.
- Thornton, E.B., Swayne, J.L., and Dingler, J.R. 1998. Small-scale morphology across the surf zone, *Marine Geology*, 145 (3-4), 173-196.
- Van Enckevort, I.M.J. and Ruessink, B.G. 2003. Video observations of nearshore bar behaviour. Part 1along shore uniform variability. *Continental Shelf Research*, 23, 501-512.
- Winant, C.D., Inman, D.L. and Nordstrom, C.E. 1975. Description of seasonal beach changes using empirical eigenfunctions. *J. Geophys. Res.*, 80, 1979-1986.
- Winjberg, K.M 1995. Morphologic behaviour of a barred coast over a period of decades, *thesis*, Univ. d'Utrecht, 215 p.

CONCEPTUAL MODELLING OF A DOUBLE CRESCENTIC BARRED COAST (LEUCATE BEACH, FRANCE)

Pierre Ferrer¹, Raphael Certain¹, Jean-Paul Barusseau¹ and Mathieu Gervais^{1,2}

Abstract

The south part of the Gulf of Lions coast (Mediterranean Sea) and its double crescentic sandbar system has been observed monthly during a 3-year long period (2005-2008) and yearly from 2000. This paper proposes a conceptual model of the morphodynamic evolution of this microtidal bar system supported by field bathymetric surveys and hydrodynamics measurements. *This model is based on the different evolutive sequences observed. It is then compared with other observations made in the literature.*

Key words: morphodynamics, crescentic sandbars, microtidal

1. Introduction

The majority of sandy coasts presents bar systems. The main classification of these bars has been proposed by Short and Aagaard (1993). Brander (1999) has completed this classification by adding some intermediate beach states. In this paper, we will focus on crescentic sand bars named Rhythmic Bar and Beach (RBB) in this classification. RBB are considered as illustrating an intermediate beach state. These beaches are characterized by two dimensionless fall velocity parameters: Ω (Gourlay, 1968) closed to 4 and K (Sunamura, 1988) between 5 and 20.

The morphological evolution of these features has been studied in different places in the world using different techniques (Goldsmith *et al.*, 1982; Wright and Short, 1984; Lippmann and Holman, 1990; Winjberg and Kroon, 2002; Stépanian *et al.*, 2003; Lafon *et al.*, 2004; Ranasinghe *et al.*, 2004; van Enckevort *et al.*, 2004; Certain and Barusseau, 2005; Castelle *et al.*, 2007; Almar *et al.*, 2008; Price and Ruessink, 2008; Quartel *et al.*, 2008; Sénéchal *et al.*, 2009). These studies describe morphological evolution of these rhythmic systems, single or multiple, in different tidal environments.

For a double bar system, the start point of the formation is a shoreline parallel outer bar (Van Enckevort *et al.*, 2004, Certain and Barusseau, 2005; Castelle *et al.*, 2007), the inner bar could present in the same time several configurations. During a storm event, the double bar system migrates seaward. When the hydrodynamic conditions become less energetic, the outer bar forms first longshore bar-trough morphology (LBT) (Castelle *et al.*, 2007) or meandering bar (Goldsmith *et al.*, 1982) before evolving toward crescentic bar, also known as lunate bar (Shepard, 1952); The inner bar could again present several intermediate configurations excluding LBT. After the storm event, the double bar system moves shoreward and the size of the rhythmic features increases (Castelle *et al.*, 2007). If the inner bar is crescentic (RBB), it can attach to the beach by its horns as a Transverse Bar and Rip (TBR) under low energetic conditions waves (De Melo Apoluceno, 2003). This configuration is very fragile. When storm events re-happen with a Hs higher than 2 m with an oblique incidence, the inner bar could stay as TBR with an oblique configuration like for i.e. at Hahoterim Beach (Goldsmith *et al.*, 1982) or Truc Vert Beach (Castelle *et al.*, 2007), and at Duck and Miyasaki beaches for a single bar system (Van Enckevort *et al.*, 2004). In TBR configuration, a rip head bar could appear following the form of the rip head current (Brander, 1999). Under high wave energy, the crescentic outer bar could wipe out and move offshore. On Aquitanian Coast, TBR inner morphology could subsist during high energy storms with Hs>5 m (Castelle *et al.*, 2007). After the peak of the storm, the

¹IMAGES, University of Perpignan Via Domitia, 52 Av. Paul Alduy, 66860 Perpignan Cedex, France. Contact:
pierre.ferrer@univ-perp.fr

²B.R.G.M. section Languedoc-Roussillon, 1039, rue de Pinville, 34000 Montpellier, France.

inner TBR morphology could reorganize itself in Low Tide Terrace morphology (LTT) if low energetic conditions happen during several weeks (Brander, 2000; De Melo Apoluceno, 2003; Castelle *et al.*, 2007). Indeed, associated to shoreward migration of both the inner bar and the rip head bar, the rips progressively infill and the bars move shoreward (Castelle *et al.*, 2007).

The objective of this paper is to propose a conceptual model of crescentic sand bars morphodynamic based on a long term survey in a microtidal environment, at Leucate Beach (France). The choice of the area was controlled by the background knowledge of this site and the persistent system of RBB bar type, or closest forms, that seems to have existed since the first observations. We expect that these observations could complete the general scheme described above and maybe incorporate new transitional states. All observed sequences will be introduced in the classification of Short and Aagaard (1993) and compared with the bibliography.

2. The study area

Leucate Beach is situated in Languedoc-Roussillon, on the southern part of the French Mediterranean coast (figure 1). The beach is almost N-S oriented, open to a large gulf, the Gulf of Lions. The sediment consists primarily of medium grained quartz sand with a median particle size around 390 µm. This microtidal environment has an annual mean tide range of 0.17 m. The coast is wave-dominated with an annual mean significant wave height of 0.62 m, a mean period around 4.12 s (source DRE Languedoc-Roussillon) and strong seasonal dependence: waves being higher in winter than in summer. During storm conditions, offshore wave heights can reach up to 9 m (at the open sea) for a maximal period of 9.2 s. Different studies have been undertaken at Leucate Beach since 1961 (Rivière, 1961; Barusseau and Saint-Guily, 1981): intensive field experiments (Adloff, 2007; Ferrer *et al.*, 2007), numerical modelling (Bujan, personal communication; Ferrer *et al.* 2008), pluri-annual morphologic surveys (Certain, 2002) and decadal data constituted by monthly bathymetric surveys (Ferrer *et al.*, 2007). It has been shown that Leucate Beach has a mean slope closed to 1.5 % and exhibits complex three-dimensional and lowly dynamic morphologies commonly involving two distinct rhythmic sandbar systems. The inner bar is located between 100 and 200 m from the coast, with a mean wavelength of the crescentic features close to 300 m (Barusseau and Saint-Guily, 1981; Certain, 2002; Ferrer *et al.*, 2007). The outer bar system is located at a distance between 400 and 500 m, with a wavelength of 600 m, the shape of which is symmetric (Barusseau and Saint-Guily, 1981; Certain, 2002; Ferrer *et al.*, 2007).

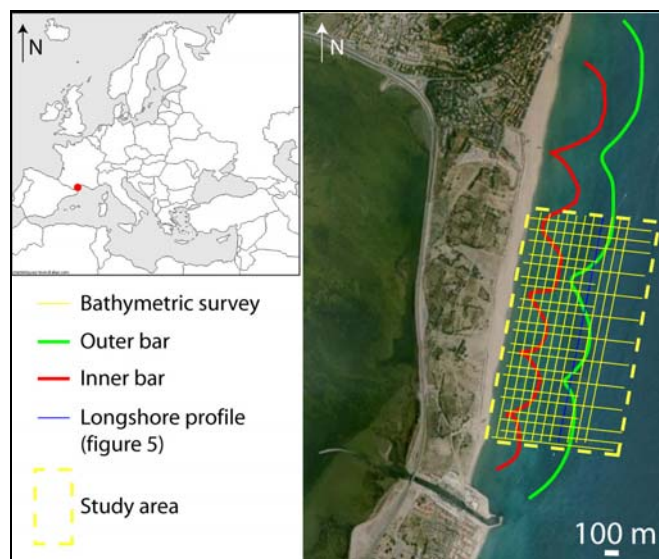


Figure 1. Location of the field study site on the French Mediterranean coast displaying a double bar system, the bathymetric survey plan and the longshore profile shown in figure 5.

3. Methodology

3.1. Bathymetric surveys

Data were acquired generally once a month from April 2006 to September 2008. This database is completed by some surveys made during summers of 2000, 2001, 2002 and after the biggest storm events in 2009. It is constituted by 28 bathymetric maps realized post-storms events. Bathymetric surveys were conducted using a GPS, an onebeam echosounder (Tritech ST500) with a depth accuracy of 0.1 m and Hypack® for the data acquisition. At each survey, 11 long-shore lines and 21 cross-shore lines were surveyed. The distance between each cross-shore transect is about 100 m up on the outer bar and 50 m up on the inner bar, and the length of the cross-shore profiles was about 1 km. The distance between each longshore transect is about 50 m, and the linear longshore length was about 1.8 km. Each bathymetric map is realized with Surfer® (Golden software). Each map is compared with the next one, the Z-level reference is the one from the first map.

3.2. Hydrodynamic data

Hydrodynamic data were obtained from the Datawell buoy at location 42°55.000'N and 3°07.500'E just offshore the studied site and fixed on a depth of 40 m (DRE Languedoc-Roussillon) during all the monthly survey. In addition, another directional buoy has been used to complete the set of data.

4. Frequency of occurrence of shoreface states

The bathymetric data of Leucate Beach (figure 2A) illustrates the presence of different types of bar systems (cf. study zone). The outer bar shows a RBB morphology with a wavelength of 600 m during the survey. It is located between 400 and 500 m from the coastline to seaward. The crest bar is between 4.5 and 5 m deep for its horns and 6.5 and 7 m for the part located offshore the trough. The inner bar shows a more complex configuration. The major configuration is a RBB morphology with a wavelength closed to 300 m. High points, which generally constitute the horns of the crescent, are located between 100 and 200 m seaward and between 1 and 2 m deep while the top of the crest in front of the trough is between 2 and 3 m deep. It is important to note that these high points could be linked to the coast initializing TBR morphology, and then sometimes TBR-LTT morphology. TBR-LTT morphologies show a longshore extension of the extremity of the transverse bar being able to create a morphological feature close to ridge and runnels (LTT morphology) with a rip-channel clearly expressed (figure 3) though the environment is microtidal. To better analyze morphologies of the inner bar, it is necessary to study independently each rhythmic morphological feature and its relation to the coast (figure 2B). This type of approach is possible by the invariant position (some meters) of the high points during all the survey. The EXT box corresponds to the main crescent of the outer bar and the F boxes to the rhythmic features of the inner bar.

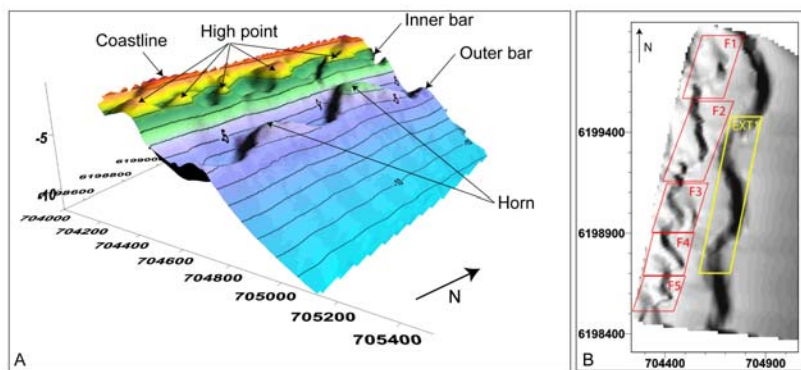


Figure 2. A- Bathymetric map of the study area displaying the outer bar with its horns and the inner bar with its high points corresponding to the horns of the crescents (in metric Lambert 93). B- Box localization of each morphological feature.

A scheme of all the features observed in the different boxes is proposed to illustrate them (figure 3). On this scheme, HP are the invariant high points of the inner bar. This scheme is based on the usual classification (Short and Aagaard, 1993) (figure 4). In TBR case, the connections of the transverse bars can be narrower than those proposed by Short and Aagaard (1993) (figure 4B). These transverse bars will be called regular TBR morphology in the following text as proposed by Castelle *et al.* (2007) in opposition to the oblique TBR morphology. In RBB case, HP are the horns of the morphological feature which presents a rhythmic feature. In TBR-LTT case, the transverse bar is attached to the coast. HP presents a longshore extension.

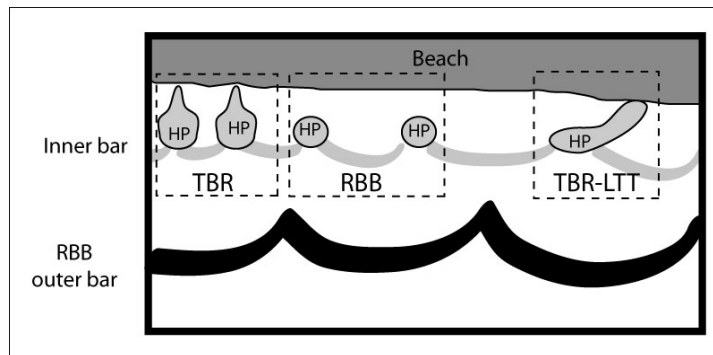


Figure 3. Schematic bathymetric map of the zone displaying the different morphologies met in the study area (HP = high point).

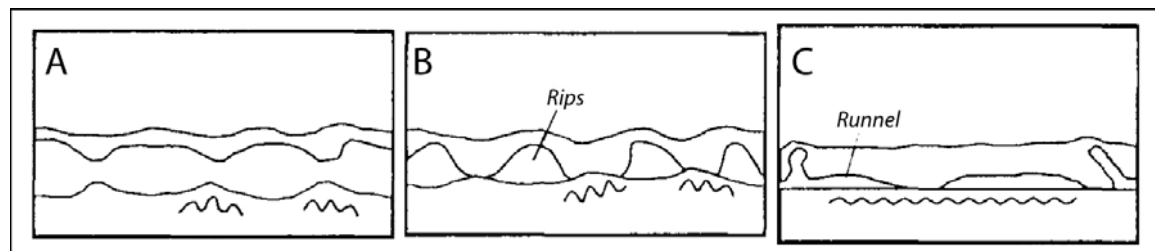


Figure 4. Classification of the beach states met in the study area. A- RBB morphology. B- TBR morphology. C – LTT morphology (adapted from Short and Aagaard, 1993)

The frequency of occurrence of each morphological feature has been calculated from the bathymetric database and compiled in the table 1. Each beach state described by Short and Aagaard (1993) is presented in this table (LBT, RBB, TBR) and the LTT morphology has been replaced by the TBR-LTT morphology which is the only feature observed at Leucate Beach. However, some other states observed in the field are not described in the usual classification, so it was necessary to add two new states: the disrupted RBB one and the disrupted TBR one. In the disrupted RBB state, the crest of the sandbar is partially disrupted, the horns are always isolated from the coast. In the disrupted TBR state, the connections to the coast are preserved and the crest of the sandbar is partially cut off.

Table 1. Percentage of each box morphological feature based on the classification of Short & Aagaard (1993) from the 28 bathymetric maps observed (from 2000 to 2008).

	EXT	F1	F2	F3	F4	F5
LBT	0	0	0	0	0	0
RBB	100	21	11	61	43	36
Disrupted RBB	0	4	48	18	11	22
TBR	0	57	22	14	39	21
Disrupted TBR	0	18	15	7	7	21
TBR-LTT	0	0	4	0	0	0

The compilation of field measurements indicates that the outer bar has always a RBB configuration during all the survey. The inner bar has various configurations but a major configuration is observed here. This configuration presents high points isolated from the coast and are linked by a crest, forming crescentic forms (RBB morphology) or disrupted crescentic forms (disrupted RBB). The high points which composed the inner bar can be at the same time the horns of the crescents and sometimes the extremities linked to the coast of the transverse bars (TBR). Rarely, the high points can be a part of the TBR-LTT morphologies.

5. Hydrodynamic conditions during the survey

During the bathymetric survey, associated swell data were available. These data come from a Datawell directional buoy located in front of Leucate Beach, moored in 40 m water depth for the hydrodynamic forcing of the period 2007-2009. To have the anterior hydrodynamic conditions, we have used others buoys in the Gulf of Lions.

Table 2. Characteristics of hydrodynamic parameters ($H_{1/3}$ and H_{max} , $T_{1/3}$ and T_{max}) recorded by Leucate's Datawell buoy.

	$H_{1/3}$ (m)			$T_{1/3}$ (s)		
	Min	Mean	Max	Min	Mean	Max
2007	0,08	0,60	4,49	2,1	4,1	9,6
2008	0,08	0,60	4,66	2,0	4,2	10,0
	H_{max} (m)			T_{max} (s)		
	Min	Mean	Max	Min	Mean	Max
2007	0,12	1,06	8,73	1,0	4,3	17,6
2008	0,10	1,06	8,07	1,0	4,4	12,9

Table 3. Swell distribution recorded by Leucate's Datawell buoy.

	H _{1/3} distribution % / number of events			H _{max} distribution % / number of events			Direction distribution (%)						
	0<...<2m	2<...<4m	4m<...	0<...<2m	2<...<4m	4m<...	Northern incidence	Frontal incidence	Southern incidence				
2007	98,1	1,9	5	0,0	2	91,4	7,3	44	1,3	6	12,2	10,0	30,8
	97,6	2,1	11	0,1	2	89,7	8,8	47	1,3	9	12,3	11,9	34,8

The hydrodynamic environment is not very dynamic during the survey, $H_{1/3}$ is between 0.6 and 0.7 m. However, the site undergoes some storm events with high energy where $H_{1/3}$ can be higher than 4 m and H_{max} higher than 8 m.

6. Morphodynamic response to storm events

During the survey, the outer bar does not evolve for storm events where $H_{1/3}$ is lower than 6 m ($H_{max} = 8.73$ m) while the inner bar is more influenced by storm events with $H_{1/3}$ higher than 1.5 m.

6.1 Outer bar response

During all the bathymetric surveys, the outer bar has never moved either longshore or crossshore. However, their horns undergo successive phases of accretion or erosion locally. On the differential volume map between summer 2002 and April 2006, the horns undergo an important accretion phase-as illustrated on a longshore profile which goes over trough and horns of the outer bar (figure 5). During this time

interval, several storm events happened. Two successive high energetic episodes have occurred during the winter 2003-2004 with $H_{1/3}$ higher than 8 m and 6 m respectively (Bourrin *et al.*, 2006) which seems to be the only episodes allowing these morphologic changes.

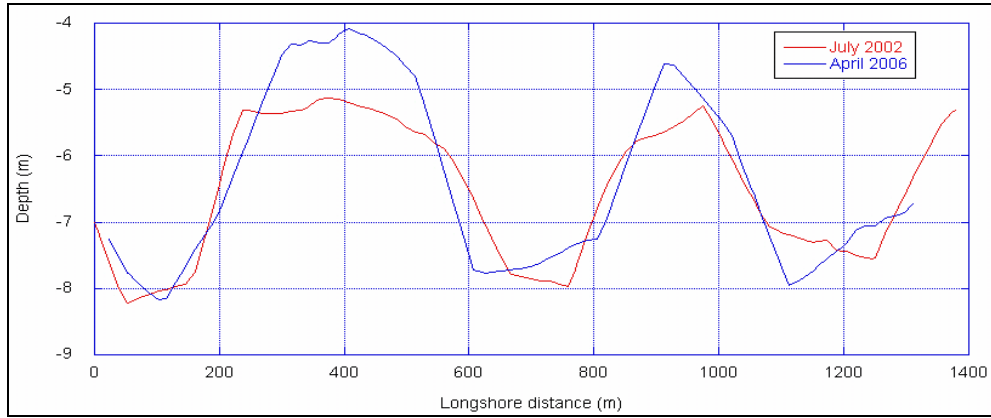


Figure 5. Longshore profile which goes over the trough and the horns of the outer bar showing the horns accretion phase.

6.2 Inner bar response

If the outer bar is stable in time and space, the inner bar is more mobile. During the bathymetric survey, the morphologies and the links of the sedimentary features to the coast have evolved. Here, the specific features of Leucate Beach will be described by characterising the morphodynamical pattern of the sandbars under the energetic conditions observed.

6.2.1 Scenario with a frontal swell.

Transition to a well formed RBB morphology (box F2)

An accentuation of the RBB morphology is observed in the inner bar after the storm event on the 14th April 2007. During this event, the inner bar was subjected to a frontal swell and a significant wave height higher than 2 m (figure 6). These modifications are shown by increases of the slope of the internal face and the height of the crest. This scenario happens each time the system was subjected to a frontal swell with a $H_{1/3}$ higher than 1.5 m. The significant wave height is higher; the RBB morphology is stronger marked. Moreover, it is possible to observe a tendency of the horns to get close to the coast.

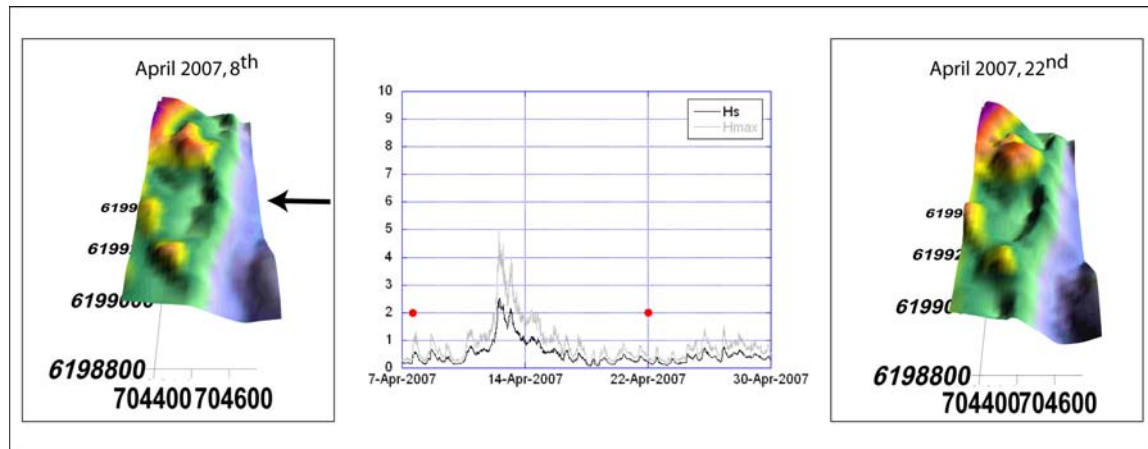


Figure 6. Morphological change of a RBB pattern after a storm event with a $H_{1/3} > 2.5$ m, a period closed to 9 s and a frontal incidence. To the left, it is possible to observe the RBB pattern on the 8th April 2007 and to the right, the same

pattern on the 22nd April 2007. The arrow shows the direction of the waves and the red dots are the date of the bathymetric maps.

Transition from a RBB morphology to a regular TBR morphology (box F2)

In addition to the deepening of the trough (some decimetres), the frontal swell is responsible for a change in the type of connection of the high points with the coast. If the storm event is energetic enough, the RBB morphology changes into a regular TBR morphology (figure 7). However, it is important to note that a small channel could remain crossing the connecting end of the transverse bar. This channel is less deep than the one before the storm event. The links to the coast are rarely identical to those proposed by the classification of Short and Aagaard (1993)

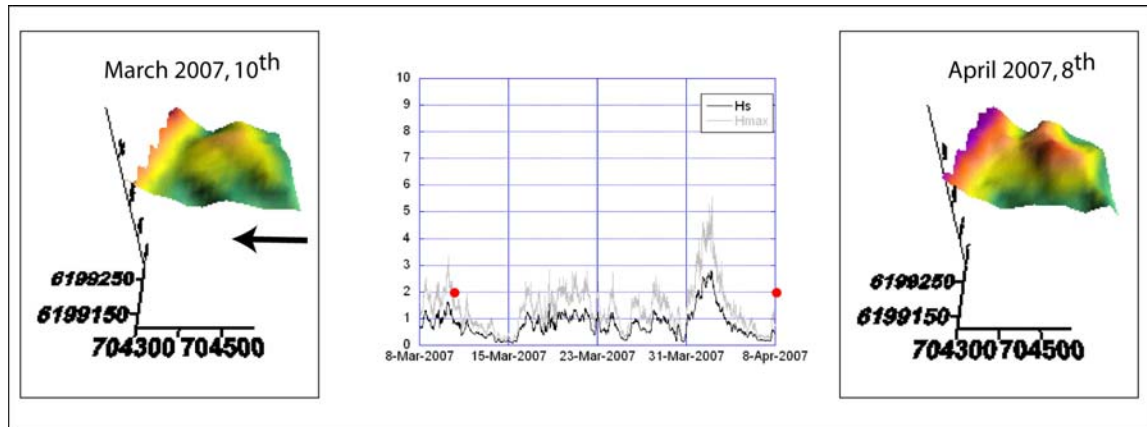


Figure 7. Morphological change of a RBB pattern after a storm event with a $H1/3 > 2.5$ m, a period closed to 8 s and a frontal incidence. On the left, it is possible to observe the RBB pattern on the 8th March 2007 and on the right, the same pattern on the 8th April 2007. The arrow shows the direction of the waves and the red dots are the date of the bathymetric maps.

6.2.2 Scenario with an oblique swell.

Transition from an oblique TBR morphology to a dissymmetric RBB morphology (box F3)

During the storm events from the 16th to the 22nd December 2007, the inner bar with an oblique TBR morphology was under two successive storm events with a northern incidence and a significant wave height higher than 2.5 m. The links to the coast were broken and a dissymmetric pattern appeared on the system (figure 8). These features are certainly due to the current organization as circulation cells and wave incidence described by Castelle *et al.* (2005). This scenario appears each time the swell is obliquely oriented and has a high energy. The dissymmetric pattern is related to the incidence of the swell. Higher the significant wave height; deeper the channels which appear between the high points and the coast.

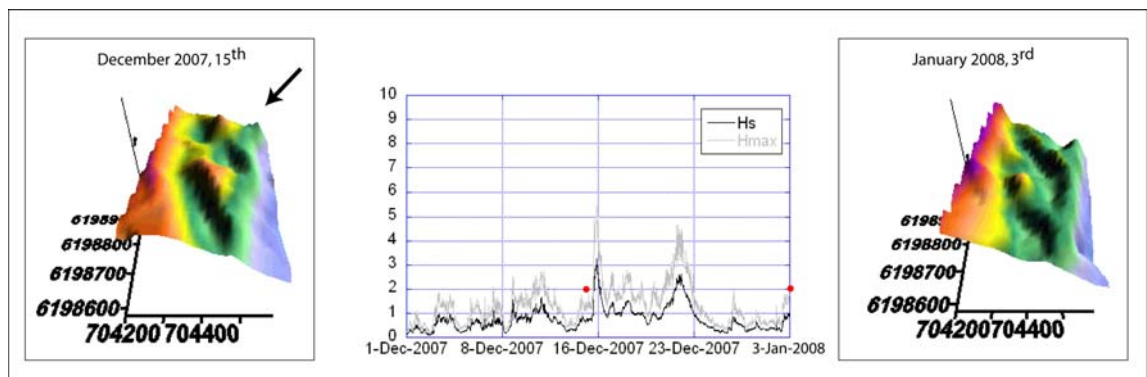


Figure 8. Morphological change of a TBR pattern after two storm events with a $H_{1/3} > 2,5$ m, period closed to 8 s and a oblique incidence from the north. On the left, it is possible to observe the TBR pattern on the 15th December 2007 and on the right, the RBB pattern of the same point on the 3rd January 2008. The arrow shows the direction of the waves and the red dots are the date of the bathymetric maps.

Transition from a RBB morphology to a disrupted RBB morphology (box F2)

In addition to the destruction of the merging part of the TBR-type bar to the beach, the oblique swell is responsible for the disruption of the crescentic bar crest (figure 9). In this instance, the system is under a northernly incident swell during a long period (June and July 2007) and the southern part of the RBB crest is consequently broken. On the other hand, the northern part of the crest can be broken if the swell has a southern incidence.

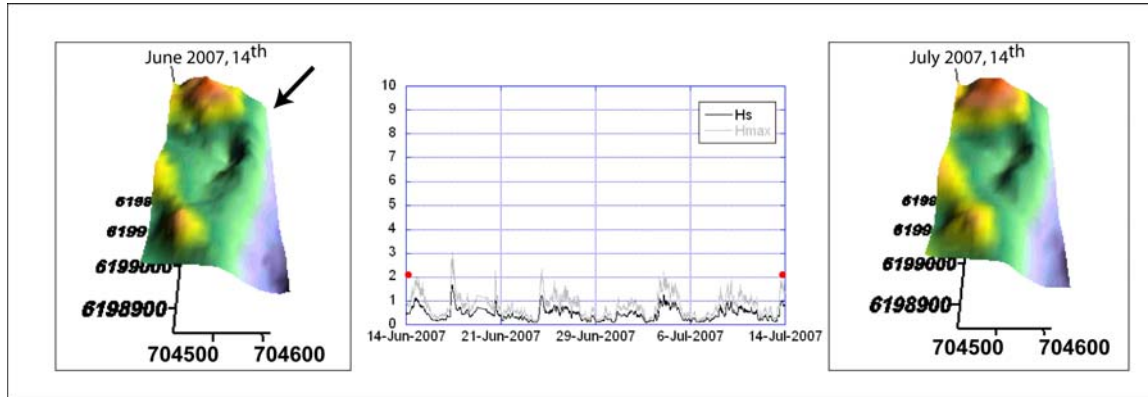


Figure 9. Morphological change of a RBB pattern after a storm event with a $H_{1/3} > 1,5$ m and an oblique incidence. On the left, it is possible to observe the RBB pattern on the 15th January 2007 and on the right, the same pattern broken on the 15th February 2007. The arrow shows the direction of the waves and the red dots are the date of the bathymetric maps.

Transition from a dissymmetric RBB morphology to an oblique TBR morphology (box F4)

Conversely to the TBR pattern shifting to the RBB one, the opposite transition is also observed. It occurred under a swell with a southern incidence and small significant wave height during a long period. The transverse bar takes the same orientation as the swell incidence-and the RBB horns weld to the beach. An oblique TBR morphology is obtained (figure 10).

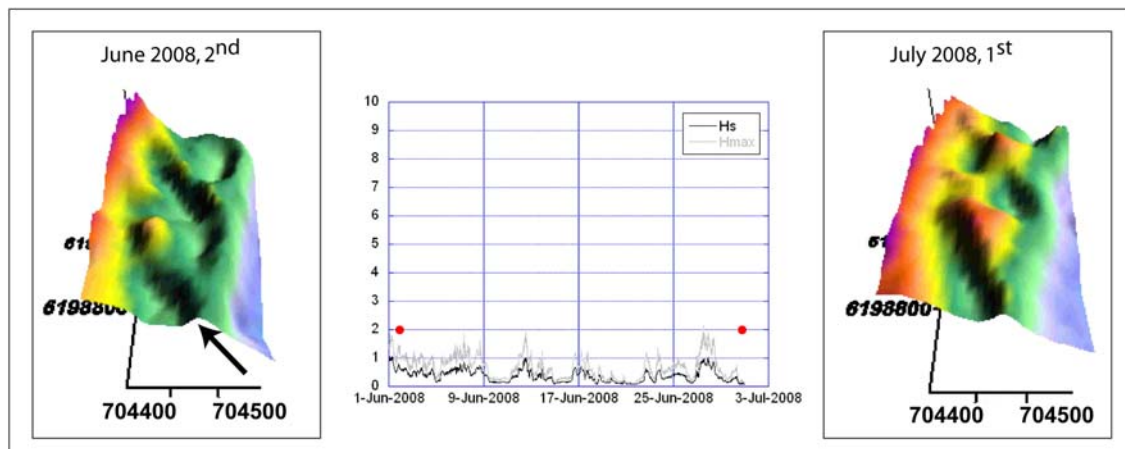


Figure 10. Morphological change of a dissymmetric RBB pattern during a low energetic event with a $H_{1/3} < 1,5$ m, a period between 3 and 8 s and a oblique incidence. On the left, it is possible to observe the dissymmetric RBB pattern on the 2nd June 2008 and on the right, the TBR oblique pattern of the same point on the 1st July 2008. The arrow shows

the direction of the waves and the red dots are the date of the bathymetric maps.

Transition from an oblique TBR morphology to a TBR-LTT morphology (box F1)

The storm events are not the only responsible factor for the inner bar morphodynamics as it has been shown earlier. A TBR morphology (oblique or regular) can become a TBR-LTT morphology if the system is under a strong northern longshore current created by a low energetic swell (figure 11). This morphological feature is rare and more present in the north part of the study zone. So to create and maintain this morphological feature, the system must be under a low energetic oblique swell.

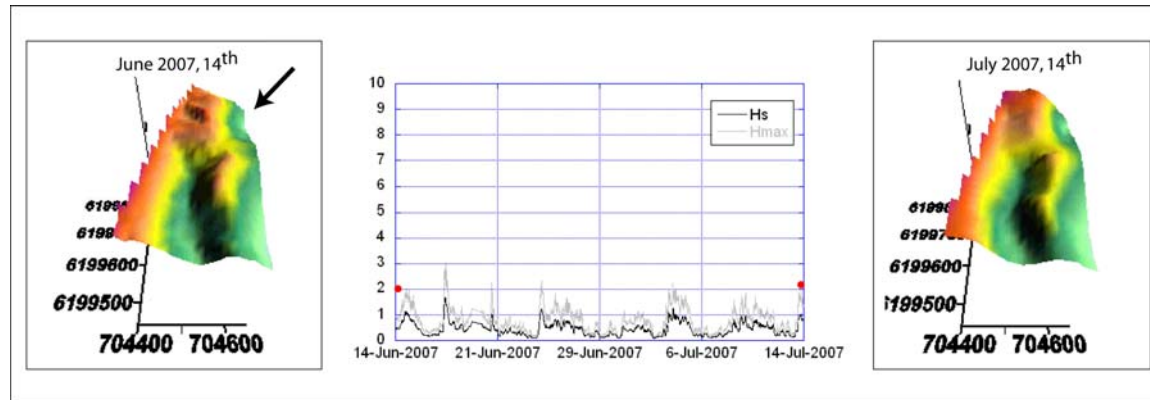


Figure 11. Morphological change of a TBR pattern during a low energetic event with a $H_1/3 < 1,5$ m, a period between 3 and 6 s and a oblique incidence. On the left, it is possible to observe the TBR pattern on the 14th June 2007 and on the right, the TBR-LTT pattern of the same point on the 14th July 2007. The arrow shows the direction of the waves and the red dots are the date of the bathymetric maps.

7. Conceptual morphodynamic model elaborate for the shoreface.

All the morphological changes described above were used to elaborate a conceptual model of Leucate Beach shoreface (figure 12). This model presents 8 observed beach states, all included in the intermediate types (Wright and Short, 1984). In this model, two types of relationship are indicated. The black lines correspond to transitions observed during the survey and the dotted lines to the assumed possible transitions. This model is a two-bars model, but the outer bar does not change during all the survey. The description of the states applies only to the morphological changes of the inner bar.

The start point of our model is a RBB morphology. This configuration is the most observed at Leucate Beach from 1961 (Rivière, 1961; Barusseau and Saint-Guily, 1981; Certain, 2002...). The horns of the inner bar constitute stable high points which have no or small variations in space. The pattern sequence described below results from the influence of various swells with a growing or decreasing significant wave height and various incidences (frontal and oblique).

When the system is under a frontal swell and a moderate significant wave height, the horns of the inner crescentic bar merge crossshore to the beach. This coalescence creates transverse bars with various forms but often regular. The first beach state is represented by the regular TBR morphology (Short and Aagaard, 1993). When the significant height wave increases, the links to the coast are broken and the crescentic shape constitute the well formed RBB morphology. If the swell has then an oblique incidence, the beach state becomes a dissymmetric RBB morphology.

On another hand, if the initial RBB configuration is submitted to obliquely incident swell, the crescentic crest of the inner bar can be broken to form a new state: the disrupted RBB morphology. If the energetic conditions decrease and are the same during a long period (some weeks to one month), the horns of the crescents attach to the coast by forming oblique transverse bars, while the crest of the crescent are always broken. The system is passing from a disrupted RBB morphology to an oblique disrupted TBR. If the system is always under low energetic and oblique swell, the crest of the crescents can reconstruct them, and the horns are always linked to the coast. The beach state is an oblique TBR morphology (Castelle *et al.*, 2007). This configuration can be obtained from a RBB morphology if the system is under a low energetic

oblique swell or from a dissymmetric RBB morphology if the system is under a decreasing energetic oblique swell. A last beach state can be obtained from an oblique TBR morphology, if the morphological feature is under a very low energetic oblique swell during a long period. The swell creates a longshore current close to the coast, the morphological feature becomes a TBR-LTT morphology. This morphological feature can also be obtained from the regular TBR morphology under the same climatic conditions.

The LBT configuration, not observed during the survey, does not appear in our model. In other places, this morphological feature needs decadal storms events to exist (Castelle *et al.*, 2007).

8. Discussion

Applicability of Leucate Beach model to other microtidal sites

Among the microtidal sites listed by Van Enckevort *et al.* (2004), the HaHoterim Beach in Israel studied by Goldsmith *et al.* (1982) offers the unique opportunity to make a comparison. As two morphodynamical sequences, 1 and 2, are described. The evolution is globally the same to the Leucate Beach one. The role of the swell incidence is emphasized, in the transition from RBB morphologies to well formed RBB morphologies (sequence 2) as well as to more or less oblique TBR morphologies (sequence 1).

Applicability of Leucate Beach model to meso- and macrotidal sites

Several examples of meso- and macrotidal sites are given in the literature, i.e. Truc Vert Beach (De Melo Apoluceno, 2003; Castelle *et al.*, 2007), Wanganui (Shand *et al.*, 2003) and Palm Beach (Brander, 1999). A comparison can be made between the morphological responses in the two types of sites, taking into account the role of the frontal and oblique waves

The frontal waves bring about similar effects in these sites. The bar crests move seaward during high energetic storm events, the RBB morphologies can become TBR morphologies if the significant wave height decreases (De Melo Apoluceno, 2003; Castelle *et al.*, 2007). However, some evolutions are more unusual like the appearance of TBR morphologies during increasing energetic events and the achievement of well shaped RBB morphology when the significant wave height increases without going to the destruction of the system (Shand *et al.*, 2003). The described sequences in meso- and macrotidal environments give information about the transition to a RBB morphology during a decreasing storm event not addressed in the Leucate Beach study.

Similarities and differences arise when oblique waves occurred. The likeness relates to the formation of dissymmetric RBB morphologies (Sénéchal *et al.*, 2008), formation of oblique TBR morphologies (Castelle *et al.*, 2007), the transition from TBR morphologies to TBR-LTT morphologies close to ridge and runnels with an oblique channel during long lasting low energetic event (De Melo Apoluceno, 2003; Castelle *et al.*, 2007), the creation of RBB morphologies which take position at the rip-current head (Brander, 1999). However, Leucate Beach model looks more complex and require the introduction of new beach states which underscore singular situations unrecorded in meso- and macrotidal sites.

Comparison of Leucate Beach model to the classification of Short and Aagaard (1993)

The classification of Short and Aagaard, supported by the former studies of Goldsmith *et al.* (1982) on HaHoterim Beach, uses the dimensionless fall velocity Ω defined by Gourlay (1968). Some observed states at Leucate Beach like RBB, regular TBR come from this classification. However, the study of the two-bar system of Leucate Beach shows that it is important to underline specific situations which seem to stress remarkable states having a long lasting occurrence. For instance, the disrupted RBB and the disrupted oblique TBR morphologies are states which can come from or drive to described states in the classification of Short and Aagaard (1993).

Otherwise, all descriptions of morphological evolution are submitted to a basic vagueness. Some authors have already proposed modifications or complements to the classification of Short and Aagaard (1993), in order to improve it. In this way, Brander has modified the TBR category introducing the rip head bar morphologies which looks like small sized RBB ($L \# 12$ m) induced by a rip current feeder. Later, Castelle *et al.* (2007) has distinguished oblique TBR morphologies, observed also in Leucate, which present a more important angular position to the coast than the TBR from Short and Aagaard (1993). Moreover, in some instances, they propose mixed beach states, i.e. the LBT-RBB or RBB-TBR configurations, and in the Leucate beach zone the transitional final low energetic TBR-LTT.

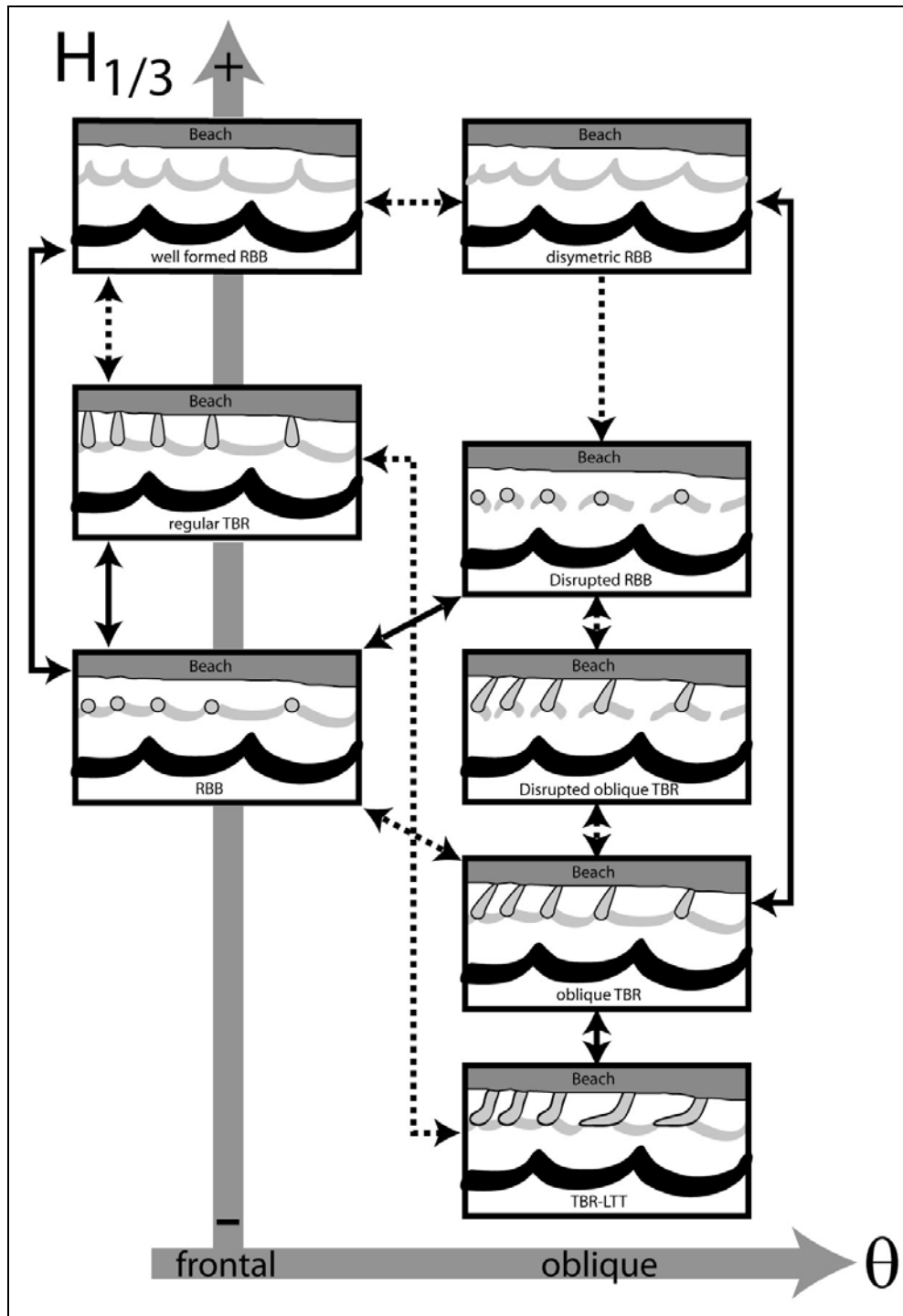


Figure 12. Preliminary beach state model exhibiting the possible range of beach state around Leucate Beach area. $H_{1/3}$ is the significant height of the waves, from small energy (-) to high energy (+) and θ is the incidence angle of the waves, from frontal to oblique). The arrows show transitions observed (black line) and non observed ones (dotted line) between the different states.

The stability of Leucate Beach system

Two sedimentological features present a particularly stable position of the post-storm bar system in Leucate Beach: the whole outer bar and the high points of the inner bar. Otherwise, the latter vary between

only two beach states: RBB and TBR. Among the factors explaining this apparent stability, it is possible to consider the outer bar as a protection of the system and the absence of high energetic storm events during our survey have a role there. The literature on this topic gives rather different results. On the basis of video survey allowing continuous and long lasting observations, it has been shown that the system presents a strong variability during and after a storm event (Shand *et al.*, 2003; Van Enckevort and Ruessink, 2003a et 2003b; Ranasinghe *et al.*, 2004; Almar *et al.*, 2008) which can be a reset factor in the bar morphogenesis (Ranasinghe *et al.*, 2004; Castelle *et al.*, 2007). Furthermore, Shand *et al.* (2003), at Wanganui (NZ), suggest that inherited non linear morphologies can resist to greater wave height and longshore current that occur during their formation. This morphological feedback has a consequence on the hydrodynamic circulation. According to Castelle *et al.* (2005) numerical modelling, stable RBB's induce stable circulation cell patterns. It's possibly be the reason why, in Leucate area, stability would be the dominant characteristics, in spite of the fact that the non-continuous investigations may introduce a bias in the form-sequence record.

9. Conclusion

Field measurements realized between 2000 and 2009 and the hydrodynamic data available were combined to study Leucate Beach microtidal system. It appears that the RBB configuration is the major component of the system. The outer bar is always RBB during the survey, while the inner bar could take others configurations like TBR or TBR-LTT.

This database has been used to elaborate a conceptual model based on the usual classification of Short and Aagaard (1993). To describe precisely this system, new states (disrupted RBB and disrupted TBR) must be introduced in this classification. All these states have been linked using significant height and incidence of the swell. 6 morphological changes have been observed and the other morphological changes are supposed to be possible. All of these states observed in microtidal environment can be included in the existing classifications.

Leucate Beach data have been acquired after storms events. In spite of this consequent database, the states transitions have not been observed during storm events. It could be interesting to associate a video survey to a bathymetric survey to observe the changes of the outer and the inner bars. Associated to this technique, the sand migration could be marked by using fluorescence marking. All these techniques could verify the stability of the system.

References

- Adloff, F., 2007. Hydrodynamique de la zone de déferlement d'un système de barres d'avant-côte festonnées. *Mémoire de Master 2 Recherche*, Université de Perpignan Via Domitia, France, 38 p.
- Almar, R., Coco, G., Bryan, K.R., Huntley, D.A., Short, A.D. and Sénéchal, N., 2008. Video observations of beach cusp morphodynamics. *Marine Geology*, 254(3-4): 216-223.
- Barusseau, J.P. and Saint-Guily, B., 1981. Disposition, caractères et formation des barres d'avant-côte festonnées du Golfe du Lion. *Oceanologica Acta*, 4(3): 297-304.
- Bowen, A., and Inman, D., 1971. Edge waves and crescentic bar. *Journal of Geophysical Research*, 76: 8662-8671.
- Brander, R.W., 1999. Field observations on the morphodynamic evolution of a low-energy rip current system. *Marine Geology*, 157(3-4): 199-217.
- Brander, R.W., 2000. Morphodynamics of a large-scale rip current system at Muriwai Beach, New Zealand. *Marine Geology*, 165: 27-39.
- Castelle, B., Bonneton, P. and Butel, R., 2006. Modélisation du festonnage des barres sableuses d'avant-côte : application à la côte aquitaine, France. *Comptes Rendus Geosciences*, 338(11): 795-801.
- Castelle, B., Bonneton, P., Dupuis, H. and Sénéchal, N., 2007. Double bar beach dynamics on the high-energy meso-macrotidal French Aquitanian Coast: A review. *Marine Geology*, 245(1-4): 141-159.
- Certain, R., 2002. Morphodynamique d'une côte sableuse microtidale à barres: le golfe du Lion (Languedoc-Roussillon). *Unpublished Thesis*, Université de Perpignan Via Domitia, France, 209 p.
- Certain, R., Barusseau, J.-P., 2005. Conceptual modeling of sand bars morpho-dynamics for a microtidal beach (Sète, France). *Bull. Soc. géol. Fr.*, 176 (4): 343-354.
- De Melo Apoluceno, D., 2003. Morpho-hydrodynamique des plages à barres en domaine méso macro-tidal: exemple de la plage du Truc Vert, Gironde, France. *Unpublished Thesis*, Université Bordeaux I, France.
- Ferrer, P., Adloff, F., Certain, R., Meulé, S., Bouchette, F. et Leredde, Y., 2007. Hydrodynamique à l'échelle événementielle d'un système de barres festonnées dans le golfe du lion (Leucate Beach, Aude). *11ème Congrès*

- Français de Sédimentologie*, Caen, France.
- Ferrer, P., Bujan, N., Certain, R., et Leredde, Y., 2008. Caractérisation hydrodynamique D'un littoral à barres festonnées du golfe du Lion (Leucate, France) : mesures in-situ et modélisation. *Xèmes Journées Nationales Génie Côtier-Génie Civil*, Sophia-Antipolis, France.
- Ferrer, P., Cance, L., Certain, R., Barusseau, J.-P., 2007. Morphodynamique pluriannuelle d'un système de barres d'avant-côte festonnées en milieu microtidal (sud du golfe du Lion). *11ème Congrès Français de Sédimentologie*, Caen, France.
- Goldsmith, V., Bowman, D. and Kiley, K., 1982. Sequential stage development of crescentic bars: Hahoterim Beach, Southeastern Mediterranean. *Journal of Sedimentary Petrology*, 52(1): 233-249.
- Gourlay, M.R., 1968. Beach and dune erosion tests. Delft: Delft Hydraulics Laboratory. Report M935/M936.
- Lippmann, T.C. and Holman, R.A., 1990. The spatial and temporal variability of sand bar morphology. *Journal of Geophysical Research*, 95(C7): 11575-11590.
- Price, T.D. and Ruessink, B.G., 2008. Morphodynamic zone variability on a microtidal barred beach. *Marine Geology*, 251(1-2): 98-109.
- Ranasinghe, R., Symonds, G., Black, K. and Holman, R., 2004. Morphodynamics of intermediate beaches: a video imaging and numerical modelling study. *Coastal Engineering*, 51(7): 629-655.
- Quartel, S., Kroon, A. and Ruessink, B.G., 2008. Seasonal accretion and erosion patterns of a microtidal sandy beach. *Marine Geology*, 250(1-2): 19-33.
- Ranasinghe, R., Symonds, K. and Holman, R., 2004. Morphodynamic of intermediate beaches: a video imaging and numerical modeling study. *Coastal Engineering*, 51, 629-655.
- Rivière, A., Arbez, F. and Vernhet, S., 1961, Remarque sur l'évolution et l'origine des structures de plage à caractère périodique. *C. R. Hebd. Séances Acad. Sci.*, 252: 767-769.
- Sénéchal, N., Ardhuin, F., Abadie, S., Almar, R., Arnaud, G., Austin, M., Barnoud, J.-M., Barthélémy, E., Berni, C., Blenkinsopp, C., Bonneton, N., Bonneton, P., Bouée, F., Bretel, P., Brown, J., Brown, J., Bujan, S., Buscombe, D., Capo, S., Castelle, B., Certain, R., Chassagneux, F.-X., Coco, G., C.D., Dallacosta, C., Dehouck, A., Delattre, M., Delvallée, S., De Vries, S., Dewez, T., Dodet, G., Emmanuel, I., Escalier, J.-M., François, B., Froidfond, J.-M., Gallagher, E., Ganderton, P., Garcin, M., Garlan, T., Gaunet, J., Gervais, M., Gluard, L., George, I., Gouaud, F., Grandjean, P., Grasso, F., Hampson, R., Hanquiez, V., Henriquez, M., Hibberd, W., Hurther, D., Lafosse, J.-M., Lagauzère, M., Lambert, A., Lecacheux, S., Le Cozannet, G., Le Drezigue, J., Le Gall, F., Lencou, P., Le Roy, R., Lusven, A., Mac Mahan, J., Magne, R., Marieu, V., Markies, H., Marron, P., Martiny, N., Masselink, G., Michallet, H., Mignot, E., Minet, M., Moon, J., Moreau, J., Morichon, D., Morisset, S., Mory, M., Nahon, A., Oman.J., Outre, M., Parisot, J.-P., Payne, G., Pedreros, R., Poate, T., Rejas, A., Reniers, A., Rey, V., Romieu, E., Rouille, P., Ruiz De Allegria, A., Ruessink, G., Russell, P., Schippers, M., Smit, M., Sotin, C., Sous, D., Stanton, T., Stockel, J., Thiebot, J., Thornton, E., Tinker, J., Tissier, M., Turner, I., Van Dam, B., Vandromme, R. and Van Maarseveen, M., 2008. ECORS – Truc Vert 2008 : Qualification des modèles de houle et de morphodynamique, *Xèmes journées nationales Génie Côtier-Génie Civil*, Sophia-Antipolis, France, pp. 635-654.
- Sénéchal, N., Gouriou, T., Castelle, B., Parisot, J.-P., Capo, S., Bujan, S. and Howa, H., 2009. Morphodynamic response of a meso- to macro-tidal intermediate beach based on a long-term data set. *Geomorphology*, 107(3-4): 263-274.
- Shepard, F.P., 1952. Revised nomenclature for depositional coastal features. *Bull. Am. Assoc. Petrol. Geol.*, 36: 1902-1912.
- Short, A. D. and Aagaard, T., 1993. Single and multi-bar beach change models. *Journal of Coastal Research*, Special Issue No. 15: 141-157.
- Stepanian, A. and Levoy, F., 2003. Sequences d'évolution morphodynamique des barres intertidales d'une plage macrotidale : l'exemple d'Omaha beach (Normandie, France): Morphodynamical evolution sequences of intertidal bars on a macrotidal beach: case study of Omaha beach (Normandy, France). *Oceanologica Acta*, 26(2): 167-177.
- Sunamura, T., 1988. Beach morphologies and their change. In Horikawa, K., (ed), *Nearshore Dynamics and Coastal Processes*. University of Tokyo Press, 133-166.
- Van Enckevort, I.M.J. and Ruessink, G., 2003a. Video observations of nearshore bar behaviour, Part I: alongshore uniform variability. *Cont. Shelf Res.*, 23, 501-512.
- Van Enckevort, I.M.J., Ruessink, B.G., 2003b. Video observations of nearshore bar behaviour. Part 2: alongshore non-uniform variability. *Cont. Shelf Res.*, 23: 513-532.
- Van Enckevort, I.M.J. et al., 2004. Observations of nearshore crescentic sandbars. *Journal of Geophysical Research*, 109(C6), C06028, doi:10.1029/2003JC002214.
- Wijnberg, K.M. and Kroon, A., 2002. Barred beaches. *Geomorphology*, 48(1-3): 103-120.
- Wright, L.D. and Short, A.D., 1984. Morphodynamic variability of surf zones and beaches: A synthesis. *Marine Geology*, 56(1-4): 93-118.

Les ondes infragravitationnelles et leur rôle éventuel dans la formation de croissants de plage : Cas de la plage de Sète

P. Ferrer¹, V. Rey², R. Certain¹, F. Adloff¹ et S. Meulé³

1 *LEGEM, Université de Perpignan, 52 av Paul Alduy, 66860 Perpignan Cedex, France*

2 *LSEET-LEPI, Université du Sud Toulon-Var, B.P 20132 F 83957, la Garde, Cedex, France*

3 *CEREGE, Europôle Méditerranéen de l'Arbois - BP 80 - 13545 Aix en Provence cedex 04*

Résumé

La génération de formes rythmiques sur les plages est un sujet riche en interrogations. Suite à une campagne intensive d'acquisition en novembre 2000 sur une plage de Sète (Hérault), une étude hydrodynamique a été menée afin de vérifier si l'infragravité était responsable de la formation des croissants de plage sur la zone. A la vue des résultats obtenus, l'infragravité ne serait pas le moteur principal de mise en place.

Abstract

Beach cusps formation is a topic with a lot of questions. After an intensive acquisition survey in November 2000, on Sète Beach (Hérault), a hydrodynamic study has been led to verify if edge waves are responsible of beach cusp formation. It seems that edge waves are not the main factor of settlement.

Mots Clés : infragravité, croissants de plage, hydrodynamique, auto-organisation.

1. Introduction.

La génération de formes rythmiques sur le littoral reste un sujet d'interrogation.

Deux théories principales sont actuellement développées pour expliquer la formation des croissants de plage : la génération due aux ondes infragravitationnelles^{1,2} et celle liée au modèle d'auto-organisation^{3,4}. La théorie proposée par Guza et Inman (1975) s'appuie sur des modulations rythmiques de la surface libre qui imposent une empreinte sur la morphologie aboutissant à la formation des croissants de plage. Pour vérifier cette théorie, il est nécessaire d'effectuer diverses mesures (espacement entre les croissants, période des ondes incidentes,

pente de la plage). Certaines études, dont notamment une étude récente de Coco et al, 1999, ont permis de vérifier l'existence d'une relation entre l'espacement des croissants et les ondes infragravitaires. Dans la seconde théorie, des hétérogénéités de la morphologie créent des rétroactions positives du champ de courant dans la zone de jet de rive qui aboutissent à la formation de structures rythmiques. Ces structures rythmiques ont un lien avec la pénétration du jet de rive sur la plage. Cependant, un grand nombre d'études^{3,6} ont été réalisées en laboratoire, avec seulement quelques validations sur le terrain (Coco et al, 2003).

Si on confronte les deux théories, on s'aperçoit qu'elles sont compatibles pour certains auteurs comme Coco et al (1999) alors que Werner et Fink (1993) montrent que, dans leur étude, des arguments les opposent. Une étude récente menée par Coco et al (2000) ne tenant pas compte de l'hydrodynamique près de la côte (vague et réfraction) a montré la possibilité de formation de croissants de plage, leur espacement étant uniquement contrôlé par l'incursion du jet de rive sur la plage. Cela a également permis de mettre en évidence que la présence d'un courant longitudinal dans la zone de jet de rive détruisait les croissants. Cela va donc à l'encontre de la théorie de Guza et Inman (1975) qui dit qu'une incidence oblique favorise le piégeage les ondes de bord dans la zone du jet de rive, ces ondes étant ensuite responsables de la formation des croissants de plage.

D'une manière générale, l'hypothèse des ondes infragravitaires reste la plus étudiée théoriquement et sur le terrain. De nombreuses études viennent confirmer ou infirmer cette théorie^{5,8,9}. Cependant, on s'aperçoit dans le détail que les séries de données hydrodynamiques utilisées sont généralement peu adaptées à ce genre d'expérimentations (mesures effectuées trop loin au large ou décalées dans le temps par rapport au moment de génération des croissants).

On se propose dans ce travail d'étudier plus spécifiquement la part possible des ondes infragravitaires comme cause dans la génération des croissants de plage à partir d'un réseau dense de capteurs de vitesses et de pression déployées en 2000 lors d'une campagne de mesure intensive dans le cadre de l'ART 7 du PNEC à Sète (golfe du Lion).

2. Site d'étude.

La zone retenue pour cette expérience se situe à Sète, dans le golfe du Lion, en Languedoc-Roussillon (fig.1). Elle correspond au site méditerranéen de l'ART 7 du PNEC (Programme National d'Environnement Côtier), qui a étudié les environnements d'avant-côte à barres sédimentaires.

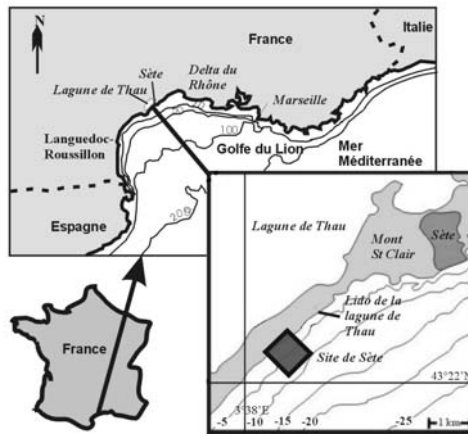


Figure 1 : Localisation de la zone d'étude.

Le site de Sète est situé en face de la lagune de Thau, au nord du lido, sur la partie la plus érodée. Il comporte une plage étroite d'une trentaine à une cinquantaine de mètres de largeur, où le cordon dunaire a disparu sous l'effet de la construction de la route nationale située en arrière.

Ce site microtidal (0,15 m de marnage) est dominé par les vagues. Les vents dominants proviennent de terre (NW) ou de mer (SE). Ils induisent des variations de niveaux importantes, qui peuvent atteindre 1m à la côte. Les vagues créées par les vents de NW sont généralement faibles (0,3m) avec des périodes allant de 3 à 4 secondes (mer du vent). Les vagues dominantes sont induites par les vents de SE. Elles atteignent régulièrement des hauteurs significatives de 2,5m avec des périodes voisines de 8 secondes. La morphologie en pente douce (1%) de l'avant-côte jusqu'au rivage est entrecoupée par les deux barres sédimentaires. La barre la plus proche du rivage est appelée barre interne, la plus éloignée barre externe. Cette terminologie est reprise pour décrire les deux fosses séparatrices. Le sédiment superficiel est fin à moyen (médiane de 125 à 320µm), généralement bien trié et sa médiane décroît du bord vers le large.

Ponctuellement, lors de la décroissance de la taille de la houle à la fin des tempêtes, la formation de croissants de plage s'observe dans la zone de jet de rive.

3. Méthodologie.

L'expérimentation de terrain s'est déroulée du 3 novembre au 3 décembre 2000¹⁰. Le dispositif instrumental se composait de trois courantomètres / houlographes Interocean de type S4 (DW et ADW), de capteurs de pression et d'un courantomètre/houlographe Nortek de type Vector pour l'étude hydrodynamique ; d'un théodolite pour la partie de l'étude morphologique. Les levés topographiques ont eu lieu suite à la formation ou à la destruction des croissants de plage.

3.1. Les outils de mesure.

Les S4 ont été fixés sur des structures a-magnétiques. Ces instruments mesurent les deux composantes du courant horizontal à une hauteur comprise entre 0,5 m et 0,9 m par rapport au fond marin et la pression, à une distance du fond de 0,4 m à 0,8 m. Ces données permettent d'évaluer les caractéristiques directionnelles des vagues. Les données brutes sont acquises à une fréquence de 2 Hz pendant 18 à 36 minutes toutes les trois heures. Une fois moyennées, elles fournissent les caractéristiques du courant horizontal moyen ainsi que les fluctuations du niveau du plan d'eau statique. Les caractéristiques de l'agitation (hauteur significative et périodes caractéristiques) sont déduites des séries temporelles des fluctuations de pression par analyse spectrale. Les S4 étaient disposés sur le glacis et dans les creux inter-barres (respectivement à -6,0 ; -4,0 et -2,5 m) afin d'étudier les conditions de houle à l'entrée du système et sa déformation après passage sur les barres (fig.2). En effet, lors des tempêtes, deux déferlements successifs peuvent se produire au passage des barres. Pour des houles plus petites, les vagues peuvent parvenir à la côte sans déferler ou seulement sur la barre interne.

Pour l'étude plus spécifique de l'hydrodynamique à la côte, au plus proche de la zone de génération des croissants, au cours de l'expérimentation de terrain, des capteurs de pression, au nombre de 5, ont été disposés sur le flanc externe et la crête de la barre interne du 14/11/2000 au 24/11/2000 (fig. 2). Ils sont situés entre -2 et -3 mètres de profondeur. L'enregistrement s'est effectué à une fréquence de 16Hz, à intervalles irréguliers sur des durées variables (5 à 90 minutes). De plus, ponctuellement, un courantomètre/houlographe de type Vector a été déployé dans la fosse de lévigation interne, au pied du talus de collision pour un enregistrement avec une fréquence de 32 Hz pendant 30 minutes. Ce déploiement a eu lieu les jours de formation de croissants de plage (7/11, 14/11 et le 24/11) ainsi qu'un jour de destruction de la topographie résiduelle (20/11/2000).

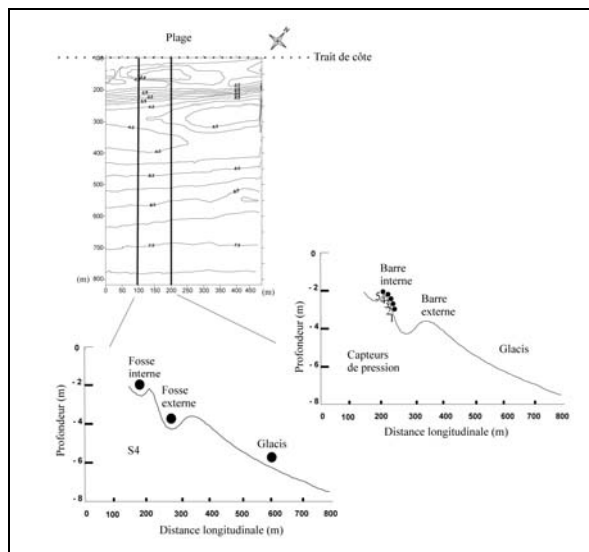


Figure 2 : Les profil transversaux instrumentés et leur morphologie au cours de la campagne (modifiée de ¹⁰).

3.2. Analyse des données.

Seules les situations de décroissance de la houle, favorables à la formation de croissants, seront présentées dans cet article. Toutes les données hydrodynamiques vont être étudiées en utilisant des transformées de Fourier rapide (FFT) avec des fréquences de coupure entre 0,003 Hz et 0,40 Hz (300 s - 2,5 s). Cette méthode permet d'obtenir des spectres d'énergie en fonction des fréquences et donc de déterminer les caractéristiques des ondes. Il a fallu ensuite différencier les ondes infragravitaires des ondes gravitaires. La limite supérieure des ondes infragravitaires a été fixée à 0,05 Hz¹¹. A partir de ces spectres, les longueurs d'onde liées aux pics des ondes infragravitaires (Le) ont été calculées à partir de la relation de dispersion (1) (en partant du postulat que les ondes étudiées sont stationnaires) puis comparées aux longueurs d'ondes des formes rythmiques observées sur le terrain (Lc). Pour le cas synchrone Lc=Le alors que pour le cas sub-harmonique Lc=Le/2.

$$Le = \frac{g}{2\pi} Te^2 \times (2n+1)\tan \beta \quad (1)$$

(où Le : la longueur d'onde de l'infragravité, g : la valeur de l'accélération de la pesanteur, Te : la période de l'infragravité, n : le mode et β : la pente de la plage)

4. Résultats.

Des représentations tridimensionnelles de la plage ont été réalisées (fig. 3). A partir de ces cartes en 3D, des profils topographiques longitudinaux ont été extraits (fig. 4). La longueur d'onde des croissants de plage (Lc) a été calculée à partir de ces profils.

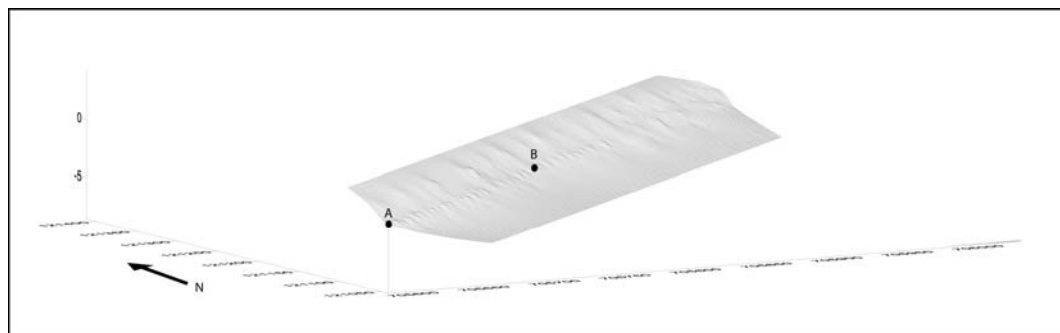


Figure 3 : modélisation 3D des croissants de plage réalisée sous Surfer pour le 14/11/2000.

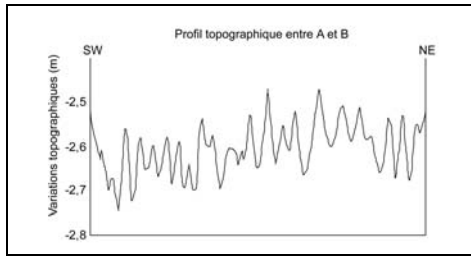


Figure 4 : profil topographique entre A et B du 14/11/2000.

Les données hydrodynamiques ont permis d'obtenir des spectres d'énergie (fig. 5 et 6) caractéristiques pour chaque journée d'analyse au moment de la formation ou de la destruction des croissants. On distingue plusieurs pics énergétiques dans ces spectres. Chaque pic correspond à un type d'onde dans le domaine infragravitaire, gravitaire ou de la mer du vent. Un zoom est effectué sur les ondes infragravitaires (fig. 7).

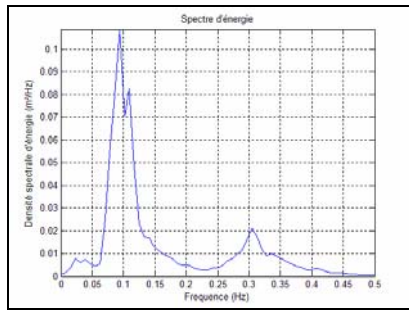


Figure 5 : spectre d'énergie du 19/11/2000.

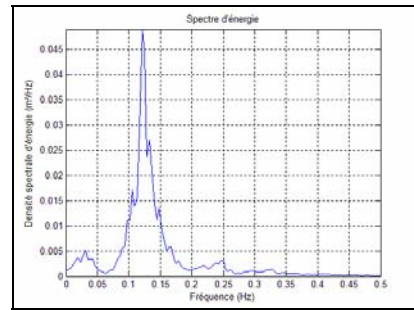


Figure 6 : spectre d'énergie du 21/11/2000.

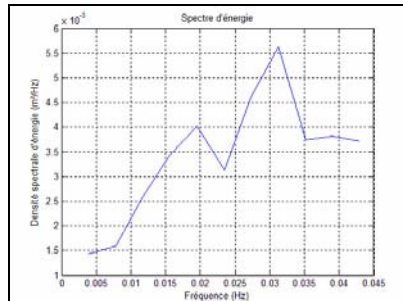


Figure 7 : spectre d'énergie de l'infragravité du 21/11/2000.

A partir de ces spectres, les fréquences des ondes gravitaires incidentes et des ondes infragravitaires observées ont été mesurées, et les périodes correspondantes ont été calculées. La longueur d'onde des ondes infragravitaires (λ_e) a été déduite de l'équation (1). Tous les résultats sont répertoriés dans le tableau 1. Un certain nombre de difficultés a été rencontré dû à la complexité du milieu. Ainsi la pente de la plage a été supposée constante dans le modèle alors qu'en réalité elle est variable dans la zone du jet de rive. Ce modèle a été testé à Sète en considérant $\tan \beta = 0,086$. Ensuite, il a fallu identifier le pic principal dans le domaine infragravitaire pour chaque spectre d'énergie. Le mode $n=0$ a été

utilisé car il correspond théoriquement à celui qui concentre le plus d'énergie à la côte.

Situation	Cas étudié	Date	Lc (m)	f _i (Hz)	T _i (s)	f _e (Hz)	T _e (s)	Le (m)	Le/2 (m)
1	Formation	07/11/2000	31	0,090	11,130	0,038	26,256	92,567	46,283
2	Formation	14/11/2000	11	0,148	6,738	0,027	36,571	179,585	89,792
3	Destruction	19/11/2000	-	0,102	9,846	0,039	25,600	87,997	43,998
4	Formation	21/11/2000	19	0,125	8,000	0,031	32,000	137,495	68,747
5	Evolution	24/11/2000	20	0,125	8,000	0,023	42,666	244,435	122,217

Tableau 1 : résultats (Lc : longueur d'onde des croissants observée sur le terrain, f_i : fréquence de l'onde incidente, T_i : période de l'onde incidente, f_e : fréquence du pic principal de l'infragravité, T_e : période de l'infragravité et Le : longueur d'onde de l'infragravité).

5. Interprétation.

Pour valider le modèle de structuration des croissants de plage à partir des ondes infragravitaires, il convient donc de mesurer les périodes des ondes infragravitaires et de vérifier que la longueur d'onde des formes rythmiques correspond à la moitié de celle calculée théoriquement à partir de la relation de dispersion (1) dans le cas subharmonique, le plus couramment admis. Plusieurs situations ont été considérées dans cette étude.

Les situations 1, 2 et 4 correspondent à la formation de croissants de plage. En comparant le pic principal de l'infragravité pour chaque situation, la longueur d'onde calculée ne correspond pas à la longueur d'onde observée des croissants. Les fréquences sont toujours trop basses pour générer de petites longueurs d'onde comme celle des croissants. Donc l'infragravité ne semble pas être le moteur principal de la formation des croissants de plage pour les situations étudiées.

Dans la situation 5, les croissants sont déjà formés. Il est intéressant de voir si l'infragravité a une influence sur l'évolution de la longueur d'onde des croissants dans le temps ou si les croissants sont en mesure de créer ou de maintenir une onde infragravitaire dont la longueur d'onde est compatible avec les croissants de plage⁸. Ici, la longueur d'onde des croissants est différente de celle du pic principal dans le domaine infragravitaire. Il est donc possible d'en déduire pour notre cas que l'infragravité n'est pas le moteur principal dans l'évolution morphologique des croissants de plage et qu'aucune onde infragravitaire spécifique ne semble maintenue par les croissants.

La situation 3 correspond à une phase de destruction des croissants. Le but est alors de voir si l'infragravité participe à leur destruction. Or, dans le spectre d'énergie du 19 novembre 2000, le pic qui correspond à celui de la mer du vent est plus énergétique que celui de l'infragravité et cette mer du vent d'influence maritime dirigée obliquement vers la côte (en provenance de sud) a manifestement participé à la destruction des croissants. Il semble donc que la cause principale de destruction des croissants soit liée à des ondes de hautes

fréquences qui viendraient déstructurer le bas de plage par une action important sur le jet de rive plutôt que par l'apparition d'ondes de basses fréquences.

6. Discussion.

La génération des croissants de plage sur le site de Sète ne semble pas liée au forçage d'ondes infragravitaire, pour les paramètres utilisés dans cette étude. Cependant, de nombreuses variables peuvent modifier fortement le calcul de la longueur d'onde des ondes infragravitaires. La plus problématique est celle concernant la pente de la plage. En effet, lors des études, personne ne définit à quoi correspond précisément la pente de la plage^{6,7,8}. Dans notre cas, la valeur utilisée $\tan\beta$ (= 0,086) correspond à la valeur mesurée à l'endroit où se forment les croissants, ce qui aboutit à des longueurs d'onde L_c calculées trop importantes par rapport à celles mesurées sur le terrain. Cependant, si on prend la pente moyenne de l'avant-côte, soit $\tan\beta = 0,01$, les longueurs d'onde calculées pour L_c peuvent être compatibles avec celles mesurées sur le terrain. Le mode n utilisé pour l'onde infragravitaire fait aussi fortement varié le calcul de la longueur d'onde mais vers des valeurs de moins en moins compatibles avec la longueur d'onde des croissants observés. De plus, la mise au carré de T dans la relation de dispersion accroît l'imprécision du calcul.

Si la génération de croissants de plage n'est pas liée à l'infragravité, elle peut être liée à l'auto-organisation. La formule théorique de Werner et Fink (1993), reliant la longueur d'onde des croissants à la distance parcourue par le jet de rive est tout à fait compatible avec les observations de terrain à Sète (des incursions du jet de rive entre 6 et 18 m pour des longueurs d'onde de croissants de 10 à 30 m). Un autre cas de figure, proche de l'auto-organisation, semble pouvoir être évoqué ici. Pour les observations faites le 07/11/2000, la formation des croissants pourrait être à rattacher à un mécanisme de propagation d'une instabilité gravitaire. En effet, il semble qu'à partir d'une hétérogénéité ponctuelle importante du relief de bas de plage on est vu les croissants se former de proche en proche dans le sens de propagation de la houle, oblique ce jour-là.. L'irrégularité de départ de la topographie aurait pu créer des perturbations hydrodynamiques qui seraient responsables de la génération de croissants de plage en aval.

Si les causes de la génération des croissants de plage n'ont pu être trouvées, il est possible d'affirmer qu'une mer du vent ($f=0,33$ Hz) avec une incidence oblique est responsable de la destruction de ces formes rythmiques. Masselink et Pattiaratchi (1998) avançaient déjà une incidence du vent et de la mer du vent sur l'évolution des croissants au fil du temps.

Dans le cadre de cette étude, un nouveau suivi hydrodynamique va être réalisé sur des durées plus longues et avec l'instrumentation d'un profil longitudinal. Cela permettra d'échantillonner les fréquences de manière plus précise. Il faudra également faire un suivi topographique plus détaillé de la pente de la plage afin de voir les différentes composantes qui peuvent entrer en jeu dans la génération des croissants.

7. Conclusion.

L'objectif de cette étude était de déterminer la part des ondes infragravitaires comme cause dans la génération des croissants de plage. A la vue des données hydrodynamiques et topographiques, les longueurs d'ondes des croissants de plage formés ne correspondent pas à celles des ondes infragravitaires. Il semble donc que l'on puisse conclure que pour les cas étudiés l'infragravité n'est pas le moteur principal dans la formation des croissants de plage.

8. Références bibliographiques.

- ¹ Guza, R. T. and Inman, D. L., (1975). Edge waves and beach cusps, *J. Geoph. Res.*, **80** (21), 2997-3012.
- ² Inman, D. L. and Guza, R. T., (1982). The origin of swash cusps on beaches, *Mar. Geol.*, **49**, 133-148.
- ³ Werner, B. T. and Fink, T. M., (1993). Beach cusps as self-organized patterns, *Science*, **260**, 968-971.
- ⁴ Coco, G., Huntley, D. A. and O'Hare, T. J., (2000). Investigation of a self-organization model for beach cusp formation and development, *J. Geoph. Res.*, **105** (C9), 21991-22002.
- ⁵ Coco, G., O'Hare, T. J. and Huntley, D. A., (1999). Beach cusps: A comparison between data and theories for their formation, *J. Coastal Res.*, **15** (3), 741-749.
- ⁶ Masselink, G. and Pattiariatchi, C. B., (1998). Morphological evolution of beach cusps and associated swash circulation patterns, *Mar. Geol.*, **146**, 93-113.
- ⁷ Coco, G., Burnet, T. K. and Werner, T., (2003). Test of self-organization in beach cusp, *J. Geoph Res.*, **108** (3), 3101-3112.
- ⁸ Holland, K. T. and Holman, R. A., (1996). Field observations of beach cusps and swash motions, *Mar. Geol.*, **134**, 77-93.
- ⁹ Holland, K. T., (1998). Beach cusp formation and spacings at Duck, USA, *Cont. Shelf. Res.*, **18**, 1081-1098.
- ¹⁰Certain, R., Meulé, S., Rey, V. and Pinazo, C., (2005). Wave transformation on a microtidal barred beach (Sète, France), *J. Mar. Sys.*, **38**, 19-34.
- ¹¹Bauer, B.O., 1990. Assessing the relative energetics of infragravity motions in lakes and seas. *J. Coast. Res.*, **6**, 853– 865.

CARACTERISATION HYDRODYNAMIQUE D'UN LITTORAL A BARRES D'AVANT-COTE FESTONNEES (GOLFE DU LION, FRANCE) : MESURES IN-SITU ET MODELISATION.

Pierre FERRER¹, Nans BUJAN², Raphaël CERTAIN¹, Yann LEREDDE²

¹ Université de Perpignan Via Domitia, E.A. 3678, Institut de Modélisation et d'Analyse en Géo-Environnement Santé, 52 av Paul Alduy, 66 860 Perpignan Cedex, France (pierre.ferrer@univ-perp.fr)

² Université de Montpellier 2, Géosciences Montpellier, UMR 5573, Laboratoire GTS, cc60, 34095 Montpellier Cedex 05

Résumé :

L'objet de cette communication est la caractérisation hydrodynamique d'un système double de barres d'avant-côte festonnées en milieu microtidal. Pour comprendre l'évolution du littoral de Leucate-Plage (Languedoc-Roussillon, France), une campagne de mesures hydrodynamiques in-situ a été réalisée, puis complétée grâce à une étude à l'aide du modèle numérique Quasi-3D SHORECIRC de la houle et des courants en simulant des conditions plus dynamiques non observées. Les mesures in-situ ont permis de réaliser des cartes de circulation hydrodynamique. Les données modélisées donnent des résultats proches de la réalité en termes de vitesses de courants dans la zone de déferlement, en termes de direction et de vitesses dans la zone de *shoaling*.

Abstract :

This paper deals with the hydrodynamic study of a microtidal double crescentic bars system. To understand the coastal evolution of Leucate-Plage (Languedoc-Roussillon, France), a hydrodynamic survey has been realized, added to numerical studies with Q-3D SHORECIRC model for more dynamic unobserved conditions. Hydrodynamic maps based on field data have been produced. The numeric modelling shows good analogies in the shoaling zone but some difference in the surf zone.

Mots clés : barres d'avant-côte en festons, microtidal, hydrodynamique, SHORECIRC.

1. Introduction.

Le littoral du golfe du Lion présente plusieurs types de morphologies sous-marines. Ainsi, dans sa partie nord (Sète) il montre un système double de barres d'avant-côte rectilignes alors qu'au niveau de Leucate, auquel on s'intéresse dans cet article, il présente un système double de barres festonnées. La génération de ces systèmes rythmiques serait liée soit à la présence d'ondes infragravitationnelles (BOWEN & INMAN, 1971), soit à un phénomène d'auto-organisation (COCO *et al.*, 2002).

Pour de tels systèmes, des études hydrodynamiques de terrain ont été menées sur la côte aquitaine en milieu méso-tidal (FROIDEFOND *et al.*, 1990 ; CASTELLE *et al.*, 2006b) mais aucune mesure n'a été réalisée en milieu microtidal.

Des études numériques sur les barres festonnées ont par ailleurs cherché à modéliser leur génération et à prédire leur évolution grâce à différents modèles hydro-sédimentaires tels que Morfo55 (GARNIER *et al.*, 2006) ou encore MORPHODYN (CASTELLE *et al.*, 2006a).

Ce travail propose d'étudier les caractéristiques hydrodynamiques d'un système double de barres festonnées en milieu microtidal : (1) à partir d'appareils de mesures hydrodynamiques (ADV et ADCP) déployés en janvier 2007 lors d'une campagne d'acquisition intensive à Leucate-Plage (golfe du Lion) et (2) grâce aux sorties de modélisations de circulation hydrodynamique faites à partir de SHORECIRC, tout en étudiant le fonctionnement de ce modèle dans un tel environnement.

2. Site d'étude.

La zone retenue pour cette expérience se situe à Leucate, dans le golfe du Lion, en Languedoc-Roussillon (voir figure 1). Elle correspond à un des sites méditerranéens des programmes Liteau 2 et Beachmed-e, qui étudient les environnements d'avant-côte à barres sédimentaires.

Ce site microtidal (0,15m de marnage) est dominé par les vagues. Les vents dominants proviennent de terre (NW) ou de mer (E à SE). Ils induisent des variations de niveaux importantes, qui peuvent atteindre 1m à la côte. Les vagues créées par les vents de NW sont généralement faibles (0,3m) avec des périodes allant de 3 à 4 secondes (mer du vent). Les vagues dominantes sont induites par les vents de E à SE. Elles atteignent régulièrement des hauteurs significatives de 3,5m avec des périodes comprises entre 5 et 9 secondes.

La morphologie en pente douce (1%) de l'avant-côte jusqu'au rivage est entrecoupée par deux barres sédimentaires rythmiques en festons (interne et externe). La barre externe a une longueur d'onde de l'ordre de 600m alors que

celle de la barre interne est proche de 400m. Cette terminologie est reprise pour décrire les deux fosses séparatrices. Le sédiment superficiel a une granulométrie de sable fin à granule, généralement bien trié et sa médiane décroît du bord vers le large.

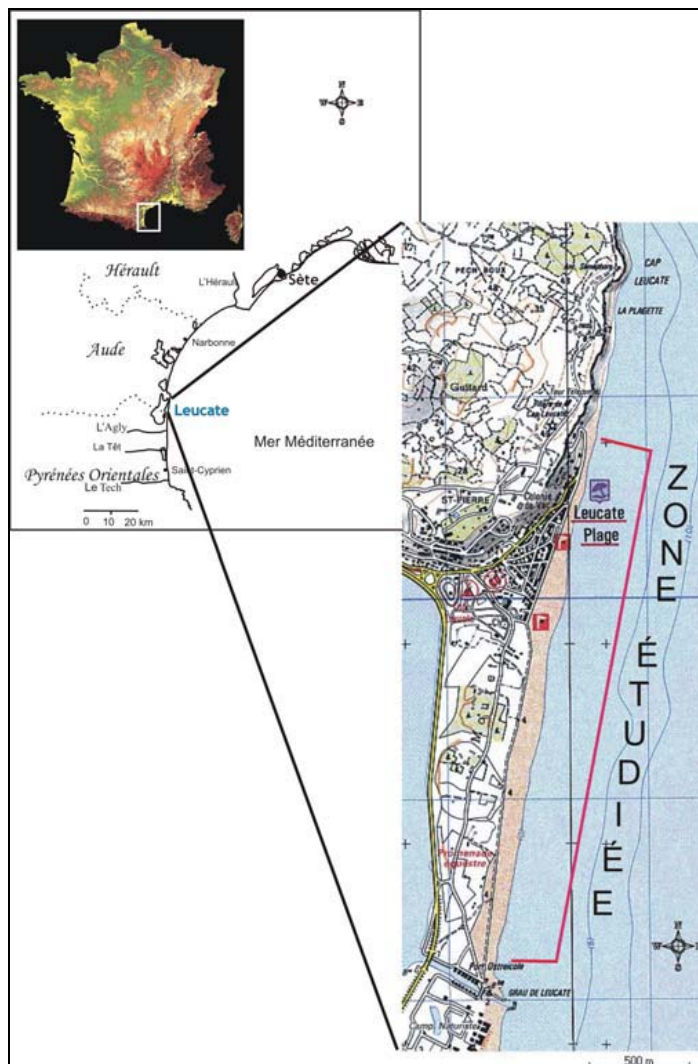


Figure 1 : localisation de la zone d'étude de Leucate.

3. Méthodologie.

3.1. Mesures hydrodynamiques in-situ.

Une campagne a été réalisée du 22 janvier au 12 février 2007 à l'aide d'appareils de mesure de la plate-forme technologique régionale GLADYS. Le dispositif instrumental était composé pour l'étude hydrodynamique de trois courantomètres / houlographes Acoustic Doppler Velocimeter ADV (type Vector

de NORTEK), de quatre courantomètres Acoustic Doppler Current Profiler ADCP (type Sentinel 600 et 1200 Hz de RD INSTRUMENTS) et d'une bouée DATAWELL positionnée au large de Leucate sur une profondeur de 40m ; d'un sondeur mono-faisceau couplé à un GPS pour l'étude bathymétrique. Un plan de positionnement précis a été utilisé afin d'instrumenter l'ensemble de la barre externe sur un feston entier afin de couvrir au mieux la circulation spatiale complexe et la partie interne correspondante (voir figure 2).

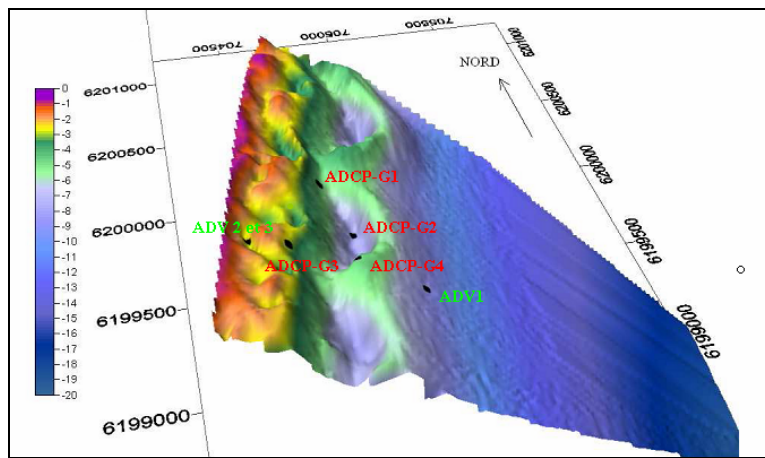


Figure 2 : plan de position des instruments lors de la campagne de mesure hydrodynamique.

Ces données ont ensuite été extraites grâce au logiciel WaveMon® développé par RD instruments avant d'être traitées grâce à des routines sous Matlab®.

3.2. Modélisation à l'aide de SHORECIRC.

SHORECIRC est un modèle développé en 1992 par l'Université du Delaware (EU). Il s'agit d'un modèle de circulation quasi-3D utilisant les courants intégrés sur la verticale (équations de Saint-Venant) couplé au modèle REFDEF qui fournit les forçages de la houle (tensions de radiations et flux de masse) (VAN DONGEREN *et al.*, 1994 ; SVENDSEN *et al.*, 2004). L'originalité de ce modèle quasi-3D est d'introduire une variation semi-empirique des courants sur la verticale et ainsi de mieux représenter les effets 3D de dispersion. On peut alors coupler courants sur le fond et vitesses orbitales sur le fond pour évaluer le transport sédimentaire dans les zones de la colonne d'eau où celui-ci a principalement lieu. Les effets de dérive due aux vents, particulièrement puissants et fréquents dans la région du Languedoc, sont pris en compte. Le modèle a subi plusieurs modifications afin de prendre en compte les phénomènes de réfraction et donc de pouvoir fonctionner sur des configurations de plage possédant des traits

de côte irréguliers et/ou des structures émergées (épis et brise-lames présents en nombre dans la région), de prendre également en compte les effets de la force de Coriolis ou encore de proposer des frontières latérales ouvertes de types Neumann.

Les premières évolutions de ce modèle furent proposées avec des travaux de thèses (VAN DONGEREN, 1997 ; SANCHO, 1997...). Dans cette même optique, des modélisations sont réalisées pour le golfe du Lion au laboratoire Géosciences Montpellier, avec les travaux de BUJAN (en cours).

4. Résultats.

A partir des données enregistrées sur la bouée Datawell, il a été possible d'observer trois coups de mer (tableau 1).

Tableau 1: caractéristiques de la houle, observées au large pour les différents coups de mers (la normale à la côte se situe autour de 100°).

Date	Direction de la houle (en degrés)	Hauteur significative (en mètres)	Période (en secondes)
22 janvier 2007	140	1,2	6
25 janvier 2007	80	1,5	7
30 janvier 2007	80	0,7	6

A partir des données traitées à la côte, des profils verticaux de courants ont été réalisés pour les différents coups de mer observés. Ces profils ont permis de dégager les différents courants littoraux qui entrent en jeu dans la circulation hydrodynamique (voir figure 3A). Nous avons ainsi pu observer des courants longitudinaux tels que la dérive littorale et le courant induit par le vent et les courants transversaux tels que le courant de retour et ceux d'arrachement.

En parallèle, afin de valider l'utilisation du modèle SHORECIRC pour la plage de Leucate-Plage, les conditions météo-marines ont été reproduites par la modélisation (voir figure 3B et 3C). Lors de cette campagne de mesures, seules des conditions de faible agitation ont pu être enregistrées. Il est plus facile de valider un modèle en conditions extrêmes (hauteur significative importante, période grande...) que pour nos observations *in-situ*. Les conditions n'étaient pas assez dynamiques pour valider le modèle dans la zone de déferlement comprise trop près de la côte et où le nombre d'appareils de mesure était insuffisant. Cependant les courants modélisés et ceux observés en un point de mesure présentent le même ordre de grandeur. Dans les zones situées plus au large (zone

de *shoaling* sous ce régime hydrodynamique), les résultats modélisés sur le système externe sont plus réalistes.

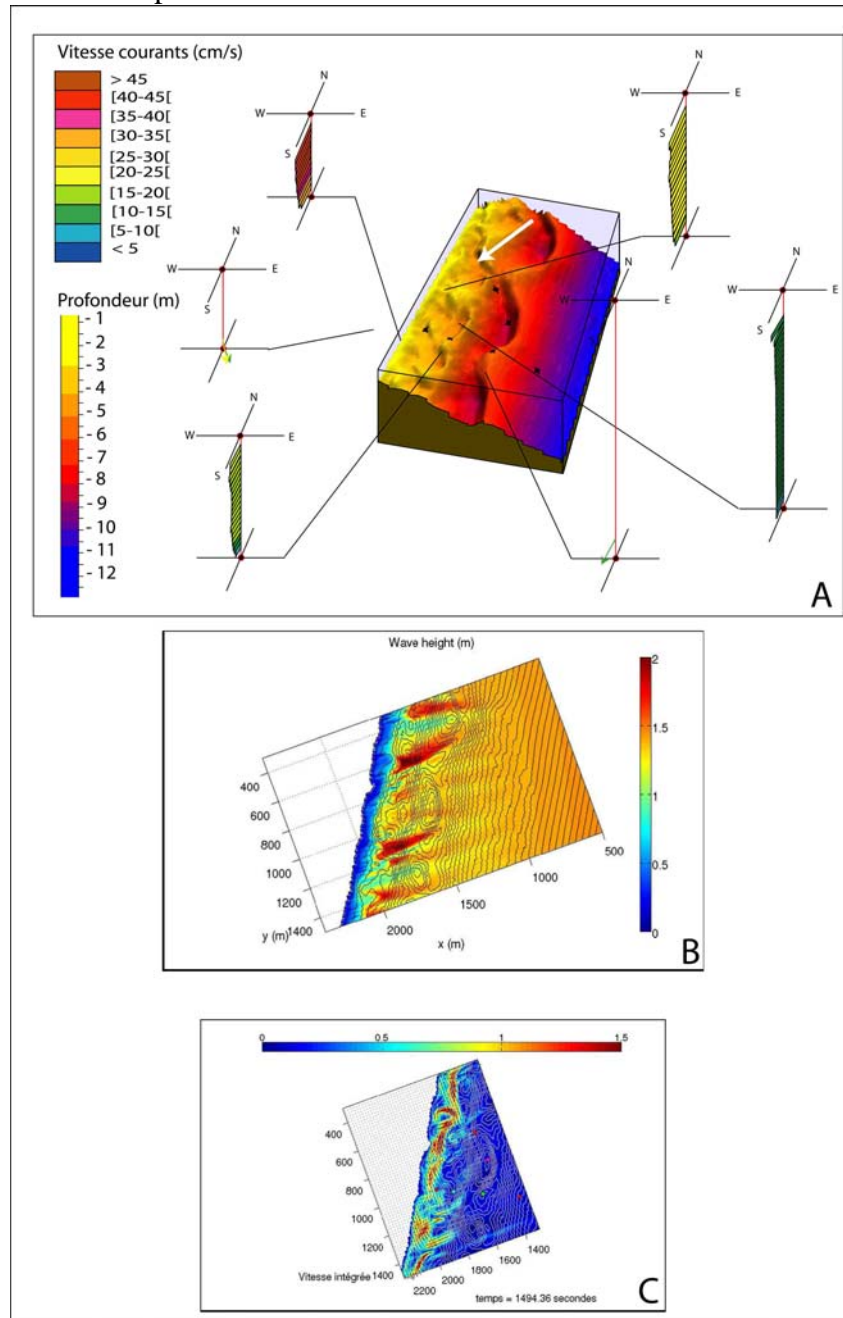


Figure 3 : Exemple de données recueillies et modélisées pour un coup de mer avec une houle de nord-est. A - Mesures in-situ. B - Modélisation de la houle avec SHORECIRC. C - Circulation intégrée sur la verticale résultante.

A partir de ces observations, des cartes de circulation hydrodynamique numériques pour des conditions plus dynamiques (zone de déferlement élargie à

tout le système de barres) ont ainsi pu être réalisées et comparées entre elles (voir figure 4). Les données de propagation de la houle, du déferlement de la houle et de circulation hydrodynamique ont pu être comparées depuis la zone externe jusqu'au bord. Les seuils d'activation des différents systèmes (interne et externe) ont pu être déduits de ces comparaisons.

A partir des données enregistrées, l'analyse du spectre d'énergie sera réalisée.

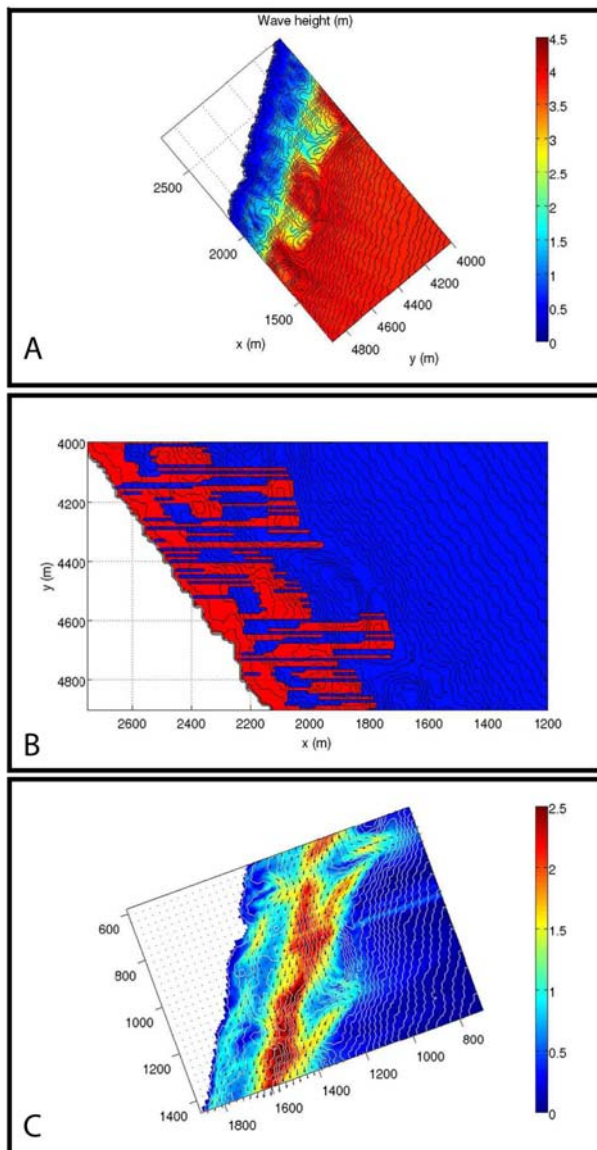
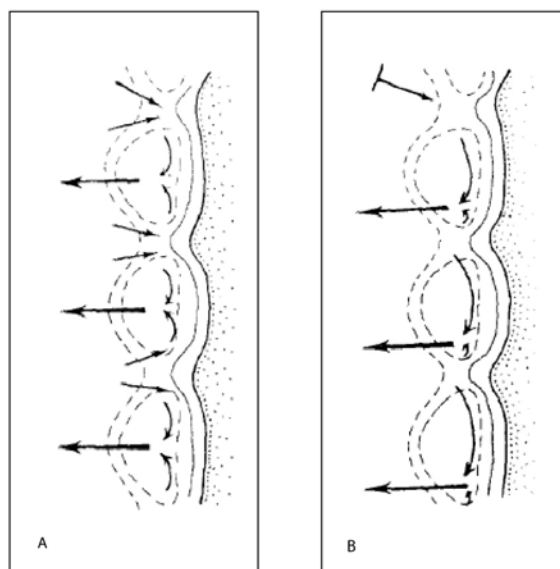


Figure 4 : Exemple de carte pour une houle d'incidence 35°, une hauteur significative de 4m et une période de 8s. A - Carte de propagation de la houle. B - Carte de déferlement de la houle. C - Carte de la circulation hydrodynamique.

5. Interprétation.

Après cette campagne de mesure mais toujours pendant le suivi morphologique mensuel du site , la hauteur significative maximale de la houle, au niveau de la bouée DATAWELL a atteint successivement 2,5m et 3,5m. , La comparaison des cartes bathymétriques a montré que pour ces valeurs extrêmes enregistrées, le système externe ne se déplace pas. Les cartes modélisées montrent que le déferlement sur le système externe se produit seulement à partir d'une hauteur significative égale à 4m, correspondant ainsi à son seuil d'activation. De même, la comparaison carte à carte des données bathymétriques a montré que le système interne évolue à partir d'une houle de hauteur significative proche de 1m. Ce seuil d'activation a pu être comparé aux données modélisées, et il est possible d'observer un déferlement sur le système interne dès cette hauteur significative ($H_s = 1m$).

Les profils verticaux mesurés et modélisés montrent bien la présence de courants transversaux et longitudinaux liés aux conditions d'entrée du système. Une comparaison des schémas de circulation (voir figure 5) proposés par FROIDEFOND *et al.* (1990) avec les cartes obtenues par modélisation numérique montre par exemple que pour une faible incidence et une hauteur significative inférieure à 4m, l'eau est évacuée par les fosses avec une bonne correspondance modèle conceptuel/modèle numérique. Dans le cas d'une augmentation de l'incidence de la houle, le schéma proposé correspond à celui modélisé numériquement avec un décalage de l'évacuation de l'eau vers les cornes.



*Figure 5 : circulation hydrodynamique au niveau d'une barre festonnée (FROIDEFOND *et al.*, 1990).*

Grâce aux différentes cartes obtenues, on constate par ailleurs que la période de la houle a une incidence sur l'intensité des courants indépendamment de la hauteur de la houle à l'approche de la barre externe mais aussi sur la position du point de déferlement. Les cartes obtenues permettent d'être en accord avec les prévisions analytiques de HSU *et al.* (2006) concernant la hauteur significative et la période de la houle.

La comparaison des spectres d'énergie de la houle observée à l'entrée du système (bouée DATAWELL) et à la côte (ADV) montre un faible transfert d'énergie vers l'infragravité à la côte.

6. Discussion et conclusion.

L'utilisation du modèle SHORECIRC présente certaines limites dans notre étude. Ces limites sont dues aux conditions limites d'utilisation de REF/DIF mais aussi au fait que la zone est peu étendue. Le modèle SHORECIRC nécessite une zone très large pour prendre en compte le vent par exemple.

Malgré les quelques divergences en terme de direction, la modélisation est en accord avec les observations de terrain. En terme de circulation hydrodynamique, les courants observés et ceux modélisés sont proches d'un point de vue intensité et direction dans la zone de shoaling. Concernant la zone de déferlement, le manque d'instruments de mesure très près de la côte pour des conditions de faible agitation ne permet pas de réaliser une comparaison entre la circulation hydrodynamique modélisée et celle observée.

Les seuils d'activation des barres déterminés par une double approche terrain/numérique dépendent des conditions hydrodynamiques. Pour la barre externe, il se situe aux alentours de 4m. Pour la barre interne, le seuil d'activation a pu être mesuré aux alentours de 1m.

Pour affiner l'utilisation de ce modèle en mer Méditerranée, une nouvelle campagne d'acquisition est en cours sur le site de l'Espiguette (golfe du Lion) afin de valider l'utilisation de ce modèle dans différentes conditions dans un système moins complexe.

7. Références bibliographiques.

- ¹ BOWEN, A.J., INMAN, D.L., 1971. *Edge waves and crescentic bars*, Journal of Geophysical Research, 76, 8662-8670.
- ² BUJAN, N. Application d'un modèle de circulation côtière quasi tridimensionnel à la dynamique des plages du Languedoc-Roussillon. Thèse de doctorat en Géosciences marines, Université de Montpellier II, *en cours*.

- ³ CASTELLE B., BONNETON P., BUTEL R., 2006a. *Modeling of crescentic pattern development of nearshore bars: Aquitanian Coast, France*, Comptes Rendus Geosciences, 338, 795-801.
- ⁴ CASTELLE, B., BONNETON, P., SENECHAL, N., DUPUIS, H., BUTEL, R., MICHEL, D., 2006b. *Dynamics of wave-induced currents over a multiplebarred sandy beach on the Aquitanian Coast*, Continental Shelf Research, 26 (1), 113-131.
- ⁵ COCO G., CABALLERIA M., FALQUÈS A., AND HUNTLEY D.H., 2002. *Crescentic bars and nearshore self-organization processes*. In Proceedings of 28th International Conference of Coastal. Engineering, ASCE.
- ⁶ FROIDEFOND, J.-M., GALLISSAIRES, J.-M., PRUD'HOMME, R., 1990. *Spatial variation in sinusoidal on a crescentic nearshore bar: application to the Cap Ferret Coast*. Journal of Coastal Research, 6, 927–942.
- ⁷ GARNIER, R., CALVETE, D., FALQUES, A., CABALLERIA, M., 2006. *Generation and nonlinear evolution of shore-oblique/transverse sand bars*. Journal of Fluid Mechanics, 567, 327-360.
- ⁸ HSU, T.W., HSU J.R.C., WENG, W.K., WANG, S.K., OU, S.H., 2006. Wave setup and set-down generated by obliquely incident waves. *Coastal Engineering*, 53, 865-877.
- ⁹ SANCHO, F.E., 1997. Unsteady Nearshore Currents on Longshore Varying Topographies. PhD Thesis in Civil Engineering, University of Delaware, Newark, USA., 319 p.
- ¹⁰ SVENDSEN, I. A., HAAS, K., ZHAO, Q., 2004, ``Quasi-3D Nearshore Circulation Model SHORECIRC: Version 2.0'', Research Report, Center for Applied Coastal Research, University of Delaware, 65 p.
- ¹¹ VAN DONGEREN, A.R., 1997. Numerical modelling of quasi-3d nearshore hydrodynamics. PhD thesis, University of Delaware, Newark, USA.
- ¹² VAN DONGEREN, A.R., SANCHO, F.E., SVENDSEN, I.A., PUTREVU, U., 1994. SHORECIRC: a quasi 3-D nearshore model. In: Proc. 24th International Conference on Coastal Engineering, ASCE, Kobe, pp. 2740–2754.

HOLOCENE SANDY BARRIEREVOLUTION AS INDICATED THROUGH LAGOONAL SEDIMENTARY INFILL. THE EXAMPLE OF THE THAU LAGOON-AND-BARRIER SYSTEM (WESTERN GULF OF LIONS, MEDITERRANEAN SEA,FRANCE)

P. Ferrer¹ *, B. Tessier², M. Benabdellouahed², R. Certain¹, J.-P. Barusseau¹

¹ LEGEM, University of Perpignan, 52 avenue Paul Alduy, 66860 Perpignan Cedex, France - pierre.ferrer@univ-perp.fr

² UMR CNRS 6143 M2C,University of Caen, 2-4 rue des tilleuls, 14000 Caen, France

Abstract

As soon as a littoralbarrier begins to construct, isolating progressively a lagoon, the sedimentaryinfill of the later can start and be potentially preserved. The differentstages of a barrier construction and evolution can be thus analyzed by studyingthe sedimentary record preserved into the lagoon. Such a study has beenperformed, using very high resolution seismic data and sediment cores, into theThau lagoon (SE France) that forms during the Holocene transgression. Two mainsedimentary units above the rocky basement have been defined into theinfilling. U1 corresponds probably to remnants of pre-Holocene continentalfacies, U2, which constitutes the main part of the infill, represents theHolocene infill. The detailed analysis of U2 allows to reconstruct thepalaeogeographic evolution of the lagoon-barrier system during the last stagesof the Holocene transgression.

Keywords : Lagoons, Seismics, Gulf Of Lions.

The Mediterranean coastline is characterized bynumerous lagoons that are separated and protected from the sea by sandybarriers (also called lidos) resulting from a process of shore regularizationby waves [1]. These lagoon/lido systems have been formed during the Holocenetransgression and more precisely during the late Holocene period when sea-levelrise slow down. Since they are protected from high energy open marine-hydrodynamics, the lagoons are the most favorable areas to preserve into theirsedimentary infilling, the different stages of construction of the beach barrierand adjacent shoreface that are usually subject to heavy wave reworking.

The Thau lagoon is one these Mediterraneanlagoons. It is located along the shore of the western Gulf of Lions(Languedoc-Roussillon, France) and belongs to a lagoon system that developsfrom the Rhone delta to the Spanish border. It is the largest and deepestlagoon. In order to study the sedimentary infill of the Thau lagoon, a veryhigh resolution seismic survey has been performed. In addition, some cores havebeen collected for lithology analysis and ¹⁴C dating.

Three main seismic units have been recognized,U0 representing the rocky substratum, U1 and U2 forming together thesedimentary infill of the lagoon [2] (Figure). U0 is represented by tilted,locally folded, reflectors interpreted as Pliocene to Miocene formations. Theupper limit of U0 is an erosional surface corresponding to the bottom of thelagoon basin. The basal unit of the infill, U1, is acoustically transparent,locally chaotic, and rests discordantly on U0. Its thickness is variable, from0 to about 6 meters. It is mainly developed where the substratumis the deepest and tends to shape the erosional top surface of U0. U1 has notbeen reached by coring and its origin is uncertain. It probably corresponds to the very early stageof the lagoon infill, either of continental or marine origin. U2 constitutes the main unit of the sedimentary infill and reaches locally about 15 m in thickness. Itsrests discordantly on U0, and concordantly on U1. Its upper surface is the lagoonbottom. U2 displays a general aggrading configuration and consists in an alternation of high amplitude and continuous parallel reflectors, and lowamplitude, poorly continuous reflectors. U2 can be divided in two sub-units,SU2-1 and SU2-2. SU2-2 is generally concordant on SU2-1, especially where U2 isthe thicker, toward the center of the lagoon. On topographic highs of thebasement, SU2-2 rests discordantly on SU2-1. A marked unconformity between the 2sub-units is also observed on the seaward edge of the lagoon, i.e. on thelandward face of the present-day lido (Figure). This unconformity isassumed to indicate a probably important landward shift of the barrier. Thus, as recorded by the lagoon infill through theseismic data, two main stages of construction of the littoral barrier seem tohave occurred, a significant retrogradational event having arised between stage1 (SU2-1) and stage 2 (SU2-2). During each of the stages,seismic facies evidences alternations of period of respectively low energy(high amplitude continuous reflectors) and high energy (low amplitudediscontinuous reflectors) deposition that could be related to more or lessprotected configuration of the lagoon, and thus to the barrier state ofstability. Cores collected in SU2-2 are composed of successivesequences consisting of thick shelly layer passing upward to organic richclayey layer. The process that could explain this sediment alteration is notfully understood but is probably due to change in biological productivity andthus could be related to climate fluctuation.

However the link between suchchanges in sedimentation, seismic facies, and barrier dynamic cannot be clearlyestablished at the present state of the study.

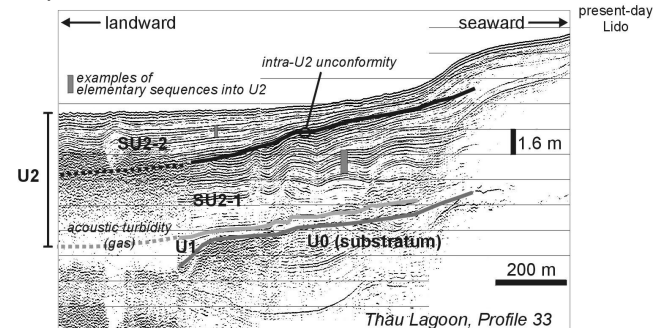


Fig. 1. southernd end of the seismic profile 33 shot into the Thau Lagoon. The unconformitywithin U2, the main holocene infill unit, is well marked below the landwardface of the present-day lido. In the center of the lagoon,the seismic image of the infill is masked by gas occurrence.

In terms of chronology, ¹⁴C AMS analyses arein course. However, we assume that the beginning of the lagoonal infill, coevalwith the initiation of barrier construction has occurred when sea-level riseslowered down, and reached almost its present-day level, i.e. around 6.000 B.P.We assume as well that the barrier retrogradational event recorded into thelagoon infill between SU2-1 and SU2-2 could be dated around 2000 B.P. Indeed,previous studies have demonstrated that the regional coastline has severelyretreated since Classical times as a result of a drastic decrease in sedimentsupply [3]. In that hypothesis, the successive sequences preserved into thelagoon infill could represent the record of millennial to multcentennialtime-scale climatic cycles that would have controlled sediment supply and thebarrier morphodynamic.

References

- 1 - Certain, R., Tessier, B., Courp, T., Barusseau,J.P. & Pauc, H., 2004. Reconnaissance par sismique très haute résolution du remplissage sédimentaire de la lagune de Leucate (Aude et Pyrénées-Orientales - SE France). Bull. Soc. Géol. Fr., 175,n°1, 35-48.
- 2 - Benabdellouahed, M., 2005. Etude du remplissageHolocene de l'étang de Thau, Golfe du lion (Analyse par prospection sismiqueTHR). Rapport de Master 2 Recherche, Université de Caen.
- 3 - Tessier B., Raphaël Certain R., Jean-Paul Barusseau J.P. & Henriet J.P. (2000) Historicalevolution of the littoral prism of the Thau lagoon barrier (Sète, South-East France). Veryhigh-resolution reflection seismic investigation. C. R. Acad. Sciences Earth and Planetary Science, 331, Issue 11, 709-716.

HYDRODYNAMICS STUDIES IN FRONT OF A SEAWALL (Véran site, Gulf of Lions, Mediterranean coast)

Olivier Samat, CEREGE-Université Aix Marseille I, France. samat@cerege.fr

Fabrice Gouaud, LSEET LEPI-Université du sud Toulon-Var, France.

Raphaël Certain, Université de Perpignan, France

Adrien Lambert, CEREGE-Université Aix Marseille I, France

Samuel Meulé, CEREGE-Université Aix Marseille I, France

François Sabatier, CEREGE-Université Aix Marseille I, France

In coastal engineering, it is current practice to use seawalls to protect the coast and limit storm floods. When these seawalls are constructed at the shoreline, their impact on bathymetric evolution remains poorly known.

A previous study (Samat et al, 2006) dealing with morphological impact of a seawall on the barred sandy coast of Véran site, (Gulf of Lions, Mediterranean coast) indicates an increase in sedimentary losses and a deepening of the trough at the foot of the structure. This evolution was supposed to be caused by an increase in turbulence due to reflective dynamics related to the presence of the seawall. (Kraus 1988)

To support this assumption we studied the hydrodynamical processes in front of this seawall. (Fig.1)

An intensive current meter survey measurement was conducted. Data were obtained over a two weeks period (21nov-05dec-2005), on two instruments station in a cross shore transect, in the inner and the outer trough. Four instruments were deployed in front and close to the seawall to study wave and current conditions. A S4-ADW was positioned in the inner trough and an ADV (Fig.2) and an ADCP in the outer trough.

Raw data were stored and analysed to obtain current information.

Concerning wave data processing, two ways were explored. On one hand assuming a progressive wave we determine incident wave spectrum on the three current meters. According to these considerations we obtained significant wave during all the period of deployment. On the other hand assuming a partially standing waves, we used an algorithm providing incident and reflective waves (Certain et al, 2005) in order to get wave reflected energy ratio.

Results on current analyses show main flow direction to the East. There is a good correlation in direction and intensity between flow characteristics and significant wave characteristics (direction and height) in both troughs.

Results on wave reflected energy ratio, compared to results of Certain et al, (2005) on a natural beach (fig.2), show an increase of reflected ratio in front of the seawall during storm conditions. We conclude

that the seawall increase significantly the reflexions processes which can explain high mobility in the upper shoreface.



Figure 1: Site location

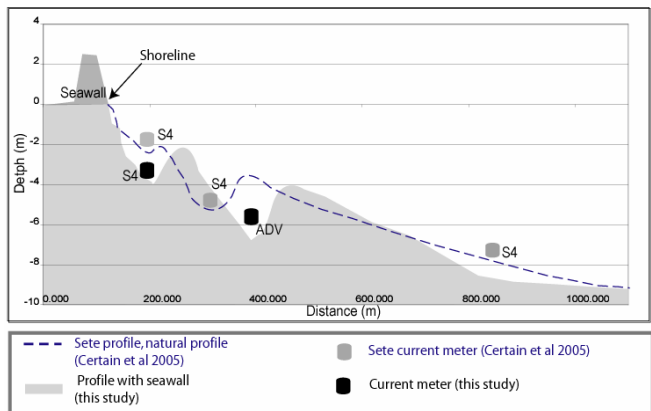


Figure 2: Cross shore hydrodynamical experiments on a natural profile (Certain et al 2005) and for this study

BIBLIOGRAPHY

- Certain R., Meulé S., Rey V., and Pinazo C., 2005. Wave transformation on a microtidal barred beach (Sète, France) *Journal of Marine Systems*, Volume 58, (Issues 1-2), October 2005, Pages 19-34.
- Kraus N.C., 1988. The effects of seawalls on the beach: an extended literature review, *Journal of coastal research* SI (4) 1-28.
- Miles J.R., Russel P.E., and Huntley D.A., 2001. Field measurement of sediment dynamics in front of a seawall, Institute of Marine Studies University of Plymouth, *journal of coastal research*, 17.(1), 195-206.
- Samat O., Sabatier F., Lambert A., 2006. Erosion of the sandy bottom in front of a seawall (Véran site, Gulf of Lions, Mediterranean coast). In: Sanchez-Arcilla, A. (Ed.), 2005, - *Coastal dynamics 2005. Proceedings of the 5th international conference*, April 4-8, Barcelona, Spain: 1-13. - ASCE. - (CD05).

HYDRODYNAMIQUE A L'ECHELLE EVENEMENTIELLE D'UN SYSTEME DE BARRES FESTONNEES DANS LE GOLFE DU LION (LEUCATE-PLAGE, AUDE).

Pierre FERRER^{*}, Fanny ADLOFF^{*}, Raphaël CERTAIN^{*}, Samuel MEULE^{**}, Frédéric BOUCHETTE^{***} et Yann LEREDDE^{***}

* Université de Perpignan Via Domitia, E.A. 3678 Laboratoire d'Etude des Géo-Environnements Marins, 52 av P. Alduy, 66 860 Perpignan Cedex, France (pierre.ferrer@univ-perp.fr)

** CEREGE, Europôle Méditerranéen de l'Arbois, BP 80, 13545 AIX EN PROVENCE cedex 04, France

*** Université de Montpellier 2, ISTEEM, UMR 5573, Laboratoire GTS, cc60, 34095 Montpellier Cedex 05, France

Résumé :

Le littoral de Leucate-Plage constitue une unité hydrosédimentaire bien identifiée. Elle est limitée au nord par les falaises de Leucate et au sud par un grau. Une campagne de mesures hydrodynamiques menée durant les mois de janvier et février 2007 a permis d'étudier l'hydrodynamique à l'échelle évènementielle de ce système à deux barres sédimentaires d'avant-côte de type festonné. Le but est de caractériser les processus du forçage responsables de la génération et du déplacement/maintien de ces morphologies remarquables. Ce site a donc été instrumenté à l'aide d'appareils de mesures hydrodynamiques (ADCP et ADV) de la plate-forme technologique régionale Languedoc-Roussillon GLADYS. Les données recueillies seront intégrées à l'atlas hydrodynamique du programme européen BEACHMED-E.

Grace à un plan de positionnement instrumental adapté (fig. 1), la circulation au niveau d'un feston de la barre externe a pu être observée dans différentes situations hydrodynamiques, variables en hauteur de houle et en direction. De plus, un profil cross-shore a également pu être instrumenté, reliant l'hydrodynamique à la côte et celle à l'entrée du système. Les premiers résultats observés ont permis de mettre en évidence l'importance des différents courants observables sur le littoral, et en particulier au niveau d'un feston. Ainsi, la prédominance de la dérive littorale est mise en évidence (fig. 1). Les autres courants tels que le courant de retour ou le courant d'arrachement sont mesurés dans certains cas de figures. Toutefois, à la vue des résultats, les conditions n'étaient pas assez dynamiques pour que l'on puisse observer des changements morphologiques au niveau de la barre externe. Cependant des changements notables dans la morphologie de la barre interne ont pu être observés. L'étude des données sur le profil cross-shore montre un transfert d'énergie généralisé du large à la côte, vers les domaines de basse fréquence (infragravité). En effet, il est intéressant d'étudier le spectre d'énergie et plus particulièrement le domaine de l'infragravité car elle est l'une des théories de formation des barres en festons (Bowen et Inman, 1971).

Enfin la comparaison des données in-situ avec des modèles hydrodynamiques devrait permettre d'affiner la modélisation et de rendre les modèles de plus en plus réalistes.

Références bibliographiques :

Bowen, A.J. and Inman, D.L., 1971. Edge waves and crescentic bars, *Journal of Geophysical Research*, 76, 8662-8670.

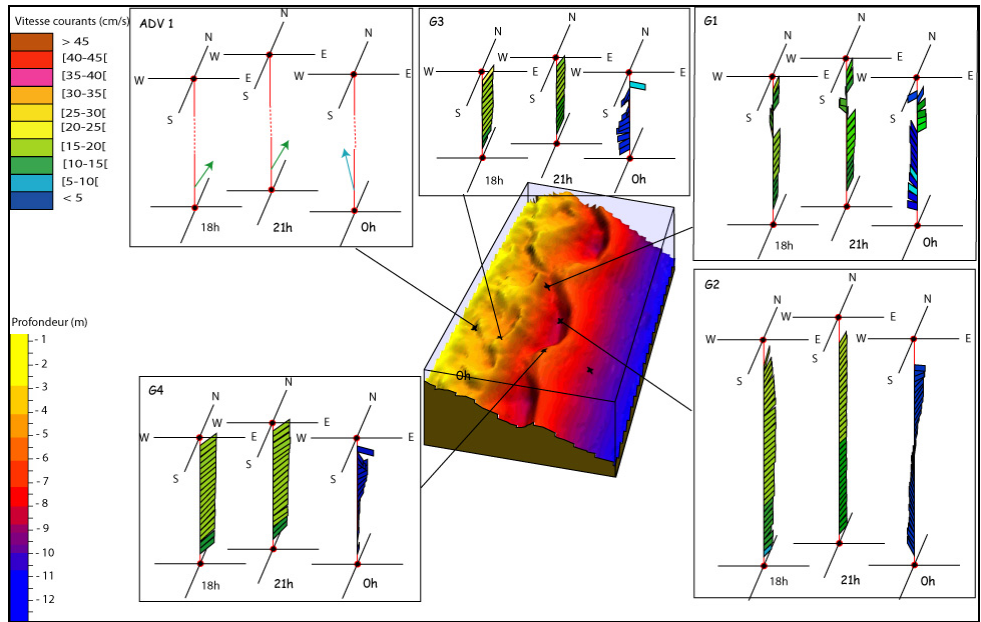


Figure 1 : positionnement des appareils sur la bathymétrie et carte des différents courants sur la colonne d'eau

MORPHODYNAMIQUE PLURIANUELLE D'UN SYSTEME DE BARRES D'AVANT-COTE FESTONNEES EN MILIEU MICROTIDAL (SUD DU GOLFE DU LION).

Pierre FERRER^{*}, Laurent CANCE^{*}, Raphaël CERTAIN^{*} et Jean-Paul BARUSSEAU^{*}

* Université de Perpignan Via Domitia, E.A. 3678 IMAGES, 52 av P. Alduy, 66 860 Perpignan Cedex, France
[\(\[pierre.ferrer@univ-perp.fr\]\(mailto:pierre.ferrer@univ-perp.fr\)\)](mailto:pierre.ferrer@univ-perp.fr)

Résumé :

La France compte 3427 km de côtes. Elle est donc un site privilégié d'étude des systèmes sédimentaires côtiers, notamment les barres d'avant-côte. Le littoral de Leucate-Plage (Aude), dans la partie sud du golfe du Lion, est peu anthropisé et présente donc un intérêt important dans la compréhension d'une plage à barres naturelles en domaine microtidal. Ce site est aussi remarquable par la présence de barres en festons, figures rythmiques parallèles à la côte. Les systèmes à barres festonnées sont présents sur un peu plus d'un tiers des côtes sableuses mondiales.

Basée sur de nombreuses études, une classification des différents systèmes sédimentaires côtiers, comportant une ou plusieurs barres sédimentaires d'avant-côte, a été proposée (Short et Aagaard, 1993). On distingue ainsi deux types de barres sédimentaires d'avant-côte, les barres rectilignes et les barres dites en festons. Les systèmes côtiers à barres sédimentaires peuvent présenter une ou plusieurs barres.

Une première observation de terrain, réalisée en l'an 2000, a permis de mettre en évidence un système à deux barres sédimentaires festonnées avec une barre interne (proche de la côte) et la barre externe (située au large) (fig. 1). La barre externe se localise sur une profondeur comprise entre 5 et 7 m, elle présente une longueur d'onde de 500 m. Alors que la barre interne se situe sur une profondeur comprise entre 2 et 4 m, elle a une longueur d'onde plus réduite de l'ordre de 250 m. Depuis cette date, un suivi bathymétrique mensuel a été mené afin d'étudier l'évolution de ce système et de réussir à le positionner dans la classification proposée ci-dessus.

Les premiers résultats ont montré que la barre externe est un système pérenne qui n'a pas beaucoup évolué. Cette barre ne migre pas géographiquement. Cependant, elle évolue sur sa hauteur. En effet, localement, on observe un engrangissement et/ou une érosion plus ou moins lié(-es) à l'évolution de la barre interne. Cette barre interne n'est pas réellement formée. Elle présente des points hauts et des chenaux plus ou moins marqués. La liaison avec la côte ainsi que la formation des festons évoluent en fonction des conditions hydrodynamiques rencontrées durant les périodes inter-relevés bathymétriques. En corrélant les données bathymétriques et les données météorologiques, il a été possible de définir des facteurs responsables de la désorganisation et de migration de la barre interne.

Le suivi bathymétrique doit se poursuivre dans le temps. Il doit être complété avec des prélèvements granulométriques. Une étude approfondie des photos aériennes de la zone devrait permettre d'être plus précis dans la classification et d'étendre la période d'observation. De plus, ce site s'intègre dans le programme Liteau 2 sur la gestion du littoral, et les données bathymétriques vont servir d'entrée aux différents modèles proposés.

Références bibliographiques :

Short, A. D. and Aagaard, T., 1993. Single and multi-bar beach change models. Journal of Coastal Research, Special Issue No. 15, 141-157.

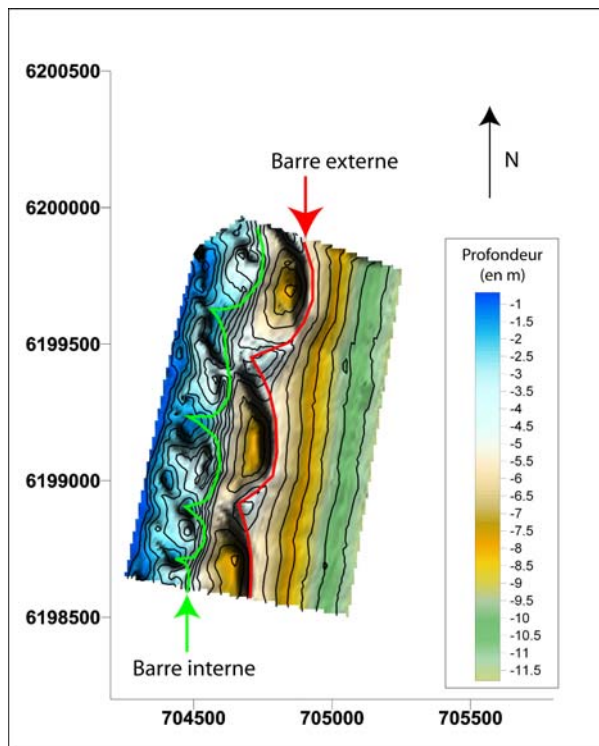


Figure 1 : Bathymétrie du système à deux barres sédimentaires d'avant-côte festonnées de Leucate-Plage

INFRAGRAVITY WAVES IN MOBILE-BED LABORATORY EXPERIMENTS

Florent Grasso, Hervé Michallet, Eric Barthélémy

Laboratoire des Ecoulements Géophysiques et Industriels (CNRS – UJF – INPG),
BP53, 38041 Grenoble Cedex 9, France.

florent.grasso@hmg.inpg.fr.

herve.michallet@hmg.inpg.fr.

eric.barthelemy@hmg.inpg.fr.

Abstract: Experiments were carried out in a flume 36 m long and 55 cm wide equipped with a piston wave generator. The sloping bottom consists of a loose material of low density (1.19 kg L^{-1}) with a median diameter $d_{50}=0.6$ mm in order that Shields and Rouse numbers are of the same magnitude as those of natural environments. Irregular waves are generated according to a JONSWAP spectrum. The waves are measured along the flume and bottom profiles are recorded in between repeated wave sequences. The infragravity modes amplitudes along the flume are obtained for different wave climates. The correlation between the incident short wave envelope and the infragravity waves clearly indicates that the latter conform to both breaking point and bound long wave release mechanisms.

INTRODUCTION

Field measurements indicate that waves in the infragravity range play a role on beach morphology. The generation of such long period waves can be explained by two different mechanisms. On one hand the breaking is thought to release bound long waves due to wave grouping (Longuet-Higgins & Stewart, 1962). On the other hand wave grouping produces a break point and set-up oscillation that acts as a piston at the wave group period (Symonds *et al.*, 1982). In both cases these incident long period waves reflect on the beach face, interfere with the incident waves to produce long period standing waves known as surf-beats.

Recently, Wang *et al.* (2002) performed velocity and concentration measurements over a beach that was shaped by breaking irregular waves in laboratory flume. A similar topography was obtained in a wave flume and allowed turbulent measurements in the surf zone suspension by Hurther *et al.* (2007). They also observed sediment suspension concentrations fluctuations at the frequency of a free standing wave. Such laboratory

experiments in wave tanks with beaches made of loose material are rare (Dette *et al.*, 2002). Most experimental studies were performed with a rigid bottom topography. Janssen *et al.* (2003) evaluated the long waves generation for a mild slope topography (1:70) molded in sand with a smooth concrete surface. They concluded that the mechanism of bound wave release is dominant. Baldock and Huntley (2002) and Baldock *et al.* (2004) observed breaking forced waves for a steeper uniform slope (1:10) and a barred beach profile. Moreover, the maximum long wave radiation occurs when the mean breakpoint closely coincides with a nodal point of the free standing long wave. The aim of the present paper is to investigate the characteristics of such surf-beats in small-scale mobile bed experiments. We will evaluate their relation to the bottom profile under controlled conditions. More specifically we will compare surf-beat characteristics for a beach at equilibrium and a barred beach in evolution.

EXPERIMENTAL SET-UP

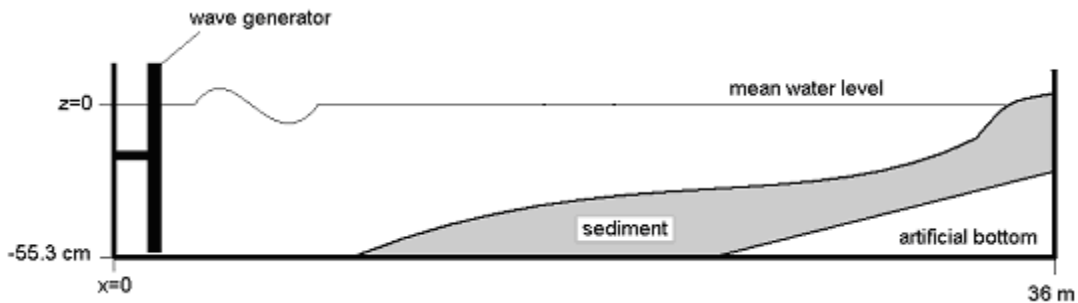


Figure 1. Experimental mobile-bed wave flume.

Our experiments were carried out in a flume 36 m long and 55 cm wide equipped with a piston wave generator (Figure 1). The still water depth is 55.3 cm. The mean overall slope is approximately 1:40. The sloping bottom consists of a loose material of low density (1.19 g cm^{-3}) with a median diameter $d_{50}=0.6 \text{ mm}$. In the experiments, the Froude number, the Shields number in the shoaling part and the Rouse number in the breaking zone (ratio of turbulent agitation to the settling velocity of the sediment) are of the same magnitude as those of natural environments. Time and length scales are roughly 1/3 and 1/10. Irregular waves are generated according to a JONSWAP spectrum (peak enhancement factor $\gamma=3.3$). For each simulation, we check that these waves conform to the expected spectrum and that they follow a Rayleigh distribution at 2 m downstream of the wave maker. Twelve wave gages mounted on trolleys measure instantaneous water elevations. Records are at least 30 mn long in order to achieve statistical convergence. Bottom profiles are recorded in between wave series.

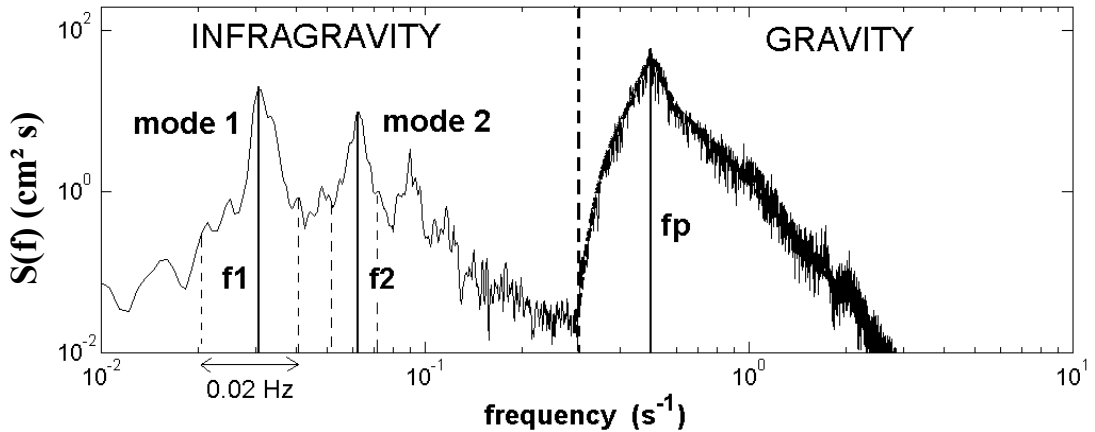


Figure 2. Surface elevation energy spectrum at $x=2$ m in the flume on the equilibrium beach plotted in Figure 3d (—). Wave parameters: $H_{rms0}=7.5$ cm, $f_p=0.5$ Hz, $h_0=55.3$ cm. First infragravity frequency peak $f_1=0.03$ Hz.

Spectral estimates $S(f)$ were obtained from Fourier transforms of five 50% overlapping data segments, each comprising 32768 points sampled at 50 Hz. A wave spectrum measured at $x = 2$ m is plotted in Figure 2. Frequencies above $3/5 \times f_p$, correspond to the generated JONSWAP spectrum and fall in the “gravity” domain. The generation of low frequency waves – resulting of gravity waves breaking – is clearly visible in the spectral power density below $3/5 \times f_p$ (this is the “infragravity” domain). A closer inspection of the low frequency range shows a broad peak at a frequency f_1 around 0.03 Hz. The first harmonic (f_2) of this peak is also clearly visible. The amplitude of the long wave motion associated with both frequencies is evaluated by estimating the energy contained in finite frequency bands of 0.02 Hz centred on peak frequencies. We choose a 0.02 Hz band cutting in order to include the main energy part of the considered peaks.

LONG WAVES STRUCTURE

Comparison for equilibrium profile, transient profile and theory

A wave climate characterized by its peak frequency ($f_p=0.5$ Hz) and the root mean square wave height at 2 m downstream the wave maker ($H_{rms0}=7.1$ cm) was run for several tens of hours. Evolutions of H_{rms} and infragravity modes amplitudes (H_{ig}) along the flume are plotted in Figure 3 for two different bottom profiles. These (plotted in Figure 3d) correspond to two different stages. One is a transient stage characterized by a bar that travels onshore at about 1 m/h. This profile shows interesting similarity with the rigid bottom profile in the experiments of Baldock *et al.* (2004). The other profile is at equilibrium in the sense that it changes very little (at plotting precision) over several hours. Note that the barred profile data is more scattered than the equilibrium profile data. The bottom changes between two sets of measurements are not entirely negligible in this case.

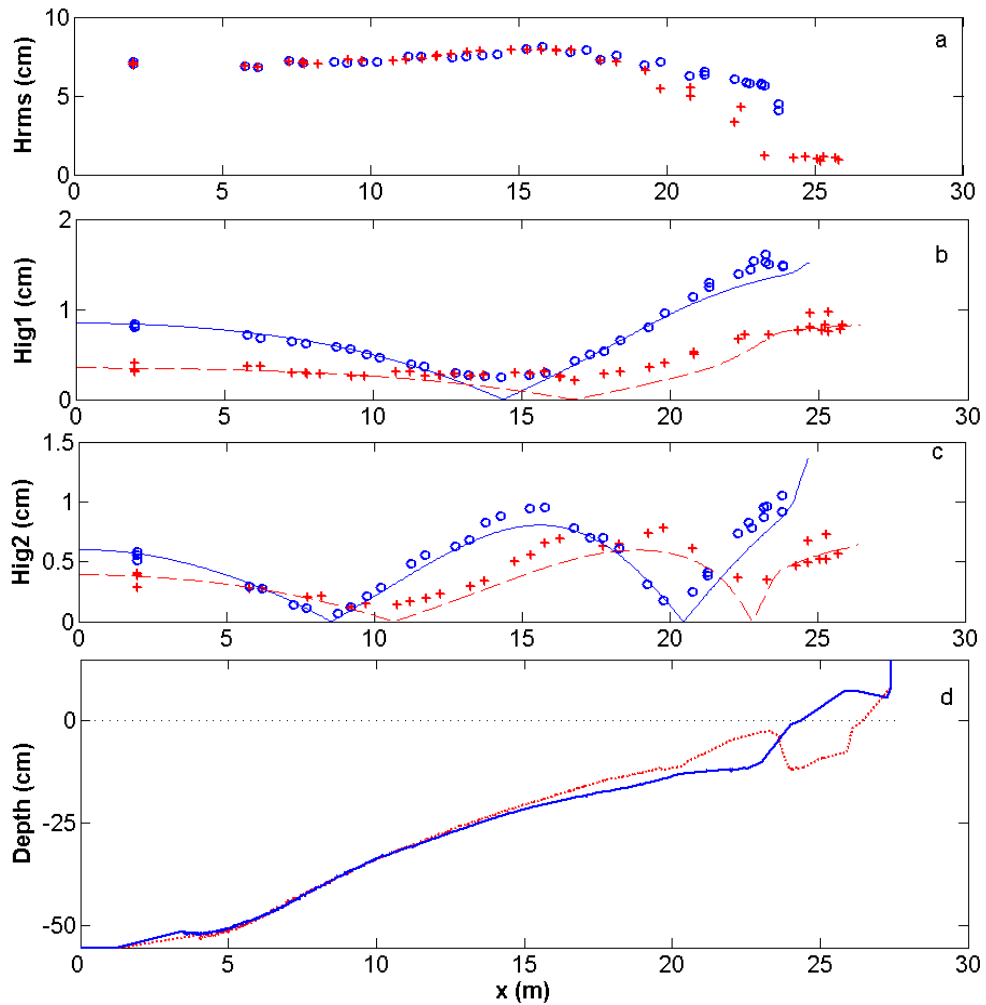


Figure 3. Wave and bottom characteristics along the flume axis for equilibrium profile (o) and transient profile (+): a) root mean square wave height, b) First mode infragravity wave amplitude, c) Second mode infragravity wave amplitude and d) equilibrium bottom profile (—) and transient bottom profile (---).

The infragravity wave energy is plotted in terms of significant amplitude in Figure 3b-c. The first mode amplitude (H_{ig1}) is maximum at the berm, minimum close to $x=15$ m and large again close to the wave maker. This indicates that a low frequency standing wave with a node somewhere around $x=15$ m is generated in the flume. Despite the fact that the equilibrium profile is far from being a plane beach, the Wilson formula for a uninodal seiche in a rectangular flume with a plane beach reported by Dean and Dalrymple (1984, p.149) gives a very good estimate of f_1 (*i.e.* 0.03 Hz). In addition, the data are compared with an analytical solution for small amplitude free standing long wave of the linearized Saint-Venant equations (plotted in Figure 3b-c as a solid line for equilibrium profile and a dashed line for the transient profile). The solution yields the modes frequencies, the nodal structure and normalized amplitudes. The overall agreement of the nodal structure is good and the peak frequencies are remarkably well predicted (*i.e.* $f_1=0.031$ Hz and $f_2=0.063$ Hz for the equilibrium profile and $f_1=0.024$ Hz and $f_2=0.047$ Hz for the transient profile).

We note on Figure 3b-c that the infragravity significant amplitudes are clearly more important for the equilibrium bottom profile. This difference may be firstly explained by the steep bar of the transient bottom profile, causing a partial waves reflection and decreasing the resonance phenomenon along the flume. . Besides, we note an important decrease of H_{rms} in Figure 3a for the transient profile (+), it corresponds to a large dissipation. Nevertheless this energy is not transferred in the infragravity domain. Figure 4 shows the mean set-up measured for the equilibrium and transient profiles. The waves breaking localised on the bar seems to enhance the time-varying breakpoint mechanism and reinforce the set-up. The energy contained in the set-up could be dissipated through an enhanced undertow current. We emphasize that those observations are only possible in our special configuration of mobile-bed experiments.

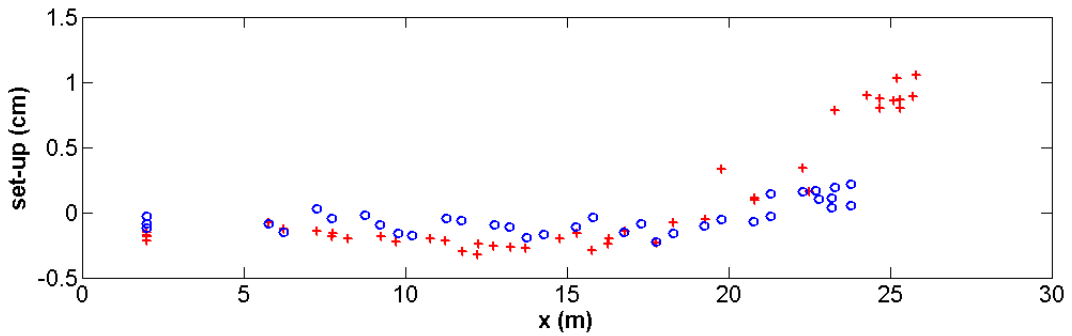


Figure 4. Mean water level along the flume axis for equilibrium profile (o) and transient profile (+) plotted in Figure 3d.

Our results in the barred case exhibit the same features, in terms of long waves amplitudes and node positions, as the results of Baldock *et al.* (2004). Their experiments were performed on a rigid bottom with a barred shape. The generated waves are similar ($H_{rms0}=5$ cm; 7.5 cm and 10 cm, for $f_p=0.6$ Hz) to our case, but the mean slope (1:10) is steeper than our transient profile mean slope (1:35). By changing the incoming wave amplitude, they might conclude that a maximum long wave radiation occurs when the mean breakpoint closely coincides with the nodal point of the long wave. In our experiments, the long waves are more energetic on the equilibrium bottom profile for which the breaking point and first mode node position are a few meters apart.

Wave spectra

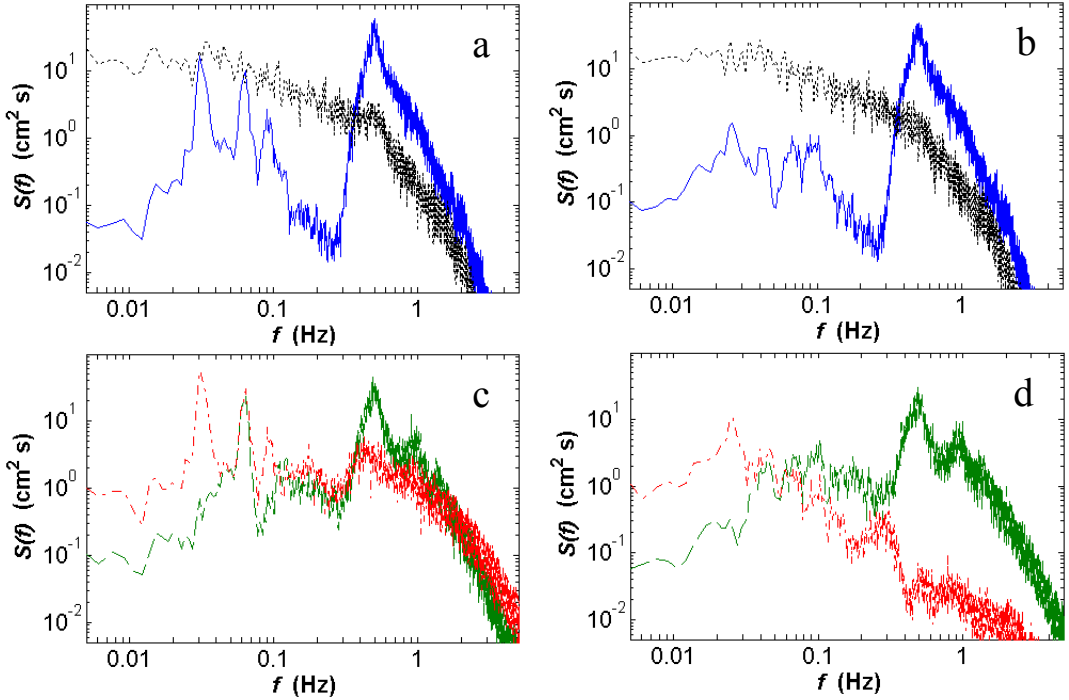


Figure 5. Total wave energy spectra at $x = 2$ m (—), $x = 15.3$ m (---), $x = 23.3$ m (- · -) and spectrum of the short wave envelope at $x = 2$ m (.....); for an equilibrium bottom profile (a,c); for a transient bottom profile (b,d).

Surface elevation energy spectra for the two different topographies are plotted in Figure 5. They are presented for three positions along the flume that correspond to the deep region, the breaking region and close to shoreline. The location of the breaking region (maximum of H_{rms} in Figure 3a) is close to the node of the first mode (Figure 3b) and the anti-node of the second mode (Figure 3c). The spectra confirm that the energy in the infragravity domain is a lot larger and the peaks more clearly defined in the case of the equilibrium profile. In the case of the transient profile, we may note that the energy in the gravity domain is very low close to shoreline. Indeed, the short waves have dissipated almost all their energy passing the bar, as indicated by the estimate of H_{rms} for $x > 23$ m in Figure 3a.

In addition, the spectrum of the short wave envelope, obtained via a Hilbert transform of the measured surface elevation data, is plotted in dotted line in Figure 5a,b. This does not account for real energy in surface elevation but as energy possibly contained in the wave packets that could be released in the breaking region. It is important to emphasize that there is no dominant frequency in the wave grouping. This confirms that the frequency peaks of the infragravity waves depend on the beach profile only.

Infragravity waves for different wave climates

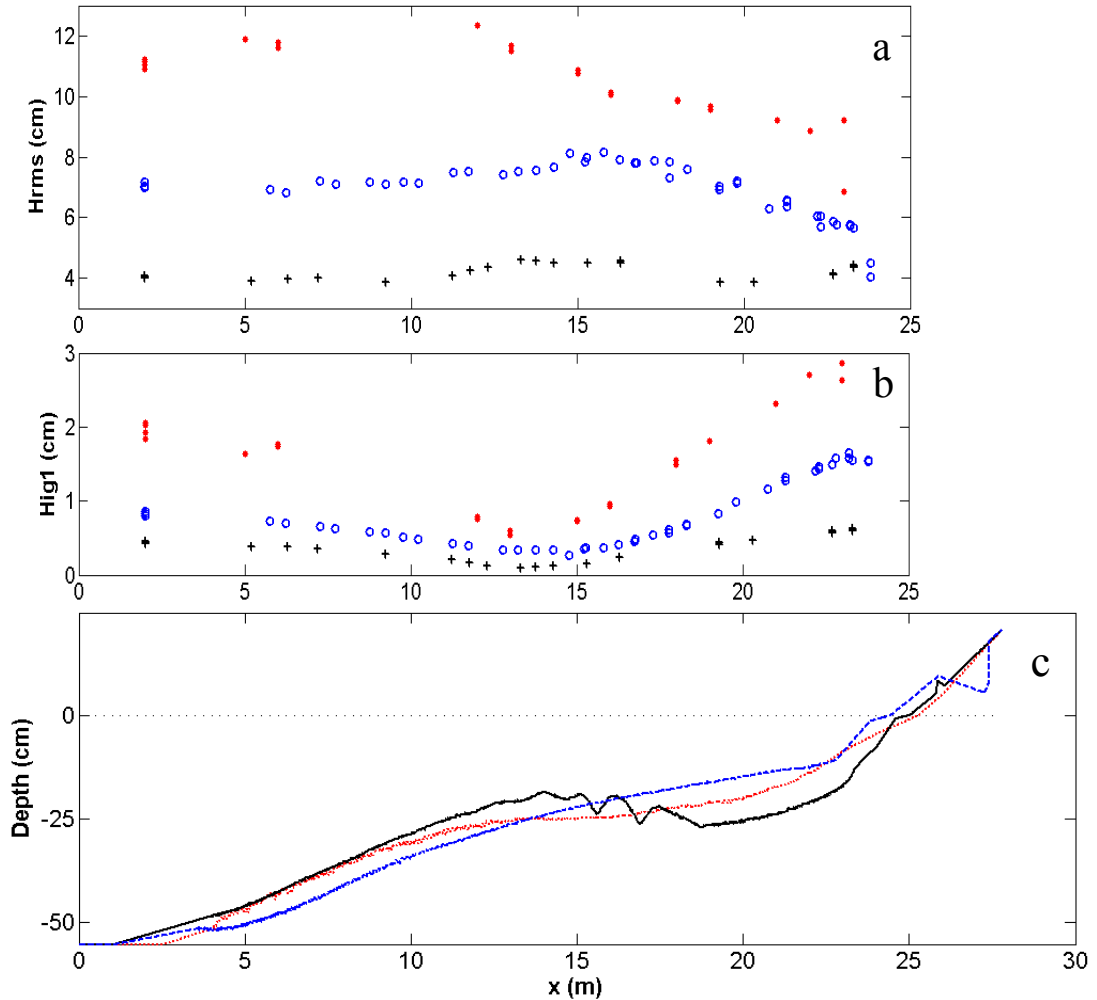


Figure 6. a) Root mean square wave height, b) First mode infragravity wave amplitude and c) bottom profile, for different wave climate: (• ; ...) $H_{rms}=11.1$ cm, $f_p=0.33$ Hz; (○ ; --) $H_{rms}=7.1$ cm, $f_p=0.5$ Hz and (+ ; —) $H_{rms}=4$ cm, $f_p=0.5$ Hz.

Different wave climates were generated (varying H_{rms} and peak frequency f_p), that reproduce storms, mild summer climates and very gentle climates. The Figure 6 synthesises the H_{rms} and H_{ig1} data for these three different climates. We note that incident short waves have a direct influence on the long waves amplitude. H_{ig1} is clearly more important for the storm type of climate (•). The maximum of the H_{rms} corresponds to the beginning of the wave breaking location and its decrease is linked to the wave energy dissipation. We observe in Figure 6 a clear distinction between break point positions of the different climates: 12 m for $H_{rms}=11.1$ cm (•); 16 m for $H_{rms}=7.1$ cm (○) and 24 m for $H_{rms}=4$ cm (+). In contrast, the first mode infragravity node position is almost the same in the three cases (13-14 m). Note that the bottom profiles corresponding to the three wave climates are similar in term of length (from the wave-maker to the shoreline) (Figure 6c). We can conclude that the long wave structure mainly depends on the beach morphology rather than on the generated wave characteristics.

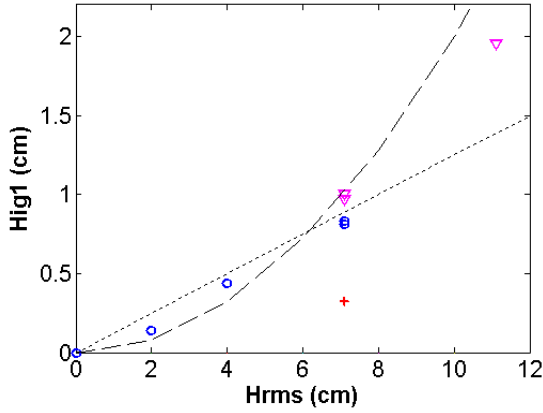


Figure 7. First mode infragravity wave amplitude versus root mean square wave height for different wave climates. (o) equilibrium bottom profile; (∇) quasi-equilibrium bottom profile; (+) transient bottom profile. Linear approximation (...) and quadratic approximation (--).

The first mode infragravity wave amplitudes for different wave climates are plotted on Figure 7 and classified in three categories that depend on the corresponding bottom profile evolution speed. This is estimated by the vertical evolution of the bottom profile ($z(x)$), averaged along the flume, during a time lap ($\Delta t = t_{i+1} - t_i$):

$$V = \frac{\int_{i=1}^{L_{\text{flume}}} |z_{i+1} - z_i| dx}{L_{\text{flume}} \times \Delta t}. \quad (1)$$

We define that an evolution speed V less than 1.5 mm/h corresponds to an “equilibrium” bottom profile (o); V between 1.5 mm/h and 4 mm/h is related to a “quasi-equilibrium” (∇) and a “transient” bottom profile is for an evolution speed V larger than 4 mm/h (+). We note again that for a same wave climate ($H_{\text{rms}}=7.1$ cm) the value of H_{ig1} is twice smaller for a transient bottom profile (the cross in Figure 8) compared to equilibrium conditions. The dependency of H_{ig1} to H_{rms} should characterize the long wave generation mechanism. A quadratic relation would correspond to the bound waves release, whereas a linear relation would characterize the break point oscillation mechanism (Baldock & Huntley, 2002). According to the experiments performed by Baldock *et al.* (2004) on a barred rigid bottom (slope 1:10), long waves are shown to be linearly dependent on the incident short wave amplitude both offshore and shoreward of the breakpoint at all frequencies. In our case, the number of different wave climates simulated is too weak to determine a clear tendency in Figure 7

LONG WAVE MOTION CORRELATION WITH THE SHORT WAVE ENVELOPE

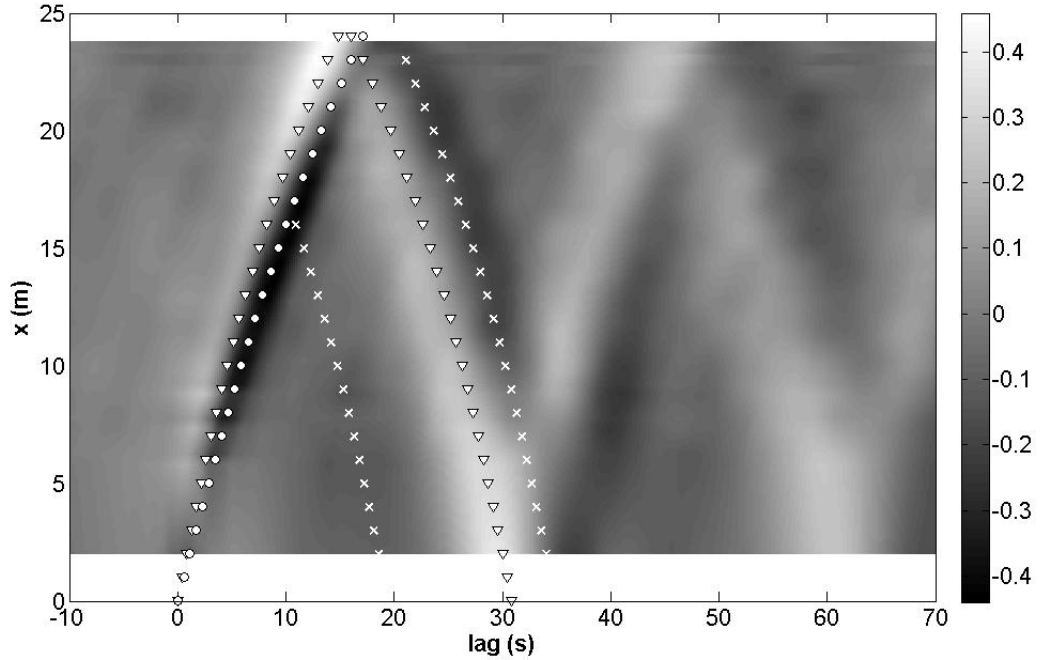


Figure 8. Cross-correlation between the infragravity waves and the short wave envelope at $x=2$ m, equilibrium bottom profile. Group celerity (for $f_p=0.5$ Hz): (o); phase celerity ($=\sqrt{gh}$) for positive correlation (∇) and negative correlation (x).

Figure 8 shows the cross-correlation between the short wave envelope in the constant depth region of the flume ($x=2$ m) and the total low pass filtered surface motion ($f<0.3$ Hz) along the flume axis. The high spatial resolution of the experimental data allows, using an interpolation function, a presentation of the sequence of correlation functions as quasi-continuous in space. A black ridge corresponds to a negative correlation and a white ridge represents a positive correlation. There is a negative correlation for lags close to zero at $x=2$ m. This corresponds to the locally forced incident bound long wave, which is out of phase with the short wave envelope (Longuet-Higgins & Stewart, 1962). This black ridge matches the phase-plane trajectory at the group celerity (represented by circular markers on Figure 8). The lag is increasing and the correlation becomes stronger further shoreward as the bound wave amplitude increases due to the shoaling of the short wave and represents a larger proportion of the total long wave energy (at $\tau \approx 10$ s and $x=15$ m). This bound wave is released during breaking and still negatively correlated to the wave envelope at lags $\tau \approx 18$ s at $x=2$ m and $\tau \approx 20$ s at $x=23$ m. The free waves resulting of the bound wave released move to the phase celerity, which is equal to \sqrt{gh} in shallow water (cross markers). We may discern a light black ridge under the white crosses which may correspond to the free wave released close to $x=15$ m at $\tau \approx 10$ s, moving offshore to reach $x=2$ m at $\tau \approx 18$ s.

On the other hand, a positive correlation is present for $\tau \approx 2$ s at $x=5$ m. It may correspond to a dynamic set-up generated by the breaking of the larger wave packets. The correlation becomes very strong at the shoreline ($\tau \approx 13$ s). We notice that the triangle markers (celerity \sqrt{gh}) match the white ridge from $\tau \approx 2$ s to $\tau \approx 16$ s. This is in agreement with Symonds *et al.* (1982) who showed that the long waves generated by breakpoint oscillations propagate freely at the phase celerity. The position and intensity representations of long waves peaks can be distorted due to the overlapping between the long wave resulting of breakpoint oscillations (positive correlation) and the bound long wave released (negative correlation).

Next, the long waves are reflected and propagate offshore (from $x=24.5$ m to 0) as seen on the correlation signature: a white ridge from $\tau \approx 17$ s to 31 s; and a black ridge from $\tau \approx 21$ s to 35 s. According to the theory, the reflected long waves travel at the phase celerity (plotted with triangle and cross markers). At larger lags, both negative and positive correlation peaks are still present but damped. This indicates that the long waves reflect on both ends of the flume but are not amplified. We recall that Janssen *et al.* (2003) concluded that the bound wave release in their mild slopes laboratory experiments ($\sim 1:70$) was dominant, while Baldock *et al.* (2004) observed breaking point forced waves for stronger slopes ($\sim 1:10$). Both mechanisms are clearly observed in our case of an equilibrium beach profile ($\sim 1:45$).

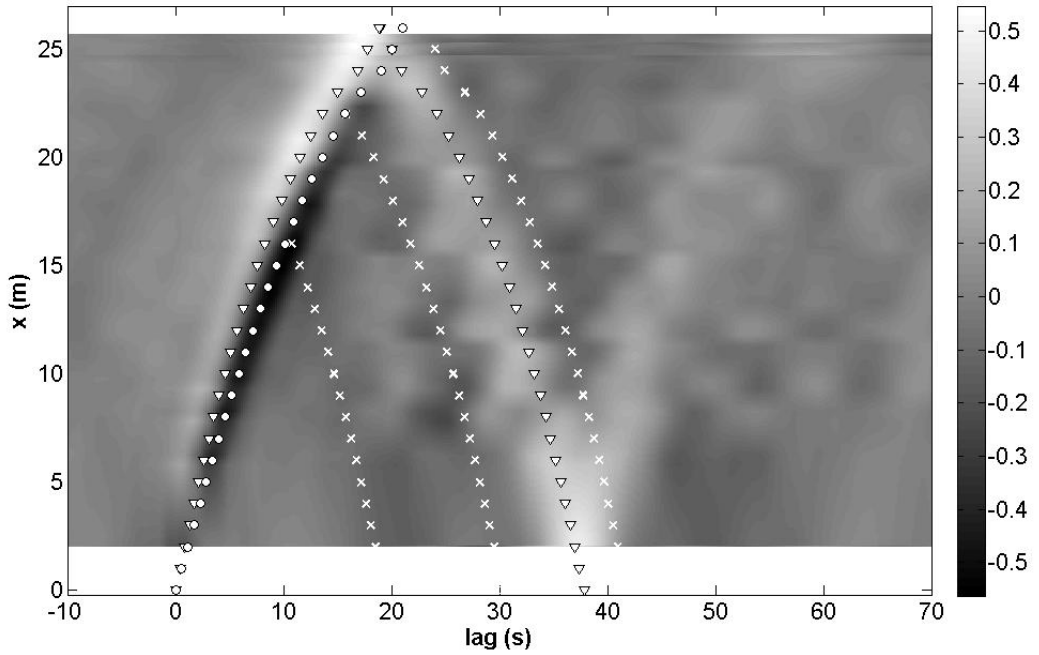


Figure 9. Cross-correlation between the infragravity waves and the short wave envelope at $x=2$ m, transient bottom profile. Group celerity (for $f_p=0.5$ Hz): (o); phase celerity ($=\sqrt{gh}$) for positive correlation (∇) and negative correlation (x).

For the transient bottom profile, the correlation picture shown in Figure 9 is in marked contrast. After reflection the correlation peaks have weaker values and we note a quicker and greater damping compared to the equilibrium case. The bound long wave signature (black ridge) is seen from $\tau \approx 0$ s at $x=2$ m to $\tau \approx 18$ s at $x=23$ m but not really at the shoreline ($x=25.8$ m). It may be due to reflection and dissipation of long waves over the bar positioned at $x=23$ m. We notice again that the bound long wave travels at the group celerity (circular markers).

Clearly, the dynamic set-up induces again a positive correlation (white ridge) evolving at phase celerity (triangle markers), starting for $\tau \approx 2$ s at $x=5$ m and becoming stronger close to $\tau \approx 18$ s at $x=25.8$ m. The break point mechanism is apparently dominant for this topography that is closer to Baldock *et al.* (2004)'s experiments. We also note that the bound long wave releases a free wave offshore at nearly $\tau \approx 12$ s and $x=15$ m (light black ridge under cross markers). We observe two negative correlations (under cross markers): from $\tau \approx 17$ s at $x=23$ m to $\tau \approx 30$ s at $x=2$ m; and from $\tau \approx 22$ s at $x=25$ m to $\tau \approx 38$ s at $x=10$ m. Those correspond to released bound long waves, partially reflected by the bar ($x=23$ m) and the berm ($x=25.8$ m). This probably leads to the weak correlation for larger time lags ($\tau > 60$ s). Bound wave release and breakpoint forcing do not reinforce the generation of the infragravity waves as for the equilibrium beach profile.

BEGINNING OF THE WAVE SEQUENCE

The presence of significant infragravity waves spectral peaks at the shoreline does not necessarily imply resonant amplification. The generated wave packets are not necessarily in phase with the radiated long waves since the incident short wave groups do not have a dominant frequency (as shown by the short waves envelope spectra in Figure 5). In that sense, seiching is not really stationary in the flume. To illustrate this point, we plot in Figure 10 the beginning of the wave sequence. In Figure 10a, the short wave packets in the deep region are visible. They induce a modulation of the mean level close to shoreline. Resulting low frequency motions are shown in Figure 10d. The main period of about 32 s, corresponding to f_l , is sometimes observed. For instance, at $x=23.8$ m, the peak for $t \approx 34$ s is enhanced for $t \approx 66$ s. In that case, a large waves packet has arrived in the breaking region in phase with the return of the generated long wave. This is not a general feature. The signature of a long wave is generally not seen after a couple of flume travel lengths. The main period of 32 s is not visible in the infragravity wave signal corresponding to the deep region for $t > 130$ s in Figure 10d. In that sense, we do not notice any amplification in the long wave generation process.

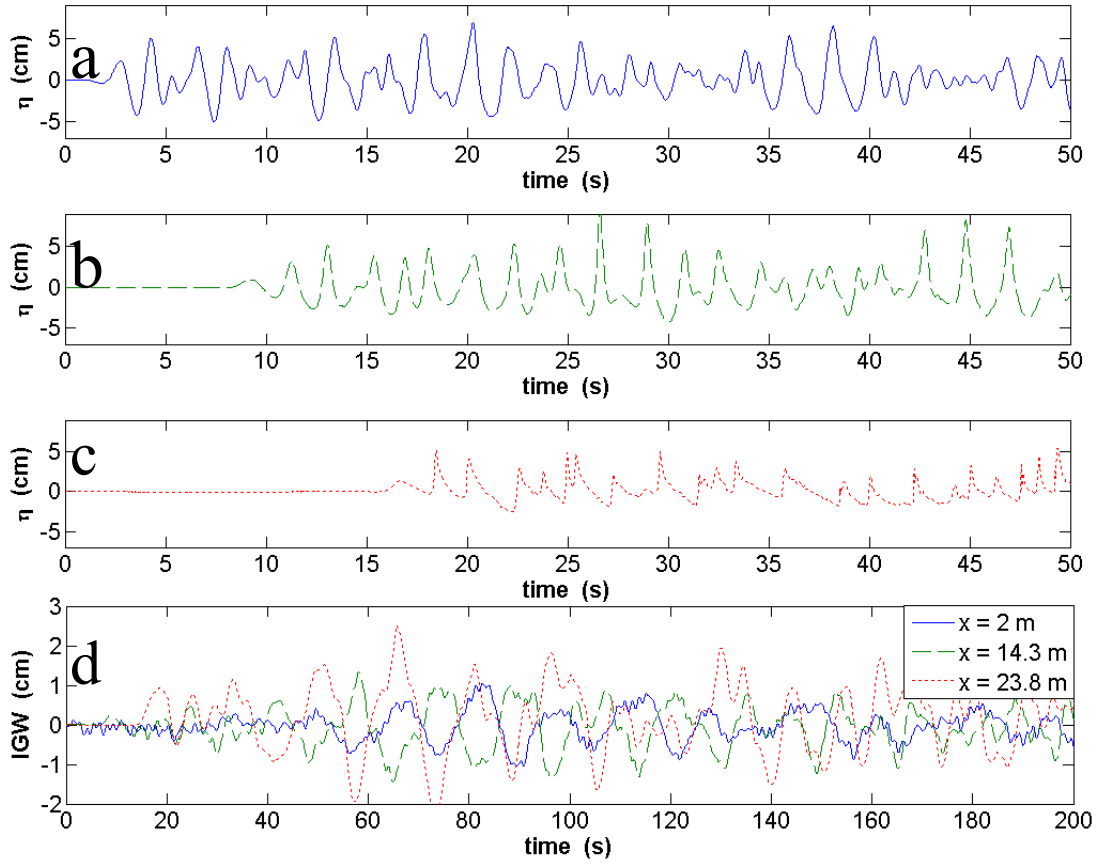


Figure 10. Surface elevation in the deep (a), breaking (b), shoreline (c) regions; and infragravity waves (d) for the equilibrium bottom profile.

CONCLUSION

The experiments show that the long wave structure strongly depends on the beach morphology rather than on the generated short wave characteristics. The nodal structure of the infragravity waves is determined by the beach shape that is, mainly the distance between the wave-maker and the shoreline.

Increasing the incoming wave amplitude increases the long wave amplitude but too few experiments were conducted for precisely determining a dependency in between linear and quadratic.

The experiments of Baldock et al. (2004) and Janssen et al. (2003) indicate that the preponderance of the breakpoint oscillation mechanism could be the result of a steep beach slope ($\sim 1:10$), while the bound wave release mechanism could be dominant for a weak beach slope ($\sim 1:70$). In our case, the loose bottom has a beach slope of about 1:40 and both mechanisms are clearly observed as shown by the correlation between the short waves envelope and the long waves.

The infragravity waves are more energetic on the equilibrium bottom profile compared to the transient barred profile. It is suggested that the beach topography evolves as to reinforce both the bound long wave release and the dynamic set-up generation.

ACKNOWLEDGEMENTS

This work has been partially funded by the CNRS-INSU PATOM and LITEAU II. The technical support of J.-M. Barnoud is gratefully acknowledged.

REFERENCES

- BALDOCK, T.E.; O'HARE, T.J. and HUNTLEY, D.A., 2004. Long wave forcing on a barred beach, *J. Fluid Mech.*, 503, 321-343.
- BALDOCK, T.E. and HUNTLEY, D.A., 2002. Long wave forcing by the breaking of random gravity waves on a beach, *Proc. R. Soc. Lond.*, A 458, 2177-2201.
- DEAN, R.G. and DALRYMPLE, R.A., 1984. *Water Wave Mechanics for Engineers and Scientists*, World Scientific.
- DETTE, H.H.; LARSON, M.; MURPHY, J.; NEWE, J.; PETERS, K.; RENIERS, A. and STEETZEL, H., 2002. Application of prototype flume tests for beach nourishment. *Coastal Eng.*, 47, 137–177.
- HURTHER, D.; MICHALLET, H. and GONDRA, X., 2007. Turbulent measurements in the surf zone suspension. *Journal of Coastal Research*, submitted.
- JANSSEN, T.T.; BATTJES, J.A. and VAN DONGEREN, A.R., 2003. Observation of long waves induced by short wave groups, *J. Geophys. Res.*, 108, 3252-3264.
- LONGUET-HIGGINS, M.S. and STEWART, R.W., 1962. Radiation stress and mass transport in gravity waves, with application to ‘surf-beats’, *J. Fluid Mech.*, 13, 481-504.
- SYMONDS, G.; HUNTLEY, D.A. and BOWEN, A.J., 1982. Two dimensional surf beat: long wave generation by a time-varying break point, *J. Geophys. Res.*, 87(C1), 492-498.
- WANG, P.; EBERSOLE, B.A.; SMITH, E.R. and JOHNSON, B.D., 2002. Temporal and spatial variations of surf-zone currents and suspended sediment concentration, *Coastal Eng.*, 46, 175-211.

MODELE MORPHODYNAMIQUE CONCEPTUEL D'UN SYSTEME DOUBLE DE BARRES FESTONNEES EN MILIEU MICROTIDAL

Pierre FERRER*, Raphaël CERTAIN*, Mathieu GERVAIS*, ** et Jean-Paul BARUSSEAU*

* Université de Perpignan Via Domitia, E.A. 3678 IMAGES, 52 av P. Alduy, 66 860 Perpignan Cedex
(pierre.ferrer@univ-perp.fr)

** B.R.G.M. section Languedoc-Roussillon, 1039, rue de Pinville, 34000 Montpellier

La plupart des littoraux sableux mondiaux présentent des morphologies d'avant-côte variées, appelées des barres sédimentaires d'avant-côte. Ces dernières sont classées en fonction de leur forme, de l'énergie incidente et de la pente de l'avant-côte. La première classification, proposée par Short et Aagaard (1993), propose 6 états depuis des plages dites réflectives à dissipatives en passant 4 états intermédiaires : LBT (Longshore Bar and Trough), RBB (Rhythmic Bar and Beach), TBR (Transverse Bar and Rip) et LTT (Low Tide Terrace). L'état dissipatif comporte des barres parallèles à la côte et l'état réflectif ne présente aucune barre. Ces états correspondent aussi en fait à des séquences dynamiques qui peuvent être observées en fonction des variations de l'énergie du milieu. Les avant-côtes microtidales à très faible marée présentant des structures rythmiques sont restées peu étudiées en comparaison de certains littoraux mésotidiaux. Afin de déterminer un modèle conceptuel morphodynamique de ce type d'environnement, le site de Leucate-Plage a été étudié. Il se base sur un suivi topo-bathymétrique mensuel de 2006 à 2008, complété par 3 levés bathymétriques durant les étés 2000, 2001 et 2002 (28 levés topo-bathymétriques) et associe les forçages hydrodynamiques (hauteur significative et direction de la houle).

Le site d'étude présente un système double de barres festonnées (figure 1). Il est composé d'une barre externe peu mobile au motif permanent en RBB, et d'une barre interne plus dynamique dont les états s'organisent autour des RBB, TBR et TBR-LTT. D'autres états ont été observés sur le site de Leucate-Plage mais non répertoriés dans la classification précédente, ce qui a nécessité la création de deux nouveaux états intermédiaires : RBB rompu et TBR oblique rompu. Le modèle s'appuie aussi sur des modifications proposées par Brander (1999) et Castelle et al. (2007), qui proposent des variantes de la classification usuelle.

Le modèle de Leucate-Plage décrit des transitions entre ces états, en tenant compte de la hauteur significative et de l'incidence de la houle. En fonction de ces critères, deux séquences principales sont déterminées. Ces séquences décrivent les passages d'une morphologie en RBB vers une morphologie en RBB mieux formée (séquence A) et vers une morphologie en TBR (séquence B). Ce modèle est ensuite comparé aux séquences d'évolution et aux classifications existantes pour les barres sédimentaires d'avant-côte.

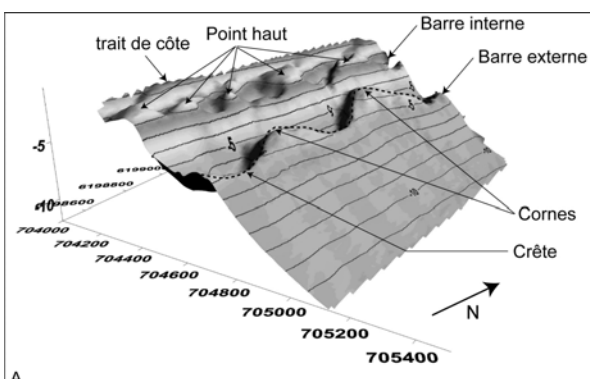


Figure 1 – carte bathymétrique de la zone d'étude (en Lambert 93) présentant un système double de barres festonnées.

BRANDER R. W. (1999) - Field observations on the morphodynamic evolution of a low-energy rip current system. *Marine Geology*, n. 157, p. 199-217.

CASTELLE B., BONNETON P., DUPUIS H. AND SÉNÉCHAL N. (2007) - Double bar beach dynamics on the high-energy meso-macrotidal French Aquitanian Coast: A review. *Marine Geology*, n. 245, p. 141-159.

SHORT A. D. and AAGAARD T. (1993) - Single and Multi-bar change models. *Journal of Coastal Research*, Special Issue n. 15, p. 141-157.

HYDRODYNAMIQUE D'UNE PLAGE A BARRE RECTILIGNE EN MILIEU MICROTIDAL

Cecile GODON (1), Nicolas ROBIN (1), Nicolas ALEMAN (1), Mathieu GERVAIS (1, 2), Raphaël CERTAIN (1), Samuel MEULE (3), Fréderic BOUCHETTE (4), Yann BALOUIN (2), Elena BRAMBILLA (4)

(1) IMAGES-Université de Perpignan Via-Domitia, 52 Av Paul Alduy, 66860 Perpignan, France ; nicolas.robin@univ-perp.fr

(2) BRGM, Service Géologique Régional du Languedoc-Roussillon, 1039, rue de Pinville, 34000 Montpellier

(3) CEREGE, Europole Méditerranéen de L4Arbois, 13545, Aix-En-Provence, France.

(4) GEOSCIENCE Montpellier, Université Montpellier 2, 34095, Montpellier, France.

La plage de Sète (Languedoc-Roussillon) est caractérisée par la présence de deux barres rectilignes subtidales évoluant dans un environnement à très faible marée. Une nouvelle campagne de deux mois s'est déroulée sur le site en fin d'année 2008 (programmes ANR VULSACO et MICROLIT RELIEF/SHOM), afin d'améliorer la compréhension des processus hydrodynamiques qui contrôlent l'évolution de ces morphologies en milieu microtidal. L'originalité de cette campagne repose sur l'immersion d'un grand nombre de courantomètres acoustiques (couplage ADV et ADCP) permettant de connaître l'intensité et la direction du courant à haute fréquence entre 10 cm du fond et la surface durant des événements hydrodynamiques et météorologiques contrastés (2 tempêtes avec des hauteurs significatives supérieures à 3 m sur le glacis et des périodes de beau temps avec fort vent de terre). Une analyse fine de la courantologie dans l'ensemble de la tranche d'eau de part et d'autre de la barre interne est proposée suite à un événement de beau temps et de forte énergie En période de beau temps, la vitesse des courants enregistrée à la fois sur le revers de la barre interne et dans la fosse interne est faible, inférieure à 0,1 m/s et suivant différentes directions. Cette tendance s'observe sur l'ensemble de la colonne d'eau. Lors de l'apex de la tempête ($H_s = 3,2$ m direction oblique), la composante longitudinale présente des vitesses élevées (entre 0,8 et 0,7 m/s) avec une décroissance de son intensité en profondeur. La composante transversale s'avère plus faible avec la présence d'un courant de retour (inférieur à 0,2 m/s) sur l'ensemble de la colonne d'eau excepté proche du fond où le courant est dirigé vers la côte. Ce nouveau jeu de données permettra dans un premier temps de mieux comprendre la dynamique des barres avant-côte et le couplage morphologie-hydrodynamique se produisant pendant les événements les plus morphogènes pour le système, puis dans un deuxième temps, pourra permettre d'affiner les modèles numériques 2DV existant.

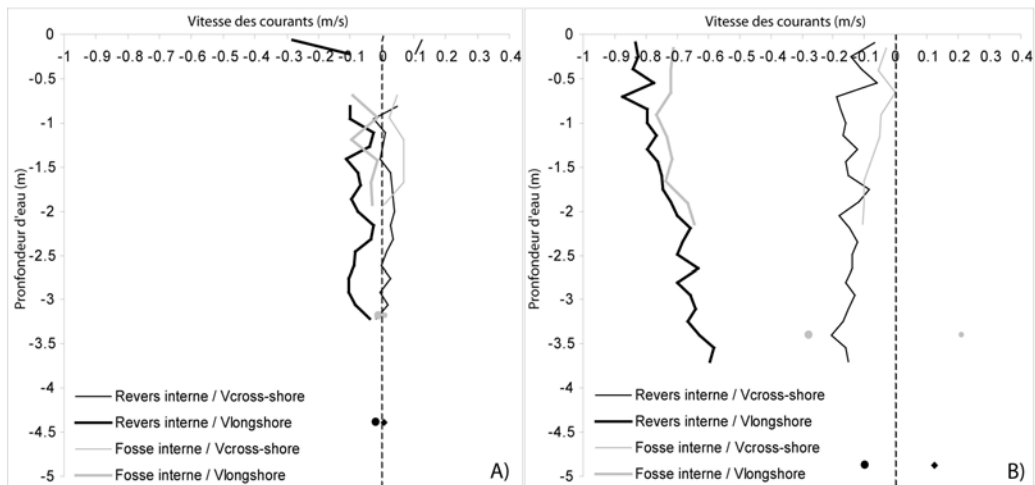


Fig.1 : Vitesse longitudinale et transversale du courant dans la fosse interne et sur le revers de la barre interne pendant une période de beau temps (a) et de tempête ($H_s = 3.2$ m) (b).



Morphological response of a double nearshore bar system under oblique waves

J. THIEBOT (1), N. ROBIN (2), R. GARNIER (3), R. CERTAIN (2), D. IDIER (1), D. CALVETE (4), A. FALQUES (4), and F. LEVOY (5)

(1) BRGM – French Geological survey - ARN/ESL - Orléans - France (j.thiebot@brgm.fr / D.Idier@brgm.fr), (2) Institut de Modélisation et d'Analyse des Géo-Environnements et de la Santé (IMAGES) - Université de Perpignan - France (nicolas.robin@univ-perp.fr / certain@univ-perp.fr), (3) School of Civil Engineering - University of Nottingham - UK (roland.garnier@nottingham.ac.uk), (4) Departament de Fisica Aplicada - Univeritat Politècnica de Catalunya (UPC) - Barcelona - Spain (calvete@fa.upc.edu / falques@fa.upc.edu), (5) UMR 6143 CNRS – Université de Caen - France (franck.levoy@unicaen.fr)

The Sète beach (Mediterranean Sea - France) is characterized by two nearshore bars which are generally considered to run parallel to the shore. However in-situ wave/current/bathymetry measurements have shown the possible reorganization of this double bar system during storms associated with oblique waves. Two situations are studied. During the field campaign in 1999, the bar system was submitted to moderately oblique stormy waves. At the end of the campaign, the inner bar was divided in segments which were oriented parallel to the wave crests and to the current. During the field campaign in 1994, the stormy waves were strongly oblique. The response of the bar system led to the appearance of rhythmic features along both bars.

The nonlinear surf zone model MORFO55 is used to understand the mechanisms which govern the bar reorganization under energetic wave conditions. This model is based on a wave and depth averaged shallow water equations solver with wave driver, sediment transport and bed updating (Garnier et al. 2006, J. Fluid Mech.). Modeling shows that the main characteristics of the bar response can be simulated from self-organization processes. The wave incidence has a tremendous influence on the bar response. Particularly, in agreement with the observations, the outer bar is stable for moderate obliquity while it is unstable for strongly oblique waves.

Experimental flume simulation of sandbar dynamics

F. Grasso[†], H. Michallet[†], R. Certain[‡] and E. Barthélemy[†]

[†] Laboratoire des Ecoulements
Géophysiques et Industriels
(CNRS – UJF – INPG)
BP 53, 38041 Grenoble cedex 9, France
Florent.grasso@hmg.inpg.fr

[‡] Université de Perpignan Via
Domitia, E.A. 3678 IMAGES
52 av P. Alduy,
66860 Perpignan Cedex, France



ABSTRACT

GRASSO, F., MICHALLET, H., CERTAIN, R. and BARTHÉLEMY, E., 2009. Experimental simulation of sandbar dynamics. *Journal of Coastal Research*, SI 56 (Proceedings of the 10th International Coastal Symposium), pg – pg. Lisbon, Portugal, ISBN.

Sandbar dynamics is a key feature of coastal hydrodynamics and plays an important role in natural shore protection. It is generally recognised that moderate wave forcing can lead to bar formation whereas storms may induce offshore bar migration. Field experiments nevertheless do not usually allow a detailed description of the evolutions due to the poor temporal resolution between topographic surveys.

Here, experiments are carried out in a 36 m long flume equipped with a piston wave generator. The sloping bottom consists of a loose material of low density (1.19 g/cm^3) with a median diameter $d_{50}=0.6 \text{ mm}$. The Shields and Rouse numbers for the experiments are of the same magnitude as those of natural environments. Time and length scales ratios are roughly 1/3 and 1/10. Irregular waves are generated according to a JONSWAP spectrum. The process of bar formation and evolution at several positions on the profile is described. On the one hand for constant wave climates of very long durations (tens of hours), bars become pitched forward and onshore migration is observed. The bar eventually merges to the berm. On the other hand, a succession of increasing, energetic and decreasing wave conditions that are characteristic of the different phases of storm events are applied. An offshore migration of mega-ripples is observed during the most energetic phase, feeding a large offshore bar. The waning conditions smooth the profile and lead to shore-face accretion. Shoreline positions during the different phases are also discussed.

ADITIONAL INDEX WORDS: Morphodynamics, irregular waves, small-scale flume, sandy beach, bar.

INTRODUCTION

Near-shore sandbars are a major feature of beach morphodynamics. They have a strong influence on shoreline position and thus are important within shore protection strategies. In spite of the observations of beaches with three-dimensional structures (HOM-MA and SONU, 1963), the two-dimensional study of cross-shore profiles is a key feature of global systems (PRICE and RUSSINK, 2008; WALSTRA *et al.*, 2008; AAGAARD *et al.*, 2002).

Two hypotheses are commonly used in the explanation of cross-shore bar generation (MASSELINK and HUGHES, 2003). The first hypothesis includes the generation of the bar near the breakpoint of short incident waves. The bar results from the convergence of sediment, because wave skewness outside the surf zone induces onshore sediment transport and bed return flow in the surf zone induces offshore sediment transport. The second hypothesis associates the generation of a bar at the (anti-) nodes of standing infragravity waves, which represent locations of sediment convergence.

Laboratory studies and field measurements conducted over many years have served to highlight bars dynamics. Hence, offshore bar migration occurs during high-energetic wave conditions, whereas low-energetic wave conditions induce

onshore bar migration (SALLINGER *et al.*, 1985; HOLMAN and SALLINGER, 1993; GALLAGHER, 1998).

Field experiments nevertheless do not usually allow a detailed description of bar evolution due to the poor temporal resolution between topographic surveys. Physical models then become an interesting alternative (ROELVINK and STIVE, 1989; DETTE *et al.*, 2002; GÜNEYDİN and KABDASLI, 2003; WANG and KRAUS, 2005; GUANDEL *et al.*, 2007; HOYNG, 2008). However, most of the latter studies have focused only on erosion or near-shore bar growth. Relatively few examples of bar migrations have been observed (HOYNG, 2008). The effects of a storm event on a barred beach, as far as we know, have never been reproduced in physical models. The experiments carried out in the LEGI wave flume put forward sandbars formations and migrations under constant wave climates (MICHALLET *et al.*, 2007; GRASSO *et al.*, submitted) and under simulated storm.

Here, we characterise bar formation and migration observed in the flume. Secondly, we focus on the morphological evolution of a barred beach for a storm simulation. We are particularly concerned by the influence of the three phases of the storm namely the rising, the apex and the waning of the event. Comparison between experimental bar evolution and natural observations is also discussed.

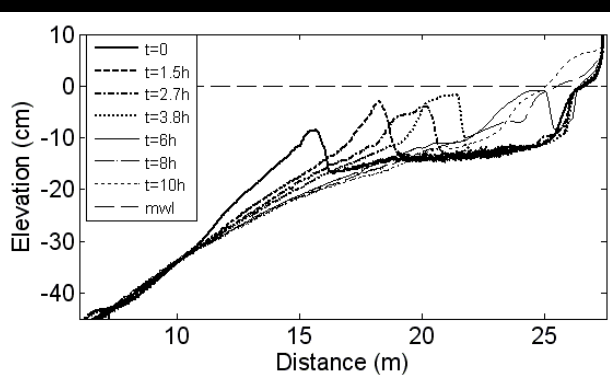


Figure 1. Bar migration and shore-face accretion for B during 10h

EXPERIMENTAL SET-UP

Our experiments were carried out in a flume 36 m long and 55 cm wide equipped with a piston wave generator. The still water depth was 55.3 cm. The mean overall slope was approximately 1/45. The sloping bottom consisted of loose material of low density (1.19 g cm^{-3}) with a median diameter $d_{50}=0.6 \text{ mm}$. The Froude number, the Shields number and the Rouse number are of the same magnitude as those of natural environments. Time and length scales are roughly 1/3 and 1/10 respectively. Irregular waves are generated (JONSWAP spectrum – peak enhancement factor=3.3). We check that these waves conform to the expected spectrum and that they follow a Rayleigh distribution at 2 m downstream of the wave maker. Bottom profiles are recorded between wave series using an acoustic profiler mounted on motorised trolley. The generated wave series are characterised by their significant wave height H_s and their peak period T_p (cf. Table 1).

EXPERIMENTAL SANDBARS EVOLUTION FOR CONSTANT WAVE CLIMATES

The experiments carried out in the flume have presented many cases of bar formations and migrations. For example in Figure 1 the constant wave climate B generated during 10 hours affects a bar formed close to the slope break at $x=15 \text{ m}$. Typically, the bar is pitched forward and onshore bar migration is observed. The bar migrates as a dune with a horizontal propagation speed around 2 m/h. Then the bar welds to the shore-face, leading to accretion and formation of a new berm.

In Figure 2 the wave climate A generated over 43 hours leads to a succession of bar formations and onshore migrations. Habitually, bars welding to the berm help nourish the shore-face and advance the shoreline seaward (black symbols in Fig. 2). Moderated wave climates (type A and B) are largely responsible for bar formations and onshore migrations.

Bar formation can occur at different positions along the profile where there is a dependence on hydrodynamics and initial bottom profile. Hydrodynamics plays a role in the sediment mobilisation. In the case of the low energetic wave climate A, waves are not able to transport significantly any sediment below depths of 25

Table 1: Wave conditions used in this study.

Wave climate	A	B	C	D	E
H_s (cm)	6	10.7	13.5	16	16
T_p (s)	1.5	2	2.5	2.7	3

cm. As we can see in Figure 2, the profile from $x=0$ to $x=20 \text{ m}$

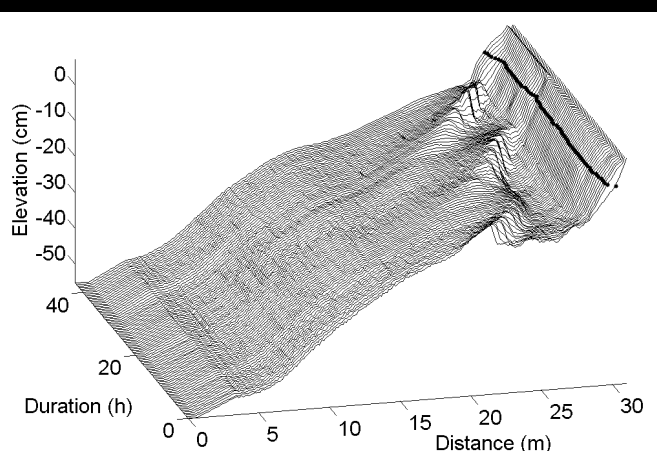


Figure 2. Bar formations and onshore migrations for climate A during 43h. Black symbols represent shoreline position

does not change for the 43 hours. Thus a sandbar could not be formed below this limit. However, energetic wave climates (type D and E) can also form a bar at a depth of 40 cm and 10 cm. The initial bottom profile appears to have an influence because the bars will largely form close to the initial profile discontinuities (this can be a slope break or an initial irregularity on the surface). The onshore bar migration is generally associated to an onshore sediment transport and the propagation speed ranging from 10 cm h^{-1} to 2 m h^{-1} .

After observing the effects of constant wave climates on sandbars, the next aspect will highlight the effects of a simulated storm on a barred beach.

EXPERIMENTAL BARRED BEACH EVOLUTION FOR A STORM EVENT

Storm event hydrodynamics

The storm event simulation is based on the hydrodynamic observations on lido beach at Sète (France) (CERTAIN *et al*, 2005). We constructed a schematic storm as a succession of different wave climates described in Table 1. The three storm phases were characterised by increasing, energetic and decreasing wave conditions respectively (Figure 3). The storm duration was 9.5 hours for an apex lasting 4.5 hours.

Experimental results

Figure 4 represents beach profile evolution during the storm. The black points on the top of the beach represent shoreline position. The black lines at 2 and 6.5 hours delineate the three

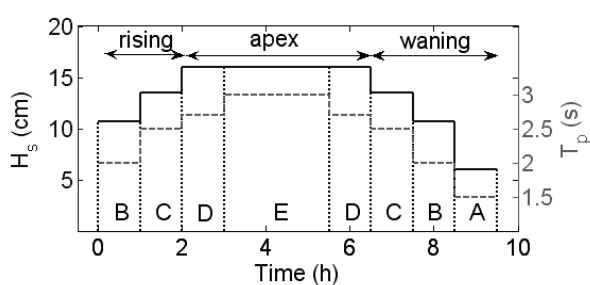


Figure 3. Storm event hydrodynamics

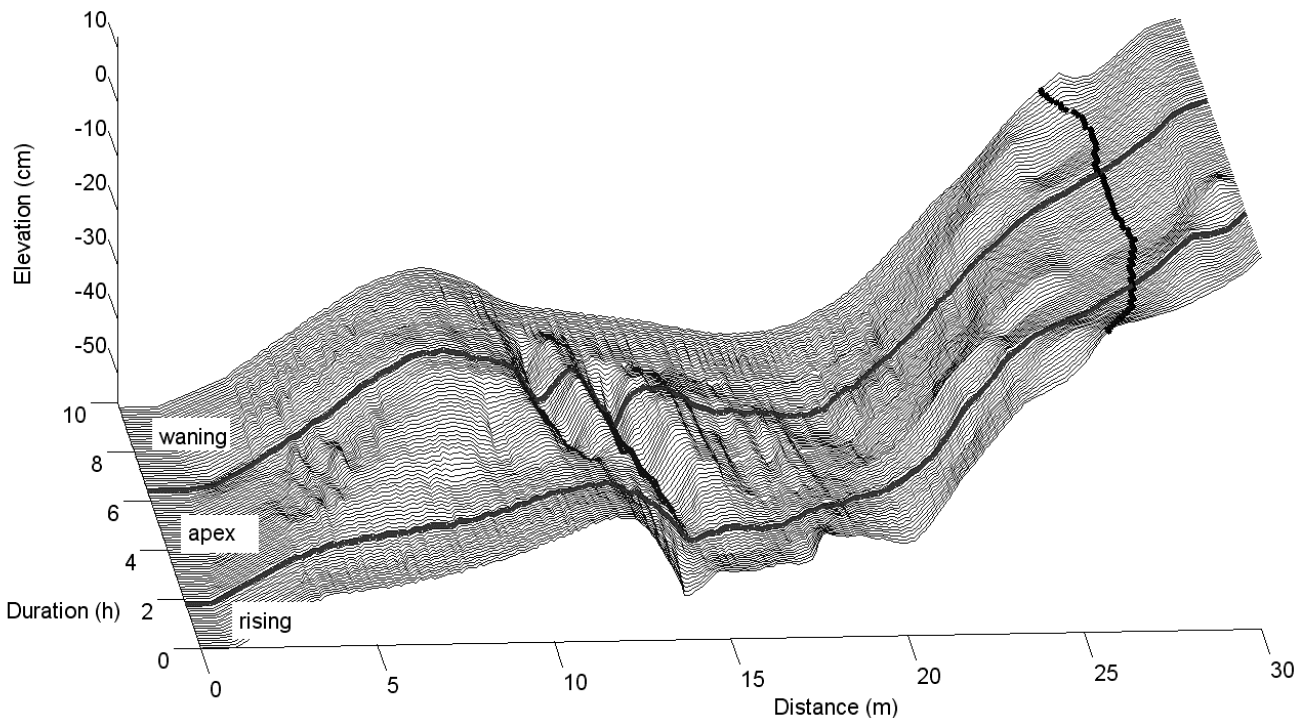


Figure 4. Beach profiles evolution during the storm event. Black symbols on top represent shoreline position and black lines delineate the three phases of the storm

phases of the storm. Beach profiles evolutions for each phase are then presented in the vertical plan (Figures 5 to 7).

During the rise of the storm (Figures 4 and 5) only the top of the beach (from -15 to +10 cm in elevation) is substantially modified. The slope is more gentle and the shoreline setback shoreward. The rest of the profile is only smoothed. The storm apex (Figures 4 and 6) leads to an offshore bar formation. It results from the convergence of sediment, onshore sediment transport from the beach foot and offshore sediment transport from the old bar. The bar crest position moves from $x=12$ m to $x=8$ m and the elevation on the bar crest increases by 5 cm. Macro sediment structures are formed in front of the main bar and tend to converge on it. A net erosion of the profile from $x=17$ m to $x=25$ m was observed. This offshore sediment flux nourishes the bar. For the waning storm (Figures 4 and 7) the wave climates C and B smooth the profile

migration in the inner zone. Climate A only reshapes the top (from -20 to +5 cm in elevation) and advances the shoreline seaward substantially leading to a new berm formation. The slope of the shore-face is clearly steeper.

We note that wave climate A does not modify the beach shape significantly below the 20 cm water depth. We used this depth as a lower limit when computing the shore volume. The upper limit is the point on the dune that stays unchanged for all the profiles. This shore volume corresponds to the sediment which is transported even by the weakest wave conditions.

In order to better quantify the shore changes we plot in Figure 8 the evolutions of the shoreline position and the shore volume during the storm. We observe a strong setback of shoreline position during the rising phase of the storm (-1.15 m). Storm apex leads to surprisingly little changes (-10 cm). But we note that

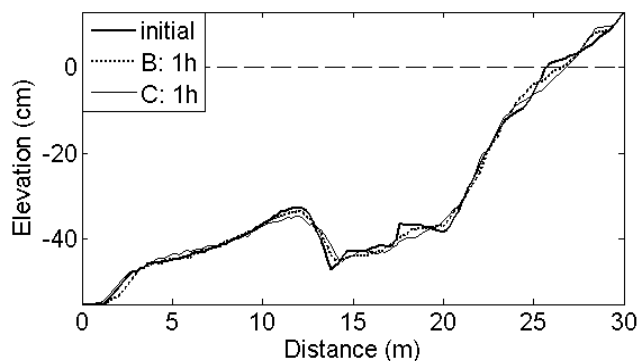


Figure 5. Beach profiles evolution during the storm rising and lead to a small bar formation at $x=25$ m and an onshore

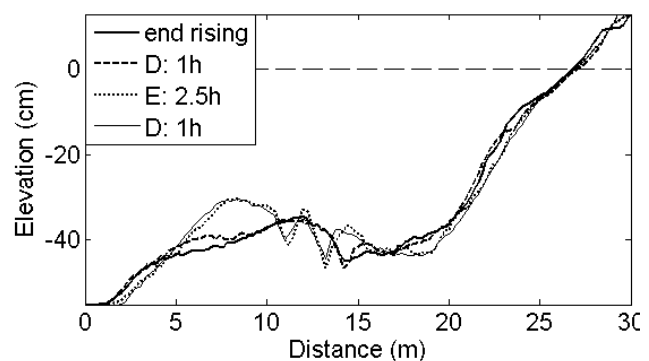


Figure 6. Beach profiles evolution during the storm apex

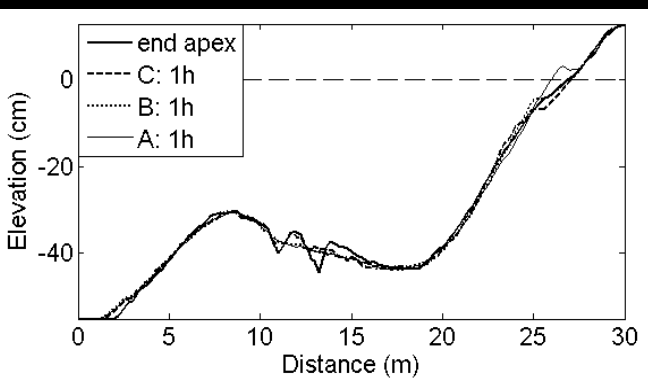


Figure 7. Beach profiles evolution during storm waning

for the storm waning, the wave climate A is responsible of the entire shoreline advancement (+90 cm).

A different behaviour for the shore volume evolution however was observed. The volume of sediment stayed almost constant during the storm rising phase. However, it decreased slightly for wave climate C (less than 1% loss compared to the initial volume). The inner zone sediment stock was generally still available for mobilisation by low energetic wave climates. During the storm apex the shore volume significantly decreased (-5%), particularly in the two first hours. This loss of sediment corresponded with an offshore sediment transport in the direction of the bar. Then, the storm waning partially reconstructed the shore-face with a volume augmentation of +2%. However, the sediment trapped in depth could not be transported to the inner zone. In general, at the time scale of the storm, the shoreline fell of -36 cm shoreward and the shore volume dropped off by -3.6%.

DISCUSSION

Experiments carried out by HOYNG (2008) in a small-scale flume (Scheldt flume) at Delft containing beaches around 20 m in length, mean water level of 0.7 m, natural sand (median diameter $d_{50}=0.13$ mm) with similar constant wave climates showed analogous morphological evolutions to our results. The accretive scenarios were mostly associated with onshore bar migrations. The bars evolved with the same asymmetric shape as observed in our experiments. Bar migration speeds were of the same order of magnitude (0.1 to 0.5 m h $^{-1}$).

If the duration of a constant wave climate is long enough (tens of hours) the bars will generally migrate and merge with the berm. In the situation where the hydrodynamic conditions decrease before the merging, the bars stop and we obtain barred beach profiles. Equilibrium beach profiles are defined as profiles which do not evolve for a constant wave climate (DEAN, 1991; WANG and KRAUS, 2005; GRASSO *et al.*, 2009). Hence, it is our understanding, that the barred beaches correspond to transient profiles tending to non-barred equilibrium profiles.

For simulations closer to the natural conditions, we can note that the storm waning contributes to shore reconstruction. It is interesting to stress the influence of the storm ratio (R_s) between the storm apex and storm waning durations:

$$R_s = T_a / T_w , \quad (1)$$

where T_a and T_w are respectively the duration of storm apex and storm waning. A scenario with a short apex and a long waning ($R_s \ll 1$) could lead to a low erosion of the inner zone and allow more time for the storm waning for reconstruction. So the shore volume balance between the beginning and the end of the storm could be positive. Whereas a scenario with a long apex and a short waning ($R_s \gg 1$) will probably lead to a strong erosion of the inner

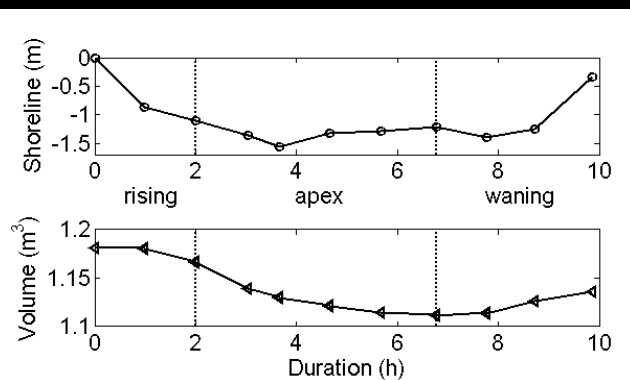


Figure 8. Shoreline and shore volume evolution during the storm event. Vertical dotted lines delineate the storm phases.

zone, without reconstruction. The shore volume balance would be negative.

We can observe some similarities between what is observed in the flume during our experiments and what is observed in nature on sandy beaches. First, the onshore migration of the bar is one of our main observations. In nature, bars are also normally shifting shoreward during periods of low waves (i.e summer) (OSTROWSKI *et al.*, 1990; HOLMAN and SALLINGER, 1993; GALLAGHER, 1998; SUNAMURA and TAKEDA, 1984). Strong correlation between inner bar evolution and shoreline evolution is also observed in nature, where the bar could weld to the shore, which moves seaward (HINE, 1979; SHORT, 1999). As in the flume for wave climate A and B (Fig. 1 and 2), storm waning conditions transport sediment onshore (KING, 1972) and advance substantially the shoreline seaward leading to a berm formation (SONU and JAMES, 1973; HINE, 1979).

The second observation is the offshore migration of the bar and erosion of the trough under dynamic conditions (Fig. 4 and 6). The seaward evolution during storm events (or/in winter) is described in nature by many authors (e.g. OSTROWSKI *et al.*, 1990). Bars could be stable over long periods of time (months to years) and then move offshore during an extreme storm event (LIPPMAN *et al.*, 1993). Long term migration speeds of the bars in nature are typically around 0.5 m day $^{-1}$ but maximum values may be considerably larger, e.g. 20 m day $^{-1}$ in Duck (USA) after extreme storms ($H_s > 4$ m) (LARSON and KRAUS, 1994). The ultimate stage of offshore migration is the destruction of the bar. The bars can degenerate and disappear (LIPPMAN *et al.*, 1993; WINJBERG, 1995). This "net offshore migration" (WINJBERG, 1995; CERTAIN and BARUSSEAU, 2005) is not observed in the flume, which may be down to the fact that an exceptional storm cannot be generated due to the configuration of the flume. Indeed, the phenomenon is initiated in nature after a particular large event (LARSON and KRAUS, 1994). The alternative phases of onshore and offshore bar migration under more or less energetic conditions has been described by several authors and known as "oscillation around an equilibrium position" (CERTAIN and BARUSSEAU, 2005). On the North Atlantic American coast, in Duck, this seasonal oscillation of the inner bar is expressed by a strong mobility (LIPPMAN *et al.*, 1993).

These experiments in the flume also stress some of the problems that can be encountered in nature. First, we saw that during the storm apex the shore volume significantly decreases (-5%), particularly in the two first hours. This highlights the lack of information and the difficulties in making measurements during storms in nature. The survey is usually done before and after each storm. This methodology does not permit a precise analysis during the event. In the same way, an offshore migration of mega-ripples is observed in our flume during the most energetic phase, feeding

the large offshore bar. This observation would be difficult to confirm in nature.

Following GRASSO *et al.* (*submitted*), it is not only the wave height but also the time duration of the dynamic conditions that have an important affect on shore-face morphology. In the flume, bars represent a transient state between equilibrium positions. Only very long time duration can permit to reach an equilibrium profile. This is never done in nature where storms are generally not exceeding days. Furthermore, there is a delay between hydrodynamic conditions and the response of morphology. The system never reaches a state of equilibrium. Thus, near-shore sandbars often represent disequilibrium features that are continuously readjusting their configuration and location (SHORT, 1999).

CONCLUSIONS

In our laboratory experiments, sandbar formation and evolution have been studied. Our results have shown that sandbars can be formed across the beach profile, depending on initial bottom profile and wave climate characteristics. For constant wave climates, bars will mostly migrate onshore and merge with the berm. For changing wave climates, bars may stop and be stranded as relict bars.

The storm simulation on a barred beach has two main effects on the morphology. Firstly, the storm apex erodes significantly the shore-face and moves the bar offshore, causing an offshore sediment transport out of the inner zone. Secondly, the storm waning partially reconstructs the shore-face. The ratio between apex and waning durations should therefore determine the shore erosion/reconstruction. Finally, we observe morphodynamic similarities between flume experiments and what is observed in nature on sandy beaches.

LITERATURE CITED

- AGAARD, T., BLACK, K.P. and GREENWOOD, B., 2002. Cross-shore suspended sediment transport in the surf zone: a field base parametrization. *Marine Geology*, 185, 283-302.
- CERTAIN, R. and BARUSSEAU, J.P., 2005. Conceptual modelling of sand bars morphodynamics for a microtidal beach (Sète, France). *Bulletin de la Société géologique Française*, 176(4), 343-354.
- CERTAIN, R., MEULÉ, S., REY, V. and PINAZO, C., 2005. Swell transformation on a microtidal barred-beach (Sète, France). *Journal of Marine Systems*, 38, 19-34.
- DEAN, R. G., 1991. Equilibrium beach profiles: characteristics and applications. *Journal of Coastal Research*, 7(1), 53-84.
- DETTE, H., LARSON, M., MURPHY, J., NEWE, J., PETER, K., RENIERS, A. and STEETZEL, H., 2002. Application of prototype flume tests for beach nourishment assessment. *Coastal Engineering*, 47, 137-177.
- GALLAGHER, E.L., 1998. Observations of sand bar evolution on a natural beach. *Journal of Geophysical Research*, 103(C2), 3203-3215.
- GRASSO, F., MICHALLET, H., BARTHÉLEMY, E. and CERTAIN, R. Intermediate cross-shore beach morphology: transients and equilibrium states. *Submitted*.
- GUANNEL, G., OZKAN-HALLER, H.T., HALLER, M.C. and KIRBY, J.T., 2007. Influence of velocity moments on sand bar movement during crosstex, *Coastal Sediment 07, ASCE*, (New Orleans, Louisiana, USA).
- GÜNEYDİN, K. and KABDASLI, M.S., 2003. Characteristics of coastal erosion geometry under regular and irregular waves. *Ocean Engineering*, 30, 1579-1593.
- HINE, A.C., 1979. Mechanisms of berm development and resulting beach growth along a barrier spit complex. *Sedimentology*, 26, 333-351.
- HOLMAN, R.A. and SALLINGER, A.H., 1993. Sand bar generation: A discussion of the Duck experiment series. *Journal of Coastal Research*, SI15, 76-95.
- HOYNG, C., 2008. Erosive and accretive coastal response, *M. sc. Thesis*, WL Delft Hydraulics.
- HOM-MA, M. and SONU, S., 1963. Rhythmic pattern of longshore bars related to sediment characteristics. *8th ICCE* (ASCE, Mexico City), 248-278.
- KING, C.A.M, 1972. Beaches and coasts. *Edward Arnold*, London, 570 p.
- LARSON, M., & KRAUS, N.C., 1994. Temporal and spatial scales of beach profile change, Duck, North Carolina, USA. *Marine Geology*, 117, 75-94.
- LIPPMAN, T.C., HOLMAN, R.A., and HATAWAY, K.K., 1993. Episodic, nonstationary behaviour of double bar system at Duck, N.C., U.S.A., 1986-1991. *Journal of Coastal Research*, 15(SI), 49-75.
- MASSELINK, G. and HUGHES, M.G., 2003. An introduction of Coastal Processes and Geomorphology. *Oxford University Press*, 368p.
- MICHALLET, H., GRASSO, F., and BARTHÉLEMY, E., 2007. Long waves and beach profiles evolutions. *Journal of Coastal Research*, SI50, 221-225.
- OSTROWSKI, R., PRUSZAK, Z., and ZEIDLER, R.B., 1990. Multi-scale nearshore and beach changes. *22nd ICCE* (ASCE, Delft, Netherlands), 2101-2116.
- PRICE, T.D. and RUSSINK, B.G., 2008. Morphodynamic zone variability on a microtidal barred beach. *Marine Geology*, 251, 98-109.
- ROELVINK, J. A., and STIVE, M.J.F., 1989. Bar-generating cross-shore flow mechanisms on a beach. *Journal of Geophysical Research*, 94(C4), 4785-4800.
- SALLINGER, A.H., HOLMANN, R.A. and BIRKEMEIER, W.A., 1985. Storm induced response of a nearshore bar system. *Marine Geology*, 64, 237-257.
- SHORT, A.D., 1999. Handbook of beach and shoreface morphodynamics. *Wiley*, 379 p.
- SONU, C. J., and JAMES, W. R., 1973. A Markov model for beach profile changes. *Journal of Geophysical Research*, 78, 1462-1471.
- SUNAMURA, T. and TAKEDA, 1984. Landward migration of inner bars. *Marine Geology*, 60, 63-78.
- WALSTRA, D.J.R.; BRIÈRE, C.; COHEN, A.B.; VAN DONGEREN, A.P.; ELSHOFF, I.J.P.; HOYNG, C.; VAN ORMONDT, M.; QUARTEL, S.; DE SONNEVILLE, B.; TONNON, P.K. AND UUNK, L., 2008. Monitoring and modelling of a shoreface nourishment. *Research Report, Overeenkomst RKZ-1821A*, WL Delft Hydraulics.
- WANG, T. and KRAUS, N.C., 2005. Beach profile equilibrium and patterns of wave decay and energy dissipation across the surf zone elucidated in a large-scale laboratory experiment. *Journal of Coastal Research*, 21(3), 522-534.
- WINJBERG, K.M., 1995. Morphologic behavior of a barred coast over a period of decades. *PhD Thesis*, Univ. Utrecht, 215p.

ACKNOWLEDGEMENT

This work has been funded by the projects LITEAU II (MEDD), Beachmed-e (INTERREG IIIC), MODLIT (ECORS – DGA) and ECOSUD-CONYCIT. The technical support of J.-M. BARNOUD is gratefully acknowledged.

Physical modeling of intermediate cross-shore beach morphology: transients and equilibrium states

F. Grasso,¹ H. Michallet,¹ E. Barthélémy¹ and R. Certain²

Abstract. Laboratory experiments on cross-shore beach morphodynamics are presented. A lightweight sediment (density $\rho_s = 1.19 \text{ g cm}^{-3}$) model is used in order to fulfill a Shields number and Rouse number scaling. This choice aims at correctly reproducing bed load transport as well as suspension dynamics. Terraces and barred beach profiles obtained in the experiments also present close similarities with profiles observed in the field. In order to question the concept of equilibrium beach profile, wave forcings conforming to a JONSWAP spectrum were imposed over long periods (up to more than a hundred hours). An average bottom evolution velocity is defined and used to determine when the profile reaches equilibrium. Usually beach profiles are characterized according to the *Wright and Short* [1984] classification based on the Dean number Ω . This well-known classification is investigated and refined in the intermediate range, that is for $1 \leq \Omega < 5$. For Ω close to one, a typical reflective profile is obtained. Terraces are obtained for the $\Omega = 2.5$ cases. For $\Omega \approx 3.7$, the profiles exhibit two parts: a mild dissipative offshore slope producing low reflection and a steeper beach face with slightly higher reflection. The wave dissipation, velocity skewness and acceleration skewness are computed from the free surface elevation time series. The dissipation and wave non-linearities patterns are similar for similar equilibrium beach profiles, that is with the same Dean number. Dissipation peaks coincide with bottom slope transitions as higher energy dissipation occurs with milder bottom slope sections. Besides, the uniformity of volumetric wave energy dissipation seems to concern only a limited zone of beaches with a widely developed surf zone.

1. Introduction

The morphology of a beach is mainly controlled by wave climate, tide and sediment characteristics. Cross-shore morphology of sandy beaches is an important issue for coastal erosion. Even though cross-shore sediment fluxes are usually a few orders of magnitude smaller than longshore transport, the cross-shore beach profile has a strong influence on longshore velocity profiles and therefore on longshore sediment fluxes. The beach profile is the result of the trade off between onshore and offshore fluxes. The direction of the cross-shore fluxes is a key point for predictive tools and is closely related to the non-linear characteristics of the incoming waves such as asymmetry and velocity skewness [Bailard, 1981; da Silva, 2006]. This complexity is very difficult to reproduce with numerical models and a physical model then becomes an interesting alternative.

Because of this complexity, the concept of equilibrium beach profile is very useful. Indeed long-term beach changes can be estimated by measuring the “distance” between the current beach profile and the equilibrium profile it should assume for a given wave climate. Using such a framework, some standard engineering tools (SBEACH for example) for cross-shore profile changes consider equilibrium profiles [Dean, 1991; Miller and Dean, 2004] as target profiles. These are essentially empirically determined but were initially justified by a physical argument of uniform volumetric wave

dissipation in the surf zone [Dean, 1977; Wang and Kraus, 2005]. These profiles have the following expression,

$$h = \alpha (x_s - x)^{2/3}, \quad (1)$$

where h is the water depth at the cross-shore position x (x oriented onshore) and x_s is the shoreline position. Dean [1977] and Moore [1982] show that the constant of proportionality α can be related to the size of the beach sediment or, alternately, the fall velocity. Other assumptions and more detailed sediment transport physics are used by Plant *et al.* [2001] who also obtain equilibrium profiles. On equilibrium beach profiles the mean cross-shore sediment fluxes are zero. Stemming from this constraint Bowen [1980] and Dronkers [2005, pp387-414], using simple sediment flux evaluations, show that these profiles are also compatible with the equilibrium between a destructive force such as gravity and a constructive force such as onshore bed load sediment transport by waves. The equilibrium beach profile formulation (1) can be obtained through a number of independent arguments that seem reasonable on physical grounds. The assumption that the equilibrium beach profile in the surf zone corresponds with uniform wave energy dissipation per unit volume, suggested by Dean [1977], has been recently analysed by Wang and Kraus [2005] for regular and irregular waves generated during runs less than ten hours in the SUPERTANK flume. The authors concluded that under irregular waves, the pattern of wave-energy dissipation across a large portion of the surf zone became relatively uniform while the profile evolved towards equilibrium. One of our aims is to question the concept of equilibrium beach profile in the framework of physical modelling. Do such profiles exist since some of the very few examples of flume experiments have focused on transients such as erosion or near-shore bar growth [Dette and Uliczka, 1987; Dally, 1987; Dette *et al.*, 2002]?

¹Laboratoire des Ecoulements Géophysiques et Industriels (UJF-INPG-CNRS), BP53, 38041 Grenoble, France

²IMAGE EA4218, Université de Perpignan, 52 av. Alduy, 66000 Perpignan, France

Clearly, because of the ever-changing wave climate in natural environments, equilibrium profiles can only be retrieved as spatial long-shore averages or mean inter-annual profiles. In detail it has been claimed that different equilibrium profiles correspond to each season in conjunction with well-defined wave climates [Larson and Kraus, 1994] leading for instance to the so-called summer profiles and winter profiles. Flume experiments can overcome the drawback of defining an equilibrium beach profile as a temporal mean. As long as one is patient enough to run lengthy experiments for given wave conditions, equilibrium profiles can be obtained [Kamalinezhad, 2004; Kamalinezhad et al., 2004; Wang and Kraus, 2005; Grasso et al., 2007; Michallet et al., 2007].

Beach profiles are generally more complex than the simple Dean concave-up equilibrium profile. Some tend to have a convex part near the shoreline and a concave part further offshore. Amongst these double convex profiles the terrace-like or step-like profiles are observed in macro-tidal wave dominated environments [Wright and Short, 1984; Black, 2002]. It has been shown that some equilibrium beach profiles are a combination of an upper profile and a lower profile [Inman et al., 1993; Bernabeu et al., 2003]. In this 2-section modelling approach a discontinuity point therefore separates the beach into two sections: the shoaling section and the surf section. The discontinuity point at depth h_r coincides with the break point. For irregular waves the breaking index γ is defined at the break point of depth h_r by,

$$h_r = \frac{1}{\gamma} H_{rms}, \quad (2)$$

with γ between 0.4 and 0.6 at the break point [Wang and Kraus, 2005], H_{rms} being the root mean square wave height. The depth h_r at the break point is expressed in terms of the significant wave height H_s to yield:

$$h_r = \beta H_s \text{ with } 1.1 \leq \beta \leq 1.7. \quad (3)$$

Longshore bars are also frequently observed on beach profiles. Some studies argue that they are perturbations of equilibrium profiles [Ribas Prats, 2003]. Observed barred profiles are constantly evolving including cyclic behaviour [Ruessink and Kroon, 1994] on time scales as long as decades. Knowledge of the seasonal variability of nearshore bars [Holman and Sallenger, 1993] has increased considerably in recent years due to the use of video remote sensing techniques [Lippmann and Holman, 1990; Van Enckevort and Ruessink, 2001]. Analysis by Lippmann and Holman [1990] shows that beach states with bars are indeed frequently observed but that they undergo frequent transitions. Analysis of Duck profiles [Larson and Kraus, 1994] shows that summer profiles are the result of an accretion process in which sand of the winter profile is transported onshore. Bar migration has been identified as one of the mechanisms of such accretion [Gallagher et al., 1998]. This beach recovery is also known to be associated with mild wave climates. Bar formation has been investigated in flume experiments but essentially as an erosion process [Roelvink and Stive, 1989; Guannel et al., 2007; Hoyng, 2008] in which undertow currents move sediment offshore [Thornton et al., 1996; Gallagher et al., 1998].

Guannel et al. [2007] investigated onshore bar migration in a specifically designed run during the CROSSTEX experiments. Onshore bar migrations are probably due to a combination of subtle mechanisms [Elgar et al., 2001; Hoefel and Elgar, 2003; Henderson et al., 2004; Hsu et al., 2006; Foster et al., 2006]. This questions the relevancy of laboratory

experiments to address such questions. It is well known that downscaled experiments with sand have difficulty in reproducing suspensions that behave dynamically as in nature. This is why a few experiments at scale 1 with sand have been recently reported in the literature [Guannel et al., 2007]. Wang and Kraus [2005] also present results from the large-scale SUPERTANK laboratory experiment. With regard to the dimensions of the flume (104 m long, 3.7 m wide), these experiments may be considered as full-scale for moderate waves ($H_s \leq 0.8$ m). The maximum duration of irregular wave runs (JONSWAP spectrum with a peak enhancement factor of 3.3) is 3 h 29 mn in the SUPERTANK experiments. It can be observed that most profile variations are restricted to shallow water such that $h < 2 H_s$. In contrast to the SUPERTANK experiment, our present experiments aim at reproducing profile changes in water as deep as 4 H_s and for long periods up to 115 h. Recently, Henriquez et al. [2008] also addressed scaling laws and concluded on the relevant use of coarse, lightweight particles for studying nearshore sediment transport in a physical model. The innovative aspect of the experiments presented in this paper is primarily the simulation of a wide range of irregular wave climates in a small-scale lightweight sediment model able to satisfy the laws of similitude over long periods.

The flume experiments and similitude conditions are described in Section 2. In this section some beach profiles at Duck and Lido beach (Sète, France) and the associated dimensionless numbers are compared to those of our experiments. Section 3 is devoted to the morphodynamics and presents a detailed description of the beach profile changes. Equilibrium states are characterized and classified in terms of the Dean number. The hydrodynamics related to the equilibrium profiles are then described in Section 4. Conclusions are given in Section 5.

2. Description of flume experiments and similitude conditions

2.1. Experimental set-up

Our experiments were carried out in a flume 36 m long and 55 cm wide equipped with a piston wave generator (Fig. 1). The still water depth at the wave-maker is $h_0 = 55.3$ cm. The sloping bottom consists of a loose material of low density ($\rho_s = 1.19 \text{ g cm}^{-3}$) with a median diameter $d_{50} = 0.6$ mm (corresponding settling velocity $w_s = 2.1 \text{ cm s}^{-1}$). It covers a rigid sloping bottom in some cases. The sediment layer over the rigid bottom is at least 5 cm thick in all the beach profiles presented in this paper. The mean overall beach slope is roughly 1/45.

Using a partially deterministic irregular wave synthesis [Hughes, 1995; p.397], irregular waves are generated according to a JONSWAP spectrum with a peak enhancement factor of 3.3 [Goda, 1985; p.26]. A linear combination of 10000 random sinusoidal components is used to define 30 mn wave sequences. There is neither wave absorption nor second-order correction on the wave-maker motion. A given 30 mn wave sequence can be repeated continuously as much as desired.

Twelve wave gages (acquisition at 50 Hz) are mounted on trolleys and measure instantaneous water elevations. The root mean square wave height H_{rms} is computed with the zero down-crossing technique for positions all along the beach profile.

It is checked that the wave field conforms to the expected spectrum and follows a Rayleigh distribution at 2 m downstream of the wave-maker, as shown for instance in Fig. 2. Limited energy is seen in the infra-gravity domain of the spectrum. This corresponds to seiching modes generated by wave breaking [Michallet et al., 2007; Grasso et al., 2007]. The contribution of these long waves to the sediment transport is expected to be weak to negligible compared to wave non-linearities and undertow effects [Ruessink et al., 2007].

Table 1. Wave conditions used in this study, related dimensionless numbers (Eq. 4–10) computed at the closure depth $h = 4 H_s$, durations of the experiments and distance from initial to equilibrium bottom profiles.

Wave climate	H_s (cm)	T_p (s)	Ω	Re ($\times 10^5$)	Fr	Θ	Rou	Duration (h)	T_{eq} (h)	Distance Δ (mm)
A	3	2	0.7	0.1	0.04	0.18	3.7	9.4	3.1	20.8
B1	10.7	2	2.5	0.7	0.08	0.38	2.6	41.3	22.7	30.3
B2	10.7	2	2.5	0.7	0.08	0.38	2.6	57.8	32.9	64.4
C	16	3	2.5	1.3	0.07	0.46	2.3	115.1	42	149.3
D	10.7	1.4	3.6	0.6	0.12	0.35	2.7	6.7	3.8	12
E	12.5	1.6	3.7	0.7	0.11	0.39	2.5	33.9	32.3	98.7
F	16	2	3.7	1.1	0.10	0.45	2.3	30.5	30.5	71.3

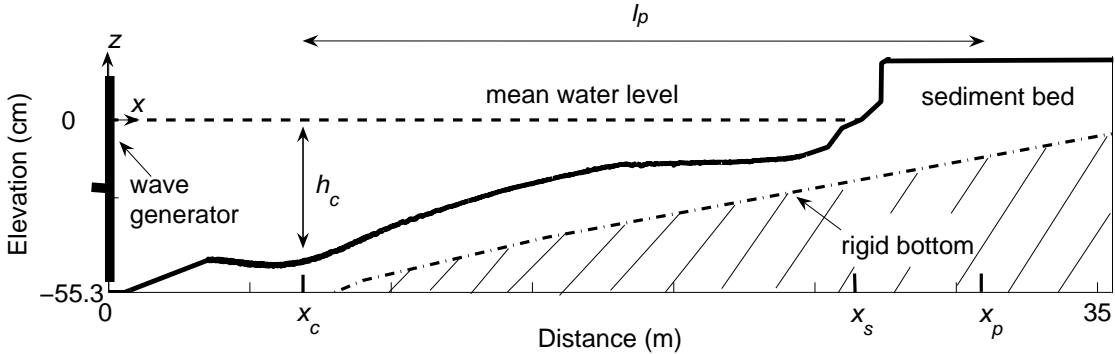


Figure 1. Schematic diagram of the LEGI wave flume: l_p is the profile length from the cross-shore position x_c of the closure depth h_c to the cross-shore position x_p of the most offshore point on the dune that does not change during an experiment, x_s is the shoreline position.

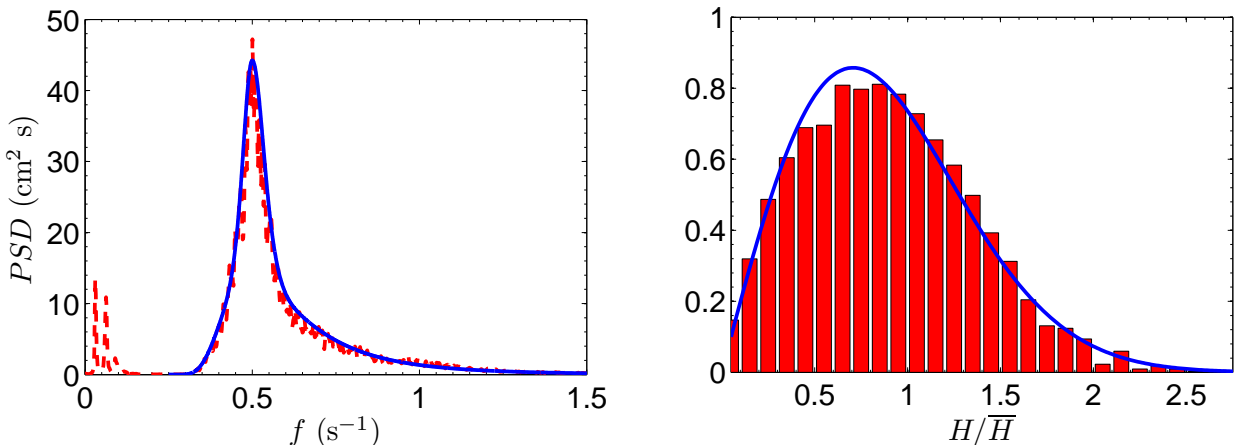


Figure 2. Experimental results and theoretical targets (solid lines) at 2 m downstream of the wave-maker for the wave climate B1: frequency distribution of power spectral density compared to the JONSWAP spectrum (a) and wave height distribution compared to the Rayleigh distribution with mean wave height $\bar{H} = 6.4$ cm (b).

Their peak frequency and structure (node and anti-node positions) mainly depend on the beach length and mean slope and are therefore similar for all the experiments presented in this paper. The variety of beach response described in the following would indicate that infra-gravity waves play a minor role on beach morphodynamics. The good agreement of the measured wave height distribution with the target Rayleigh distribution (Fig. 2b) also suggests that a reflected waves absorption device is not needed for producing the desired irregular wave climates. Each wave sequence corresponds to a wave climate characterized by the significant wave height at the wave-maker H_s and the spectrum peak

period T_p . A summary of the wave climates prescribed during the experiments is given in Table 1.

Bottom profiles are recorded between wave series using an acoustic profiler mounted on a motorized trolley. Starting from a given bottom profile, wave sequences are repeated until an equilibrium state is reached. The equilibrium state is characterized in Section 4. The initial bottom profile of an experiment is a profile produced by previous wave sequences. The initial profile corresponds to an equilibrium state only for experiment C, produced previously by experiment F. The duration of each experiment, the time to reach equilibrium state and the distance from initial to equilibrium profiles are also indicated in Table 1. These are discussed further in Section 3.1. Although it should depend on the

bed slope [*Unal and Bayazit, 1998*], the closure depth in all our set of experiments was found to be roughly $4 H_s$. This is probably due to the fact that in all our runs the mean beach slopes are similar. Attempts to compare our findings with empirical relations based on extreme wave heights obtained in natural environments [*Hallermeier, 1978; Komar, 1998*] were inconclusive.

Values of dimensionless numbers are also indicated in Table 1. The choice of the sediment and wave conditions was determined through similitude considerations, as detailed in the next section.

2.2. Dimensionless numbers

Our laboratory experiments are designed to reproduce natural beach profiles and changes. The physics and hydraulics of movable bed models depend on:

- the wave parameters: H_s the significant wave height and T_p the peak wave period;
- the sediment parameters: d the sediment diameter and ρ_s the density of the sediment;
- the water depth h , the fluid density ρ , the fluid kinematic viscosity ν and the gravity g .

Hence these models are characterized by 8 independent parameters [*Kamphuis, 1985*]. This implies that the ideal downscaling would require scaling 5 dimensionless numbers, which is known to be very difficult. In the following we discuss which scaling is favoured. The Froude scaling is the primary requirement for physical models involving waves [*Dean and Dalrymple, 2001*]. The Froude number is written:

$$F = \frac{H_s \omega_p}{2 \sqrt{gh}}, \quad (4)$$

where H_s is the significant wave height, $\omega_p = 2\pi/T_p$ the angular frequency and h the water depth. We also choose an undistorted model since wave dynamics, shoaling, breaking and turbulence generation by the waves are phenomena to be modelled correctly. As a consequence a single length scale λ_t will be chosen (λ_i is the ratio of the model value to the prototype value of parameter i). The Froude similitude between nature and the model implies that the time scale is:

$$\lambda_t = \sqrt{\lambda_l}. \quad (5)$$

The wave Reynolds number is usually not scaled even in movable bed models, and will not be here. Nonetheless this number reads:

$$Re = \frac{A \omega_p h}{\nu}, \quad (6)$$

where ν is the fluid viscosity and A the particle excursion at the bottom:

$$A = \frac{H_s}{2 \sinh kh},$$

k being the wave number. The sediment transport similitude is achieved in both shoaling and surf zones by adopting Shields and Rouse scalings. On the one hand the Shields number is defined by:

$$\Theta = \frac{1}{2} f_w \frac{(A \omega_p)^2}{g(\rho_s/\rho - 1) d_{50}}, \quad (7)$$

where f_w is a wave friction factor which, according to *Swart [1974]*, can be approximated as:

$$f_w = \exp \left[5.213 \left(\frac{2.5 \times d_{50}}{A} \right)^{0.194} - 5.977 \right].$$

In the present context, the Shields number measures whether the sediment is set in motion by the waves and what the transport regime is (bed load, suspension, sheet flow, etc). It also indicates if ripples can form [*Nielsen, 1992*]. On the other hand the Rouse number reads:

$$Rou = \frac{w_s}{u'}, \quad (8)$$

where u' is the turbulent intensity of the flow field, which is approximated by:

$$u' = \kappa \sqrt{f_w/2} A \omega_p,$$

with κ the von Karman constant (0.4) [*Soulsby, 1997*]. This number is relevant for characterizing sediment particle motions in a turbulent flow as in the breaking and outer surf zones, where sediment suspension is triggered and fueled by different turbulence sources (boundary layers, breaking). Considering a characteristic length (the water depth for instance), it can be thought of as the ratio of a turbulent time scale to a settling time scale.

Choosing a length scale and prescribing Froude scaling in an undistorted model imposes all the hydrodynamic scaling. The remaining parameters to be chosen are thus the sediment density and diameter, both of which will be determined with the Shields and Rouse scalings. These requirements led to the choice of a coarse lightweight sediment, as described in the previous section. Consequently the immersed weight of the sediment ($\rho_s/\rho - 1$) is not scaled since water is the fluid in both the experiments and nature.

The scaling choice will be more thoroughly justified in the next section in comparison with natural beaches. Our approach is somewhat different from that of *Dean and Dalrymple [2001, p.310]*, who argued that morphological models with sand can be based on Froude and Dean scaling only. Other dimensionless numbers can be derived from those just described and are useful for the following.

The particle Reynolds number is one of them. It is written:

$$Re_p = \frac{A \omega_p d_{50}}{\nu} = Re \frac{d_{50}}{h}. \quad (9)$$

This Reynolds number quantifies the inertia of the flow around the sedimentary particle compared to the viscous drag. It indicates whether the flow around the particle is laminar or turbulent. The particle Reynolds number is linked to the wave Reynolds number by a factor d_{50}/h , which is a sort of Keulegan-Carpenter number. The parameter Re_p is one used in the Shields diagram to decide whether the sediment is set in motion or not.

The Dean number [*Dean, 1973*] is often used for discussing morphological beach states. It reads:

$$\Omega = \frac{H_s}{T_p w_s}. \quad (10)$$

This number is commonly interpreted as being the ratio of a particle settling time (H_s/w_s) to the wave period and therefore indicates whether phase-lag effects occur in sediment transport processes [*da Silva et al., 2006*]. This interpretation shows that it is merely a rewriting of the Rouse number and not an independent dimensionless number. Since *Wright and Short [1984]*, this number has been known to

be relevant for the modal classification of cross-shore beach profiles. Dissipative beaches characterized by a mild slope and spilling breakers are expected for $\Omega \geq 5$ while reflective beaches with a steep slope and surging breakers correspond to $\Omega \leq 1$ [Wright and Short, 1984; Masselink and Short, 1993; Bernabeu et al., 2003]. In the intermediate range defined by $1 \leq \Omega \leq 5$ beaches tend to have a moderate mean slope, breaking can be either plunging or spilling, and longshore bar-trough systems, rhythmic bars and terraces can be observed.

Wright and Short [1984] also used an equivalent of the surf parameter ξ [Battjes, 1974], which is defined as:

$$\xi = \frac{m}{\sqrt{H_s/L_\infty}}, \quad (11)$$

with m the local beach slope and L_∞ the deep water wavelength.

The choice of the scaling just described is now assessed by comparison with natural beach morphologies which relate to the intermediate range $1 \leq \Omega < 5$.

2.3. Natural beach examples

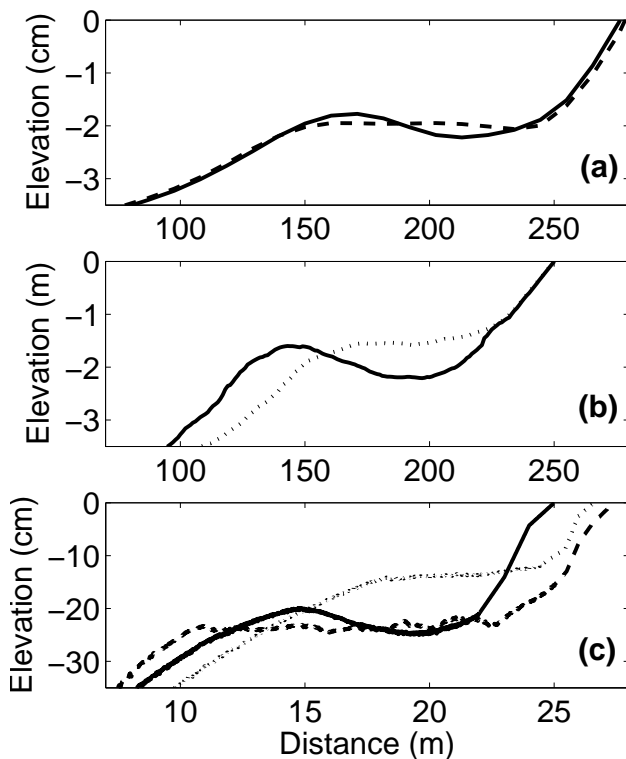


Figure 3. Measured beach profiles. (a) Duck: 4 Oct. 1994 (—), 7 Sept. 1994 (—); (b) Lido: 25 Nov. 2000 (—), 1 Nov. 2000 (···) and (c) LEGI wave flume: during climate B1 (—), climate C (—), climate B2 (···). Duck and Lido cross-shore profiles are averaged over a 500 m longshore section. The mean water level is at 0.

It is obviously impossible to match simultaneously the Froude, Shields, Rouse and density ratio numbers of down-scaled laboratory movable bed experiments with those encountered in nature. As discussed in the previous section, a good compromise has been found by using a lightweight sediment with a relatively large diameter.

To confirm that this choice is morphologically relevant, we consider two examples of natural beaches, namely Duck

(North Carolina, USA [Lee et al., 1998]) and the Lido beach (Sète, France [Certain et al., 2005; Certain and Barusseau, 2005]). The tidal range is about 1.5 m at Duck and 0.2 m at Lido, thus both sites fall into the micro-tidal category. These two sites are therefore interesting for comparison with our 2-D constant mean water level laboratory experiments. At the year scale the closure depth is about $h_0 = 4.5$ m at approximately 300 m from the shoreline at both sites. The lower part of the profiles is only modified by extreme storms. Since we cannot reproduce very large waves in the flume ($H_s \leq 20$ cm), we focus on the morphodynamics of the upper part ($h < 3.5$ m) of the profiles. At Duck beach [Birkemeier et al., 1985; and Bayram et al., 2001] the sediment median diameter is ranging from 0.18 mm by 5 m depth to 0.4 mm at the shoreline. Grain size distribution at Sète beach follows the same tendency [Akouango, 1997]. It induces a mean sediment median diameter in the upper beach of 0.3 mm, which yields a fall velocity of $w_s \simeq 4.5 \text{ cm s}^{-1}$.

Beach profiles observed at Duck, Lido, and produced in the LEGI flume are plotted in Fig. 3. The Duck and Lido cross-shore profiles correspond to averages of cross-shore profiles surveyed along a 500 m stretch of the shore. It clearly appears that both sites have very close morphological length scales. The profiles were chosen so as to feature a bar and a terrace. The experiments have profiles very similar to those of the natural beaches with a length scale of $\lambda_t \simeq 1/10$. More precisely, bar cross-shore position, bar shape, water depth at the crest, depth at the trough, terrace depth, and mean slopes are very similar. In more detail, it can be seen that the Lido terrace profile (Fig. 3b) is similar to the B2 experimental terrace profile (Fig. 3c), whereas the Duck terrace profile (Fig. 3a) is closer to the C experimental terrace profile (Fig. 3c). The profiles observed at Duck feature bars presenting longshore variability, such as crescentic bars (type C, D, E, F of Lippmann and Holman, [1990]). Therefore the terrace profile of Duck is a consequence of the longshore averaging of the ridge and runnel rhythmic system.

As the consequence of the choice of the length scale, the time scale is $\lambda_t \simeq 1/3$. The dimensionless numbers (4) – (10) for both natural sites and the wave climates that are related to the profiles of Fig. 3 are given in Table 2. The numbers are computed in the shoaling region at the closure depth estimated at $4 H_s$ (see discussion in section 2.1). A comparison of these values with those in Table 1 clearly shows that in our experiments the Froude, Shields and Dean numbers vary in the same range, indicating that our scaling is correct, at least in the ranges of the experiments. Note that, as foreseen, the wave Reynolds number is about 30 times smaller in the experiments than in nature but large enough in the breaking region ($\sim 10^5$) for the flow to be turbulent. The Keulegan-Carpenter numbers in nature and in the experiments evaluated at the bar crest are respectively 2×10^{-4} and 3×10^{-3} , implying that the particle Reynolds numbers at both sites and in our experiments are very close. Hence both the Shields numbers and the particle Reynolds numbers of our experiments are close to those found at Duck and Lido. This places our experiments and in-situ conditions at the same point in the Shields diagram. It is clear that the field wave conditions fall in the intermediate range as defined by Wright and Short [1984] since Ω is between 2.4 and 4.

On the one hand, the Duck and Lido barred profiles (Fig. 3a and Fig. 3b, respectively) were observed after mild wave climates lasting one day. Average wave conditions for these events are $H_s = 1.2$ m and $T_p = 8$ s on October 3 (1994) at Duck beach and $H_s = 1$ m and $T_p = 7$ s on November 24 (2000) at Lido beach. On the other hand, the Duck terrace profile (Fig. 3a) was preceded by 3 days

Table 2. Field measurements (see related profiles of Duck and Lido beaches in Fig. 3) and other laboratory experiment wave conditions; corresponding dimensionless numbers (computed for $h = 4 H_s$).

Site	date	H_s (m)	T_p (s)	d_{50} (mm)	Ω	Re ($\times 10^6$)	Fr	Θ	Rou
Duck	3-6 Sept. 94	1.75	12	0.3	3.2	4.8	0.06	0.42	2.5
Duck	3 Oct. 94	1.2	8	0.3	3.3	2.6	0.07	0.31	2.9
Duck ^a	1986-87	0.9	8.2	0.3	2.4	1.8	0.06	0.25	3.3
Duck ^a	1986-87	0.9	8.2	0.2	4	1.8	0.06	0.33	2
Lido	20-25 Oct. 00	1.2	8	0.3	3.3	2.6	0.07	0.31	2.9
Lido	24 Nov. 00	1	7	0.3	3.1	2	0.07	0.27	3.1
Delft flume ^b	–	0.17	2	0.1	10.8	0.12	0.10	0.15	1.3
Delft flume ^c	–	0.17	2.3	0.13	5.7	0.13	0.09	0.14	1.9
Delft flume ^c	–	0.10	3	0.13	2.6	0.06	0.05	0.09	2.2
HWRL ^d	–	0.6	4	0.22	4.9	0.83	0.10	0.21	2.7
HWRL ^d	–	0.3	8	0.22	1.2	0.36	0.03	0.14	3.4
SUPERTANK ^e	–	0.8	4.5	0.22	5.8	1.26	0.10	0.26	2.5
SUPERTANK ^e	–	0.4	8	0.22	1.6	0.55	0.04	0.17	3.1

^a field measurement analysis reported in *Lippmann and Holman* [1990]

^b laboratory experiments reported in *Roelvink and Stive* [1989]

^c laboratory experiments reported in *Hoyng* [2008]

^d laboratory experiments reported in *Guannel et al.* [2007]

^e laboratory experiments reported in *Wang and Kraus* [2005]

of an energetic wave climate ($H_s \approx 1.75$ m and $T_p \approx 12$ s that took place from September 3 until September 6 1994). The terrace profile at Lido (Fig. 3b) was measured after 6 days of weaker conditions than that of Duck ($H_s \approx 1.3$ m and $T_p \approx 8$ s that took place from October 20 up to October 25, 2000). The aim here is not to explain in details the morphodynamics of these two beaches. It is suggested that beach profile changes could be the result of relatively energetic wave conditions over a relatively short duration. Moreover, these in-situ examples show that, in the intermediate range, beach profiles exhibit both terraces and bars. Following the results of a two-years video-survey at Duck beach [*Lippmann and Holman*, 1990], the wave climate corresponding to the most likely observed beach profile (of the attached rhythmic bar type) is characterized by $H_s = 0.9$ m and $T_p = 8.2$ s. The associated dimensionless numbers are given in Table 2. Considering a smaller sediment size relative to the lower beach (0.2 rather than 0.3 mm) does not change much the dimensionless numbers range.

Examples of wave conditions and dimensionless numbers in other laboratory experiments are also given in Table 2. These configurations use fine sand (median diameter from 0.1 mm to 0.22 mm). The closest conditions to nature are obtained in the largest wave flume (88 m long, 3.7 m deep [*Guannel et al.*, 2007]). Shields numbers are generally notably smaller compared to field conditions, which probably indicates that the onset of sand transport and the transport regime are not well reproduced. This also emphasizes that it is not possible to match Θ , Rou and Ω numbers simultaneously in a small-scale experiment using fine non-cohesive sand.

For our present experiments the dimensionless numbers Fr , Rou , Θ and Ω given in Table 1 are of the same order of magnitude as those of the Duck and Lido natural sites in Table 2. Note that during the shoaling process up to the breaking point, Fr and Θ tend to increase while Rou tends to decrease in both laboratory and natural conditions. The important point is that the choice of the lightweight sediment enables us to obtain Dean numbers in the intermediate range $0.7 \leq \Omega \leq 3.7$.

3. Morphodynamics

3.1. Beach profile changes

Before discussing the equilibrium states, the present section gives an insight into how the experimental beach morphology evolves and what type of transients are observed. Three characteristic changes are presented in Figs. 4, 5, 6.

Wave climate C leads to beach face erosion and the formation of a so-called terrace (Fig. 4). The initial profile of this experiment was a steep beach shaped by a $\Omega = 3.7$ Dean number wave climate (F in Table 1). In this transition to a lower Dean number ($\Omega = 2.5$), sediment is transported offshore from the upper shoreface and the overall beach slope is reduced. This kind of change can be observed in nature in the case of storm events during which the upper part of the beach is eroded and the profile switches to form a deep terrace [*Günaydin and Kabdasli*, 2003]. It has also been reproduced in large-scale experiments (see test A7 by *Dette et al.*, [2002]). We note that the growth of the incident wave energy in the field generally corresponds to an increase in the value of Ω . In contrast, the beach face erosion shown in Fig. 4 corresponds to a decrease in Ω although the wave energy, which is proportional to H_s^2 , has been kept constant.

Wave climate E (Fig. 5) corresponds to a Dean number $\Omega = 3.7$ in the upper part of the intermediate range. As it evolves, the beach slope becomes steeper as sediment is transported onshore to the berm. The berm is clearly nourished. This is typical of beach profile reconstruction by fair weather waves following erosion by a strong storm [*King, 1972; Sonu and James, 1973; Certain and Barusseau, 2005*].

In the case of climate B2 (Fig. 6), the bar on the initial profile migrates onshore as a dune propagation. During migration it develops an asymmetric shape with a steeper slope shoreward. The bar sand eventually fills the trough to generate a perched terrace similar to that of case C. Onshore bar migration has been widely observed in nature, documented and discussed [e.g. *Trowbridge and Young, 1989; Gallagher et al., 1998; Ruessink et al., 2007*].

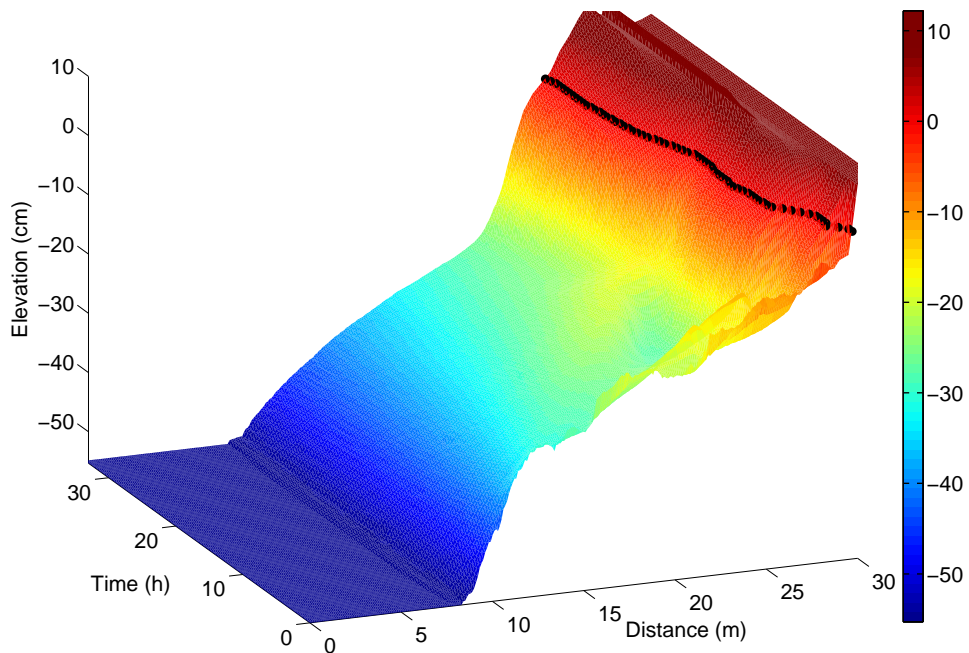


Figure 5. Beach profile changes. Bar formation, onshore migration and beach face accretion for climate E ($\Omega = 3.7$). The bold black symbols represent the shoreline position.

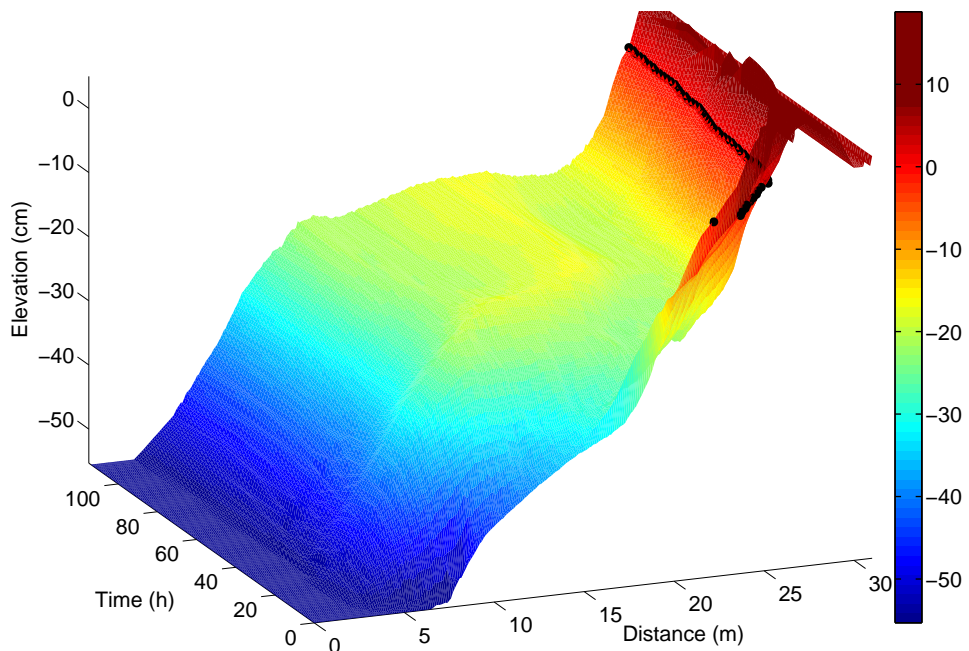


Figure 4. Beach profile changes. Terrace formation and beach face erosion for climate C ($\Omega = 2.5$). The bold black symbols represent the shoreline position.

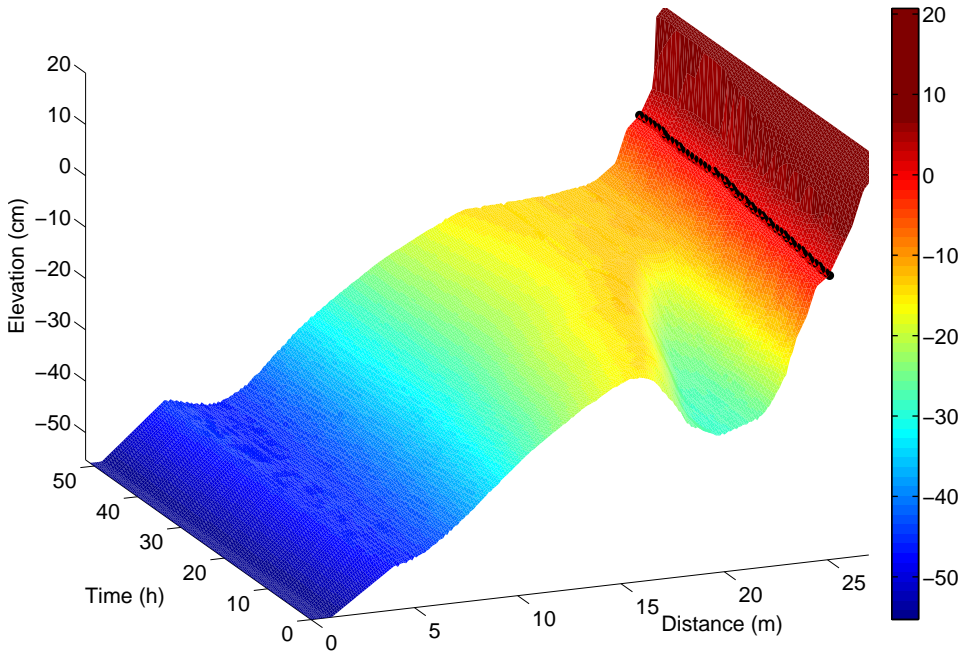


Figure 6. Beach profile changes. Onshore bar migration for climate B2 ($\Omega = 2.5$). The bold black symbols represent the shoreline position.

Fig. 7 presents the initial (dashed) and final (solid) beach profiles for experiments B1, B2, C, D, E and F given in Table 1. It is worth noting that the Ω value alone does not determine whether upper shoreface of profiles are eroding or accreting. Nor does it in combination with the offshore wave steepness H_s/L_0 , with L_0 being the offshore wavelength at the wave-maker [Dette *et al.*, 2002]. In experiments B1 and B2, the same wave forcing was imposed on two different initial profiles. This results in similar terrace shapes. Nonetheless B1 produces less shoreface accretion while B2 produces less shoreface erosion. This is due to the fact that the initial conditions in tests B1 and B2 differ strongly. However, it can be observed that B1, B2 and C ($\Omega = 2.5$) lead to beach face erosion. No back-shore is noticed and the dune is close to the shoreline. This highlights the fact that steep aerial beach profiles are probably a feature of erosional profiles. In contrast, climates D, E and F ($\Omega \approx 3.7$) produce a steeper mean profile that promotes beach face accretion. This is a striking result since one would at first guess think that the higher the Dean number the milder the beach slope. However, one should recall that in Wright and Short [1984] analysis this trend applies for the three states of their classification. A reflective beach has a steeper slope than an intermediate

beach which in turn has a steeper mean slope than a dissipative one. The Wright and Short [1984] classification does not give any refined comparison of beach slopes within the intermediate state. We also note a berm formation for $\Omega \simeq 3.7$. From a large set of field data, Ortega-Sánchez *et al.* [2008] concluded that a beach berm is mostly found under mean or short wave periods. For a given wave height in our experiments, a larger Ω values corresponds to a smaller wave period.

The rate of change of the beach is evaluated by computing a mean velocity of bottom profile variation defined as:

$$V_m(t) = \frac{1}{l_p} \int_{x_c}^{x_p} \left| \frac{\partial h}{\partial t} \right| dx, \quad (12)$$

where l_p is the profile length from the cross-shore position x_c of the closure depth $h_c = 4 H_s$ to the cross-shore position x_p of the most offshore point on the dune that does not change during an experiment (Fig. 1). The velocity of the shoreline is also computed as:

$$V_s(t) = \frac{dx_s}{dt}, \quad (13)$$

where x_s is the shoreline abscissa. $V_s \leq 0$ indicates seaward displacement whereas $V_s \geq 0$ corresponds to shoreward displacement. Examples of V_m and V_s varia-

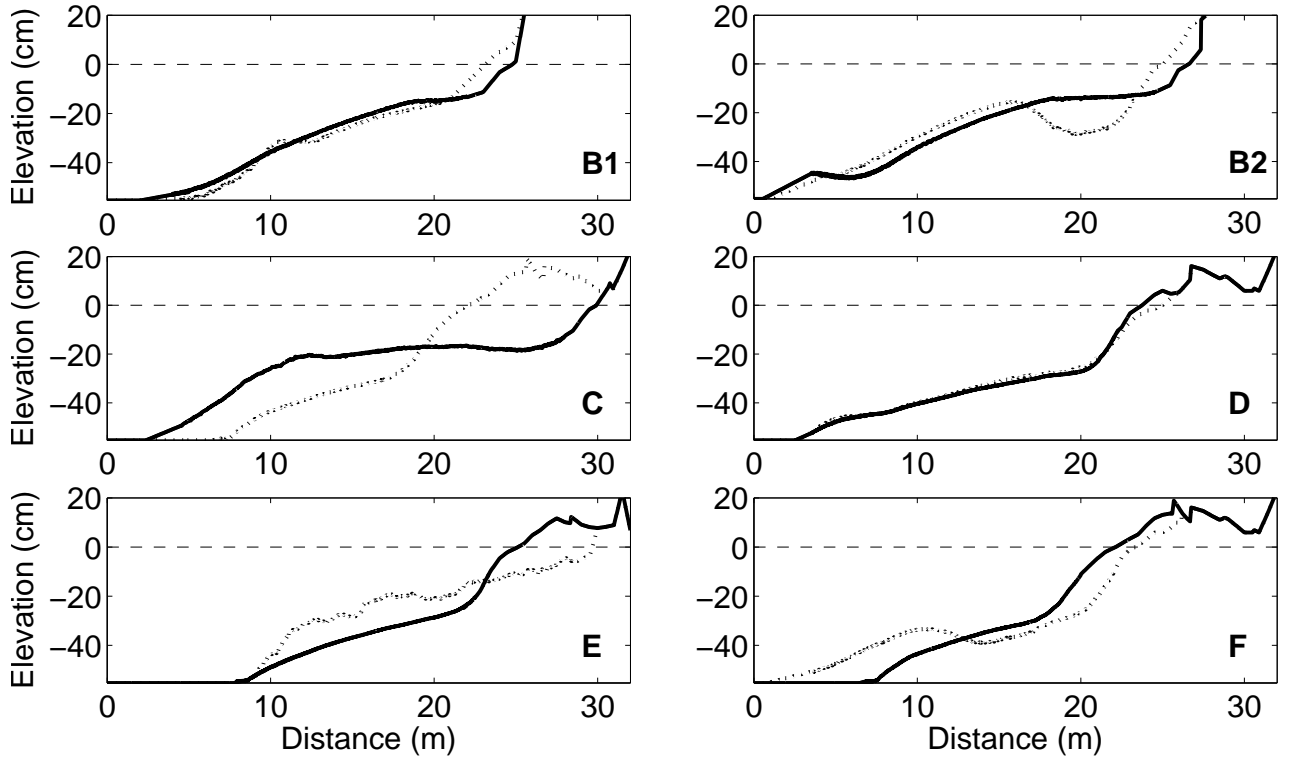


Figure 7. Initial (···) and final (—) beach profiles for the wave climates given in Table 1. B1, B2 and C ($\Omega = 2.5$), D ($\Omega = 3.6$), E and F ($\Omega = 3.7$)

tions with time are shown in Fig. 10. The change at the bottom is generally rapid ($V_m \sim 10 \text{ mm h}^{-1}$) just after a new wave climate is initiated ($0 \leq t < 2 \text{ h}$). If the wave conditions are very different compared to those that have produced the initial profile, several hours may elapse before a new general shape is observed. For climate C for instance, V_m remained higher than 5 mm h^{-1} for the first 20 hours, which corresponds to the formation of the terrace shown in Fig. 4. Similarly the shoreline velocity V_s also drops from 100 cm h^{-1} to a few cm h^{-1} in 30 hours. Once the general shape is reached, V_m decreases to less than 2 mm h^{-1} . This signifies slow erosion of the foreshore and an increase in the terrace length. It is worth noting that an experimental time of 30 hours up-scales to about 4 days in nature. Constant wave conditions for such a long time are rare in nature. The variation velocity V_m never decreases to zero. The small values of V_m observed after long experimental runs may correspond to small oscillations of the beach profile around the equilibrium state. These may be due to sediment size sorting along the profile and vertical size segregation within the bed. These slow phenomena induce small cross-shore variations in the sediment settling velocities and very long-term and slow changes in the beach.

The distance between the initial and the equilibrium profiles may be characterized by the averaged distance Δ defined as:

$$\Delta = \frac{1}{l_p} \int_{x_c}^{x_p} |\Delta h| \, dx, \quad (14)$$

where Δh is the difference between initial and final water depth. As shown in Fig. 11, the duration to reach an equilibrium state is well correlated to the distance from the initial to the final bottom profile. The trend does not depend on the wave height which implicitly enters the computation of Δ through the closure depth. The increase rate of T_{eq} with Δ is not uniform and presents an asymptotic behavior. For large Δ values, increasing Δ also increases V_m at the beginning of the experiment and consequently does not increase much T_{eq} .

As a general conclusion, a profile is deemed to be at equilibrium when $V_m \approx 2 \text{ mm h}^{-1}$. This criterion is applied to sort out the equilibrium states of our flume experiments. These equilibrium states are discussed with respect to the values of the dimensionless numbers.

3.2. Equilibrium profile morphologies

The equilibrium beach profiles for all the wave climates listed in Table 1 are plotted in Figs. 8 and 9.

Wave climate forcing A with $\Omega = 0.7$ (Fig. 8) is weak ($H_s = 3 \text{ cm}$) and the closure depth evaluated as $4 H_s \simeq 12 \text{ cm}$ is close to the beach face. Hence only the upper beach is re-shaped while the rest is a relict due to previous wave climates. A close-up of the active

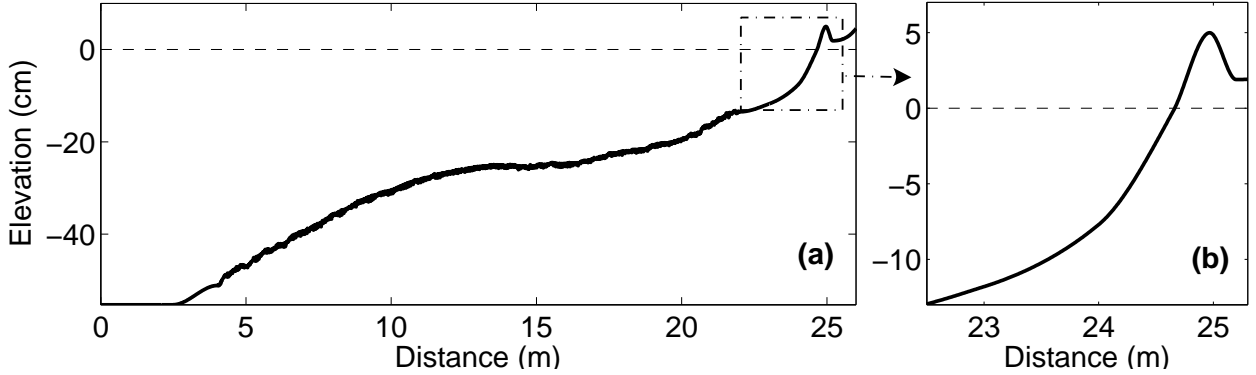


Figure 8. Equilibrium beach profile for wave climate A ($\Omega = 0.7$ see Table 1). (a) entire beach profile; (b) close-up from the closure depth to the top of the berm.

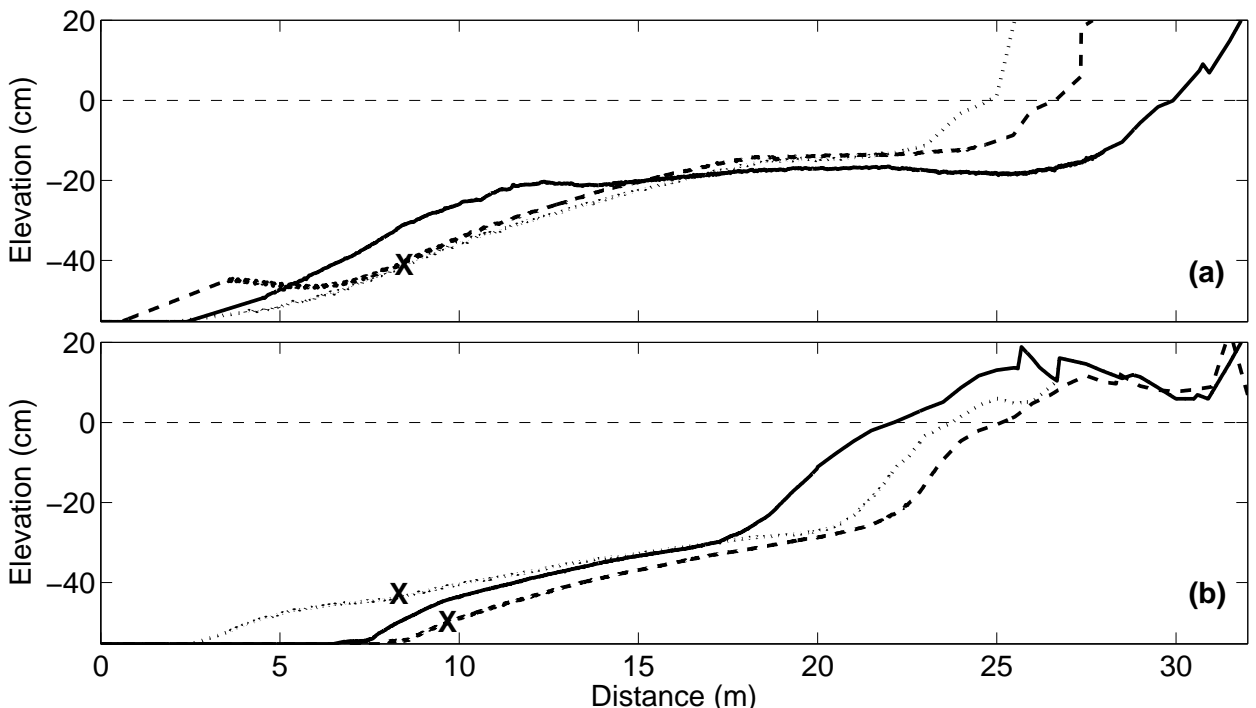


Figure 9. Equilibrium beach profiles for the wave climates given in Table 1. (a) B1 (· · ·), B2 (— · —) and C (—); $\Omega = 2.5$ and (b) D (· · ·); $\Omega = 3.6$; E (— · —) and F (—); $\Omega = 3.7$. Symbols **X** indicate the closure depths observed during profile formation.

part is given in Fig. 8. The beach face is steep with $m \sim 1/7$. This is typical of reflective profiles as defined by *Wright and Short* [1984]. This is also substantiated by computing the reflection coefficient. The surf parameter has a value of $\xi \simeq 2.1$, which yields a strong reflection coefficient of roughly 45% [*Mei*, 1992].

We now present 2 series of experiments in the intermediate Dean number range: 1 to 5. First of all, three wave climates with $\Omega = 2.5$ (Fig. 9a) associated with three beach profiles that are very similar and that display a terrace between the beach face and the lower shoreface. The terraces are at a depth $h \sim 1.1 \times H_s$ with mean slopes of less than 1/200. These experimental runs tend to show that the lower bound of β in (3) is the more appropriate as pointed out by *Bernabeu et*

al. [2003]. The terraces force a large surf zone of spilling breakers. At the scale of the wavelength (3 m on the terrace) the beach faces are characterized by a steep slope ($m \sim 1/10$) with associated surf parameters ξ between 0.76 and 0.94, which indicates beach face reflections of roughly 10 %. The shoaling sections, which coincide with the lower shorefaces, have a slope of about 1/50 that yield surf parameters between 0.15 and 0.19. These are the lowest values obtained in our experiments. It hence appears that these profiles are a combination of a surf zone dissipative profile section and a reflective beach face.

A second series of experiments with $\Omega \approx 3.7$ has been selected and plotted in Fig. 9b. These profiles are characterized by a break point very close to the shoreline and located in the lower part of the beach

face. These beach faces at the scale of the wavelength (roughly 3.5 m at the toe of the beach face) have slopes similar to the previous $\Omega = 2.5$ cases, that is $m \sim 1/10$. The surf parameter computed with these slopes ranges between 0.53 and 0.62, which indicates very small reflection coefficients. This series of profiles also shows offshore shoaling sections ($2 H_s \leq h \leq h_0$) that have a mild slope ($m \sim 1/25$). For this slope the surf zone parameter is even smaller, at about 0.2. Although the overall mean beach slope for the $\Omega \approx 3.7$ cases is steep, they fall in the dissipative category with regard to the surf similarity parameter.

In the intermediate range explored here, the profiles show combined reflective/dissipative profiles. The associated hydrodynamic characteristics leading to these morphologies are explored in the next section.

4. Hydrodynamics on equilibrium profiles

The wave-forced hydrodynamics of beaches is a very complex topic and still of interest for coastal research. Its combination with sediment transport raises this complexity a level higher. Indeed many competing sedi-

imentary effects take place on a beach and are usually categorized into destructive and constructive forces [Dean and Dalrymple, 2001]. However the most obvious element in this picture is the dissipation of the wave energy. Unbroken waves feed energy to the sediment phase by dissipation in the boundary layer while breaking waves will do so by both the boundary layer and the turbulence generated by breaking. Hence a first approach is to analyse how wave energy losses are distributed in the cross-shore direction. Energy loss in the surf zone is also known to generate an undertow current, which has long been recognized as a bar generation mechanism [King and Williams, 1949].

4.1. Wave transformation and currents

In the shoaling zone, wave amplitude prediction can be based on the wave energy flux balance. The same energy balance equations can, with ad-hoc sink terms, be used to predict wave height decay in the surf zone. These energy flux balance models can even properly predict wave modifications over non-monotonic bottom profiles such as wave reformation [Battjes and Janssen, 1978; Thornton and Guza, 1983; Ruessink et al. 2003]. The energy balance equation reads:

$$\frac{\partial(E C_g)}{\partial x} = - < \epsilon > = - [< \epsilon_b > + < \epsilon_f >] , \quad (15)$$

where E is the energy density, C_g is the group velocity, $< \epsilon_b >$ the dissipation by breaking per unit area, and $< \epsilon_f >$ the frictional dissipation. At natural sites, the frictional dissipation is negligible compared with the dominant wave breaking dissipation, except in very

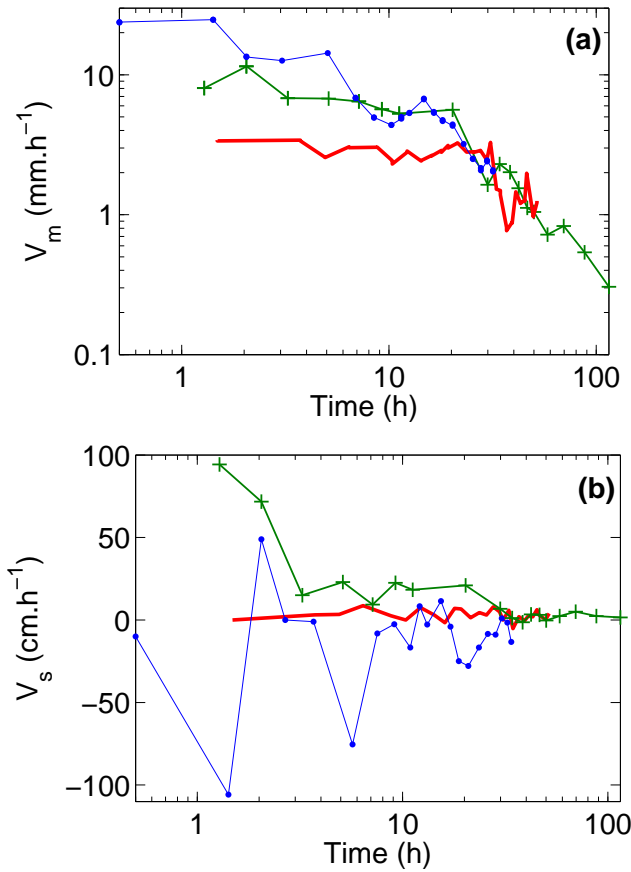


Figure 10. Bottom variation velocity for wave climates B2 (—), C (+) and E (·). (a): mean velocity of bottom profile variation V_m and (b): horizontal velocity of shoreline variation V_s .

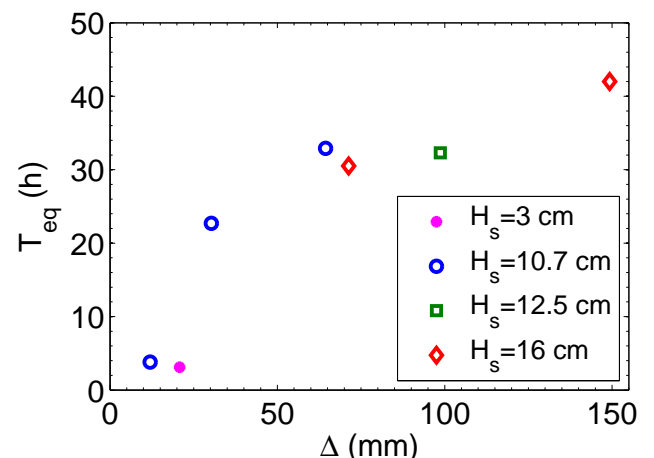


Figure 11. Time to reach equilibrium (T_{eq}) as a function of the distance from initial to equilibrium bottom profiles (Δ). The 7 wave climates given in Table 1 are sorted by their significant wave height (H_s).

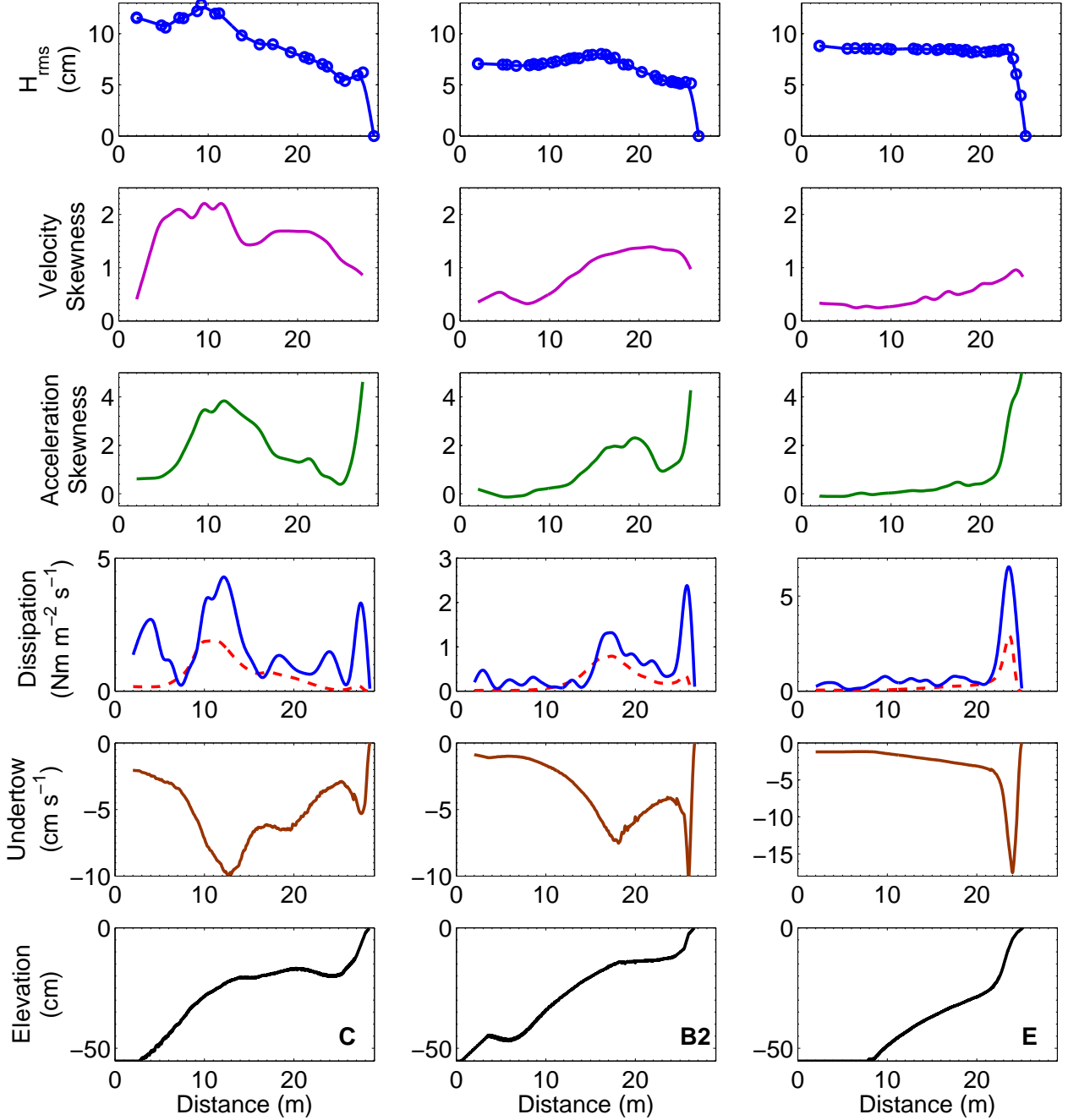


Figure 12. Hydrodynamic characterization of equilibrium states C, B2 and E with, from top to bottom: root mean square wave height, velocity skewness, acceleration skewness, measured dissipation $\langle \epsilon \rangle$ (solid) and modeled dissipation $\langle \epsilon_b \rangle$ (dashed), undertow and bottom profile.

shallow water. Assuming that the linear theory applies both in the shoaling and surf zones, E is written:

$$E = \frac{1}{8} \rho g H_{\text{rms}}^2, \quad (16)$$

and $C_g = \sqrt{gh}$ in shallow water. Substituting (16) in (15) gives a relationship to evaluate dissipation from measured wave height decay,

$$\langle \epsilon \rangle = -\frac{1}{8} \rho g^{3/2} \frac{\partial (H_{\text{rms}}^2 h^{1/2})}{\partial x}. \quad (17)$$

According to Thornton and Guza [1983], the bore dissipation can be evaluated as:

$$\langle \epsilon_b \rangle = -\frac{3\sqrt{\pi}}{16} \rho g \frac{B^3 H_{rms}^5}{T_p \gamma^2 h^3} \left[1 - \frac{1}{\left(1 + (H_{rms}/\gamma h)^2 \right)^{5/2}} \right], \quad (18)$$

where B and γ are breaker coefficients, respectively 1 and 0.42 for developed rollers. Relation (18) has been widely verified with field measurements. Relations (17) and (18) provide two independent methods to estimate wave dissipation in our experiments.

The undertow current partly induced by wave breaking is estimated from the time-averaged continuity equation [Dally and Brown, 1995; Cienfuegos et al., 2009]:

$$\frac{d}{dx} [U(h + \bar{\eta})] + \frac{dQ_W}{dx} + \frac{dQ_R}{dx} = 0, \quad (19)$$

where U is the depth-averaged mean current, $\bar{\eta}$ is the mean water level, Q_W is the volume flux per unit crest width associated with the organized wave motion, and Q_R is the fluid volume flux due to the roller. In the following we use the model developed by Dally and Brown, [1995] for undertow estimates. The bottom profile is often considered as the result of the balance between wave non-linearities that transports the sediment on-shore and the undertow current that distributes the sediment offshore. For long-waves, the wave velocity is proportional to the free surface elevation. The crest-to-trough asymmetry or velocity skewness may be estimated as:

$$Vel.Sk = \frac{\langle (\eta - \bar{\eta})^3 \rangle}{\langle (\eta - \bar{\eta})^2 \rangle^{3/2}} \quad (20)$$

where $\langle \rangle$ is the time averaging operator. The front-to-lee asymmetry can be characterized by the skewness of the acceleration or the third order moment of the Hilbert transform [Kennedy et al., 2000]. Here, the acceleration skewness is estimated as:

$$Acc.Sk = \frac{\langle (d\eta/dt - \langle d\eta/dt \rangle)^3 \rangle}{\langle (d\eta/dt - \langle d\eta/dt \rangle)^2 \rangle^{3/2}}. \quad (21)$$

4.2. Predicted hydrodynamics

In Fig. 12 we plot some of the hydrodynamic features corresponding to equilibrium beach profiles C, B2 and E. The root mean square wave height H_{rms} (top line panels) is used to compute wave energy dissipation per unit area and undertow current (lower-middle line panels). The cross-shore structure of the total dissipation $\langle \epsilon \rangle$ and of the bore dissipation $\langle \epsilon_b \rangle$ are comparable. The difference observed between the total dissipation (solid) and the model dissipation (dashed)

can be seen as the frictional dissipation $\langle \epsilon_f \rangle$. This is stronger near the shoreline. The bore dissipation model parameters were calibrated by Thornton and Guza [1983] with field measurements. Note however the good overall agreement between $\langle \epsilon \rangle$ and $\langle \epsilon_b \rangle$ in the present experiments even though we chose not to recalibrate the parameters. This gives extra strength to the experimental scaling chosen.

Terrace profiles C and B2, which have the same $\Omega = 2.5$, display similar tendencies. The waves begin to break slightly before the depth discontinuity (at $x = 10$ m for C; $x = 16$ m for B2) and break further up-beach after reforming as traveling waves on the terrace. This induces two main dissipation peaks. A lag is observed between the beginning of wave breaking and the maximum dissipation owing to the time required for the rollers to form. This is in line with previous analyses and models [Dally and Brown, 1995]. The cross-shore undertow distribution is clearly correlated to that of the dissipation. In these two cases the undertow current acts over the entire length of the step. With climate C ($H_s = 16$ cm, $T_p = 3$ s) the undertow can reach 10 cm s^{-1} at $x = 12.5$ m, where the dissipation is maximum. This value is of the same order of magnitude as the undertow estimations by Roelvink and Stive [1989] for waves with $H_s = 16$ cm and $T_p = 2$ s. In case E ($\Omega = 3.7$) wave breaking is limited to the upper beach, that is for $x \geq 23$ m. The corresponding dissipation peak induces a strong but very localized undertow (from $x = 22$ to 25 m) at which position the beach also shows a slope transition.

It is important to note that in all cases, the dissipation peaks are located at slope transitions in the beach profiles ($x = 12.5$ and 28 m for C; $x = 17.5$ and 26 m for B2; $x = 24$ m for E). Moreover the beach slope usually becomes milder as wave energy dissipation increases. It should also be emphasized that narrow beach face dissipation occurs for a basically similar steep beach face slope in all cases. Following Dean [1991], Wang and Kraus [2005] suggest that equilibrium beach profiles in the surf zone correspond to uniform volumetric wave energy dissipation. In the present experiments, relatively uniform wave energy dissipation is only observed for climate C ($x \simeq 15$ –25 m). Hence, the uniform surf zone dissipation does not appear to characterize all the equilibrium beach profiles. It appears to concern the beach profiles with a widely developed surf zone.

The acceleration skewness (upper-middle line panels) follows a similar trend as dissipation and undertow. It reaches maximum values where dissipation is also maximum. On one hand, this occurs in the outer surf zone ($x = 10$ to 15 m for case C and $x = 16$ to 20 m for case B2). It also strongly increases in the upper beach face in all three cases. Of course this indicates that zones where the acceleration skewness is strong, the velocity as well as the surface displacement are pitched forward with “saw-tooth” shapes [e.g. Elgar and Guza, 1985].

The velocity skewness does not show two maximum as the acceleration skewness does. Velocity skewness increases in the shoaling zones. It is a measure of how non-linear the waves are. Waves that reach large values of velocity skewness have sharp crests and broad troughs. A comparison of cases C and B2, that have the same $\Omega = 2.5$ value, clearly shows that both cases are similar in a similitude sense.

The present experiments show that the cross-shore dissipation structure and the wave non-linearities are clearly correlated to the beach profile type. Different wave climates characterized by the same Dean number induce similar hydrodynamic features.

5. Discussion and conclusions

In this work it is shown that careful scaling of beach morphology is possible with lightweight sediment. In particular the Froude, Shields and Rouse scaling is shown to be paramount. This was checked by comparing some beach profiles from our experiments with those of Duck and Lido beaches.

It is shown that equilibrium profiles can be obtained in flume experiments. Beach profiles reaching equilibrium are quantified by using a bottom variation velocity. It is even conjectured that while the initial beach profile condition determines the time needed to reach equilibrium it does not strongly influence the final shape.

This work also extends previous work on micro-tidal beach profile classification based on the Dean number. The classical classification is refined for $0.7 \leq \Omega \leq 3.7$, corresponding to the intermediate range as defined by *Wright and Short* [1984]. For Ω close to one, a typical reflective profile is obtained in accordance with all previous classifications. Long terraces are obtained at a depth of about $h_r = 1.1 H_s$ for the $\Omega = 2.5$ cases. These profiles consist of 3 sections, an offshore shoaling section with very little reflection, an essentially dissipative terrace and a beach face producing significant reflection. With $\Omega \approx 3.7$, the profiles are divided into 2 parts. The lower part ($h > 2 H_s$) has a mildly dissipative slope producing little reflection, while the beach face ($h < 2 H_s$) is steeper and produces slightly more reflection.

The Ω value alone does not determine whether profiles are eroding or accreting. Erosion or accretion depend not only on wave conditions but also on the initial profile and how “distant” it is from the equilibrium profile. For a given wave climate, knowledge of the initial and target equilibrium profiles certainly determines how dynamic the morphological variations are.

It is shown that the cross-shore dissipation and wave non-linearity patterns are similar for similar beach profiles, that is with the same Dean number. The velocity skewness increases in the shoaling zone and remains large in the surf zone. The acceleration skewness is very large in the breaking zone and on the upper beach

face. The dissipation peaks also coincide with bottom slope transition. More precisely, greater energy dissipation comes with milder bottom slope sections. This fits with the *Wright and Short*, [1984] classification. While the uniformity of volumetric wave energy dissipation for equilibrium beach profiles was widely accepted, in our experiments it is not characteristic of all the equilibrium profiles. It appears to concern only a limited region of the beach profiles with a widely developed surf zone.

The examination of the sediment transport along with the determination of wave non-linearities in transient states is left aside for future work. Boussinesq-type numerical models [*e.g.* *Cienfuegos et al.*, 2006; 2007] could also help for better understanding the coupling between hydrodynamics, sediment transport and morphodynamics.

In our experiments, very slow profile changes are identified. This needs to be further investigated. It may be due to very slow sediment segregation along the profile but also vertically in the bed. In general barred profiles are transients in our experiments (see also *Grasso et al.* [2009]). What we suspect is that the bars are shaped by subsiding wave conditions after storms and under such conditions they tend to migrate to the shore and eventually merge with the berm. However if the wave height decays very rapidly after the storm, the hydrodynamics may not be sufficient to set the sediment in motion on the bar. Beach profile changes resulting from a succession of different wave climates of defined durations is therefore an important issue.

Acknowledgments. This study was funded by the LITEAU program of the French Ministry of Ecology, the INSU (LEFE-IDAO and RELIEF-MODLIT), the EC INTERREG-IIIC program under project BEACHMED-e and the ECOS-Sud program with CONYCIT (contract C07U01). The authors acknowledge the use of Duck beach data provided by the Coastal and Hydraulics Laboratory of the US Army Corps of Engineers. The technical assistance of J.-M. Barnoud is gratefully acknowledged.

References

- Akouango, E. (1997), *Morphodynamique et dynamique sédimentaire dans le golfe du Lion. Contribution à l'étude de la zone côtière dans l'actuelle et le quaternaire récent*, PhD Thesis, Univ. de Perpignan.
- Baird, J. A. (1981), An energetics total load sediment transport model for a plane sloping beach, *J. Geophys. Res.*, 86(C11):10,938–10,954.
- Battjes, J. A. (1974), Surf similarity, *Proceedings 14th International Conference on Coastal Engineering*, ASCE, Copenhagen, Denmark, pp.466–480.
- Battjes, J. A., and Janssen, J. P. F. (1978), Energy Loss and Set-Up Due to Breaking of Random Waves, *Proceedings 16th International Conference on Coastal Engineering*, ASCE, Hamburg, Germany, pp.569–587.
- Bayram, A., M. Larson, H. C. Miller, N. C. Kraus (2001), Cross-shore distribution of longshore sediment transport: comparison between predictive formulas and field measurements, *Coastal Engineering*, 44:79–99.
- Bernabeu, A. M., R. Medina, and C. Vidal (2003), A morphological model of the beach profile integrating wave and tidal influence, *Marine Geology*, 197:95–116.
- Birkemeier, W. A., H. C. Miller, S. D. Wilhem, A. E. Dewall, and C. S. Gorbics (1985), A user's guide to the Coastal Engineering Research Center's (CERC's) Field Research Facility.,

- Instruction report CERC-85-1.*, U.S. Army Engineer Waterways Experiment Station.
- Black, K. P., R. M. Gorman, and K. R. Bryan (2002), Bars formed by horizontal diffusion of suspended sediment, *Coastal Engineering*, 47:53–75.
- Bowen, A. J. (1980), *The coastline of Canada*, Vol. 80-10, Geological Survey of Canada.
- Certain, R., and J.-P. Barusseau (2005), Conceptual modelling of sand bars morphodynamics for a microtidal beach (Sète, France), *Bull. Soc. Géol. Fr.*, 176(4):343–354.
- Certain, R., S. Meulé, V. Rey, and C. Pinazo (2005), Swell transformation on a microtidal barred-beach (Sète, France), *Journal of Marine Systems*, 38:19–34.
- Cienfuegos, R., E. Barthélémy, and P. Bonneton (2006), A fourth-order compact finite volume scheme for fully nonlinear and weakly dispersive Boussinesq-type equations. Part I: model development and analysis, *Int. J. Num. Meth. Fluids*, 51(11):1217–1253.
- Cienfuegos, R., E. Barthélémy, and P. Bonneton (2007), A fourth-order compact finite volume scheme for fully nonlinear and weakly dispersive Boussinesq-type equations. Part II: boundary conditions and validation, *Int. J. Num. Meth. Fluids*, 53(9):1423–1455.
- Cienfuegos, R., E. Barthélémy, and P. Bonneton (2009), A wave-breaking model for Boussinesq-type equations including roller effects in the mass conservation equation, *Journal of Waterw., Port, Coastal, and Oc. Eng.*, accepted.
- da Silva, P. A., A. Temperville, and F. Seabra Santos (2006), Sand transport under combined current and wave conditions: A semi-unsteady, practical model, *Coastal Engineering*, 53:897–913.
- Dally, W. R., and C. A. Brown (1995), A modelling investigation of the breaking wave roller with application to cross-shore currents, *J. Geophys. Res.*, 100(C2):24,873–24,883.
- Dally, W. R. (1987), Longshore bar formation, In *Coastal Sediments'87*, ASCE, New Orleans, Louisiana, USA, pp.71–86.
- Dean, R. G. (1973), Heuristic models of sand transport in the surf zone, in *Proc. Conf. Engineering Dynamics in the Surf Zone*, Sydney, Australia, pp.208–214,
- Dean, R. G. (1977), Equilibrium beach profiles: U.S. Atlantic and Gulf coasts, *Ocean engineering report no. 12*, Dept of Civil Engineering, Univ. of Delaware.
- Dean, R. G. (1991), Equilibrium beach profiles: characteristics and applications, *J. Coastal Res.*, 7(1):53–84.
- Dean, R. G., and R. A. Dalrymple (2001), *Coastal Processes with Engineering Applications*, Cambridge University Press, ISBN 0521495350.
- Dette, H., and K. Uliczka (1987), Prototype investigation on time-dependent dune recession and beach erosion, In *Coastal Sediments'87*, ASCE, New Orleans, Louisiana, USA, pp.1430–1444.
- Dette, H., M. Larson, J. Murphy, J. Newe, K. Peter, A. Reniers, and H. Steetzel (2002) Application of prototype flume tests for beach nourishment assessment. *Coastal Engineering*, 47:137–177.
- Dronkers, J. (2005), *Dynamics of Coastal Systems, Advanced Series on Ocean Engineering* (Vol. 25), World Scientific.
- Elgar, S., E. L. Gallagher, and R. T. Guza (2001), Nearshore sand bar migration *J. Geophys. Res.*, 106(C6):11,623–11,627.
- Elgar, S., and R. T. Guza (1985), Observations of bispectra of shoaling surface gravity waves. *J. Fluid Mech.*, 161:425448.
- Foster, D. L., A. J. Bowen, R. A. Holman, and P. Natoo (2006), Field evidence of pressure gradient induced incipient motion *J. Geophys. Res.*, 111(C5):C05004, 1–8.
- Gallagher, E. L., S. Elgar, and R. T. Guza (1998), Observation of sand bar evolution on a natural beach, *J. Geophys. Res.*, 193(C2):3203–3215.
- Goda, Y. (1985), *Random Seas and Design of Maritime Structures*, University of Tokyo Press.
- Günaydin, K., and M. S. Kabdasli (2003), Characteristics of coastal erosion geometry under regular and irregular waves, *Ocean Engineering*, 30:1579–1593.
- Grasso, F., H. Michallet, and E. Barthélémy (2007), Infragravity waves in mobile-bed laboratory experiments, In *Coastal Sediments'07*, ASCE, New Orleans, Louisiana, USA, pp.235–247.
- Grasso, F., H. Michallet, R. Certain, and E. Barthélémy (2009), Experimental flume simulation of sandbar dynamics, *J. of Coastal Res.*, SI56:54–58.
- Guannel, G., H. T. Ozkan-Haller, M. C. Haller, and J. T. Kirby (2007), Influence of velocity moments on sand bar movement during crosstex, In *Coastal Sediments'07*, ASCE, New Orleans, Louisiana, USA.
- Hallermeier, R. J. (1978), Uses for a calculated limit depth to beach erosion, *Proceedings 16th International Conference on Coastal Engineering*, ASCE, Hamburg, Germany, pp.1493–1512.
- Henderson, S. M., J. S. Allen, and P. A. Newberger (2004), Nearshore sandbar migration by an eddy-diffusive boundary layer model, *J. Geophys. Res.*, 109:C06024.
- Henriquez, M., A. J. H. M. Reniers, B. G. Ruessink, M. J. F. Stive, T. P. Stanton and D. L. Foster (2008), On the scaling of sediment transport in the nearshore, In *COASTLAB 2008 Conference*, Bari, Italy.
- Hoefel, F., and S. Elgar (2003), Wave-induced sediment transport and sandbar migration, *Science*, 299:1885.
- Holman, H., and E. Sallenger (1993), Sand bar generation: A discussion of the Duck experiment series, *J. Coastal Res.*, SI15:76–95..
- Hooyng, C. (2008), *Erosive and accretive coastal response*, M.Sc. Thesis, WL Delft Hydraulics.
- Hsu, T.-J., S. Elgar, and R. T. Guza (2006), Wave-induced sediment transport and onshore sandbar migration, *Coastal Engineering*, 53:817–824.
- Hughes, S. A. (1995), *Physical models and laboratory techniques in coastal engineering, Advanced Series on Ocean Engineering* (Vol. 7), World Scientific.
- Inman, D. L., M. H. S. Elwany, and S. A. Jenkins (1993), Shoreline and bar-berm profiles on ocean beaches, *J. Geophys. Res.*, 98(C10):18,181–18,199.
- Kamalinezhad, M., H. Michallet, and E. Barthélémy (2004), Equilibre morphologique de barres de déferlement: expériences. In *VIIIe Journées Nationales Génie Civil - Génie Côtier*, Compiègne, France.
- Kamalinezhad, M. (2004), *Plages en équilibre morphologique et hydrodynamique associée*, PhD Thesis, Institut National Polytechnique de Grenoble, France.
- Kamphuis, J. W. (1985), On understanding scale effect in coastal mobile bed models, *Physical modelling in coastal engineering*, R.A. Dalrymple, ed., Rotterdam, A.A. Balkema, 141–162.
- Kennedy, A. B., Q. Chen, J. T. Kirby, and R. A. Dalrymple (2000), Boussinesq modelling of wave transformation, breaking and runup. I: 1D, *J. Waterw. Port Coastal and Oc. Eng.*, 126(1):39–48.
- King, C. A. M., and W. E. Williams (1949), The formation and movement of sand bars by wave action, *Geographical Journal*, 113:70–85.
- King, C. A. M. (1972), *Beaches and coasts*, Edward Arnold, London.
- Komar, P. D. (1998), *Beach Processes and Sedimentation*, Prentice Hall, New Jersey, USA.
- Larson, M., and N. C. Kraus (1994), Temporal and spatial scales of beach profile change, Duck, North Carolina, *Marine Geology*, 117:75–94.
- Lee, G.-h., R. J. Nicholls, and W. A. Birkemeier (1998), Storm-driven variability of the beach-nearshore profile at Duck, North Carolina, USA, 1981–1991, *Marine Geology*, 148(3–4):163–177.
- Lippmann, T. C., and Holman, R. A. (1990), The spatial and temporal variability of sand bar morphology, *J. Geophys. Res.*, 95(C7):11,575–11,590.
- Masselink, G., and A. D. Short (1993), The effect of tide range on beach morphodynamics and morphology: A conceptual beach model, *J. Coastal Res.*, 9(3):785–800.
- Mei, C. C. (1992), *The applied dynamics of ocean surface waves* (2 ed.), Advanced Series on Ocean Engineering (Vol. 1), World Scientific.
- Michallet, H., F. Grasso, and E. Barthélémy (2007), Long waves and beach profiles evolutions, *J. Coastal Res.*, SI50:221–225.
- Miller, J. K., and R. G. Dean (2004), A simple new shoreline change model, *Coastal Engineering*, 51:531–556.
- Moore, B. D. (1982), Beach profile evolution in response to changes in water level and wave height, *MCE thesis, Department of Civil Engineering, University of Delaware*.
- Nielsen, P. (1992), *Coastal bottom boundary layers and sediment transport*, Advanced Series on Ocean Engineering (Vol. 4), World Scientific.

- Ortega-Sánchez, M., S. Fachin, F. Sancho, and M. A. Losada (2008), Relation between beachface morphology and wave climate at Trafalgar beach (Cadiz, Spain), *Geomorphology*, 99:171–185.
- Plant, N. G., B. G. Ruessink, and K. M. Wijnberg (2001), Morphologic properties derived from a simple cross-shore sediment transport model, *J. Geophys. Res.*, 106(C1):945–958.
- Ribas Prats, F. (2003), *On the growth of nearshore sand bars as instability processes of equilibrium beach states*, PhD Thesis, Universitat Politècnica de Catalunya, Spain.
- Ruessink, B. G., and A. Kroon (1994), The behaviour of a multiple bar system in the nearshore zone of Terschelling, the Netherlands: 1965–1993, *Marine Geology*, 121:187–197.
- Ruessink, B. G., D. J. R. Walstra, and H. N. Southgate (2003), Calibration and verification of a parametric wave model on barred beaches, *Coastal Engineering*, 48:139–149.
- Ruessink, B. G., Y. Kuriyama, A. J. H. M. Reniers, J. A. Roelvink, and D. J. R. Walstra (2007), Modeling cross-shore sandbar behavior on the timescale of weeks, *J. Geophys. Res.*, 112:F03010.
- Roelvink, J. A., and M. J. F. Stive (1989), Bar-generating cross-shore flow mechanisms on a beach, *J. Geophys. Res.*, 94(C4):4785–4800.
- Sonu, C. J., and W. R. James (1973), A Markov model for beach profile changes, *J. Geophys. Res.*, 78:1462–1471.
- Soulsby, R. L. (1997), *Dynamics of marine sands*, Thomas Telford, London.
- Swart, D. H. (1974), A schematization of onshore-offshore transport, *Proceedings 14th International Conference on Coastal Engineering, ASCE*, pp.884–900.
- Thornton, E. B., and R. T. Guza (1983), Transformation of wave height distribution, *J. Geophys. Res.*, 88(C10):5925–5938.
- Thornton, E. B., R. T. Humiston, and W. A. Birkemeier (1996), Bar-trough generation on a natural beach, *J. Geophys. Res.*, 101:12,097–12,110.
- Trowbridge, J., and D. Young, (1989), Sand transport by unbroken water waves under sheet flow conditions, *J. Geophys. Res.*, 94:10,971–10,991.
- Unal, N. E., and M. Bayazit (1998), Incipient motion of coarse particles on a slope by regular or irregular waves, *J. Waterw., Port, Coastal, and Oc. Eng.*, 124(1):32–35.
- van Enckevort, I. M. J., and B. G. Ruessink (2001), Effect of hydrodynamics and bathymetry on video estimates of nearshore sandbar position, *J. Geophys. Res.*, 106(C8):16,969–16,979.
- Wang, T., and N. C. Kraus (2005), Beach profile equilibrium and patterns of wave decay and energy dissipation across the surf zone elucidated in a large-scale laboratory experiment, *J. Coastal Res.*, 21(3):522–534.
- Wright, L. D., and A. D. Short (1984), Morphodynamic variability of surf zones and beaches: a synthesis, *Marine Geology*, 56:93–118.
-
- F. Grasso, LEGI, BP53, 38041 Grenoble Cedex, France.
(florent.grasso@hmg.inpg.fr)
- H. Michallet, LEGI, BP53, 38041 Grenoble Cedex, France.
(herve.michallet@hmg.inpg.fr)
- E. Barthélémy, LEGI, BP53, 38041 Grenoble Cedex, France.
(eric.barthelemy@hmg.inpg.fr)
- R. Certain, IMAGE EA4218, 52 av. Alduy, 66000 Perpignan, France. (certain@univ-perp.fr)



Methodology of seasonal morphological modelisation for nourishment strategies on a Mediterranean beach

Philippe Larroudé

Laboratoire des Ecoulements Géophysiques et Industriels, LEGI, BP 53, Grenoble, France

ARTICLE INFO

Keywords:

Large-scale features
Near shore region
Morphological evolution
Sediment transport
Nourishment
Numerical simulation 2DH and Multi1DH model

ABSTRACT

A modified 2DH morphodynamical model was employed to simulate the evolution of large-scale features with major implications for beach nourishment. The study was focused on modelling the evolution of material artificially placed in different parts of the profile, extracting or adding material to the natural bars, and quantifying how the profile responds to different wave climates and nourishment placements. The simulated results were compared with field data from a Mediterranean beach.

© 2008 Elsevier Ltd. All rights reserved.

1. Introduction

Examples of nourishment tests carried out on the near shore zone are few and far between in relevant literature, compared to the number undertaken directly on the beach. SAFE, the latest European project within the MAST program, acknowledges the absence of reference documents on this question, although such a technique could presumably constitute a less costly alternative (Hamm et al., 2002).

The use of offshore bars to fight beach erosion, dating back to the 90s, was based on the fact that they represented a substantial reservoir of sediments. That theory turned out to be irrelevant, as beach nourishment requires coarser grain sizes. However, the essential role these bars can play in wave mitigation was shown by recent studies. Hence, working on reinforcing existing bars or even adding extra bars is a convincing approach, for they constitute a line of defence with no visual impact and are therefore environment-friendly. The method offers the added benefit of tapping abundant fine sands which are easily available offshore, to build up the bars.

In addition, adequate depths in the inner shelf area would facilitate dredging and discharge operations and as the material reclaimed is usually clean, it can therefore be used directly without any processing. The core of the additional bar could also be made from marine muds, which are equally easily available. All these assumptions should, of course, be systematically checked, the purpose of the exercise being to assess, through mid-term bathymetric evolution simulation, the consequences of the implementation of offshore bar nourishment and define the best location.

The understanding of these processes needs, at this time, *in situ* data but also the development of mathematical models and numerical codes. Hence, following the work of De Vriend (1987) and De Vriend and Stive (1987), we tried to improve the classic quasi-steady procedure. The objectives of this work will be therefore to mode and to simulate processes of sedimentary transport on sandy beaches with varied weather conditions in the medium term time scale (from a few days to a few months).

2. Procedure and description of the beach

Certain and Barusseau (2006) showed that the morphodynamic evolution of offshore bars in a microtidal environment and bimodal moderate wave regime follows two different conceptual models, the main one being a seasonal pattern in line with the observed cycle of hydrodynamic conditions.

The morphological evolution in the near shore region, including its large-scale features, was first investigated using a combination of a commercial 2DH model and a Multi1DH model (Camenen and Larroudé, 2003a,b). Simulation of the wave-driven currents was carried out with Telemac, a finite-volume elements model, and the Sisyphe sand transport module served to compute sediment transport rates and bed evolution. Since the sediment transport in the surf zone is mainly controlled by undertow, an undertow model (based on Svendsen, 1984) was added to account for that process.

These models were used in the framework of a simulated meteorological cycle describing the seasonal evolution of hydrodynamic factors. Results from monthly 2DH evolution simulations showed a perfect fit with field data obtained on the “plage de la Corniche” in Sète (Southern France) (the site is presented in Certain, 2002).

E-mail address: larroude@hmg.inpg.fr

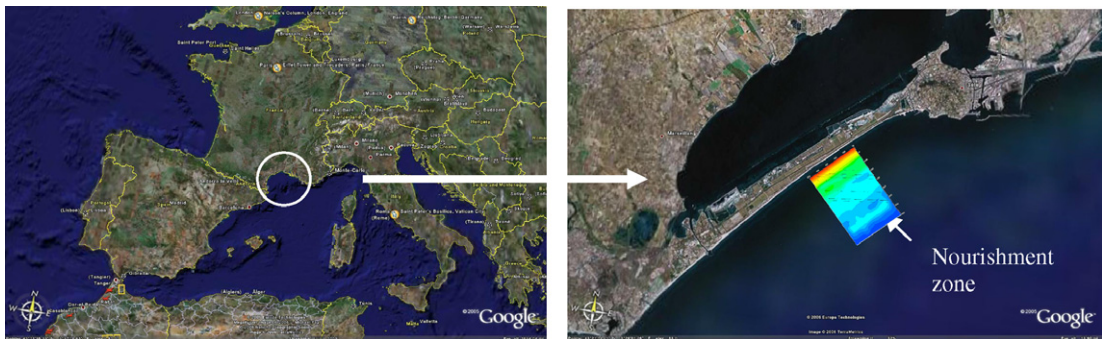


Fig. 1. Localisation of the “plage de la Corniche”, France, Mediterranean sea coast, and zoom on the study area with the creation of an artificial offshore bar.

Morpho-hydrodynamic feedback of a bar having undergone reinforcement is also examined (see Fig. 1).

3. The codes

The sedimentary evolution was modelled under the action of the oblique incident waves and was coupled with different numerical tools dedicated to the other process involved in the near shore zone. We can mention the following modules:

- a wave module takes into account the surge energy dissipation (hyperbolic equation of extended Berkhoff), ([LNHE](#), [Artemis](#), [2002](#)). The Artemis code (Agitation and Refraction with Telemac2d on a Mild Slope) solves Berkhoff equation taken from Navier–Stokes equations with some other hypothesis (little camber of the surface wave, little slope...). The main results are, for every node of the mesh, the height, the phase and the incidence of the waves. Artemis can take into account the reflection and the refraction of waves on an obstacle, the bottom friction and the breakers. One of the difficulties with Artemis is that a fine mesh must be used to have good results whereas Telemac2d do not need such a fine mesh;
- a module that calculates currents induced means by the surge of the waves, from the concept of radiation constraints obtained according to the module of waves, ([LNHE](#), [Telemac2d](#), [2002](#)). Telemac2d is designed to simulate the free surface flow of water in coastal areas or in rivers. This code solves Barré Saint–Venant equations taken from Navier–Stokes equations vertically averaged. Then, main results are, for every node of the mesh, the water depth and the velocity averaged over the depth. Telemac2d is able to represent the following physical phenomena: propagation of long periodic waves, including non-linear effects, wetting and drying of intertidal zone, bed friction, turbulence;
- a sedimentary module integrating the combined actions of the waves and the wave currents (2D or 3D) on the transport of sediment, ([LNHE](#), [Sisyphe](#), [2002](#)). The Sisyphe code solves the bottom evolution equation which expresses the conservation of matter using directly a current field result file given by Telemac2d. Four of the most currently empirical or semi-empirical formulas are already integrated in Sisyphe (Peter–Meyer, Einstein–Brown, Engelund–Hansen and Bijkar formulas). We integrated two others which seem more appropriate to coastal sediment transport ([Bailard](#), [1981](#); [Dibajnia and Watanabe](#), [1992](#)). The main results are, for every node of the mesh, the bottom evolution and the solid transport. The equations of the three modules are detailed in [Hervouet](#) ([2007](#)). This methodology was tested and explained for morphodynamic simulations in [Falqués et al.](#) ([2008](#));
- a hydrodynamic simplified model (called Multi1DH) used the following assumptions: a random wave approach, in a 1DH

(cross-shore) direction. An offshore wave model (shoaling + bottom friction + wave asymmetry) was used with the break point estimation. The waves in the surf zone were modelled with the classic model of [Svendsen](#) ([1984](#)) with an undertow model (roller effect, [Svendsen](#), [1984](#); [Dally et al.](#), [1984](#)). As a long shore current model, we used the [Longuet Higgins's](#) model ([1970](#)). This model was already used and tested in [Camenen](#) and [Larroudé](#) ([2003b](#)).

4. Results

4.1. Comparison for validation

Firstly we set up a procedure to use the coupled codes Artemis–Telemac2d–Sisyphe and more particularly we improved the treatment of the boundary conditions in order to be able to work on fields of calculations close to the coastal zone and equivalents in dimension for the three codes. We also used the Multi1DH code for the medium term simulations. Both these models take into account the breaker zone of waves as presented in paragraph 3. On the other hand only the parametric model can represent the set up. This methodology of morphodynamic modelling for sandy beaches was already improved in terms of mesh, time step and convergence in [Camenen](#) ([2002](#)), [Larroudé and Camenon](#) ([2004](#)) and [Falqués et al.](#) ([2008](#)). These models were used for monthly simulations taking account the weather conditions. These weather conditions were drawn from the ground data for the period of November 2000 and were simplified in terms of height of swell, period of swell and direction by dividing the month into 9 significant periods (see Table 1). One can notice that using the average height of the swells during each simulation period attenuated the weather events this November.

We obtain a good adequacy between numerical bathymetries after one month and those raised on the ground (see Fig. 2).

We began simulations with a nourishing of the study zone at the beginning of November 2000 and we could compare the results

Table 1

Simplified weather data: November 2000 (θ angle in degree in the trigonometrically direction reverses compared to the normal with the beach)

Time	Hs (m)	Tp (s)	θ
0j à 1j 21 h	0.244	7.45	25.475
1j 21 h à 3j 12 h	1.703	7.92	27.861
3j 12 h à 7j 21 h	0.351	7.13	28.094
7j 21 h à 10j 9 h	1.787	6.76	6.065
10j 9 h à 18j 12 h	0.222	6.2	3.97
18j 12 h à 20j 3 h	1.358	6.78	14.9
20j 3 h à 24j 15 h	0.251	7.03	14.33
24j 15 h à 30j	1.259	6.27	-5

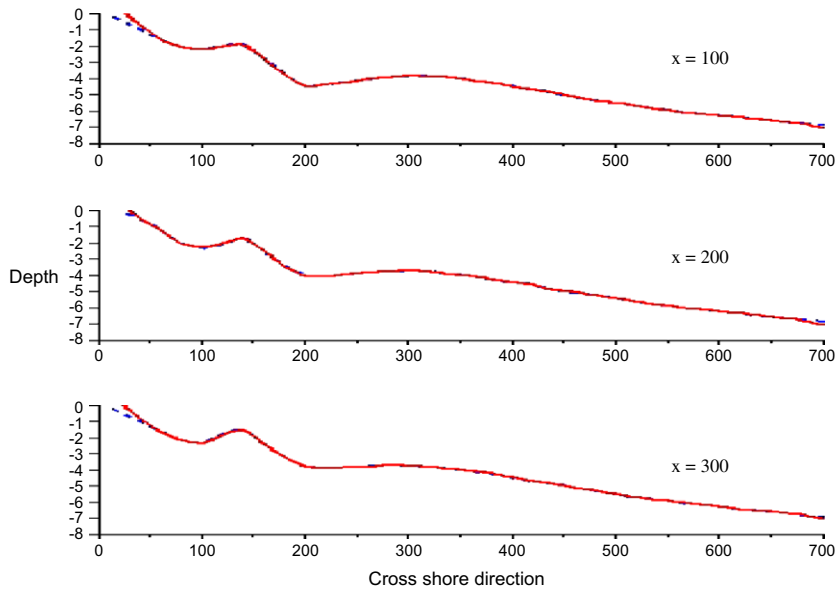


Fig. 2. Sea bed for three location on the beach at the 25 November 2000, comparison between *in situ* data and numerical simulation after one month using the 2DH model with the meteorological model.

obtained with model 2DH (waves, hydrodynamics and transport) and the simplified model Multi1DH.

Secondly, we regarded as basic state a profile of the bathymetry of November 16, 2000, the P5 profile with $X = 200$ m (longshore distance compared to the beginning of the study zone). This approach enabled us to more easily compare the models of calcula-

tion used by the various partners of the program. For these simulations we agreed to consider three cases of climatic conditions (see Table 2): Traditional Storm (TS), falling from Storm (FS) and Exceptional Storm (ES). All the simulations were carried out with the model Multi1DH and the results will be presented later. We also made some calculations with the chain of Artemis-Telemac2d-Sisyphus code.

In the case of FS, the swells do not have any effects on the internal and external bars. For TS simulations the swells erode the internal bar but do not seem to attack to a significant degree, the beach and the external bar. Only one longer-term erosion of the internal bar can be prejudicial for the protection of beach.

The case of the exceptional storms was used as a basis to present the differences obtained with the model Multi1DH between the different recharging option. The case, on the basic profile of

Table 2
Weather data simplified for the three cases of storm (θ angle in degree in the trigonometric direction reverses compared to the normal with the beach)

	Time (h)	Hs (m)	Tp (s)	θ
TS	24	1	6.5	0° and 20°
FS	24	2.5	7	0° and 20°
ES	24	4	10	0° and 20°

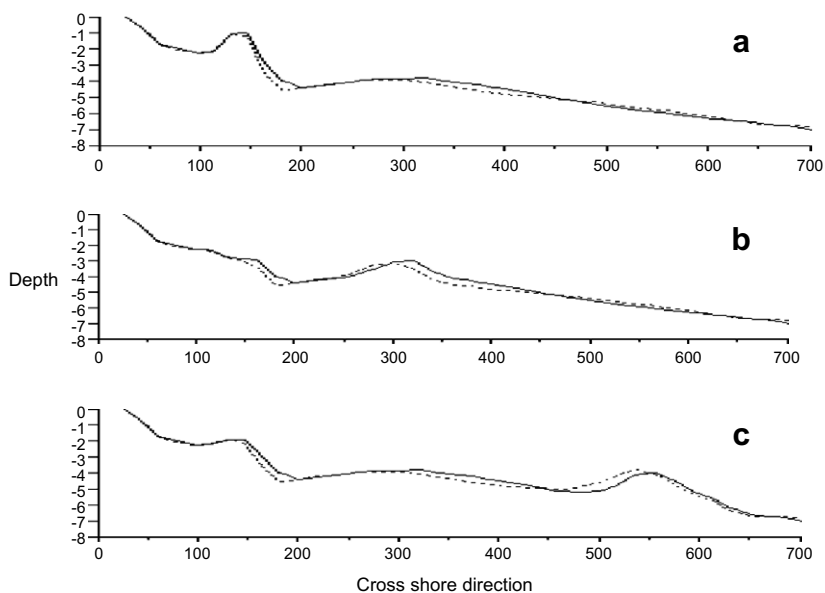


Fig. 3. Sea bed evolution on 24 h calculated with the Multi1DH model for three location of nourishment: (a) on the inner bar, (b) on the offshore bar and (c) with the creation of new bar offshore.

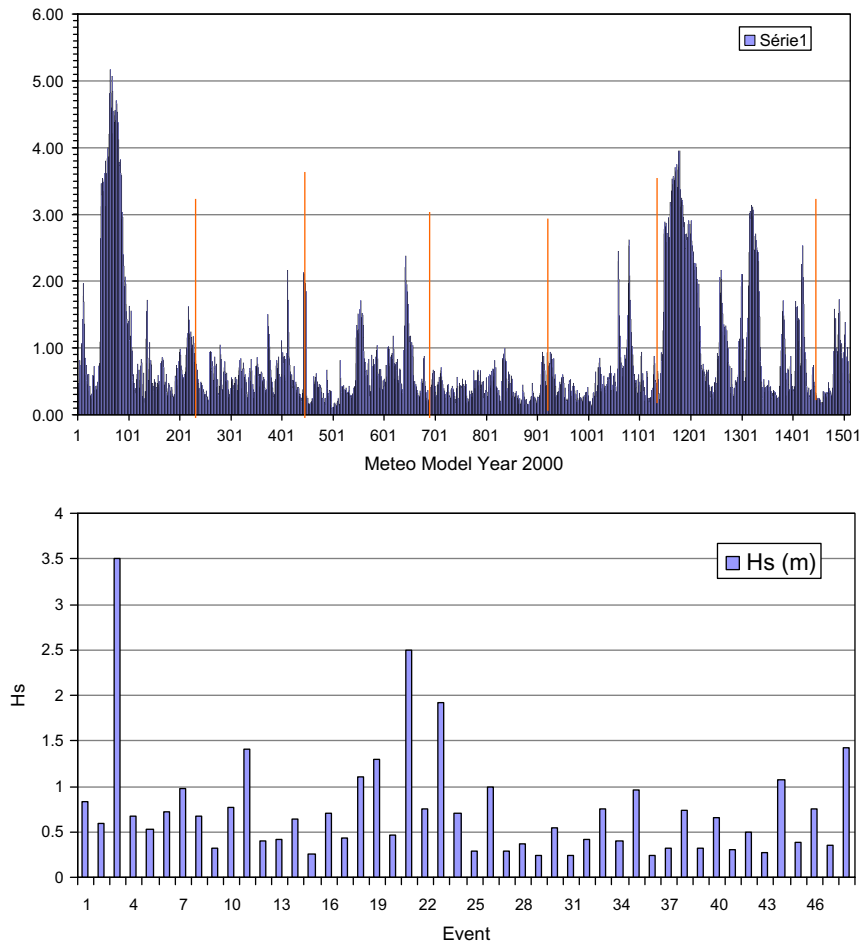


Fig. 4. The meteorological model is based on the data (Certain, 2002) collected on the “plage de la Corniche” in Sète during the year 2000.

November 16, 2000, shows us an erosion of the internal and external bars with a transport of these bars further offshore and thus one can consider a weakening of the protection of the beach (see

Fig. 3). The internal bar was eroded of approximately 10 m and the external bar of 40 m, the deposit offshore with a maximum of 25 m is very spread out.

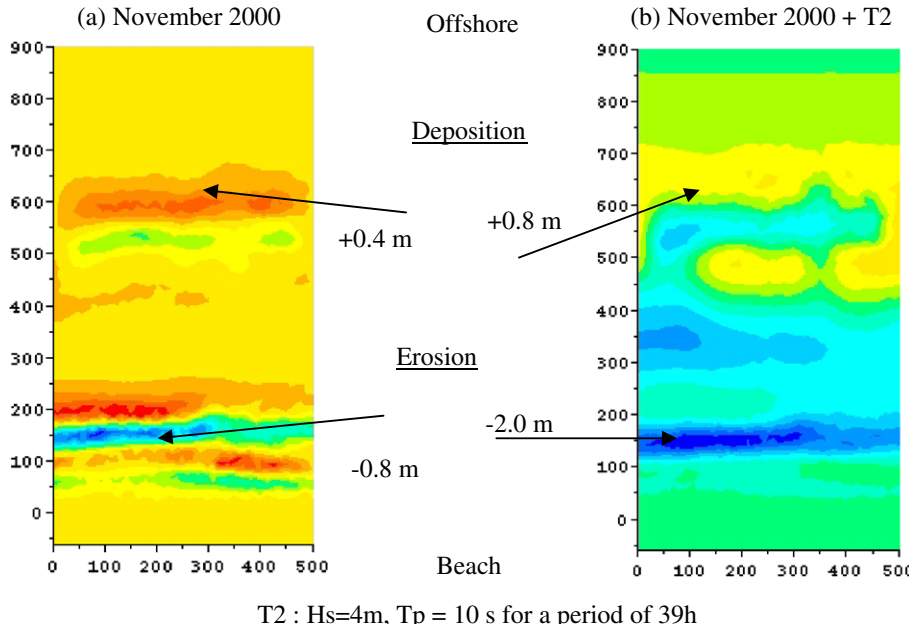


Fig. 5. (a) Sea bed evolution for a monthly simulation from the 4 November to the 25 November 2000 with nourishment and (b) the same with a storm of 39 h.

These values are indicative of a possible comparison with other simulations but cannot be used as quantitative values for real estimates of the quantities of sands put into motion. We will further see that these values are still strongly dependent on the models and in particular on the formulas of sedimentary transport.

4.2. Long term simulation

The accuracy of this first result allowed us to create a methodology of simulation for a longer time scale. We are now looking with the coupled codes Artemis-Telemac2d-Sisyphé, the morpho-evolution of the beach with and without nourishment. The aim was to find the best way to create the simplified meteorological model from the *in situ* data. In the study presented in the paper, we show the first step of this methodology which is to compare seasonal simulation with different script of meteorolog-

ical events during each season. The principal question is do we have to cut out each hour, day? Each meteorological event has time duration issued from the data (see graphics on Fig. 4). Figs. 5 and 6 show the importance of the storm in the destruction of the offshore nourishment bar. The major modification of the sea bed was numerically obtained because the time loop of the coupled codes Artemis-Telemac2d-Sisyphé was shorter than the time duration of the storm. The principal criteria to cut out could be the current velocity due to the waves. Indeed, when we have calm weather condition (e.g. small waves height) the feedback between the hydrodynamics and the sea bed evolution could be longer. Figs. 7 and 8 show the numerical difference due to number of hydro-sedimentary loop we simulated for the same monthly or seasonal modelling. The differences are very important in the very near shore region and close the beach. Fig. 8 shows a complete year of simulation (the 4 seasons) with

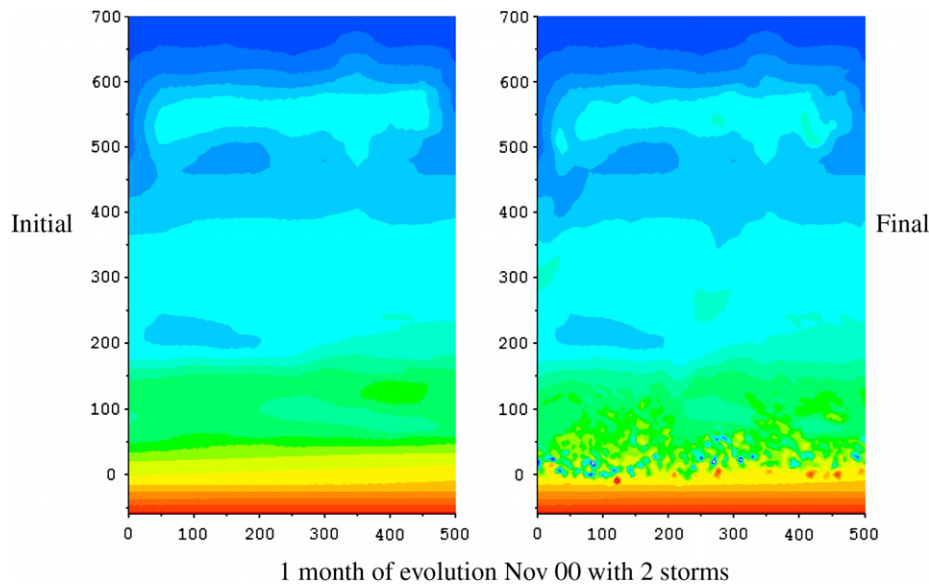


Fig. 6. Iso-bathymetry of a monthly simulation from the 4 November to the 25 November 2000 with nourishment and with two consecutive storms.

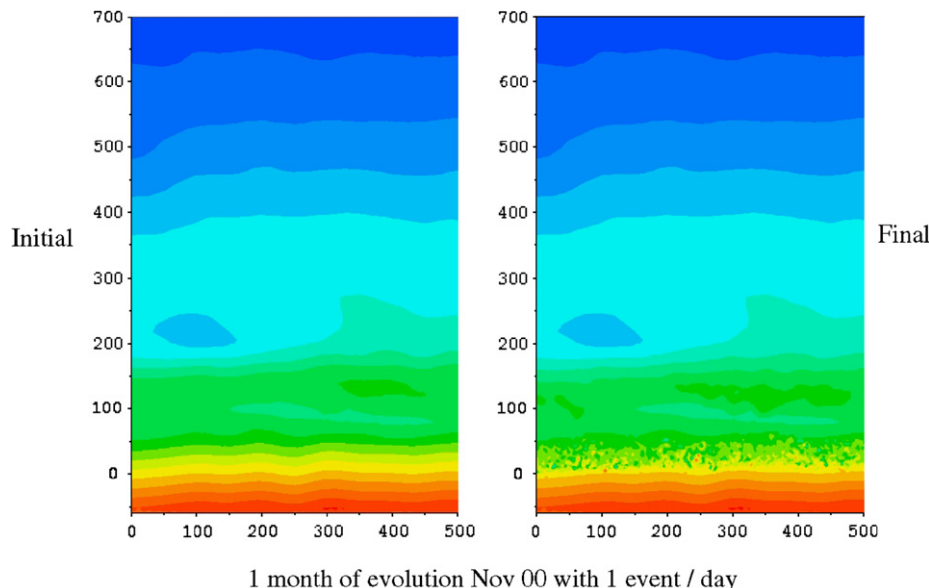


Fig. 7. Iso-bathymetry of a monthly simulation from the 4 November to the 25 November 2000 without nourishment and with one meteorological event per day.

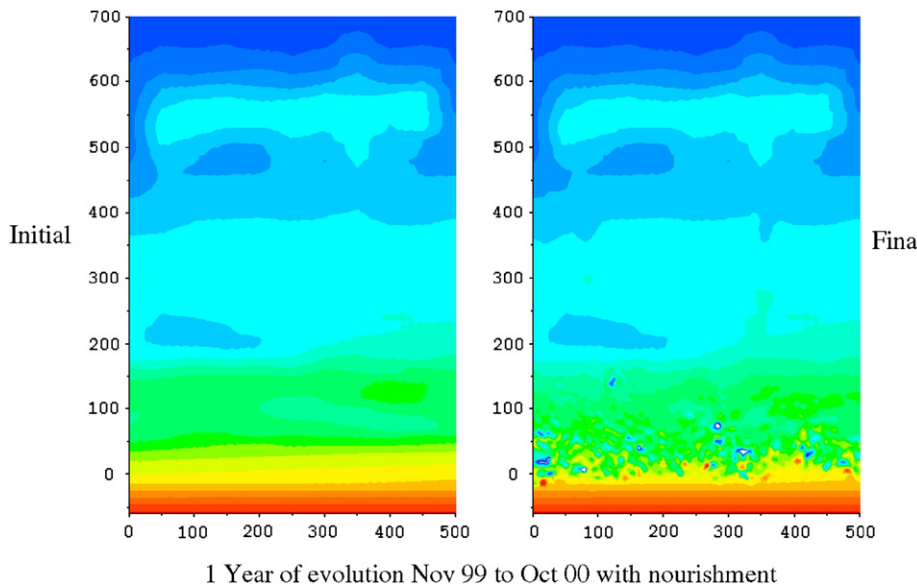


Fig. 8. Iso-bathymetry of a yearly simulation from November 1999 to October 2000 with nourishment.

nourishment and with a cut out of 48 events. The simulation took 24 h on a 2.36 GHz processor. The aim was to find at the same time the best accuracy of the yearly sea bed evolution and the lowest computational time. The other main goal was to be able to predict the best placement of the nourishment bar to protect the beach over five to ten years.

5. Conclusion

The interesting thing about this study is that we could compare our numerical results to the *in situ* data. Then, it could be easier to modulate time steps to have the most realistic results. A modified 2DH morphodynamical model was employed to simulate the evolution of large-scale features with major implications for beach nourishment. The study was focused on modelling the evolution of the sea bed and artificial material in the near shore region, extracting or adding material to the natural bars, and quantifying how the profile responds to different wave climates and nourishment placements. The simulated results were compared with field data from a Mediterranean beach over storm, monthly and yearly time scales. The results are good in terms of quality and also in terms of quantity for the velocity field due to waves. The next step of the study will be to simulate a large number of seasons from the year 1994 to 2005 to be able to elaborate a criterion for the meteorological cut out. The second goal is to predict the next five years with different nourishment placements to have a good strategy for beach protection.

Acknowledgements

This paper is largely based on research work carried out in the task group Coastal Morphology of the LITEAU program supported by the French Government and the HUMOR program supported by the European Community.

References

- Bailard, J.A., 1981. An energetic total load sediment transport model for a plane sloping beach. *Journal of Geophysical Research* 86 (C11), 10938–10954.
- Camenen, B., 2002. Modélisation numérique du transport sédimentaire sur une plage sableuse. Ph.D. Thesis. Université Joseph Fourier, Grenoble, 298p.
- Camenen, B., Larroudé, Ph., 2003a. Comparison of sediment transport formulae for a coastal environment. *Journal of Coastal Engineering* 48, 111–132.
- Camenen, B., Larroudé, Ph., 2003b. Un modèle morphologique côtier pour la création de barres rythmiques. *Revue française de génie civil, Génie côtier* 7, 1099–1116.
- Certain, R., 2002. Morphodynamique d'une côte sableuse microtidale à barres: le golfe du Lion (Languedoc-Roussillon). Ph.D. Thesis. University of Perpignan, 199p.
- Certain, R., Barusseau, J.P., 2006. Conceptual Modelling of Straight Sand Bars Morphodynamics for a Microtidal Beach (Gulf of Lions, France). ICCE, San Diego.
- Dally, W.R., Dean, R.G., Dalrymple, R.A., 1984. A Model for Breaker Decay on Beaches. In: 19th Coastal Engineering Conference Proceeding. ASCE, pp. 82–88.
- De Vriend, H.J., 1987. 2DH Mathematical modelling of morphological evolutions in shallow water. *Coastal Engineering* 11, 1–27.
- De Vriend, H.J., Stive, M.J.F., 1987. Quasi-3D modelling of nearshore currents. *Coastal Engineering* 11, 565–601.
- Dibajnia, M., Watanabe, A., 1992. Sheet flow under nonlinear waves and currents. *Coastal Engineering*, 2015–2029.
- Falqués, A. et al., 2008. Rhythmic surf zone bars and morphodynamic self-organization. *Coastal Engineering*.
- Hamm, L., Capobianco, M., Dette, H.H., Lechuga, A., Spanhoff, R., Stive, M.J.F., 2002. A summary of European experience with shore nourishment. *Coastal Engineering* 47, 237–264.
- Hervouet, J.M., 2007. *Hydrodynamics of Free Surface Flows: Modelling with the Finite Element Method*. John Wiley & Sons., 360p.
- Larroudé, Ph., Camenen, B., 2004. 2DH and multi1DH morphological model for medium term evolution of large scale features and nourishment in the nearshore region: application to TrucVert and Corniche beach (France) and la Barrosa beach (Spain). In: 29th International Conference on Coastal Engineering. ASCE, Lisbon.
- LNHE-Chatou, 2002. Telemac2d – modelisation system of Telemac, version 5.2 – user-validation manual. Technical report, edf-gdf.
- LNHE-Chatou, 2002. Sisyphe – modelisation system of Telemac, version 5.2 – user-validation manual. Technical report, edf-gdf.
- LNHE-Chatou, 2002. Artemis – modelisation system of Telemac, version 5.2 – user-validation manual. Technical report, edf-gdf.
- Longuet Higgins, M.S., 1970. Longshore currents generated by obliquely incident sea waves. *Journal of Geophysical Research* 75 (33), 60778–60801.
- Svendsen, I.A., 1984. Mass flux and undertow in the surf zone. *Coastal Engineering* 8, 347–365.

EXPERIMENTAL FLUME SIMULATION OF SHOREFACE NOURISHMENTS UNDER STORM CONDITIONS

Florent Grasso¹, Hervé Michallet¹ and Eric Barthélémy¹

Abstract

This study focuses on barred beach shoreface nourishments physically simulated in a wave flume. The attack of a schematic storm on three different nourishments is analysed. The apex and waning storm phases lead respectively to off-shore and on-shore sediment transport. The trough and outer bar nourishments are feeding the bar and increase wave dissipation off-shore. The bar acts as a wave filter and reduces shore erosion (lee effect). In contrast, nourishment in the inner zone leads mostly to shore feeding and beach face reconstruction (feeder effect). Along the successive nourishments, the upper beach face is clearly steepening and on-shore sediment transport is reduced during moderate wave climates. The surface sedimentological analysis reveals marked variations. Coarser sediments are sorted on the bar and the upper beach face. These locations correspond to large wave dissipation zones during the storm apex.

Key words: beach morphodynamics, sediment transport, grain size variation, changing wave climates.

1. Introduction

The large impact of human activities on coastal morphodynamics is now widely admitted. Beach protection and shore reconstruction strategies are at the forefront of coastal engineering issues. One traditional way to maintain beaches consists in beach nourishment (Hamm *et al.*, 2002; Hanson *et al.*, 2002). However, shoreface nourishment appears as a good compromise between efficiency, ecology and operating cost. It draws an increasing interest of the scientific community (Walstra *et al.*, 2008). According to Van Duin *et al.* (2004) and Grunnet *et al.* (2005), the shoreface nourishments may have two different effects, namely the lee and feeder effects. The lee effect refers to the ability to increase wave dissipation off-shore for protecting the beach face. It would reduce undertow and increase wave non-linearities, promoting on-shore sediment transport (Ruessink *et al.*, 2007). The feeder effect comprises the on-shore movement of nourished sand, restoring the beach profile.

Besides, the influence of nourished grain size on beach slope stability is frequently discussed (Van Duin *et al.*, 2004; Grunnet and Ruessink, 2005). Nonetheless, not many studies investigate evolution of sediment grain size variation along cross-shore beach profiles. Benedet *et al.* (2004) present sediment surface samples on post-nourished profiles but with poor spatial and temporal discretizations (around 50 m and 1 year). They observed a mean grain size increasing on the beach face. In a non-nourished intertidal beach, Masselink *et al.* (2007) measured surface sedimentological evolutions during 20 days at a high resolution (5 m and 12 h). They conclude that, in the intertidal zone, grain size distribution of surface sediments did not vary consistently across the beach profile, and temporal changes in the sedimentology were unrelated to the morphological response. The only noticeable temporal trend in the grain size data was the coarsening of sediment size near the end of the survey period during relatively high wave energy conditions.

In the last decades, important efforts have been done in surveying natural shoreface nourishments (Grunnet and Ruessink, 2005). Field experiments nevertheless do not usually allow a detailed description of beach changes due to the poor temporal resolution between topographic surveys. The video systems (e.g. Argus) allow a continuous survey of morphological changes (Ojeda and Guillén, 2004; Ojeda *et al.*, 2008). However, such systems can not follow beach changes for energetic wave conditions with widely developed surf zone. These conditions are yet known to be mostly responsible for beach morphodynamics. Hence, physical models are particularly useful because of high temporal and spatial discretizations (e.g. Roelvink

¹LEGI (CNRS – UJF – Grenoble-INP), BP 53, 38041 Grenoble cedex 9, France. Florent.Grasso@legi.grenoble-inp.fr

and Stive, 1989; Dette *et al.*, 2002; Hoyng, 2008). Few shoreface nourishment experiments were carried out in the laboratory (e.g. Walstra *et al.*, 2008) and, as far as we know, all of these were subjected to constant wave conditions. The purpose of the present study involves shoreface nourishments forced by storm scenario in flume experiments. Besides, such experiments enable a full beach sedimentology analysis.

Firstly, the morphological response of shoreface nourishments affected by storm events will be described. Focusing on the beach face, the changes will be quantified as evolutions of both shoreline position and shore volume. Wave hydrodynamics and sediment transport along beach profiles will then be compared for energetic and moderate wave conditions. Evolution of sediment grain size variations over storm simulations will be presented too. Finally, the discussion will bring out main ideas and address previous observations reported in the literature.

2. Methodology

Our experiments were carried out in the 36 m long and 55 cm wide LEGI flume, equipped with a piston wave generator. The still water depth is 55.3 cm. The mean overall slope is approximately 1/45. The sloping bottom consists of loose material of low density (1.19 g cm^{-3}) with a median diameter $d_{50}=0.6 \text{ mm}$ (corresponding settling velocity $w_s=2.1 \text{ cm s}^{-1}$). The Froude number, the Shields number and the Rouse number are of the same magnitude as those of natural environments (Grasso *et al.*, 2009a). Time and length scales are roughly 1/3 and 1/10 respectively. Irregular waves are generated (JONSWAP spectrum – peak enhancement factor=3.3). Using capacitive wave probes, it is checked that these waves conform to the expected spectrum and that they follow a Rayleigh distribution at 2 m downstream of the wave-maker. Bottom profiles are recorded between wave series using an acoustic profiler mounted on a motorised trolley. The generated wave series are characterised by their significant wave height H_s and their peak period T_p (Table 1). The associated Dean number, defined as $\Omega=H_s/(T_p w_s)$, is also given in Table 1.

The storm event simulation is based on the hydrodynamic observations on Lido beach at Sète, France (Certain *et al.*, 2005). A schematic storm is constructed as a succession of different wave climates described in Table 1. The three storm phases (rising, apex, and waning) are characterised by increasing, energetic and decreasing wave conditions respectively (Figure 1). The storm duration is 10.5 hours (~35 h in nature) for an apex lasting 4.5 hours (~15 h in nature). The wave generation is stopped at least each hour for recording the beach profile. This schematic storm is repeated four times (42.7 h total duration), firstly for a reference case without nourishment (N0) and next for three shoreface nourishments.

Table 1. Wave conditions used in this study.

Wave climate	A	B	C	D	E
H_s (cm)	6	10.7	13.5	16	16
T_p (s)	1.5	2	2.5	2.7	3
Ω	1.9	2.5	2.6	2.8	2.5

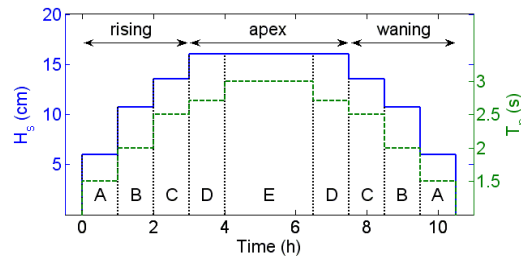


Figure 1. Storm event hydrodynamics.

The shoreface nourishments are simulated as localized sediment deposits. These are located: (N1) in the bar trough, (N2) on the outer bar, and (N3) in the inner zone (cf. Table 2 and Figure 2). All nourishment designs have comparable volumes ($0.16\text{-}0.18 \text{ m}^3$) which, on prototype scale, represent approximately $291\text{-}327 \text{ m}^3/\text{m}$. The sediment median diameter is ranging from $d_{50}=602$ to $756 \mu\text{m}$.

Sediment grain size distribution is measured for the four cases N0, N1, N2, and N3. Surface sediment samples are taken in the first centimetre layer for pre- and post-storm beach profiles. Sediment cores are realised on the N3 final profile at six cross-shore positions, they are then split in 3 cm high layers. All samples are analysed using a laser particle sizer (“Mastersizer 2000”, Malvern Instruments). Herein, the grain size is ranging from 400 to $1000 \mu\text{m}$. The measurements reproducibility for samples taken closely on the beach is of about 5%. Our measurements reveal similar sorting for d_{10} , d_{50} and d_{90} ; hence the choice is done to present only median grain size diameter results.

Figure 2 gives an overview of the beach changes for the four storm simulations. It illustrates the beach profile evolutions, split into three phases of the storm event, and highlights the shoreline position. The initial beach profile of N0 case results from various wave conditions. The initial profile of each other case corresponds to the final profile of the previous one. The following section is based on the analysis of these four cases. Note that the overall sediment volumes are not identical for all the cases. The beach sediment volume has increased of about 10% for N3 compared to N0 as a result of successive nourishments.

Table 2: Shoreface nourishments characteristics.

Nourishment	Location	Volume (m^3)	$d_{50} (\mu\text{m})$
N1	Trough ($x\sim 15.5\text{-}18 \text{ m}$)	0.16	756
N2	Outer bar ($x\sim 8\text{-}10.5 \text{ m}$)	0.16	602
N3	Inner zone ($x\sim 21\text{-}24 \text{ m}$)	0.18	702

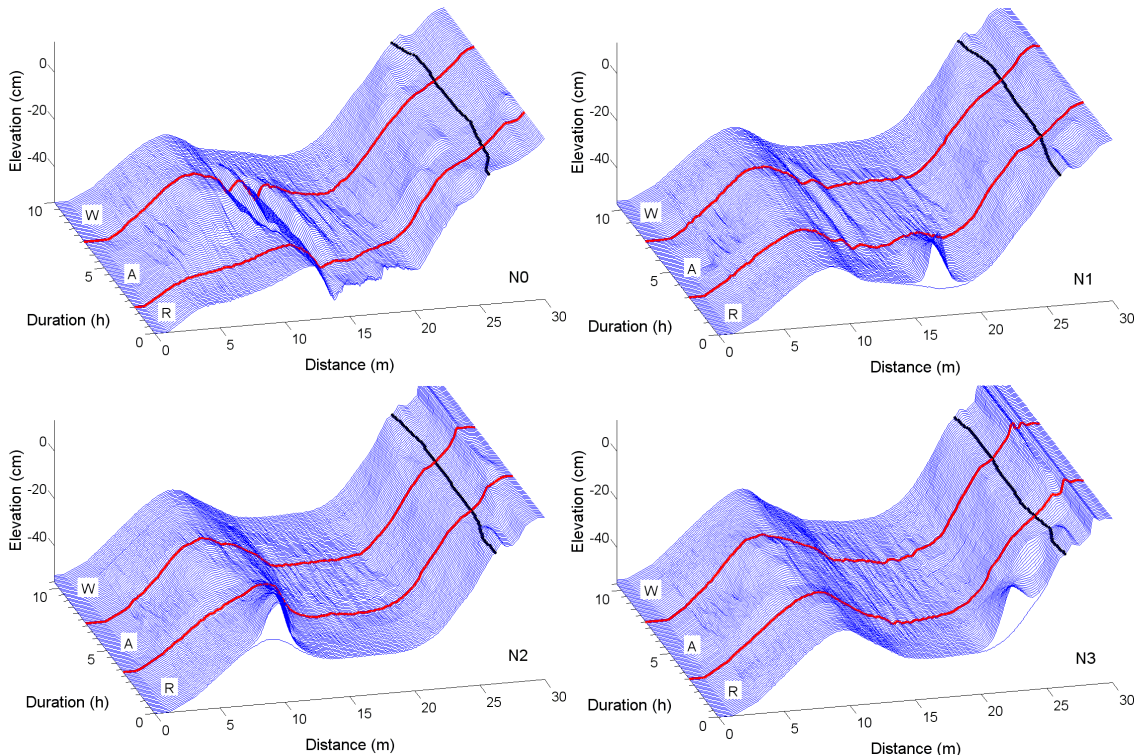


Figure 2. Beach profile changes during the four storm simulations: N0, N1, N2, and N3. Black lines on top represent shoreline position and grey/red lines delineate the three phases of the storm (Rising, Apex, and Waning). The distance $x=0$ corresponds to the wave-maker position; the zero-elevation corresponds to still water level.

3. Results

3.1. Morphological response

Figure 4 presents the beach profiles after each storm phase for the four simulations. In the first case (Figure 4.N0), the rise of the storm only modifies substantially the upper beach face above the 15 cm water depth. The slope is flattening and the shoreline is retreating. The rest of the profile is only smoothed. The storm apex leads to an off-shore bar formation. The bar crest moves from $x=12$ to 8 m and its elevation increases by 5 cm. A net erosion of the beach is observed from $x=17$ to 25 m. The storm waning results in smoothing the lower shoreface and reshaping the upper part. The shoreline moves seaward and the berm is reconstructed shoreward to its initial position. The slope of the upper beach face is clearly steeper. A focus on beach changes inner each storm phases has been more intensely discussed in Grasso *et al.* (2009b).

Starting from the N0 final profile, the nourishment N1 is done nearby $x=16.5$ m (Figure 4.N1). As for the N0 simulation, the storm rising leads to upper beach face erosion and berm destruction. The sediment deposit is dispersed in the trough. The storm apex leads the outer bar to grow by 4 cm and erodes the beach face from $x=22$ to 26 m. The storm waning is still only acting on the upper shoreface which experiences a berm reconstruction and a beach face steepening.

The bar nourishment N2 (Figure 4.N2) follows the same trend as previously. Nevertheless, the water depth above the sediment deposit being sufficiently shallow, the storm rising waves affect the lower shoreface and the bar is pitched forward as it starts to migrate on-shore. The bar crest is then retreating of about 2 m during storm apex. The bar crest is 5 cm higher on the final profile compared to N1 final profile.

A quite different trend is observed in N3 storm rising (Figure 4.N3). The sediment deposit on the lower beach face induces a strong accretion in upper shoreface and shoreline is not retreating. However, the bar is again accreting for storm apex but less than N1 and N2 (only by 2 cm). Conversely to the previous cases, the storm waning reconstructs and advances the berm ahead its initial position. After each simulation, the bar positions are close (from $x=8.5$ to 9.5 m) and beach profiles present very similar shapes. The beach face slopes are steepening along successive shoreface nourishments.

In order to better quantify the morphological changes, the beach profile has been divided in several parts. The beach volume is split in lower and upper shoreface volumes, delineated by the vertical dashed line at $x=16.5$ m in Figure 3. The shore volume is an upper shoreface subpart. It is computed above the 20 cm water depth to the most off-shore point on the dune that does not change during experiments. This shore volume would represent the sediment which may be transported even by the weakest wave conditions. The shoreline position x_s is defined at still water level.

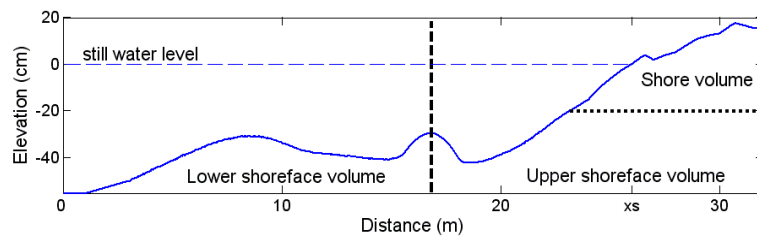


Figure 3. Schematic diagram of a beach profile. Vertical dashed line delineates lower (on the left-hand) and upper (on the right-hand) shoreface volumes. The shore volume is computed above the 20 cm water depth and x_s is the shoreline position.

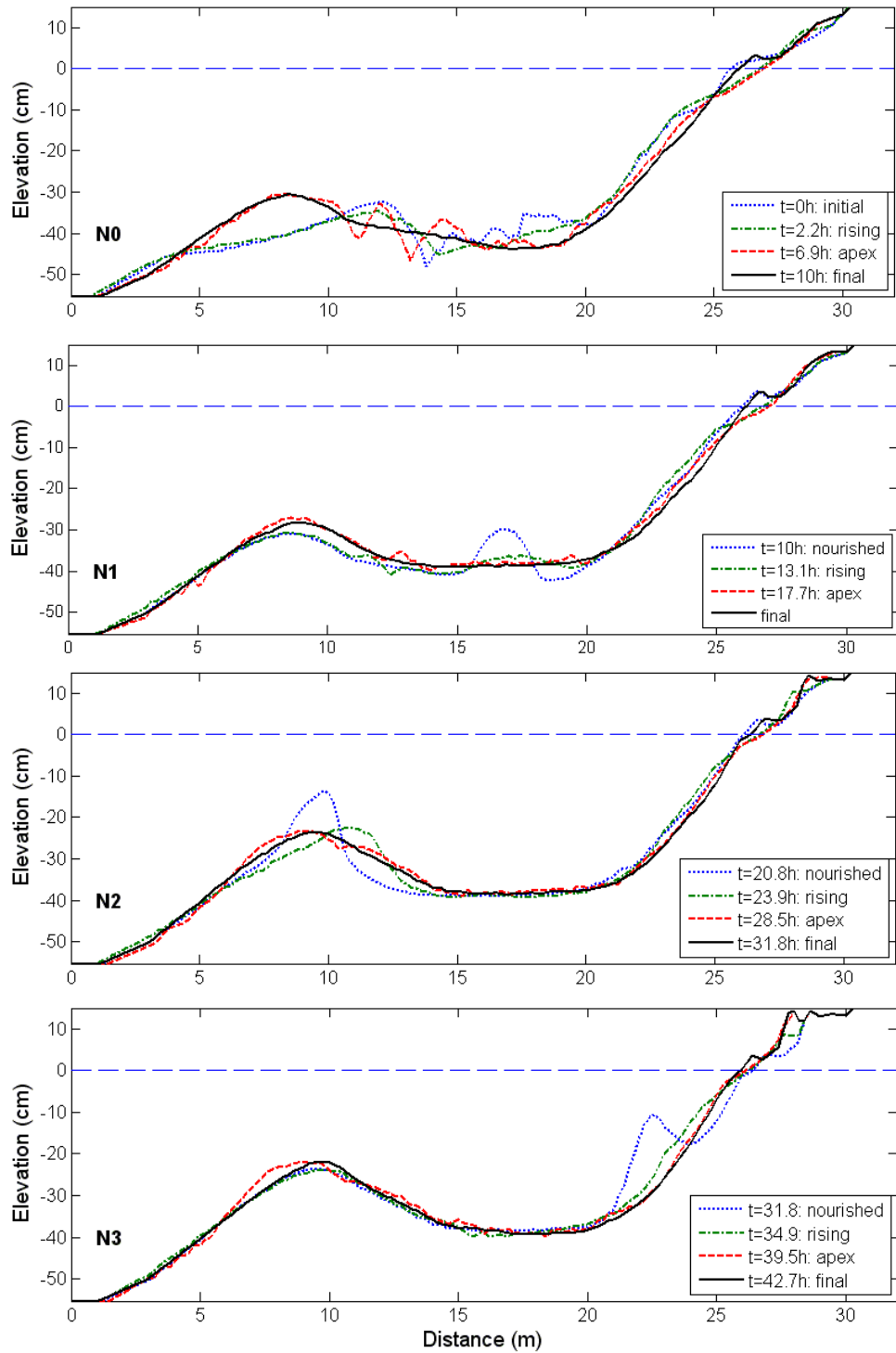


Figure 4. Initial (dotted), end of rising (dash-dotted), end of apex (dashed) and final (solid) beach profiles for storm simulations: N0, N1, N2, and N3.

Figure 5 synthesizes the beach changes characteristics for the four successive storm simulations delineated by vertical solid lines. Morphological evolutions of N0, N1, and N2 follow similar trends. The shoreline (top line panel) is strongly retreating during storm rising phases and in a lesser extent during apex phases (-156 cm for N0, -116 cm for N1, and -76 cm for N2). It is then moving seaward for waning phases but does not recover fully its initial position. At the time scale of the storm, the shoreline retreats by -36 cm for N0, -19 cm for N1, and -17 cm for N2. The shoreline retreat thus decreases by 50% for these two nourished cases compared to the reference case. The nourishment in the inner zone has a quite different trend (N3) as the shoreline is advancing by 39 cm. This tendency is confirmed by the shore volume (second line panel), increasing by 1.5%. Shore volume variations from previous simulations present a nuanced feature. The apex phases strongly erode the shore: -4.6% for N0, -3.8% for N1, -3% for N2. Whereas waning phases are mainly responsible for sediment accretion: 2.2% for N0, 1.4% for N1, 0.7% for N2. In spite of these final reconstructions, the shore volumes present a decreasing but constant loss of sediment (-3.3% for N0, -2.5% for N1, -1.2% for N2).

Such sediment losses are explained by sediment exchanges between lower and upper shorefaces (third line panel). The lower shoreface volume is almost continuously increasing, conversely to the upper shoreface volume. Rapid volume evolutions during apex phases characterize a strong off-shore sediment transport from the upper to the lower shorefaces. Nevertheless, these sediment exchanges weaken through the nourishments. It is pointed out that only the nourishments located in the upper shoreface (at $t=10$ and 31.8 h) partially succeed in slowing down the erosion of this part. Out of shoreface nourishments, the total sediment volume evolution reveals some fluctuations (bottom line panel). These variations are one order larger than the measurement uncertainty (the latter estimated of the order of $5 \times 10^{-3} \text{ m}^3$). The sediment mass being constant for a given case, these small variations correspond to apparent volume changes. The trend is an increase of the apparent volume during the storm apex and a decrease afterwards (clearly seen in the first storm simulation N0 in the bottom line panel of Figure 5). This point will be addressed in the Discussion.

Shoreface morphodynamics and post-storm beach profiles appear to be mostly concerned by the apex and the waning of the storm (Grasso *et al.*, 2009b). The effects of these energetic and moderate wave conditions on the sediment transport are investigated in the next section.

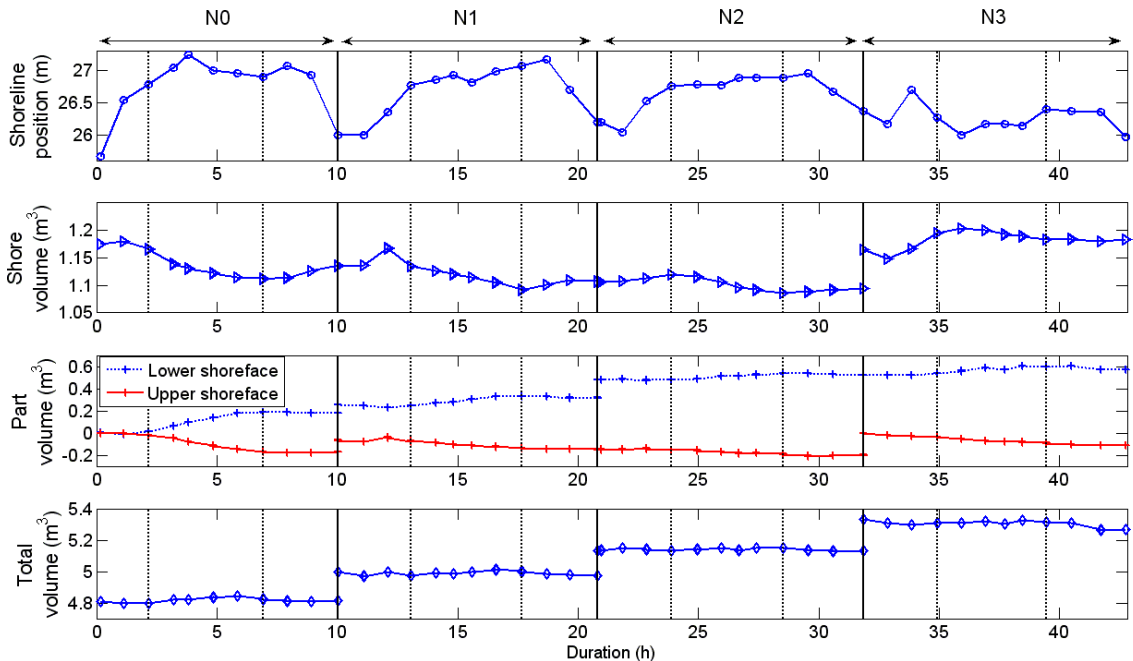


Figure 5. From top to bottom: time evolution of shoreline position, shore volume, subparts volume variations, and total beach volume. Vertical solid lines delineate the four storm simulations (N0, N1, N2, and N3) and dotted lines delineate the three phases (increasing, energetic, and decreasing) in each storm.

3.2. Wave hydrodynamics and sediment transport associated

For characterising storm apex (storm waning), wave climate E (B) is chosen. Figure 6 sums up the root mean square wave height evolution H_{rms} (top line panel) across corresponding beach profile (bottom line panel) for the four simulations. Measured from the wave height decay, the dissipation per unit area (second line panel) is given by:

$$\langle \varepsilon \rangle = -\frac{1}{8} \rho \cdot g^{3/2} \frac{\partial (H_{rms}^2 h^{1/2})}{\partial x}, \quad (1)$$

where ρ is the water density, h the water depth, g the gravity, and x is on-shore oriented (Grasso *et al.*, 2009a). The mean sediment transport rate over each climate period Q_s (third line panel) is derived from profile development over considered wave climate (E or B):

$$\frac{\partial q_s}{\partial x} = \frac{\partial h}{\partial t}, \quad (2)$$

$$Q_s = \frac{1}{\Delta t} \int_t^{t+\Delta t} q_s dt, \quad (3)$$

where q_s is the sediment transport rate and Δt the wave climate period.

For energetic wave conditions ($H_s=16$ cm, $T_p=3$ s, Figure 6.E) the cross-shore wave height evolutions present two breaking zones. One begins on the outer bar ($x=7-8$ m) and the second on the beach face (23-24 m). This induces two main dissipation peaks. The bar is growing during the successive nourishments, it enhances (reduces) the wave breaking on the bar (the beach face). As a consequence, the dissipation follows the same trend. Note that the N1 dissipation peak ($x=9-11$ m) is poorly captured due to a lower discretization in the measurement locations for this case. The steeper beach face for case N3 induces a stronger dissipation at $x \sim 24$ m compared to cases N1 and N2. For these energetic conditions, the sediment transport is globally off-shore directed. However, the total transport rate (Q_s summed along the beach profile), weakens with successive nourishments (Table 3). This in line with the previous observations (Figure 5) for which the sediment exchanges from the upper to the lower shorefaces weaken through the apex simulations. Moreover, the sediment transport over the bar may be on-shore directed and is increasing with the bar growing. This tendency is also observed for moderate wave climates ($H_s=10.7$ cm, $T_p=2$ s, Figure 6.B) where waves are rising without breaking ($x=5-10$ m). The climate B hydrodynamics draws yet a different feature with a total sediment transport directed on-shore (Table 3). The waves are only breaking on the beach face leading to one dissipation peak close to $x=25$ m. This peak has approximately the same magnitude for successive nourishments ($5 \text{ Nm}^{-2} \text{ s}^{-1}$). The on-shore sediment transport on the upper beach face is clearly decreasing as the slope is steepening. Once more, this is in agreement with the decreasing shore volume deposit through succeeding waning phases (Figure 5). For a better understanding of these beach slope changes and associated sediment transport processes, the beach sedimentology is investigated in the next section.

Table 3: Total sediment transport rate for energetic (E, apex) and moderate (B, waning) wave conditions for the four storm simulations (N0, N1, N2, and N3).

Storm simulation	N0	N1	N2	N3
ΣQ_s E, apex ($10^{-3} \text{ m}^2 \text{ s}^{-1}$)	-4.1	-1.1	-1.3	-0.9
ΣQ_s B, waning ($10^{-3} \text{ m}^2 \text{ s}^{-1}$)	0.75	0.41	0.23	0.43

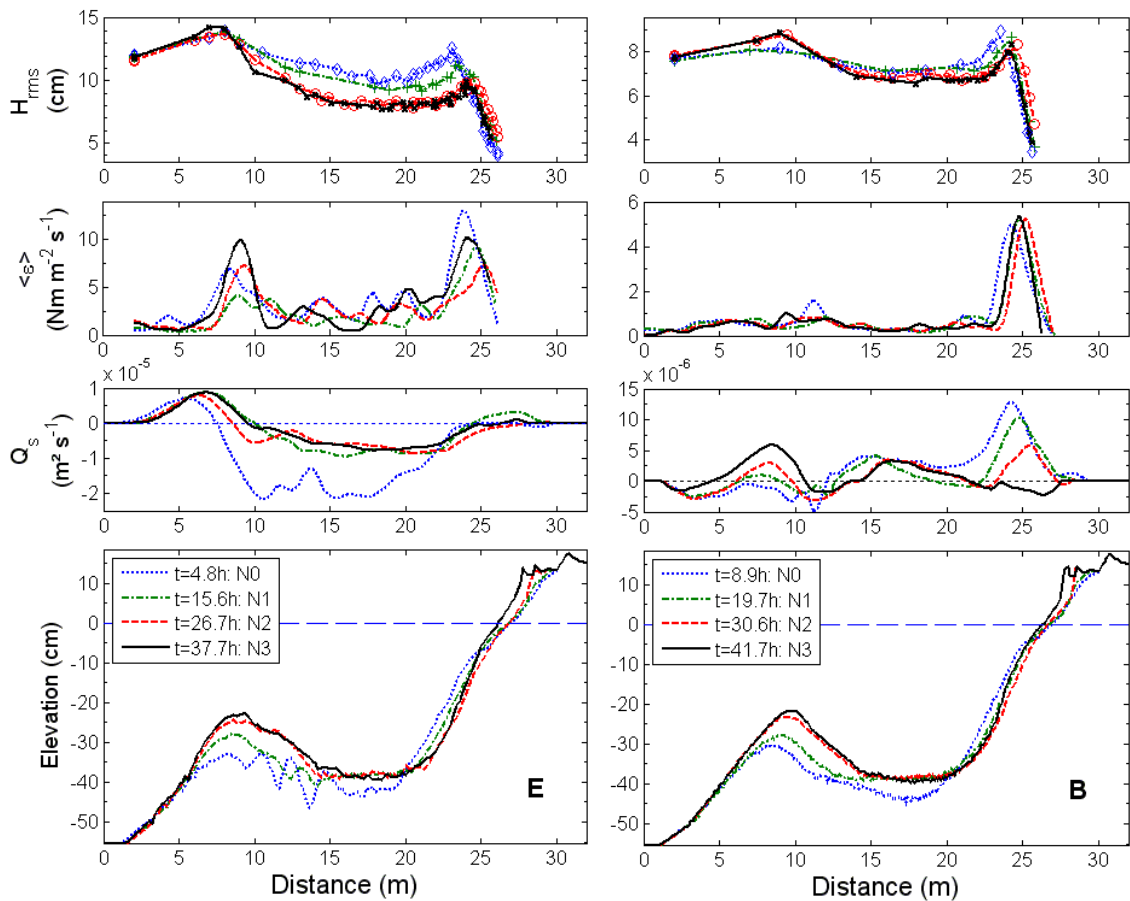


Figure 6. From top to bottom: root mean square wave height (H_{rms}), dissipation ($\langle \varepsilon \rangle$), sediment transport rate (Q_s), and beach profiles for N0 (dotted), N1 (dash-dotted), N2 (dashed), and N3 (solid). On the left-hand, storm apex energetic wave conditions (E: $H_s=16$ cm, $T_p=3$ s); and on the right-hand storm waning moderate wave conditions ($H_s=10.7$ cm, $T_p=2$ s).

3.3. Sediment grain size variation

The following sedimentological analysis is based on two points: i) the sediment median size variations along the beach profiles; and ii) the temporal evolution of these variations through the nourishments. Figure 7 synthesises sediment median diameters (d_{50}) measured for pre- and post-storm simulations. The N0 initial grain size is relatively homogeneous along the beach (crosses in Figure 7.N0). In contrast, the storm is clearly sorting the sediment. Coarser sediments are on the outer bar ($d_{50}=858 \mu m$) and on the dune ($742 \mu m$), while finer sediments are in the trough ($550 \mu m$) and at the beach foot ($657 \mu m$). The first nourishment (Figure 7.N1) consists in a coarser sediment deposit at $x=18$ m ($d_{50}=756 \mu m$). Once more, the storm concentrates coarser sediments on the upper beach face ($759 \mu m$). The coarsening on the bar is not verified here as the sample at $x=10$ m is missing. As finer sediment is deposited on the bar ($d_{50}=602 \mu m$ at $x=10$ m, Figure 7.N2), the storm simulation overdoes this tendency with $d_{50}=874 \mu m$ on the bar and $790 \mu m$ on the upper beach face. The storm after the third nourishment ($d_{50}=702 \mu m$, Figure 7.N3) is again gathering coarser sediments on the upper beach face. The deposited sediment is clearly spread off-shore as deduced from the final samples on the left side of the trough and on the forefront of the bar ($x=10-14$ m, $d_{50}=718$ and $736 \mu m$). We note grain size evolutions at $x=2$ and 6 m that may be explained by a vertical sorting.

Sediment cores were sampled along the N3 final beach profile and the corresponding median size variations are presented in Figure 8. The vertical grain size variations present irregular trends for different cross-shore positions. In agreement with surface samples on the bar, coarser sediments are also present in the vertical structure ($x=10$ m, $z=-22$:-40 cm). Besides, it appears at $x=14$ m for $z=-46$:-36 cm that coarser sediments are only in surface as a result of the last nourishment spreading.

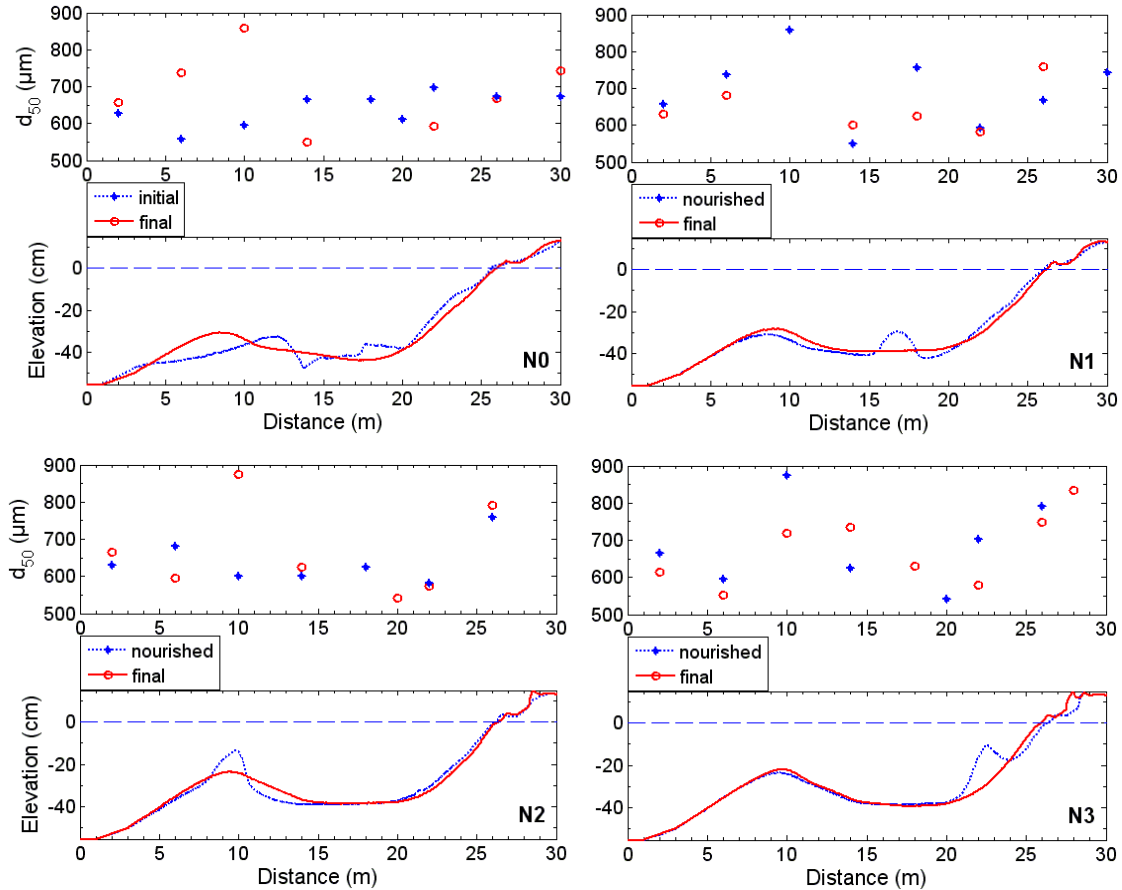


Figure 7. Sediment median diameter (d_{50}) along initial (dotted, +) and final (solid, o) beach profiles, for N0, N1, N2, and N3.

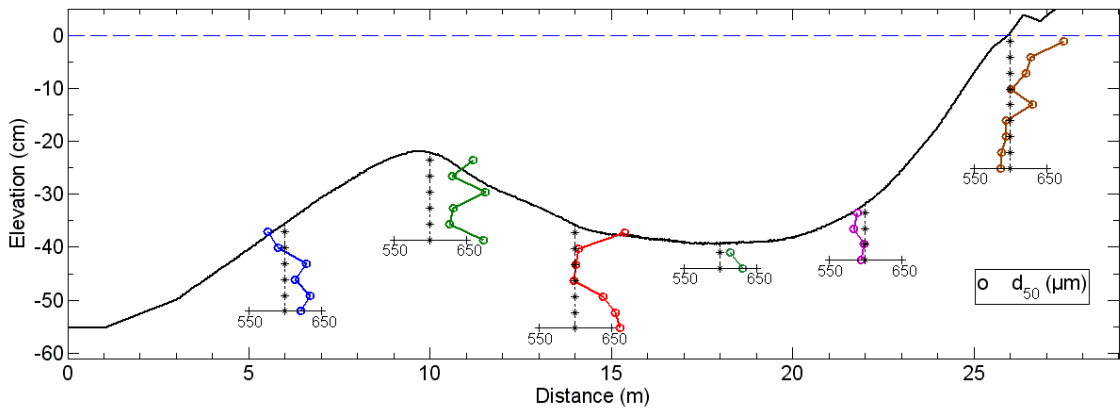


Figure 8. Vertical distribution of sediment median diameter (d_{50}) along N3 final beach profile.

4. Discussion

The storm simulations have typical effects on the beach morphodynamics. The apex phases lead to strong off-shore sediment transport rates, eroding the beach face and accreting the outer bar. These evolutions are described in nature during storm events (or/in winter) by many authors (e.g. Ostrowski *et al.*, 1990). In contrast, the rising and the waning phases correspond to on-shore sediment transports and beach face accretion. This is also in line with field observations for moderate wave conditions (King, 1972; Sonu and James, 1973). In our experiments, the low and moderate wave conditions are not able to transport on-shore the sediment trapped in the bar trough. This explains negative shore volume balances at the time scale of the storms.

Throughout successive nourishments, the apex destructive waves are dissipating more energy on the outer bar (+43%) and less on the beach face (-22%). Such behaviour due to bar growing leads to decrease both off-shore sediment transport and shore erosion. This is typical of the lee effect where the bar acts as a wave filter dissipating the energy of the larger breaking waves (Van Duin *et al.*, 2004; Grunnet *et al.*, 2005). Undertow and wave non-linearities effects, which certainly play an important role on the morphodynamics (e.g. Ruessink *et al.*, 2007), were not quantified in this study. It is difficult to compare the different nourishment efficiencies because the initial beach profile is not identical for each case. Nevertheless, a marked trend is observed for the nourishment in the inner zone (N3). The deposited sediment is transported on-shore and nourishes directly the upper beach face. The berm is reconstructed seaward to its initial position. This corresponds to the namely feeder effect characterized by an on-shore propagating active bar merging the berm (Walstra *et al.*, 2008). The totality of the sediment nourished in the shore volume is still in place at the end of the storm. Another part located in the lower beach face is yet transported off-shore feeding the trough and the bar.

Walstra *et al.* (2008) conducted extensive laboratory experiments on morphological nourishment responses. They noted that, besides the direct influence on bar dynamics, an indirect result of the nourishments may be the steepening of the nearshore profile. There is a very similar tendency in our experiments. This may be explained by the sediment size sorting. Strong wave dissipations on the bar and the upper beach face are linked to two significant suspension zones. Finer sediments of these zones are mobilized and diffused to lesser agitated water depths (at the lower beach face and in the trough). This results in coarser sediment concentrations on the bar and upper beach face, leading to steeper slopes. This is in line with Benedet *et al.* (2004) who obtain sediment coarsening on the beach face; and Masselink *et al.* (2007) who observe, in the intertidal beach, the coarsening of sediment size during relatively high wave energy conditions. For the upper beach face during waning phases, the slope steepening may explain the decreasing on-shore sediment transport as the gravity influence is relatively enhanced. Several nourishment grain sizes are involved ($d_{50}=602$, 702, and 756 μm) but similar features are obtained. It requires further investigation with more dispersed sediment size deposits for observing substantial differences in nourishment simulations. Besides, sediment cores show that the sediment size varies greatly over the active layer. Other experiments with multiple core samplings between each different wave climate would be needed to better understand the relationships between the sorting process and the beach morphological response.

Other shoreface nourishments were carried out in the Scheldt flume at Delft (Hoyng, 2008; Walstra *et al.*, 2008). This small-scale flume (length-scale of 1/10 to 1/20) uses fine sand ($d_{50}=0.13$ mm) and deposit volumes correspond approximately to 400 m^3/m in nature. As for our experiments, the total beach volume presents variations during experiments. According to Walstra *et al.* (2008), it is thought that the initial profile, measuring before any waves, would be settled after 1 h wave action. In our understanding, these fluctuations correspond to apparent volume variations and thus beach porosity changes. Energetic wave conditions (i.e. storm apex) mobilize a large sediment layer that is put into suspension. The bed made of settled sediment is probably less compact. As a consequence, energetic waves may increase the bed porosity and the apparent volume. In contrast, bed load transport is the main mechanism under moderate and low wave conditions (i.e. storm rising and waning). This may promote sand grains arrangement leading to a decrease in both bed porosity and apparent volume.

5. Conclusion

This study focuses on shoreface nourishments physically simulated in the LEGI wave flume. A barred beach profile is nourished in three different ways corresponding to three cross-shore positions of sand deposits (outer bar, trough, and inner zone). A schematic storm event is reproduced in terms of successive varying wave climates. The morphological response of the three nourishments to this storm is analysed. Energetic wave conditions lead to off-shore sediment transport, beach face erosion, and bar growing. Moderate wave conditions lead to on-shore sediment transport and beach face accretion. The trough and bar nourishments are feeding the bar and increase wave dissipation off-shore. The bar acts as a wave filter and reduces shore erosion, which is known as the lee effect. In contrast, nourishment in the inner zone leads mostly to shore feeding and beach face reconstruction (known as the feeder effect). Through successive nourishments, the upper beach face is clearly steepening and the on-shore sediment transport reduces during moderate wave climates. This is linked to the coarsening of the sediment on the upper beach face. The surface sedimentological analysis reveals marked variations significant of sediment sorting along the beach profile. The coarser sediments are located on the bar and the upper beach face. These locations correspond to maximum wave dissipation zones. Sediment cores present interesting features that would indicate in-depth sediment sorting.

Acknowledgements

This study is funded by the LITEAU program of the French Ministry of Ecology, the INSU (LEFE-IDAO and RELIEF-MODLIT/SHOM-DGA), the EC INTERREG-IIIC program under project BEACHMED-e and the ECOS-Sud program with CONYCIT (contract C07U01). The technical assistance of J.-M. Barnoud is gratefully acknowledged.

References

- Benedet, L., C.W. Finkl, T. Campbell, and A. Klein, 2004. Predicting the effect of beach nourishment and cross-shore sediment variation on beach morphodynamic assessment. *Coastal Engineering*, 51:839-861.
- Certain, R., S. Meulé, V. Rey, and C. Pinazo, 2005. Swell transformation on a microtidal barred-beach (Sète, France). *Journal of Marine Systems*, 38:19-34.
- Dette, H., Larson, M., Murphy, J., Newe, J., Peter, K., Reniers, A. and Steetzel, H., 2002. Application of prototype flume tests for beach nourishment assessment. *Coastal Engineering*, 47:137-177.
- Grasso, F., H. Michallet, E. Barthélémy, and R. Certain, 2009a. Physical modelling of intermediate cross-shore beach morphology: transients and equilibrium states. *Journal of Geophysical Research*, in press.
- Grasso, F., H. Michallet, R. Certain, and E. Barthélémy, 2009b. Experimental flume simulation of sandbar dynamics. *Journal of Coastal Research*, SI56:54-58.
- Grunnet, N.M., and B.G. Ruessink 2005. Morphodynamic response of nearshore bars to a shoreface nourishment. *Coastal Engineering*, 52(2):119-137.
- Grunnet, N.M., B.G. Ruessink and D.J.R. Walstra, 2005. The influence of tides, wind and waves on the redistribution of nourished sediment at Terschelling, The Netherlands. *Coastal Engineering*, 52:617-631.
- Hamm, L., M. Capobianco, H.H. Dette, A. Lechuga, R. Spanhoff, M.J.F. Stive, 2002. A summary of European experience with shore nourishment. *Coastal Engineering*, 47:237-264
- Hanson, H., A. Brampton, M. Capobianco, H.H. Dette, L. Hamm, C. Lastrup, A. Lechuga, and R. Spanhoff, 2002. Beach nourishment projects, practices, and objectives—a European overview. *Coastal Engineering*, 47:81-111.
- Hoyng, C., 2008. Erosive and accretive coastal response, *M. sc. Thesis*, WL Delft Hydraulics.
- King, C.A.M., 1972. Beaches and coasts. *Edward Arnold*, London, 570 p.
- Masselink, G., N. Auger, P. Russell, and T. O'Hare, 2007. Short-term morphological change and sediment dynamics in the intertidal zone of a macrotidal beach. *Sedimentology*, 54:39-53.
- Ojeda, E., and J. Guillén, 2004. Monitoring beach nourishment based on detailed observations with video measurements. *Journal of Coastal Research*, SI48:100-106.
- Ojeda, E., B.G. Ruessink, and J. Guillén, 2008. Morphodynamic response of a two-barred beach to a shoreface nourishment. *Coastal Engineering*, 55:1185-1196
- Ostrowski, R., Z. Pruszak, and R.B. Zeidler, 1990. Multi-scale nearshore and beach changes. *22nd International Conference on Coastal Engineering* (ASCE, Delft, Netherlands), 2101-2116.

- Roelvink, J.A., and M.J.F. Stive, 1989, Bar-generating cross-shore flow mechanisms on a beach. *Journal of Geophysical Research*, 94(C4):4785-4800.
- Ruessink, B.G., Y. Kuriyama, A.J.H.M. Reniers, J.A. Roelvink, and D.J.R. Walstra, 2007. Modelling cross-shore sandbar behaviour on the timescale of weeks. *Journal of Geophysical Research*, 112, F03010.
- Sonu, C. J., and James, W. R., 1973. A Markov model for beach profile changes. *Journal of Geophysical Research*, 78:1462-1471.
- Van Duin, M.J.P., N.R. Wiersma, D.J.R. Walstra, L.C. Van Rijnand, and M.J.F Stive, 2004. Nourishing the shoreface: observations and hindcasting of the Egmond case, The Netherlands. *Coastal Engineering*, 51(8-9):813-837.
- Walstra, D.J.R., C. Brière, A.B. Cohen, A.P. Van Dongeren, I.J.P. Elshoff, C. Hoyng, M. Van Ormondt, S. Quartel, B. De Sonneville, P.K. Tonnon, and L. Uunk, 2008. Monitoring and modelling of a shoreface nourishment. *Research Report, Overeenkomst RKZ-1821A*, WL Delft Hydraulics.

ETUDE DE FAISABILITE PAR MODELISATION NUMERIQUE ET CANAL A SEDIMENT DE RECHARGEMENTS SEDIMENTAIRES SABLEUX D'AVANT-COTE EN MILIEU MICROTIDAL, UNE NOUVELLE METHODE DE LUTTE CONTRE L'EROSION COTIERE

**Raphaël CERTAIN¹, Florent GRASSO³, Karine SPIELMAN²,
Dominique ASTRUC², Philippe LARROUDE³, Hervé MICHALLET³, Eric
BARTHELEMY³, François SABATIER⁴, Jean-Paul BARUSSEAU¹**

¹Université de Perpignan Via Domitia, E.A. 3678 IMAGES, 52 av P. Alduy,
66860 Perpignan Cedex, France (certain@univ-perp.fr)

²Institut de Mécanique des Fluides de Toulouse (IMFT), UMR 5502
CNRS/INPT/UPS, Allée du Pr. Soula, 31400 Toulouse, France.

³Laboratoire des Ecoulements Géophysiques & Industriels (LEGI), UMR CNRS
5519, BP 53 38041 Grenoble Cedex 9

⁴CEREGE, Europôle Méditerranéen de l'Arbois, 13545 Aix en Provence, France

Résumé :

Une des méthodes de restauration de plage les plus courantes consiste à recharger la plage émergée en sable, procédé toutefois pénalisé par la limitation des sources de sable disponibles et par des contraintes fortes pesant sur le respect des critères granulométriques. Le matériel sableux à disposition a souvent une granulométrie trop faible par rapport au matériel *in situ*, ce qui le rend très instable. L'idée vient alors de prélever ce sédiment en mer et de recharger directement dans les petits fonds ayant une granulométrie plus compatible. Les résultats obtenus pour deux programmes en cours actuellement, LITEAU II (MEDAD) et GESA Beachmed-e (Programme européen Interreg III C), sont présentés ici. Ils étudient un certain nombre de scénarios de rechargements d'avant-côte à l'aide de plusieurs modèles numériques complémentaires et de simulations en canal à sédiment.

Abstract:

One way to recover beaches consists in beach nourishment. Sometimes the grain size of the borrow sand is however too thin to be in equilibrium on the beach. A solution can be to make shoreface nourishment, where sand is generally thinner.

The results of two programs LITEAU II (MEDAD) and GESA Beachmed-e (European Program) are presented here. Several scenarios of shoreface nourishments in a microtidal environment are tested by numerical and physical modelling.

Mots clés :

Rechargement sédimentaire d'avant-côte, modélisation numérique, modélisation physique, érosion côtière, barres sédimentaires d'avant-côte.

1. Introduction

Les communes littorales méditerranéennes souffrent dans leur grande majorité de problèmes d'érosion de leurs littoraux sableux ; qu'ils soient liés aux conditions de

l'évolution naturelle des milieux ou qu'ils soient induits par des aménagements.

Les rechargements classiques en sable réalisés sur la plage émergée sont une des techniques de lutte mais le matériel sableux à disposition a souvent une granulométrie trop faible par rapport au matériel *in situ*. Prélever ce sédiment en mer et recharger directement dans les petits fonds ayant une granulométrie fine plus compatible peut être une alternative.

Cette technique a pu être testée sur certains littoraux mésotidiaux (Burke *et al.*, 1991 ; Basinski & Szmytkiewicz, 1991 ; Foster *et al.*, 1994). Le programme européen Nourtec (MAST-II) reste à ce jour le plus ambitieux (NOURTEC, 1997). Les résultats ont été encourageants puisque le sédiment a été remonté vers la côte et a pu bénéficier à la plage (Hoekstra *et al.*, 1996). Cette expérience concluante a amené les autorités hollandaises à commanditer une quinzaine de rechargements d'avant-côte depuis 1997 (Spanhoff *et al.*, 2003).

Peu de modèles numériques 2DV, 2DH et 3D ont déjà été mis en oeuvre pour modéliser le comportement des rechargements des barres et/ou creux d'avant-côte (Van Duin *et al.*, 2004 ; Grunnet *et al.*, 2005). Les résultats ont montré l'utilité de ces modèles, bien que des améliorations soient nécessaires.

En milieu microtidal, aucune étude préalable n'a pour l'instant été menée. Deux programmes en cours actuellement LITEAU II (MEDAD) et GESA Beachmed-e (Programme européen Interreg III C) étudient un certain nombre de scénarios de rechargements d'avant-côte à l'aide de plusieurs modèles numériques complémentaires et de simulations en canal à sédiment. La faisabilité de tels rechargements sur différentes avant-côtes microtidales est testée. Des scénarios impliquant des volumes sédimentaires différents ainsi que différentes conditions de forçage caractéristiques de la zone sont simulés. Les auteurs présenteront ici

les résultats techniques finaux obtenus pour GESA Beachmed-e et de mi-parcours pour le programme LITEAU II.

2. Site d'étude et méthodologie

2.1 Sites d'étude

Notre choix s'est porté sur six sites qui subissent des érosions diverses et qui sont représentatifs de l'ensemble des avant-côtes menacées du Languedoc-Roussillon : la plage de la Corniche à Sète, ainsi que celles de Vendres, Ingril, Maguelonne et Petit-Travers (Hérault) ; plus au sud celle de Leucate (Aude).

2.2 Méthodologie pour la modélisation numérique

Les modèles qui sont utilisés dans cette étude sont les suivants.

Le code numérique 2DV MODHYS a été développé au sein de l'IMFT (Spielmann, 2002) pour analyser les bénéfices que l'on pourrait retirer d'une modification des profils de plage barrée vis-à-vis de l'érosion littorale. Ce modèle permet de prédire l'évolution à court et moyen terme d'un profil de plage (24 h dans ce travail), essentiellement dans des conditions hydrodynamiques de moyenne et de forte houle.

En utilisant le code de calcul Telemac, les modifications apportées par le LEGI ont consisté en la mise en place d'une procédure quasi-permanente liant les calculs de houle, d'hydrodynamique et de transport sédimentaire. Différentes formules de transport semi-empiriques pouvant être utilisées pour ce code ont été également testées. La chaîne de calcul Telemac constitue un modèle complet utilisant la méthode aux éléments finis et permettant la réalisation de différents calculs hydrodynamiques sédimentaires.

Le modèle 2DV S-Beach est un modèle à vocation appliquée qui permet lui aussi de répondre aux attentes du projet. C'est un logiciel qui calcule les transformations d'un profil topo-bathymétrique, en fonction des conditions de houle au large.

Sur les six profils naturels retenus, des rechargements ont été « effectués » soit 1) au niveau de la barre externe (Fig. 1), soit 2) en créant une barre surnuméraire au large. On a fait le choix volontairement de choisir de gros volumes de rechargement. Les conditions de houle imposées ont été déduites de l'analyse des données décennales qui ont permis de déduire des scénarios types (Tabl. 1).

2.3 Méthodologie pour le modèle physique

Le LEGI a développé depuis quelques années une modélisation physique dans un canal de 36m (hauteur d'eau de 55,3 cm) équipé d'un batteur générant une houle irrégulière.

L'originalité des expériences réside dans l'utilisation d'un sédiment mobile non cohésif de faible densité (PMMA, $\rho_s = 1,19 \text{ g.cm}^{-3}$), de diamètre médian $d_{50} \approx 0,6 \text{ mm}$ (vitesse de chute $W_s = 1,95 \text{ cm/s}$). L'échelle géométrique étant de l'ordre de 1/9 par rapport aux plages naturelles (la similitude de Froude implique une échelle de temps d'environ 1/3), ce choix de sédiment permet de respecter la similitude du transport sédimentaire (nombres de Shields et de Rouse en particulier). Des houles irrégulières (spectre de JONSWAP) respectant une distribution de Rayleigh se propagent et déferlent sur la plage de sédiments.

La stratégie retenue consiste, une fois un profil d'équilibre barré obtenu, à réaliser une série de rechargements en étudiant le devenir du matériel rajouté.

Tableau 1: Les trois scénarios de forçage hydrodynamique retenus.

	Hs (m) (sur les fonds de -6m)	Ts (s)
Tempête exceptionnelle TE	4	10 s
Tempête classique TC	2,5	7 s
Tombant de tempête TT	1	6,5 s

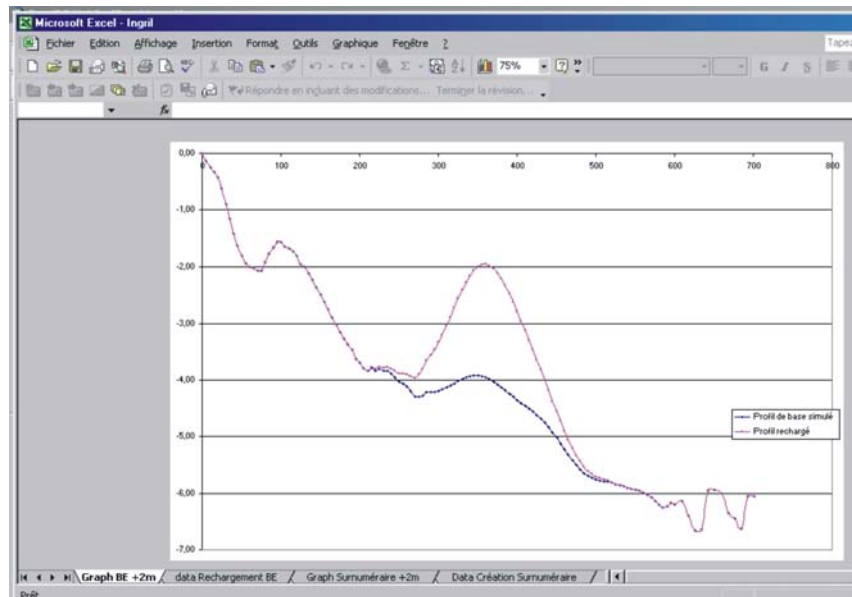


FIG. 1 : Exemple de rechargement d'avant-côte pour Ingril avec représentation d'un onglet de graphique correspondant. En bleu le profil naturel ; en rose le profil recharge qui fera l'objet de modélisation.

3. Résultats

Les résultats des simulations numériques et physiques diffèrent notablement. Ils seront présentés séparément puis une synthèse/discussion sera réalisée à partir des conclusions.

3.1 Les modèles numériques

3.1.1 Modhys

La figure 2 présente un exemple de résultats obtenus à l'aide de Modhys pour un cas de rechargement surnuméraire. On constate que malgré la réalisation du rechargement au large, la barre interne subit une érosion notable et que l'énergie incidente arrivant à la plage est importante.

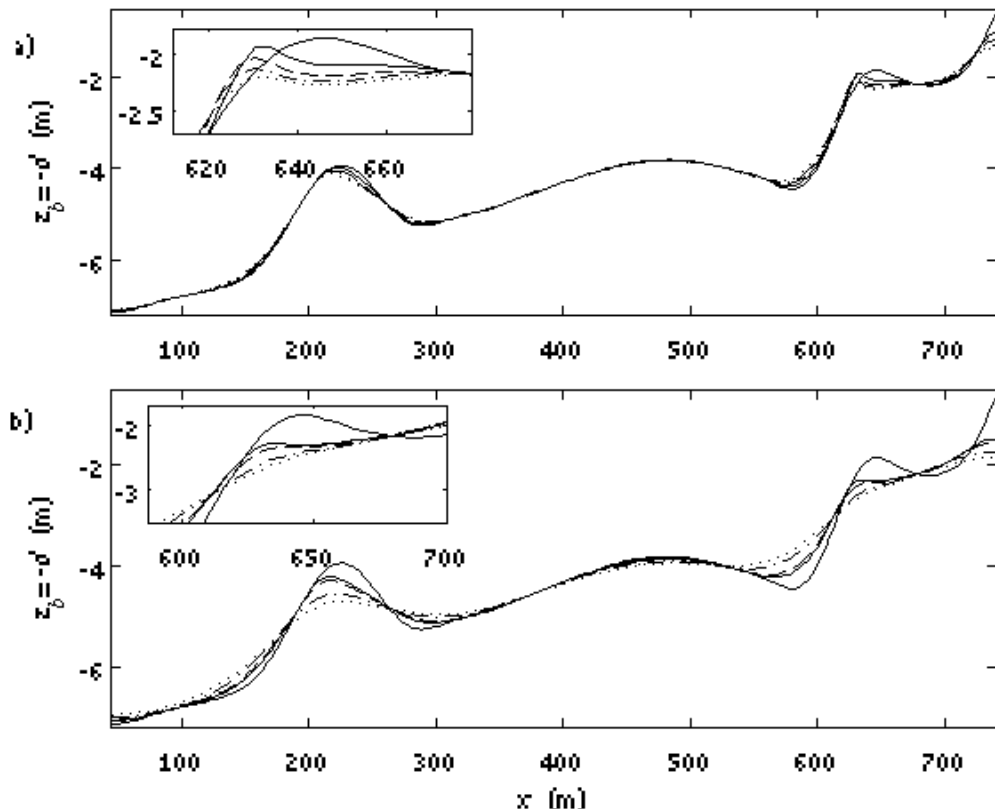


FIG. 2 : Evolution à Sète du profil de bathymétrie à 3 barres (—) pour différentes heures à partir du début d'une tempête classique : (a) (—) $t=1h$, (- -) $t=2h$, (- \circ -) $t=3h$, (...) $t=4h$, (b) (—) $t=6h$, (- -) $t=8h$, (- \bullet -) $t=16h$, (...) $t=24h$.

Dans l'ensemble, à l'échelle de temps de la tempête de 24h, les simulations réalisées à l'aide de Modhys ne semblent pas très favorables aux rechargements d'avant-côte. Les rechargements par création d'une barre surnuméraire ne jouent

qu'un rôle très faible de brise-lame immergé, alors que les rechargements directement sur la barre externe semblent eux plus favorables en terme de dissipation de l'énergie et de transport de sédiment vers la côte.

On peut aussi noter que les conditions initiales du profil de plage jouent un grand rôle et qu'on peut observer des comportements différents du système interne en fonction de la forme initiale du profil d'avant-côte (le rechargement surnuméraire apparaît comme une bonne solution pour Petit-Travers par exemple). Il apparaît dès lors que toute généralisation est difficile et que chaque cas reste un cas d'étude particulier.

3.1.2 S-Beach

Les résultats sont ici illustrés pour la plage du Petit-Travers. On observe sur ce profil une diminution assez importante de la perte de sable pour la plage grâce au recharge sur la barre externe et aucun changement pour le recharge surnuméraire. De surcroît, la barre externe réapprovisionnée a atténué le recul du rivage contrairement au profil avec recharge surnuméraire (Figs. 3 et 4). Par conséquent pour ce site, le recharge sur barre externe peut être une solution alternative pour atténuer l'érosion de cette plage pendant des événements extrêmes.

En conclusion pour ce modèle qui permet de bien prendre en compte l'évolution de la plage émergée, le recharge sur la barre externe semble être plus efficace que le recharge surnuméraire sur tous les profils mais ne permet une diminution de l'érosion par rapport au profil initial que sur deux avant-côtes, Maguelonne et Petit-Travers. Ces spécificités par rapport aux conditions des profils initiaux de plage sont identiques à ce qui avait été diagnostiquée par le modèle Modhys.

Il semble par ailleurs que les temps des simulations ne soient pas assez longs, notamment en situation de tombant de tempête, pour voir des évolutions positives pour la berme de la plage, ce qui est pourtant observé en nature.

3.1.3 Télémac

Le modèle Télémac utilisé pour des tempêtes de 24 h avec Hs constante montre globalement les mêmes types de conclusion que les deux précédents modèles. Cependant, la situation diffère si on élargit l'échelle de temps considérée, et qu'on rallonge notablement la durée de la phase de tombant de tempête (Fig. 5).

En opposition, on remarque alors que le recharge surnuméraire évolue peu mais que la tendance de la barre interne est à la migration vers la côte, l'érosion de la plage étant par ailleurs atténuée. On montre finalement avec TELEMAC que

pour des situations de simulations sur des temps plus longs (10j) en situation de tombant de tempête ou de petites houles pour une création de barre surnuméraire, les conclusions sont beaucoup plus nuancées. Les résultats apparaissent plus favorables et plus en similitude avec ce qui a pour l'instant été observé en milieu naturel et en canal à sédiment.

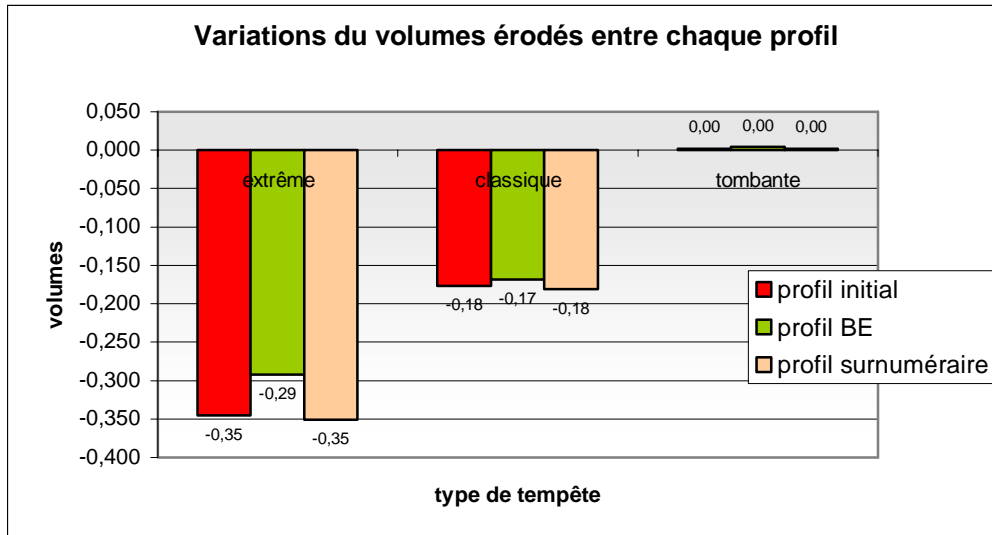


FIG. 3: Variation des volumes de sables sur la plage du Petit-Travers en fonction des types de rechargement surnuméraire ou barre externe (BE)

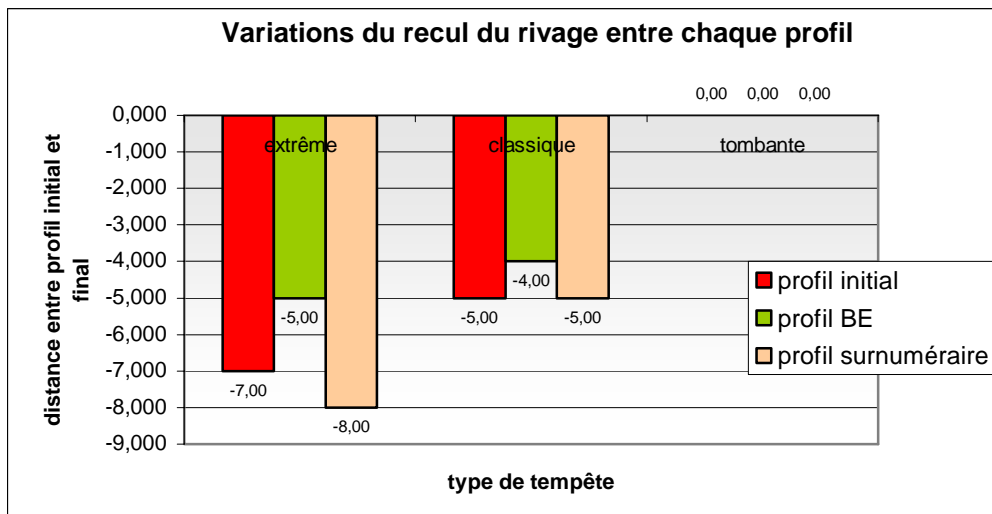


FIG. 4: Histogramme des variations du recul du rivage en fonction de chaque profil sur la plage du Petit-Travers

3.1.4 Conclusions pour la modélisation numérique

Le fait de créer une troisième barre surnuméraire au large n'a pas d'effet sauf si cette barre est suffisamment volumineuse, assez près du bord ou en position bathymétrique suffisamment haute sur le profil pour créer un déferlement de la houle. Ce qui n'était pas dans la plupart des cas élaborés et simulés.

Le rechargement directement sur les barres externes est la méthodologie qui semble la plus efficace pour diminuer l'action de la houle à la côte lors d'une tempête mais l'énergie reste importante dans le système interne, ce qui amène à penser que cette solution puisse être accompagnée aussi par du rechargement de plage. Il est important de noter que ces observations sont faites pour des situations de tempêtes caractéristiques de la zone étudiée (24h) mais que les résultats diffèrent si on simule sur des temps plus longs.

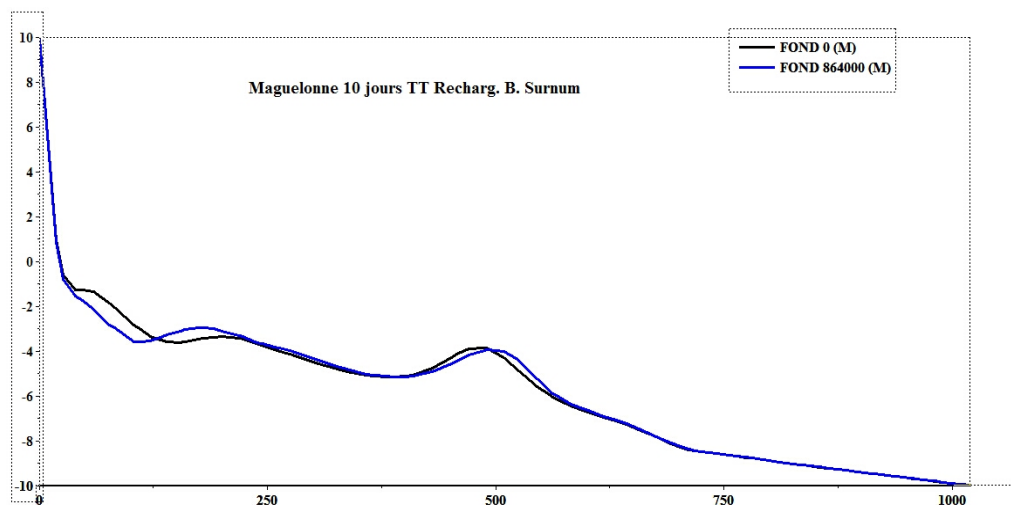


Fig. 5: Simulation à Maguelone pour un temps long de 10 jours (en noir le profil initial, en bleu le profil final) en situation de tombant de tempête.

Les simulations sur des temps plus longs (plusieurs jours) de faible agitation sont très favorables à la remontée de matériel de l'avant-côte vers la plage, comme cela a pu être observé sur les sites méso-tidaux hollandais et pour le modèle physique. Cette meilleure prise en compte du temps semble avoir une influence prépondérante sur la qualité des résultats alors que l'on pensait initialement que les problèmes survenaient des formules de transport utilisées qui ne prenaient pas assez en compte le charriage, qui joue un grand rôle dans la remontée du sédiment vers la côte.

Le scénario retenu au départ de simulation de fortes tempêtes définies par une Hs constante sur 24h induit une exagération des réponses observées et une

minoration des effets des rechargements d'avant-côte. En effet, c'est uniquement lors de la phase de tombant successive à la tempête (non simulées ici) que les phases d'accrétion surviennent.

La réponse des différents profils testés n'est pas uniforme et dépend des conditions morphologiques intrinsèques du site.

Enfin, on observe des difficultés à modéliser l'évolution de la plage émergée.

3.2 Le modèle physique

3.2.1 Description des résultats

On note par exemple (figure 6) que le sédiment rechargé sur la barre externe dans des conditions de tempête classique en simulant un montant et un tombant de tempête pour des correspondances en temps réel de 10 jours participe à la construction de la barre et que du sédiment vient se placer en haut de plage en construisant une berme en fin de tempête. Il faut noter que la plage émergée est érodée durant le montant et engrasse seulement durant le tombant.

3.2.2 Conclusions pour la modélisation physique

On remarque en canal à houle et sédiment une bonne efficacité des rechargements d'avant-côte, quelle que soit leur position sur le profil, du moment que le tombant de tempête est suffisamment long et bien modélisé et que les conditions d'agitations ne sont pas extrêmes.

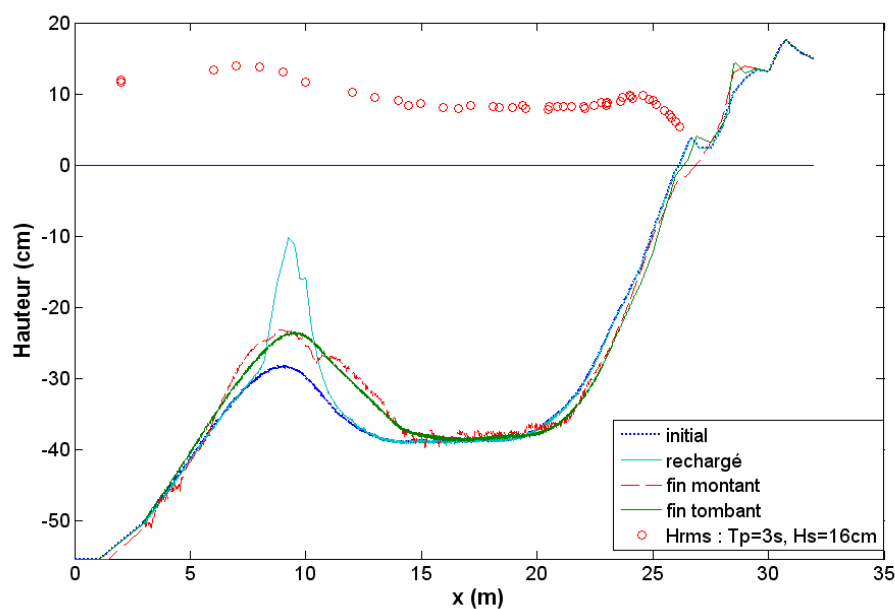


Fig. 6 : Rechargement sur la barre externe. Evolution des profils de fond et mesures des vagues de fin de montant au cours d'une tempête caractéristique.

Pour des conditions de tempêtes qui se rapprochent (car les dimensions du canal ne permettent pas de créer de fortes tempêtes) des tempêtes exceptionnelles simulées numériquement, on observe par contre des érosions du rechargement et une remontée difficile du matériel post-tempête.

La méthodologie qui consiste à découper la tempête en deux phases, le montant et le tombant s'avère payante et valide. L'analyse séparée de ces deux phases permet de montrer que la phase de montant érode et que la phase de tombant engrasse la plage. C'est surtout le tombant de tempête qui conditionne la réponse finale. C'est donc le ratio entre ces deux phases, peut être plus que la hauteur maximum lors de l'apex de la tempête, qui conditionne la réponse du profil. Ceci permet d'expliquer une bonne part des divergences entre modèles numériques et modèle physique. Cela souligne aussi le problème des études in-situ qui ne permettent pas, par des approches de bathymétrie classiques avant et après tempêtes, de diagnostiquer l'évolution réelle du profil pendant le forçage.

Dans ce cadre, on peut aisément imaginer que ce sont les successions rapprochées de tempêtes qui auront les effets les plus dévastateurs pour les rechargements.

4. Discussion et comparaison des deux types de modélisations

L'utilisation conjointe de modèles numérique et d'un modèle physique s'avère efficace. Les modèles numériques simulent bien l'érosion, tout en l'exagérant dans certains cas ; à l'inverse le modèle physique reproduit bien les phases d'accrétion et d'engrissement de la plage mais les réductions d'échelles réalisées, le place de fait dans des situations plutôt favorables de tempête classique. L'approche croisée permet de diagnostiquer précisément le principal point de divergence des réponses des deux approches de simulations : pour les modèles numériques la tempête est mal discrétisée et le temps de tombant minoré ; alors que la phase de tombant de tempête est clairement identifiée dans le canal comme le seul moment du retour du sable vers la côte.

L'analyse détaillée des échelles temporelles entre les modèles numériques et le modèle physique montre l'influence forte des durées de simulations considérées. Dans le canal, l'équivalent nature des tombants de tempête serait de plusieurs jours, alors que les modèles numériques s'attachent surtout à simuler l'évolution du rechargement à l'échelle événementielle (tempête de 24 h par exemple en configuration d'apex permanent). Lorsqu'on teste numériquement des simulations plus longues de faible houle, les résultats des modèles numériques convergent

vers celui des expérimentations en canal. Dans le futur, seuls des modèles capables de simulations sur des temps longs (saisonniers par exemple) devront servir aux diagnostics d'études appliquées comme les rechargements. Mais ces modèles restent à construire et doivent passer par des validations sur des cas *in-situ* mesurés, comme les cas de rechargements hollandais méso-tidaux.

5. Conclusion

L'utilisation de techniques scientifiques performantes s'avère une solution efficace pour l'aide au diagnostic dans les études appliquées, même si l'amélioration des modèles doit rester une priorité. Ce projet peut constituer un des outils à venir visant à orienter le choix des aménageurs du littoral parmi un ensemble de solutions possibles vers une solution douce, économiquement compétitive, et ayant un impact paysagé minimal.

Remerciements. – Nous remercions le programme LITEAU du MEDAD qui a permis cette étude, ainsi que la communauté européenne et les gestionnaires locaux de la région Languedoc-Roussillon pour leur intérêt pour cette thématique.

6. Références bibliographiques

- ¹ BASINSKI, T., & SZMYTKIEWICZ, M., 1991. *Effectiveness of different artificial nearshore and beach nourishment technologies*. Proc. 3rd Int. Conf. On Coastal and Port Eng. In Developing Countries, Kenya, vol. 1.
- ² BURKE, C.E., MCLELLAN, T.N., & CLAUSNER, 1991. *Nearshore berms- Update of the United States Experience*. CEDA-PIANC Conference, Amsterdam, The Netherlands.
- ³ FOSTER, G.A., HEALY, T.R., & DE LANGE, W.P., 1994. *Sediment budget and equilibrium beach profiles applied to renourishment of an ebb tidal delta adjacent beach, Mt Maunganui, New Zealand*. J. of Coas. Res., 10, N°3, 564-575.
- ⁴ GRUNNET, N.M., RUSSINK, B.G. AND WALSTRA, D.-J. R., 2005. *The influence of tides, wind and waves on the redistribution of nourished sediment at Terschelling, The Netherlands*. Coastal Eng., 52: 617-631.
- ⁵ HOEKSTRA, P., HOWMAN, K.T., KROON, A., RUSSINK, G., ROELVINK, J.A. & SPANOFF, R., 1996. *Morphological development of the Terschelling shoreface nourishment in response to hydrodynamic and sediment transport process*. Proceedings 25th International Conference on Coastal Engineering 1996, 2897-2909.

- ⁶ NOURTEC, 1997. *Innovative Nourishment Techniques Evaluation- Final Report*. Coord. Rijkwaterstaat, National Institute of Coastal and Marine Management/ RIKZ, The Hague, The Netherlands, 105 pp with figures.
- ⁷ SPANHOFF, R., BIEGEL, E.J., BURGER, M., & DUNSBERGEN, D.W., 2003. *Shoreface nourishments in the Netherlands*. Proceedings of Coastal Sediment 2003.
- ⁸ SPIELMANN K., 2002, *Modélisation de la dynamique morphologique d'un profil de plage*, Thèse de doctorat, Univ. de la Méditerranée, 270 p.
- ⁹ VAN DUIN, M.J.P., WIERSMA, N.R., WALSTRA, D.J.R., VAN RIJN, L.C. & STIVE, M.J.F., 2004. *Nourishing the shoreface: observations and hindcasting of the Egmond case, The Netherlands*. Coastal Eng., 51: 813-837.

Etudes expérimentales des profils cross-shore de plages sableuses

**Florent GRASSO¹, Eric BARTHELEMY¹, Raphaël CERTAIN²,
Hervé MICHALLET¹**

¹ CNRS-UJF-INPG, LEGI, BP 53, 38041 Grenoble Cedex 9, France

florent.grasso@hmg.inpg.fr

eric.barthelemy@hmg.inpg.fr

herve.michallet@hmg.inpg.fr

² IMAGE EA4218, Université de Perpignan, 52 av. Alduy,
66000 Perpignan Cedex, France

certain@univ-perp.fr

Résumé :

Les principaux objectifs de cette étude sont d'une part de tester en canal le concept d'équilibre morphologique pour un climat de houle donné. Nos expériences se sont déroulées dans le canal à houle à fond sédimentaire du LEGI. Nous avons pu mettre en évidence huit climats de houle menant à un équilibre morphologique. Des profils d'équilibre ont pu être classés en fonction du nombre de Dean. D'autre part, l'évolution des profils de fond reproduit bien les différents scénarios que nous observons en nature, tels que l'érosion ou l'accrétion sédimentaire du haut de plage et les migrations de barres.

Abstract:

The main objectives of this study are on one end to test with a physical model the concept of equilibrium beach profile for a wave climate. Our experiments were conducted in the sedimentary LEGI wave-flume. We were able to identify eight wave climates leading to an equilibrium. Equilibrium profiles have been sorted according to their Dean number. On the other end, the evolution of profiles correctly reproduces the different scenarios observed in nature, such as erosion and sediment accretion at the shore and bar migrations.

Mots-clés :

Houle irrégulière – morphodynamique – profils d'équilibre – canal à houle.

1 Introduction

La morphodynamique des plages sableuses est au centre du problème de l'érosion des littoraux. La direction des flux sédimentaires *cross-shore* est un point clé des outils de prédiction et il est fortement corrélé aux caractéristiques non-linéaires des vagues incidentes, comme l'asymétrie et le *skewness* (Bailard¹, 1981 ; da Silva *et al.*⁵, 2006). Cette complexité est très difficile à reproduire avec des modèles numériques, ainsi la modélisation physique devient une alternative intéressante.

Les outils habituels utilisés en ingénierie pour l'évolution *cross-shore* considèrent des profils d'équilibre (Dean⁸, 1991 ; Miller & Dean²¹, 2004) comme profils cibles. Ces profils se justifient par la notion d'énergie de dissipation volumique des vagues uniforme en zone de *surf* (Dean⁷, 1977 ; Wang *et al.*²³, 2003). Pour les profils de plage à l'équilibre, le flux sédimentaire moyen *cross-shore* est nul. Partant de cet état de fait Bowen³ (1980) et Dronker¹¹ (2005), utilisant une estimation simplifiée du flux sédimentaire, montrent que ces profils sont aussi compatibles avec un équilibre entre une force destructive comme la gravité et une force constructive comme le transport sédimentaire par charriage dû aux vagues. Ainsi, la notion de profil de plage à l'équilibre semble raisonnable. Un de nos objectifs est de tester ce concept d'équilibre morphologique avec un modèle physique, sachant que la plupart des études en laboratoire se sont focalisées sur l'érosion ou la formation de barre en zone littorale (Dette & Uliczka⁹, 1987 ; Dette *et al.*¹⁰, 2002 ; Dally⁶, 1987).

Du fait du perpétuel changement de climat de houle en nature, les profils d'équilibre peuvent être retrouvés à partir de profils moyens annuels. Différents profils d'équilibre peuvent correspondre à chaque saison, reliés à un climat de houle défini (Larson & Kraus¹⁹, 1994). Les expériences en canal peuvent surmonter l'inconvénient de définir un profil de plage à l'équilibre comme une moyenne temporelle. Pour des temps d'expérience suffisant, des profils d'équilibre pourront être atteints (Grasso *et al.*¹⁴, 2007 ; Michallet *et al.*²⁰, 2007 ; Wang & Kraus²², 2005 ; Kamalinezhad¹⁷, 2004 ; Kamalinezhad¹⁸, 2004).

Les profils de plages sont plus compliqués qu'un simple profil d'équilibre de Dean. Ils tendent à avoir une convexité proche du trait de côte et une partie concave plus au large. Ces profils de type terrasse sont observés dans les environnements dominés par la houle (Wright & Short²⁴, 1984). Les barres au large sont également fréquemment observées sur les profils de plage.

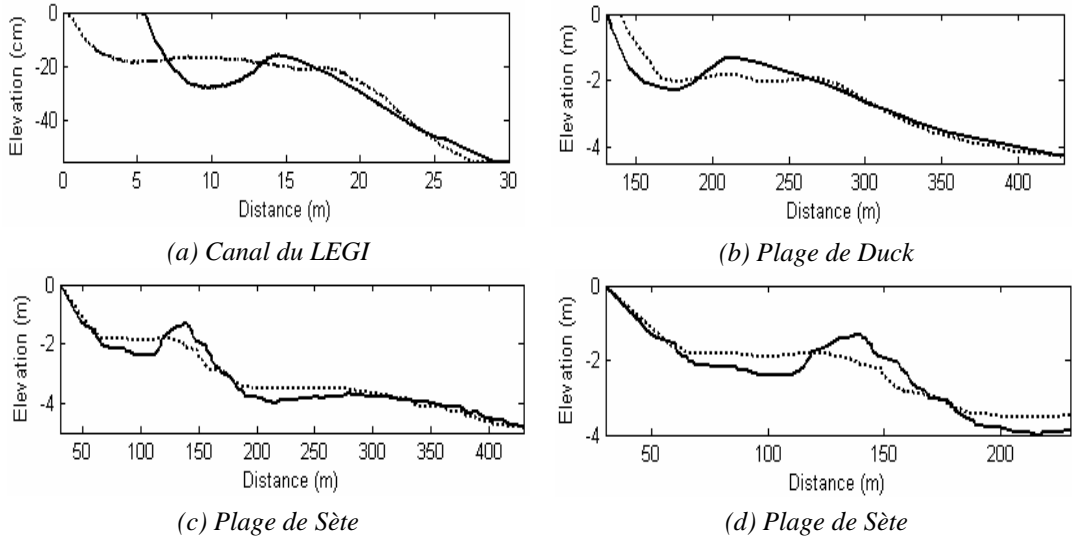


Figure 1. Profils de fond : a) canal LEGI b) Duck, 20 oct 1994 Y1250 (—) et 7 septembre 1994 Y1113 (...) c) et d) Sète, 25 nov 2000 (—) et 1 nov 2000 (...).

Nous avons examiné deux sites : la plage du Lido à Sète (Certain & Barusseau⁴, 2005) et celle de Duck en Caroline du Nord (campagne Duck94). Ces plages sont caractérisées par une houle principalement frontale et par de faibles variations *long-shore* du profil de fond. Elles se rapprochent ainsi des profils de plage *cross-shore* expérimentaux barrés ou de type terrasse (Figure 1). Nous pouvons définir, à l'échelle de l'année, une profondeur de coupure de la plage de Sète vers -5 m qui se situe à environ 400 m du trait de côte (Figure 1.c), et vers -4.5 m à 300 m du trait de côte pour la plage de Duck (Figure 1.b). En appliquant une réduction d'échelle géométrique de l'ordre de 1/10, nous remarquons une forte similitude entre les profils de fond des plages naturelles et ceux obtenus en canal (Figure 1.a). Cela est particulièrement visible en terme de positionnement de la barre par rapport au trait de côte et des profondeurs d'eau au niveau de sa crête et son creux.

Notre étude vise à mieux comprendre les liens entre les caractéristiques de la houle et l'évolution long terme de la morphologie des plages. Très peu d'expériences ont été menées sur ces questions car elles requièrent une durée très longue (plusieurs dizaines d'heures en laboratoire, Kamalinezhad¹⁷, 2004). Selon Wright & Short²⁴ (1984) le nombre de Dean permet de classer les profils de plage *cross-shore*, nous pouvons le calculer de la manière suivante :

$$\Omega = \frac{H_s}{T_p w_s} \quad (1)$$

où H_s est la hauteur significative des vagues au batteur, T_p la période pic du

spectre des vagues et w_s la vitesse de chute du sédiment. Ce nombre peut être interprété comme la mobilisation de la particule par les vagues pendant sa chute. Pour un même nombre de Dean, deux profils de fond seraient similaires. Pour nos expériences, $\Omega < 5$, ce qui dans la classification de Wright & Short²⁴ (1984) correspond à des plages dites réflectives et intermédiaires, caractérisées par des barres *long-shore* ou cycliques, des terrasses à double convexité (Black *et al.*², 2002) et des profils raides uniformes.

2 **Dispositif expérimental**

Les expériences se sont déroulées dans un canal de 36 m de long et 55 cm de large équipé d'un générateur de vague de type « piston ». La profondeur d'eau au batteur est de 55.3 cm. Le fond du canal est constitué de sédiment mobile de faible densité ($\rho = 1.19 \text{ g/cm}^3$) ayant un diamètre moyen $d_{50}=0.6 \text{ mm}$. Le lit sédimentaire recouvre un faux fond rigide pour certains essais. Les nombres de Froude, Shields et Rouse sont du même ordre de grandeur que ceux des plages naturelles. Les échelles de temps et de longueur sont environ 1/3 et 1/10. Des houles irrégulières sont générées (spectre d'énergie de type JONSWAP - facteur de pic = 3.3). Nous vérifions que ces vagues respectent la distribution de Rayleigh à 2 m du batteur. Douze sondes à vagues (acquisition à 50 Hz), montées sur des chariots, enregistrent l'élévation instantanée de la surface libre et permettent de mesurer la hauteur quadratique H_{rms} ($H_{rms} \sim 0.7H_s$) et la période pic des vagues (T_p) (Tableau 1). Les profils de fond sont relevés entre chaque série de vagues grâce à un profileur acoustique monté sur un chariot motorisé.

Tableau 1. Climats de houle générés dans le canal, utilisés pour cette étude.

Série	H_s (mm)	T_p (s)	Ω	Durée (h)	Temps pour atteindre l'équilibre (h)	Type
A	30	2	0.8	9	6	estival
B	60	1.5	2	82	70	
C1	107	2	2.7	41	25	tombant de tempête
C2	107	2	2.7	52	35	tombant de tempête
D	160	3	2.7	115	45	tempête
E	107	1.4	3.9	7	4	
F	125	1.6	4	33	30	
G	160	2	4.1	30	30	

3 Résultats et discussions

3.1 Profils de fond à l'équilibre

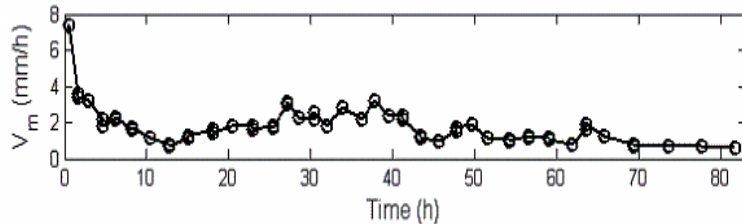


Figure 2. Vitesse moyenne d'évolution des profils de fond calculée pour la série de vagues B.

L'état d'équilibre du fond est déterminé par le calcul de la vitesse moyenne:

$$V_m = \frac{1}{l_p} \int_1^{l_p} \left| \frac{dh_s}{dt} \right| dx \quad (2)$$

où l_p est la longueur du profil de fond étudié, h_s la hauteur de sédiment le long du profil et t la durée de génération des vagues. Nous estimons avoir atteint l'équilibre lorsque $V_m \sim 1$ mm/h (environ 70 heures pour la série B, cf. Figure 2). Nous obtenons ainsi huit conditions d'équilibre morphologique (Figure 3).

Le temps nécessaire à l'obtention des états d'équilibre peut être plus ou moins long en fonction de l'éloignement du profil de fond initial au profil de fond final (par exemple pour A et E l'équilibre est très vite atteint: 6 et 4 h). Notons que la présence du fond fixe ne semble pas limiter l'érosion et influencer la dynamique sédimentaire (profils similaires Figure 3.f, g et h). Pour des profils de fond initiaux différents, les profils finaux à l'équilibre sont fortement similaires pour des conditions identiques (C1 et C2). Nous retrouvons le plateau à la même profondeur et les pentes de bas et de haut de plages sont identiques, avec toutefois une différence de positionnement du trait de côte (Figure 3.c, d). L'évolution de profils de fond différents soumis au même climat de houle ne sont pas exactement reproductibles mais similaires en termes de forme. L'action des vagues est limitée à une certaine profondeur, définissant ainsi une plage d'influence. La similarité de forme des profils à l'équilibre pour un climat de houle donné serait donc correcte sur la partie du profil délimitée par la profondeur d'action de cette houle. Cela est clairement visible sur la Figure 3.a: seule la partie haute du profil de fond est remodelée par la série A (pour une profondeur d'eau inférieure à environ 20 cm).

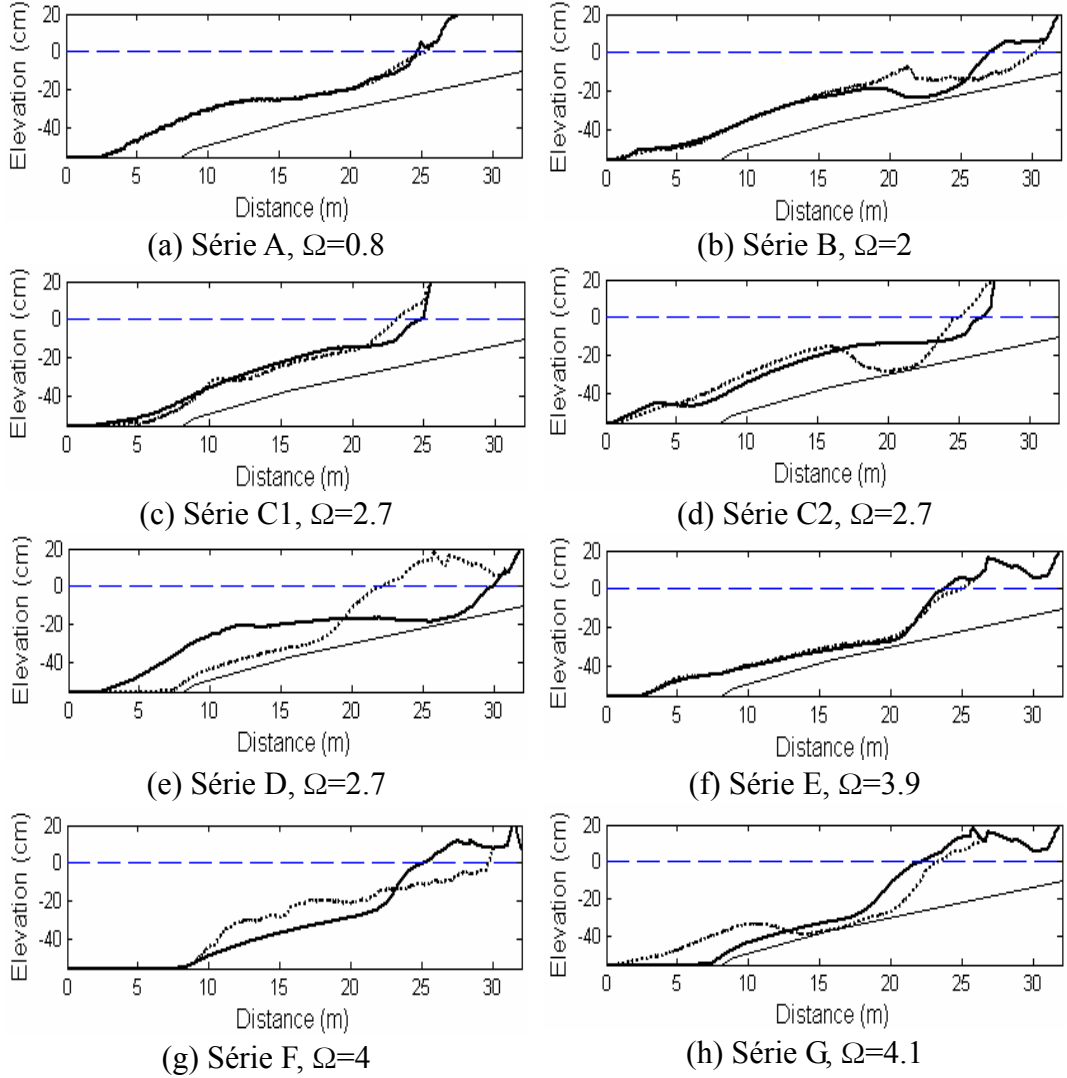


Figure 3. Profils de fond initiaux (...) et finaux à l'équilibre (—) pour huit séries de houles.

3.2 Classification des profils d'équilibre en fonction du nombre de Dean

Wright & Short²⁴ (1984) ont présenté une classification des profils de plage en fonction de Ω (1): les plages dissipatives caractérisées par de faibles pentes et un déferlement glissant ($\Omega > 6$), les plages intermédiaires de pentes modérées et un déferlement plongeant ($1 < \Omega < 6$), les plages réflectives à fortes pentes et déferlement principalement frontal (ou gonflant) pour $\Omega < 1$. Nos expériences permettent de simuler des climats de houle dont le nombre de Dean est compris entre 0.8 et 4.1. Pour les séries A et B (Figure 3.a et b), le bas de plage est considéré comme immobile car l'influence des vagues est limitée aux environs de 20 et 30 cm de profondeur, le profil global est donc peu représentatif du nombre

de Dean. Les profils de fond à l'équilibre des Figure 3.c, d et e correspondent aux séries C1, C2 et D pour lesquelles $\Omega=2.7$: des profils de type terrasse dont la profondeur varie avec l'amplitude de la houle. La pente moyenne des profils (calculée du trait de côte au pied de plage) est de l'ordre de 1/45. Pour les profils d'équilibre des Figure 3.f, g et h (E: $\Omega=3.9$, F: $\Omega =4$ et G: $\Omega =4.1$), nous remarquons des formes très similaires caractérisées par une partie très raide en haut de plage qui s'adoucit ensuite en profondeur. Cela se traduit par des pentes moyennes plus raides avoisinant 1/30. Les profils de plage raides associés à un $\Omega<1$ s'expliquent par un temps de chute du sédiment très court devant la période pic des vagues, privilégiant ainsi le transport sédimentaire par charriage. Le profil est donc influencé par l'association de la granulométrie (à travers la vitesse de chute) et de l'hydrodynamique. Les processus sont plus complexes lorsque le temps de chute du sédiment devient plus important ($\Omega>1$), une particule peut être mobilisée par plusieurs vagues et la présence d'un courant de retour plus ou moins établi pourra influencer la distribution sédimentaire. Nous retrouvons dans ces expériences que les plages intermédiaires peuvent être vues comme la composition d'une partie réfléctrice et d'une autre dissipative.

3.3 Profils de fond transitoires

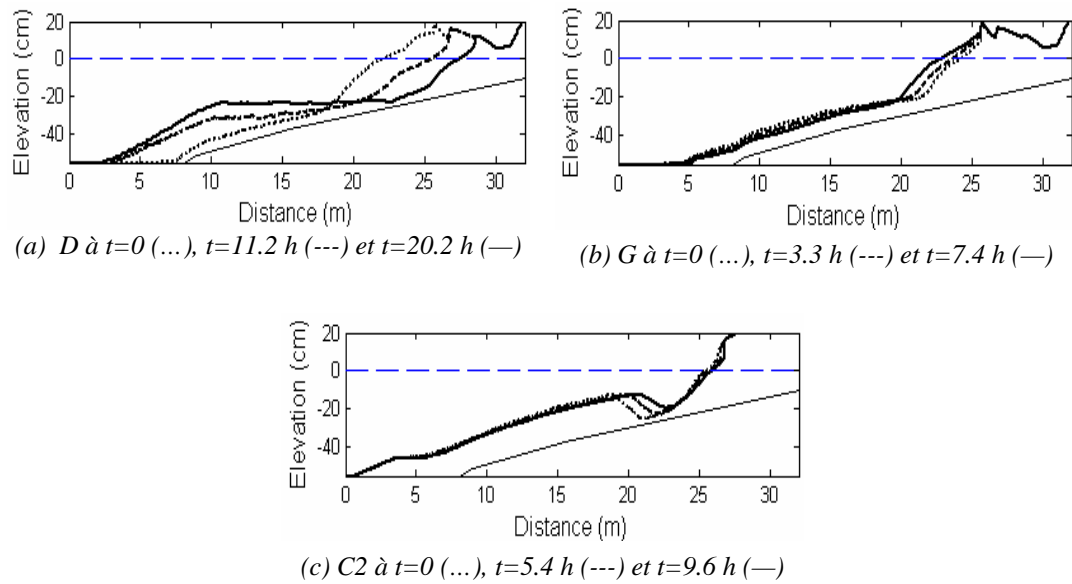


Figure 4. Profils de fond transitoires caractéristiques : érosion du haut de plage (a), accrétion du haut de plage (b) et migration de barre vers la côte (c).

Un profil de fond est défini comme « transitoire » quand sa morphologie évolue en fonction du temps pour un climat de houle généré, cela se visualise par une

vitesse moyenne d'évolution importante. Prenons l'exemple de la Figure 2, suite à un important pic d'intensité (7.4 mm/h) la vitesse moyenne suit une forte décroissance pendant les 13 premières heures d'expérience chutant à 0.7 mm/h, puis cette vitesse augmente à nouveau vers 3 mm/h par pics successifs. Ces variations de vitesse d'évolution sont liées à la formation de barres et leur migration vers la côte.

Nous présentons sur la Figure 4 trois scénarios d'évolutions caractéristiques menant chacun à un état d'équilibre. La Figure 4.a représente une phase d'érosion du haut de plage avec la formation d'un plateau horizontal, qui correspond au passage d'un climat de houle de fort nombre de Dean (série G, $\Omega=4.1$) à un plus faible (série D, $\Omega=2.7$). Cela se traduit par un transport sédimentaire du haut de plage vers le bas, qui vient adoucir la pente moyenne. Nous retrouvons ce type de scénario en nature pour les cas de tempêtes où le profil de haut de plage s'érode et bascule pour former une terrasse plus en profondeur (Günaydin & Kabdasli¹³, 2003).

Le scénario inverse est représenté sur la Figure 4.b avec une accrétion du haut de plage au détriment du bas. Le nombre de Dean fort ($\Omega=4.1$) de la série de houle générée (G) tend à raidir le profil de fond, le sédiment est mobilisé dès le pied de plage pour aller engranger le haut et faire avancer le trait de côte vers le large. Cela est typique des observations faites sur la reconstruction d'un profil de plage après une forte érosion (Certain & Barusseau⁴, 2005).

Enfin, la Figure 4.c met en avant le cas d'une migration de barre vers la côte, sous l'action des vagues C2 la barre se déplace à la manière de la propagation d'une dune avec une asymétrie de forme entre la pente amont (plus raide) et aval. La barre vient alors se coller en haut de plage, suite à un temps de génération de vagues suffisamment long. La dynamique des barres sédimentaires a été largement observée en nature (Gallagher *et al.*¹², 1998 ; Hoefel & Elgar¹⁵, 2003 ; Hsu *et al.*¹⁶, 2006), mais leur discréétisation temporelle reste très limitée. Ainsi, les cas de migration de barre, n'ayant à notre connaissance jamais été simulés auparavant en laboratoire, apportent de nombreuses informations sur la dynamique des plages naturelles.

4 Conclusions

Un des principaux objectifs de cette étude était de tester en canal le concept d'équilibre morphologique pour un climat de houle donné. Grâce à l'utilisation d'un sédiment de faible densité permettant de respecter les similitudes hydro-sédimentaires, nous reproduisons en laboratoire (échelle de réduction géométrique d'environ 1/10) des profils de plages observés en nature (lido de Sète et plage de Duck).

Un équilibre morphologique a été atteint pour huit climats de houle. Nous avons également établi une classification des profils de fond à l'équilibre en fonction du nombre de Dean (Ω): il apparaît clairement une similarité de forme des profils de type « terrasse » pour $\Omega=2.7$ et des profils raides et plus uniformes pour $\Omega\sim4$.

Les profils de fond en régime transitoire reproduisent des scénarios observés en nature : des phases d'érosion ou d'accrétion du haut de plage, mais aussi des cas de formations de barres et leurs migrations vers la côte. Le couplage des différents processus hydrodynamiques (*undertow*, asymétrie des vagues) et sédimentaires (charriage, suspension) étant particulièrement complexe, ces expériences présentent ainsi un intérêt pour la calibration des modèles numériques de morphodynamique.

5 Remerciements

Cette étude a bénéficié du support technique de Jean-Marc Barnoud, de financements LITEAU II et INTERREGIV-Beachmed-e et de données recueillies par l'US Army Corps of Engineers lors de la campagne Duck94 (<http://www.frfr.usace.army.mil/duck94/DUCK94.stm>).

6 Références bibliographiques

- [1] J.A. Bailard. An energetics total load sediment transport model for a plane sloping beach. *J. Geophys. Res.*, 86(C11):10938-10954, 1981.
- [2] K.P. Black, R.M. Gorman, K.R. Bryan. Bars formed by horizontal diffusion of suspended sediment. *Coastal Engineering*, 47(1):53-75, 2002.
- [3] A.J. Bowen. Simple models of nearshore sedimentation; beach profiles and longshore bars. In McCann S.B., editor, *The Coastline of Canada*, volume Paper 80-10:1-11. Geological Survey of Canada, 1980.
- [4] R. Certain, J.-P. Barusseau. Conceptual modelling of sand bars morphodynamics for a microtidal beach (Sète, France). *Bull. Soc. géol. Fr.*, t.176, no 4, pp. 343-354, 2005.
- [5] P.A. da Silva, A. Temperville, F. Seabra Santos. Sand transport under combined current and wave conditions: a semi-unsteady, practical model. *Coastal Engineering*, 53:897-913, 2006.
- [6] W.R. Dally. Longshore bar formation. In *Coastal Sediments'87*, ASCE, 71-86, New Orleans, Louisiana, USA, 1987.
- [7] R.G. Dean. Equilibrium beach profiles: U.S. Atlantic and Gulf coasts. Ocean engineering report no. 12, Department of Civil Engineering, University of Delaware, 1977.
- [8] R.G. Dean. Equilibrium beach profiles: characteristics and applications. *J. Coastal Res.*, 7(1):53-84, 1991.
- [9] H. Dette, K. Uliczka. Prototype investigation on time-dependent dune recession and beach erosion. In *Coastal Sediments'87*, ASCE, 1430-1444, New Orleans, Louisiana, USA, 1987.

- [10] R.G. Dette, M. Larson, J. Murphy, J. Newe, K. Peter, A. Reniers, H. Steetzel. Application of prototype flume tests for beach nourishment assessment. *Coastal Engineering*, 47:137-177, 2002.
- [11] J. Dronkers. *Dynamics of Coastal Systems*, volume 25 of *Advanced Series on Ocean Engineering*. World Scientific, pp.387-414, 2005.
- [12] E.L. Gallagher, S. Elgar, R.T. Guza. Observation of sand bar evolution on a natural beach. *J. Geophys. Res.*, 193(C2):3203-3215, 1998.
- [13] K. Günaydin, M.S. Kabdasli. Characteristics of coastal erosion geometry under regular and irregular waves. *Ocean Engineering*, 30:1579-1593, 2003.
- [14] F. Grasso, H. Michallet, E. Barthélémy. Infragravity waves in mobile-bed laboratory experiments. In *Coastal Sediment 07*, ASCE, New Orleans, Louisiana, USA, 2007.
- [15] F. Hoefel, S. Elgar. Wave-induced sediment transport and sandbar migration. *Science*, 299:1885, 2003.
- [16] T.-J. Hsu, S. Elgar, R.T. Guza. Wave-induced sediment transport and onshore sandbar migration. *Coastal Engineering*, 53:817-824, 2006.
- [17] M. Kamalinezhad. *Plages en équilibre morphologique et hydrodynamique associée*. PhD Thesis, Institut National Polytechnique de Grenoble, France, 2004.
- [18] M. Kamalinezhad. Equilibre morphologique de barres de déferlement: expériences. *VIII^e Journées Nationales Génie Civil - Génie Côtier*, Compiègne, France, 2004.
- [19] M. Larson, N.C. Kraus. Temporal and spatial scales of beach profile change, Duck, North Carolina. *Marine Geology*, 117:75-94, 1994.
- [20] H. Michallet, F. Grasso, E. Barthélémy. Long waves and beach evolution profiles. *J. Coastal Res.*, SI50, 221-225, 2007.
- [21] J.K. Miller, R.G. Dean. A simple new shoreline change model. *Coastal Engineering*, 51:531-556, 2004.
- [22] P. Wang, N.C. Kraus. Beach profile equilibrium and patterns of wave decay and energy dissipation across the surf zone elucidated in a largescale laboratory experiment. *Journal Coastal Research*, 21(3):522-534, 2005.
- [23] T. Wang, B.A. Ebersole, E.R. Smith. Beach-profile evolution under spilling and plunging breakers. *J. Waterway, Port, Coastal and Ocean Eng.*, 129(1):41-46, 2003.
- [24] L.D. Wright and A.D. Short. Morphodynamic variability of surf zones and beaches: a synthesis. *Marine Geology*, 56:93-118, 1984.

Etude de faisabilité par modélisation numérique et canal à sédiment de rechargements sédimentaires sableux d'avant-côte en milieu microtidal, une nouvelle méthode de lutte contre l'érosion côtière.

Raphaël Certain¹, Dominique Astruc², Karine Spielman², Philippe Larroudé³, Hervé Michallet³, Florent Grasso³, Barthélémy Eric³, François Sabatier⁴, Jean-Paul Barusseau¹

¹Université de Perpignan Via Domitia, E.A. 3678 IMAGES, 52 av P. Alduy, 66860 Perpignan Cedex, France (certain@univ-perp.fr)

²Institut de Mécanique des Fluides de Toulouse (IMFT), UMR 5502 CNRS/INPT/UPS, Allée du Pr. Soula, 31400 Toulouse, France.

³Laboratoire des Ecoulements Géophysiques & Industriels (LEGI), UMR CNRS 5519, BP 53 38041 Grenoble Cedex 9

⁴CEREGE, Europôle Méditerranéen de l'Arbois, BP 80, 13545 Aix en Provence cedex 04, France

Les communes littorales méditerranéennes souffrent dans leur grande majorité de problèmes d'érosion de leurs littoraux sableux ; qu'ils soient liés aux conditions de l'évolution naturelle des milieux ou qu'ils soient induits par des aménagements antérieurs. Ceci entraîne un coût important de lutte contre ces phénomènes et des conséquences socio-économiques sur le tourisme et les activités nautiques. Une des méthodes de restauration les plus courantes consiste à recharger la plage émergée en sable, procédé toutefois pénalisé par la limitation des sources de sable disponibles et par des contraintes fortes pesant sur le respect des critères granulométriques. Le matériel sableux à disposition a souvent une granulométrie trop faible par rapport au matériel *in situ*, ce qui le rend très instable. L'idée vient alors de prélever ce sédiment en mer et de recharger directement dans les petits fonds ayant une granulométrie plus compatible. Les avantages de cette technique de recharge (mis en évidence dans le programme du MEDD LITEAU I) résident dans un coût limité par la réduction du transport du matériel de recharge, dans l'utilisation de matériel granulométriquement favorable et dans la proposition d'une méthode « douce », sans impact paysager, respectueuse de l'environnement.

Ceci, cependant, ne peut être réalisé sans étude préalable. Deux programmes en cours actuellement LITEAU II (MEDD) et GESA Beachmed-e (Programme européen Interreg III C) étudient un certain nombre de scénarios de rechargements d'avant-côte à l'aide de plusieurs modèles numériques complémentaires et de simulations en canal à sédiment. Les équipes de l'IMFT, du LEGI, du CEREGE et d'IMAGES (LEGEM UPVD) testent en particulier la faisabilité de tels rechargements à l'aide des modèles Modys, de la plateforme Télémac, de S-Beach sur les différentes avant-côte microtidales sélectionnées dans le cadre de ces programmes. Des scénarios impliquant des volumes sédimentaires différents ainsi que différentes conditions de force caractéristiques de la zone sont étudiés.

Les auteurs présenteront les résultats techniques de mi-parcours obtenus, les programmes comportant par ailleurs des volets sur l'impact biologique de ces rechargements et la faisabilité économique des différents scénarios.

Ce projet peut constituer un des outils à venir visant à orienter le choix des aménageurs du littoral parmi un ensemble de solutions possibles vers une solution douce, économiquement compétitive, et ayant un impact paysagé minimal.

Simulations morphodynamiques long terme pour la protection du littoral

Philippe Larroudé

LEGI
BP 53 38041 Grenoble, France,
larroude@hmg.inpg.fr

Résumé :

L'utilisation des barres en mer pour combattre l'érosion des plages, remonte aux années 90, et est basée sur le fait qu'elles représentent un réservoir substantiel de sédiment. De plus, le rôle essentiel que ces barres peuvent jouer dans la réduction de l'énergie des vagues a été démontré par des études récentes. Par conséquent, travailler à renforcer les barres existantes ou même à ajouter des barres supplémentaires est une approche prometteuse, parce qu'elles constituent une ligne de défense et respectent l'environnement. Le premier objectif de cette étude est de montrer que la simulation numérique peut être un outil d'aide à la décision pour définir le meilleur emplacement de recharge. Le deuxième but de cette étude est de définir une méthodologie pour simuler les conditions atmosphériques réelles sur une saison, un an ou une décennie grâce à un nombre approprié d'événements climatiques représentatifs.

Abstract :

The use of offshore bars to fight beach erosion, dating back to the 90th, was based on the fact that they represented a substantial reservoir of sediments. That theory turned out to be irrelevant, as beach nourishment requires coarser grain sizes. However, the essential role these bars can play in wave mitigation was demonstrated by recent studies. Hence, working on reinforcing existing bars or even adding extra bars is a convincing approach, for they constitute a line of defence with no visual impact and are therefore environment-friendly. The method offers the added benefit of tapping abundant fine sands, easily available offshore, to build up the bars.

All these assumptions should, of course, be systematically checked, the purpose of the exercise being to assess, through mid-term and long-term bathymetric evolution simulation, the consequences of the implementation of offshore bar nourishment and define the best location. The second aim of this study is to define a parameterization of the screenplay of the weather condition over a season, one year or a decade in an appropriate number of climatic events for the simulation.

Mots-clefs :

Modélisation ; Evolution morpho-dynamique ; Rechargement sédimentaire

1 Introduction

Le présent projet de recherche vise à étudier la possibilité d'utiliser les barres sédimentaires d'avant-côte dans la lutte contre l'érosion des plages sableuses. Ces barres constituent des stocks disponibles de sable, susceptibles d'être utilisés (Hamm *et al.*, 2002). Les avantages de cette technique de rechargement résident dans un coût limité grâce à la réduction du transport, dans l'utilisation de matériel granulométriquement favorable et dans la proposition d'une méthode « douce », sans impact paysagé, respectueuse de l'environnement.

A partir de la sélection d'un site naturel pilote (voir figure 1, collaboration avec l'université de Perpignan, Certain (2002)), l'étude repose sur la modélisation numérique saisonnière des processus mis en jeu pour ce type de configurations. Certain & Barusseau (2006) montrent que l'évolution morphodynamique des barres d'avant côte dans un environnement micro-tidal et un régime modéré bimodal de vague suit deux modèles conceptuels différents, le principal étant un modèle saisonnier en conformité avec le cycle observé des conditions hydrodynamiques.

Nous avons étudié l'évolution morphologique de ces barres et des rechargements en utilisant une combinaison d'un modèle 2DH commercial et d'un modèle de Multi1DH (Camenen et Larroudé, 2003, 2003b). Nous avons effectué ces simulations à long terme pour estimer l'impact sur l'hydrodynamique et sur l'évolution locale de fond marin dû au placement de la barre sableuse de rechargement de longueur finie. L'évolution morphologique de ce rechargement est étudiée pour différents emplacements dans la région littorale.

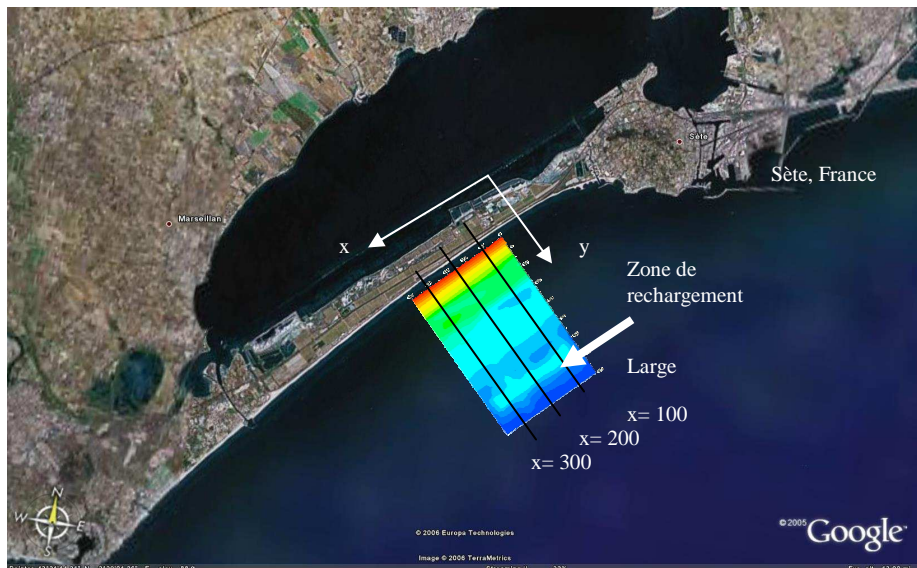


FIG. 1 – Site de « la plage de la Corniche » à Sète montrant la zone modélisée ainsi que l'emplacement du rechargement et des profils cross-shore ($x=100$, 200 et 300 m) utilisés pour les comparaisons avec les données in-situ.

2 Les modèles numériques

Les calculs numériques ont été réalisés à l'aide de la chaîne de calcul Telemac (LNHE-Chatou, 2002). Ce code constitue un modèle complet utilisant la méthode des éléments finis, permettant la réalisation de différents calculs hydrodynamiques sédimentaires.

La modélisation de la houle se fait par l'intermédiaire du code Artemis qui résout l'équation de Berkhoff avec intégration des processus de dissipation par déferlement et frottement sur le fond. La modélisation des courants se fait en utilisant le code Telemac2d (résolution des équations de Barré Saint-Venant) ; le transport solide est simulé à l'aide du code Sisyphe (résolution de l'équation de conservation de la matière).

La modélisation du transport sédimentaire se fait à l'aide du code Sisyphe, pour lequel différentes formulations peuvent être utilisées pour prendre en compte les effets combinés de la houle et du courant de houle sur la remise en suspension et le transport du sédiment.

Il est important de choisir la formule de transport la plus appropriée à notre domaine d'étude afin d'obtenir les résultats les plus réalistes possible. Certaines formules parmi les plus courantes sont déjà intégrées dans le code de calcul (formules de Peter-Meyer, Einstein, Engelund-Hansen, Bijkér et Ribberink). Nous avons également programmé les formules de Bailard (1981), Van Rijn (1984), et Dibajnia-Watanabe (1992) qui sont mieux adaptées au transport sédimentaire sur le littoral (interaction houle-courant). Une étude et des conclusions sur ces formules ont fait l'objet d'un article dans Journal of Coastal Engineering (Camenen and Larroudé 2003).

Nous utilisons également un modèle morphodynamique Multi-1DH pour des plages sableuses. Un intérêt du modèle vient de l'intégration des effets du courant de retour, jouant un rôle primordial dans la construction de la barre de déferlement.

L'évolution des fonds est ensuite calculée en imposant comme contraintes hydrodynamiques le courant le long de la côte selon la formule de Longuet-Higgins (1970) et le courant de retour (modèle basé sur l'approche de Svendsen (1984). Le processus est répété à chaque fois que la variation des fonds est susceptible de modifier l'hydrodynamique. Ainsi, la construction de la barre pré littorale, sa propagation du fait du courant "longshore", et les perturbations de la barre (chenaux des courants d'arrachement) sont calculées simultanément. Ce modèle permet ainsi de simuler la création de barres (par exemple rythmiques comme dans l'étude sur la plage du Truc-Vert, sur la côte atlantique du bassin d'Arcachon Camenen et Larroudé (2003b)). Il permet également de simuler la migration de barres et l'évolution des fonds à des échelles temporelles plus longues. C'est que nous avons fait pour cette étude sur le site de Sète.

3 Résultats

3.1 Comparaisons et validations

Nous avons établi une procédure de calcul avec un couplage externe des codes Artemis-Telemac2d-Sisyphe. Nous avons plus particulièrement amélioré le traitement des conditions aux frontières afin de pouvoir travailler sur des maillages équivalents pour les trois codes. Ces modèles ont été employés pour des simulations mensuelles et annuelles avec prise compte des conditions atmosphériques réelles. Ces conditions atmosphériques sont tirées des données mesurées in situ pour la période -entre autres cas- de novembre 2000. Les valeurs de hauteur, période et direction de houle sont obtenues en moyennant sur une durée correspondant à des conditions de vagues similaires et significatives (voir le tableau 1).

temps (s)	Hs (m)	Tp (s)	θ (degré)
0j à 1j 21h	0.244	7.45	25.475
1j 21h à 3j 12h	1.703	7.92	27.861
3j 12h à 7j 21h	0.351	7.13	28.094
7j 21h à 10j 9h	1.787	6.76	6.065
10j 9h à 18j 12h	0.222	6.2	3.97
18j 12h à 20j 3h	1.358	6.78	14.9
20j 3h à 24j 15h	0.251	7.03	14.33
24j 15h à 30j	1.259	6.27	-5.

Table 1 : Données météorologiques simplifiées: Novembre 2000 (Θ angle d'incidence en degré)

On peut noter que la hauteur des houles au large, moyennée sur chaque période, atténue les événements de tempête de ce mois de novembre. Nous ferons donc des simulations en rajoutant spécifiquement une ou plusieurs tempêtes suivant les mois étudiés au modèle météorologique simplifié.

Nous obtenons une bonne adéquation entre les bathymétries numériques après un mois de calcul et celles mesurées in situ (voir figure 2).

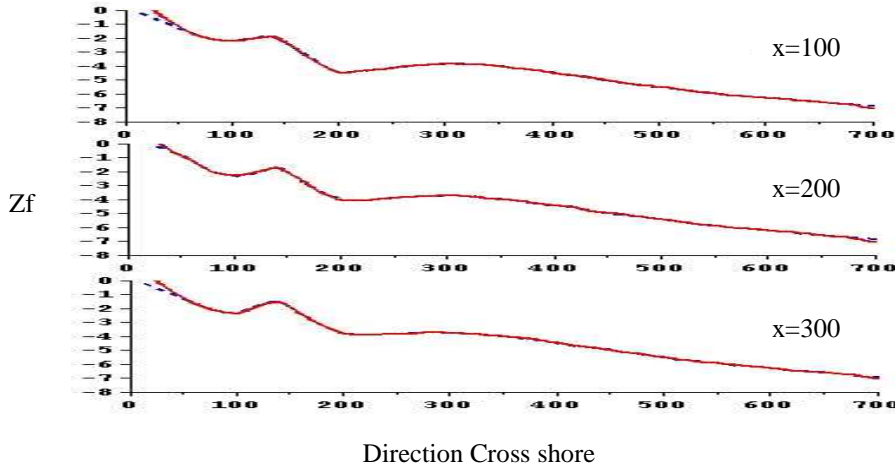


FIG. 2 – Côte du fond (Zf) pour 3 profils cross-shore le 25 novembre 2000, comparaison entre les données in situ (---) et numériques (—) après un mois avec le modèle 2DH.

Nous avons effectué également des simulations avec plusieurs emplacements de rechargement sur la zone d'étude et nous comparons les résultats obtenus entre le modèle 2DH (vagues, hydrodynamique et transport) et le modèle Multi-1DH simplifié. Ces simulations ont fait l'objet d'un rapport d'activité du programme national Liteau I. L'ensemble de cette étude nous permet de mieux envisager la dimension et le lieu du rechargement sur l'avant-plage. La méthodologie du découpage des données météorologiques va nous permettre le passage des simulations mensuelles à annuelles.

3.1 Simulations long-terme

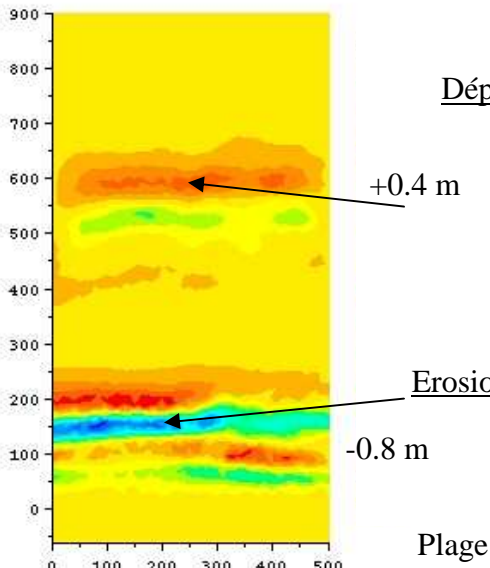
Nous observons à présent avec les codes couplés Artemis-Telemac2d-Sisyphé, la morpho-évolution de la plage avec et sans rechargement. Le but est de trouver la meilleure façon de créer un modèle météorologique simplifié des données in-situ.

Dans l'étude présentée ici, nous testons la méthodologie qui nous permet de comparer sur des simulations saisonnières les différentes moyennes en temps des événements météorologiques. Il faut effectuer une moyenne sur une durée temporelle plus courte que la durée de l'événement climatique que l'on veut représenter. La figure 3 montre l'évolution du fond marin obtenue par les codes couplés Artemis-Telemac2d-Sisyphé pour un découpage temporel inférieur à la tempête (T2). Les différences des quantités de sédiment érodées et déposées montrent que dans une simulation long terme (annuelle ou plus) il faudra prendre en compte certains événements prédominants du climat en plus du modèle météo moyené.

Nous avons effectué par la suite une simulation d'une année complète (découpée par saison) avec rechargement et utilisant un modèle météo composé de 48 événements. La simulation a

pris 24 heures de calcul sur un processeur de 2.36 gigahertz. L'objectif est de pouvoir prévoir grâce aux simulations le meilleur placement de la barre d'alimentation pour protéger la plage sur cinq à dix ans.

a) Novembre 2000



b) Novembre 2000 + T2

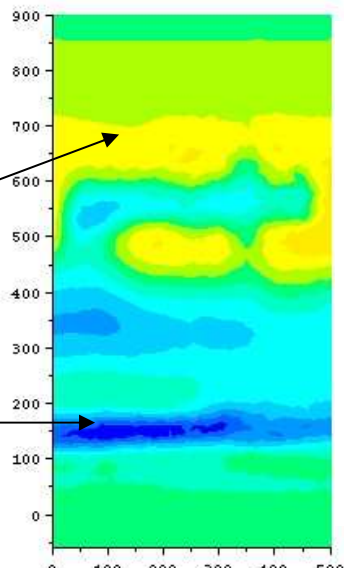


FIG. 3 – Evolution morphodynamique pendant un mois avec un rechargement : a) sans tempête et b) avec une tempête : T2 : Hs=4m, Tp = 10 s pendant 39h.

4 Conclusion

Un modèle 2DH morphodynamique issu d'un couplage externe de trois codes a été utilisé pour simuler l'évolution morphodynamique des rechargements de sable sous marin pour la protection du trait de côte. Un modèle simplifié multi1DH a été également utilisé pour les tests de scénarios de tempêtes et de formules de transport sédimentaire. Nos études nous ont permis d'optimiser l'emplacement de la dune sous marine de protection de la plage. Nos simulations permettent, grâce à la méthodologie mise en place, d'étudier des événements pour différentes échelles de temps (de la durée d'une tempête à celle d'une année complète). Pour toutes les simulations mensuelles, des comparaisons avec les données de terrain ont été effectuées et montrent une bonne adéquation entre les évolutions numériques et naturelles.

La prochaine étape de l'étude est de simuler un grand nombre de saisons de l'année 1994 à l'année 2005 afin de valider le modèle de simulation météorologique. L'objectif est de pouvoir prévoir pour les cinq années à venir le placement idéal pour un rechargement dans le cadre de la protection des plages.

Références

- Bailard J.A., 1981, An energetic total load sediment transport model for a plane sloping beach, *Journal of geophysical research*, vol.86 C11 pp. 10938-10954.
 Camenen B. and Larroudé Ph., 2003, *Comparison of sediment transport formulae for a coastal environment*, *Journal of Coastal Engineering*, 48, pp. 111-132.

- Camenen B. and Larroudé Ph., 2003b, Un modèle morphologique côtier pour la création de barres rythmiques, *Revue française de génie civil, Génie côtier*, vol. 7, pp. 1099-1116, 2003.
- Certain, R., 2002, Morphodynamique d'une côte sableuse microtidale à barres : le golfe du Lion (Languedoc-Roussillon). PhD Thesis, University of Perpignan, 199 pp.
- Certain, R. and Barusseau J.P., 2006, Conceptual modelling of straight sand bars morphodynamics for a microtidal beach (Gulf of Lions, France), ICCE 2006, San Diego.
- Dally W.R., Dean R.G., and Dalrymple R.A. , 1984. A model for breaker decay on beaches. In *19th Coastal Eng. Conf. Proc.*, pages 82-88. ASCE.
- De Vriend H.J., 1987, 2DH Mathematical Modelling of Morphological Evolutions in Shallow Water, *Coastal Engineering* ,11, pages 1-27
- De Vriend H.J. and Stive M.J.F., 1987, Quasi-3D Modelling of Nearshore Currents, *Coastal Engineering* ,11, pp. 565-601.
- Dibajnia M. and Watanabe A., 1992, Sheet flow under nonlinear waves and currents, *Coastal Engineering*, pp. 2015-2029.
- Hamm, L., Capobianco, M., Dette, H.H., Lechuga, A., Spanhoff, R., Stive, M.J.F, 2002, Asummary of European experience with shore nourishment, *Coastal Engineering*, 47, 237-264.
- LNHE-Chatou, 2002, Telemac2d - modelisation system of Telemac, version 5.2 – user-validation manual, Technical report, edf-gdf
- LNHE-Chatou, 2002,Sisyphe - modelisation system of Telemac, version 5.2 – user-validation manual, Technical report, edf-gdf
- LNHE-Chatou, 2002, Artemis - modelisation system of Telemac, version 5.2 – user-validation manual, Technical report, edf-gdf
- Longuet Higgins M..S., 1970, Longshore currents generated by obliquely incidentsea waves, *Journal of geophysical research*, vol 75, n°33, pp. 60778-60801
- Svendsen I.A. 1984, Mass flux and undertow in the surf zone, *Coastal . Eng.* , 8, pp. 347-365.
- Van Rijn L.C. 1984, Sediment transport: part1 : bed load transport ; part2 : suspended load transport ; part3 : bed forms and alluvial roughness, volume 110. ASCE.

Remerciements : Ce travail est supporté financièrement par les programmes LITEAU II et Beachmed-e, InterReg IIIC

YEARLY SIMULATION WITH A COMPLET NON LINEAR 2DH MODEL FOR NOURISHMENT STRATEGIES ON MEDITERRANEAN BEACHES

Philippe Larroudé¹

A modified 2DH morphodynamic model was employed to simulate the evolution of large-scale features with major implications for beach nourishment. The study is focused on modeling the evolution of material artificially placed in different parts of the profile, extracting or adding material to the natural bars, and quantifying how the profile responds to different wave climates and nourishment placements. The simulated results were compared with field data from a Mediterranean beach.

INTRODUCTION

Examples of nourishment tests carried out on the near shore zone are few and far between in the relevant literature, compared to the many ones undertaken directly on the beach. SAFE, latest European project within the MAST program, acknowledges the absence of reference documents on this question, although such a technique could presumably constitute a less costly alternative (Hamm *et al.*, 2002).

The use of offshore bars to fight beach erosion, dating back to the 90th, was based on the fact that they represented a substantial reservoir of sediments. That theory turned out to be irrelevant, as beach nourishment requires coarser grain sizes. However, the essential role these bars can play in wave mitigation was evidenced by recent studies. Hence, working on reinforcing existing bars or even adding extra bars is a convincing approach, for they constitute a line of defence with no visual impact and are therefore environment-friendly. The method offers the added benefit of tapping abundant fine sands, easily available offshore, to build up the bars.

In addition, adequate depths in the inner shelf area would facilitate dredging and discharge operations and, the material reclaimed being usually clean; it can therefore be used directly without any processing. The core of the additional bar too could be made from marine mud, also easily available. All these assumptions should, of course, be systematically checked, the purpose of the exercise being to assess, through mid-term bathymetric evolution simulation, the consequences of the implementation of offshore bar nourishment and define the best location.

The understanding of these processes needs at this time the *in situ* data but also the development of models mathematics and numerical codes. Hence, following the work of De Vriend (1987) and De Vriend & Stive (1987), we try to improve

¹ LEGI, University Joseph Fourier, BP 53, 38041 Grenoble, France,

the classic quasi-steady procedure. Objectives of this work will be therefore to simulate processes of sedimentary transport on sandy beaches with varied weather conditions in the medium term time scale (from few days to few months).

PROCEDURE AND DESCRIPTION OF THE BEACH

Certain & Barusseau (2006) show that morphodynamic evolution of offshore bars in a microtidal environment and bimodal moderate wave regime follows two different conceptual models, the main one being a seasonal pattern in line with the observed cycle of hydrodynamic conditions.

The morphological evolution in the near shore region, including its large-scale features, was first investigated using a combination of a commercial 2DH model and a Multi1DH model (Camenen and Larroudé, 2003, 2003b). Simulation of the wave-driven currents was carried out with Telemac, a finite-volume elements model, and the Sisyphe sand transport module served to compute sediment transport rates and bed evolution. Since the sediment transport in the surf zone is mainly controlled by undertow, an undertow model (based on Svendsen, 1984) was added to account for that process.

These models were used in the framework of a simulated meteorological cycle describing the seasonal evolution of hydrodynamic factors. Results from monthly 2DH evolution simulations show a perfect fit with field data obtained on the beaches in Sète and in Leucate (Certain, 2002). Morpho-hydrodynamic feedback of a bar having undergone reinforcing is also examined.

THE CODES

The sedimentary evolution is modeling under the action of the oblique incident waves and is coupling with different numerical tools dedicated to the other process involved in the near shore zone. We can mention the following modules:

- Module of wave with hold in account of the energy dissipation by surge (hyperbolic equation of extended Berkhoff), (LNHE, Artemis, 2002). The Artemis code (Agitation and Refraction with Telemac2d on a Mild Slope) solves Berkhoff equation taken from Navier-Stokes equations with some other hypothesis (little camber of the surface wave, little slope...). Main results are, for every node of the mesh, the height, the phase and the incidence of the waves. Artemis can take into account the reflection and the refraction of waves on an obstacle, the bottom friction and the breakers. One of the difficulties due to Artemis is that a fine mesh must be used to have good results when Telemac2d do not need such a fine mesh.

- Module that calculates currents induced means by the surge of the waves, from the concept of radiation constraints gotten according to the module of waves, (LNHE, Telemac2d, 2002). Telemac2d is designed to simulate the free surface flow of water in coastal areas or in rivers. This code solves the Barré-Saint-Venant equations taken from Navier-Stokes equations vertically averaged. Then, main results are, for every node of the mesh, the water depth and the velocity averaged over the depth. Telemac2d is able to represent the following physical phenomena : propagation of long periodic waves, including non-linear effects, wetting and drying of intertidal zone, bed friction, turbulence, ...
- Sedimentary module integrating the combined actions of the waves and the current of waves (2D or 3D) on the transport of sediment, (LNHE, Sisyphe, 2002),
The Sisyphe code solves the bottom evolution equation which expresses the conservation of matter using directly a current field result file given by Telemac2d. Four of the most currently empirical or semi-empirical formulas are already integrated in Sisyphe (Peter-Meyer, Einstein-Brown, Engelund-Hansen and Bijkar formulas). We integrate two other ones which seem more appropriate to coastal sediment transport (Bailard, 1981 and Dibajnia-Watanabe, 1992). Main results are, for every node of the mesh, the bottom evolution and the solid transport.
- An hydrodynamic simplified model (called Multi1DH) uses the following assumptions: a random wave approach, in a 1DH (cross-shore) direction. A offshore wave model (shoaling + bottom friction + wave asymmetry) is used with the break point estimation. The waves in the surf zone are simulated with the classic model of Svendsen (1984) with an undertow model (roller effect, Svendsen, 1984, Dally et al. 1984).The long shore current model is the Longuet-Higgins's model (1970).

RESULTS

Comparison with in situ data

Firstly we set up a procedure to use the coupled codes Artemis-Telemac2d-Sisyphe and especially we improved the treatment of the boundary conditions in order to be able to work on fields of calculations close to the coastal zone and equivalents in dimension for the three codes. We also used the Multi1DH code

for the medium term simulations. These models were used for monthly simulations taking of account the weather conditions. These weather conditions are drawn from the data of ground for the period of November 2000 and are simplified in terms of height of swell, period of swell and direction by dividing the month into nine significant periods. One can notice that the average height of the swells to broad during each period attenuated the weather events this November.

We obtain a good adequacy between numerical bathymetries after one month and those raised on the ground (see Larroudé, 2007).

We began simulations with a fattening of the zone of study at the beginning of November 2000 and we can compare the results obtained with model 2DH (waves, hydrodynamics and transport) and the model simplified Multi-1DH.

Secondly, we regarded as basic state a profile of the bathymetry of November 16, 2000, the P5 profile with $X = 200\text{m}$ (distance longshore compared to the beginning of the zone of study). This approach will enable us to more easily compare the models of calculation used by the various partners of the program. For these simulations we agreed to consider three cases of climatic conditions (see Table 1): Traditional Storm (TS), falling from Storm (FS) and Exceptional Storm (ES).

	temps	Hs (m)	Tp (s)	θ
TS	24 h	1 m	6,5 s	0° et 20°
FS	24 h	2,5 m	7 s	0° et 20°
ES	24 h	4 m	10 s	0° et 20°

Table 1: Weather data simplified for the three cases of storm (Θ angle in degree in the trigonometrically direction reverses compared to the normal with the beach).

The whole of simulations was carried out with the model multi1DH and the results will be presented in the continuation. We also made some calculations with the chain of Artemis-Telemac2d-Sisyphus code.

For case FS, the swells do not have effects on the internal and external bars. For simulations TS the swells erode the internal bar but does not seem to attack to a significant degree the beach and the external bar. Only a long-term erosion of the internal bar can be prejudicial for the beach.

The case of the exceptional storms will be used to us as a basis to present the differences obtained with the model multi1DH between different the option from recharging.

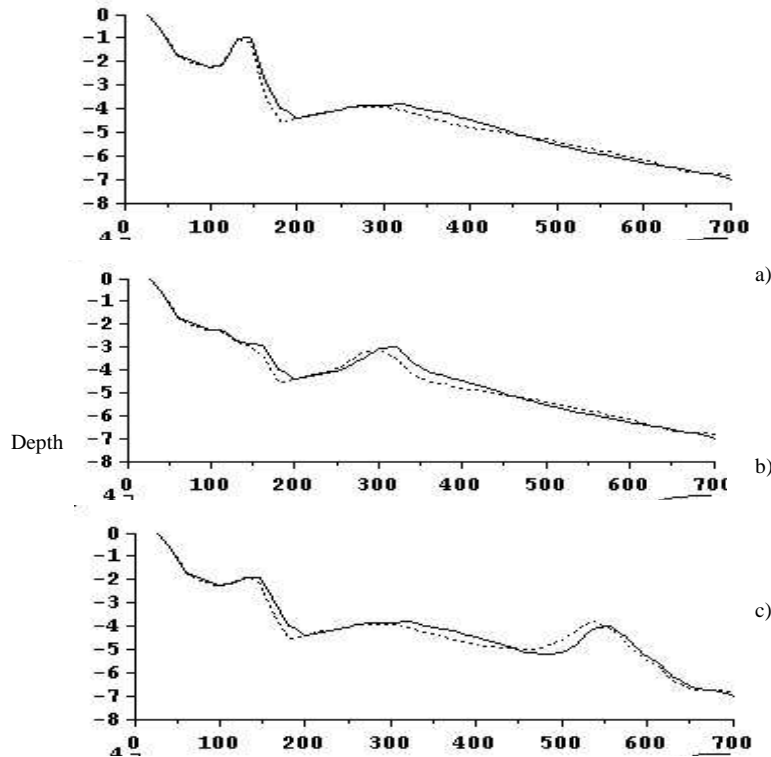


Figure 1: Sea bed evolution (solid line for initial bed and dash line for the final bed) on 24 hours calculated with the multi1DH model for three location of nourishment: a) on the inner bar, b) on the offshore bar and c) with the creation of new bar offshore

The case, on the basic profile of November 16, 2000, shows us an erosion of the bars internal and external with a transport of these bars towards the broad one and thus one can consider a weakening of the protection of the beach (see figure 1). The internal bar is eroded of approximately 10m and the external bar of 40m, the deposit with broad with a maximum of 25m but is very spread out.

long term simulation

The good accuracy of this first result allows us to create a methodology of simulation for longer time scale. We are looking now with the coupled codes Artemis-Telemac2d-Sisyphe, the morpho-evolution of the beach with and

without nourishment. The aim is to find the best way of create the simplified meteorological model from the in-situ data. In the study presented in the paper, we show the first step of this methodology which is to compare seasonal simulation with different script of meteorological event during each season. The principal question is do we have to cut out each hour, day ... Each meteorological event has time duration issued from the data (see graphics on figure 2).

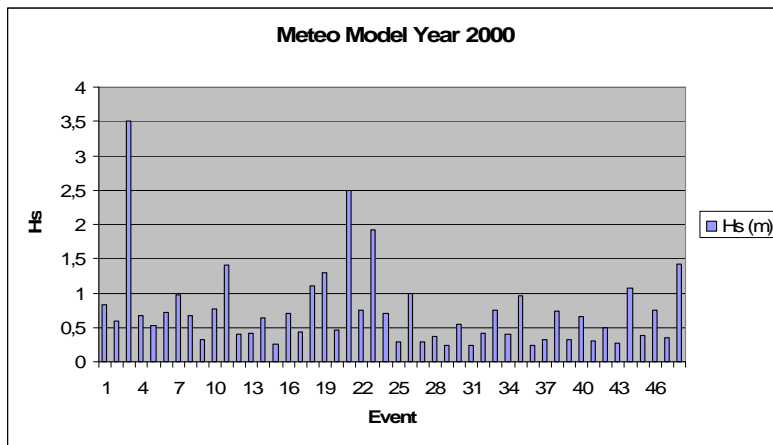


Figure 2: Meteorological model is based on the data (Certain, 2002) collated on the beaches in Sète during the year 2000. We show here one (the significant wave height) of the different parameter needed for a simulation. We create the same Meteorological model for the other parameters.

The major modification of the sea bed is numerically obtained because the time loop of the coupled codes Artemis-Telemac2d-Sisyphé is shorter than the time duration of the storm. The principal criteria to cut out could be the current velocity due to the waves. Indeed, when we have calm weather condition (e.g. small waves height) the feedback between the hydrodynamics and the sea bed evolution could be longer. The numerical difference due to number of hydro-sedimentary loop has been simulating for the same monthly or seasonal period. The differences are very important in the very near shore region and close the beach. The figure 3 shows a complete year of simulation (the 4 seasons) with nourishment and with a cut out of 48 events. The simulation took 24 hours on a 2.36 GHz processor. The aim is to find in the same time the best accuracy of the yearly sea bed evolution and the lowest computational time. The other main goal is to be able to predict the best placement of the nourishment bar to protect the beach over five to ten years.

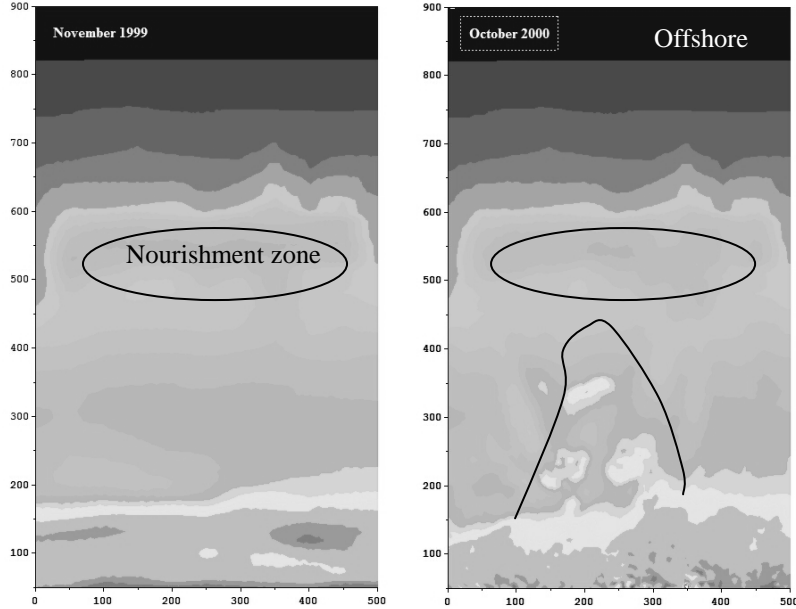


Figure 3: Iso-bathymetry of a yearly simulation from November 1999 to October 2000 with nourishment and creation of a classical tombolo.

CONCLUSION

The interesting thing of this study is that we can compare our numerical results to the in-situ data. Then, it could be easier to modulate time steps to have the most realistic results. A modified 2DH morpho-dynamical model was employed to simulate the evolution of large-scale features with major implications for beach nourishment. The study is focused on modelling the evolution of sea bed and artificial material in the near shore region, extracting or adding material to the natural bars, and quantifying how the profile responds to different wave climates and nourishment placements. The simulated results were compared with field data from a Mediterranean beach over storm, monthly and yearly time scale. The results are good in term of quality and also in term of quantity for the velocity field due to waves. The next step of the study is to simulate a large amount of seasons from the year 1994 to 2005 to be able to elaborate a criterion for the meteorological cut out. The second goal is to predict the next five years with different nourishment placement to have a good strategy for the beach protection. To achieve this simulation over several years we are going to try two approaches. The first one is to create as in this paper several years of simplified

meteorological model from the in-situ data. The second solution could be to simulate with the Multi1DH model a significant numbers of one year simulation. Each one year simulation is different from the previous from a parameter point of view (for instance change the number of storm in the year). We can, therefore, use a probabilistic method (as in Payo et al., 2004) to obtain a standard year and repeating it for a five or ten years simulation.

ACKNOWLEDGEMENTS

This paper is largely based on research work carried out in the task group Coastal Morphology of the LITEAU II and VULSACO program supported by the French Government and the BeachMed-e program supported by the European Community.

REFERENCES

- Bailard J.A., 1981, An energetic total load sediment transport model for a plane sloping beach, Journal of geophysical research, vol.86 C11 pp. 10938-10954.
- Camenen B. and Larroudé Ph., 2003, Comparison of sediment transport formulae for a coastal environment, Journal of Coastal Engineering, 48, pp. 111-132.
- Camenen B. and Larroudé Ph., 2003b, Un modèle morphologique côtier pour la création de barres rythmiques, Revue française de génie civil, Génie côtier, vol. 7, pp. 1099-1116, 2003.
- Certain, R., 2002, Morphodynamique d'une côte sableuse microtidale à barres : le golfe du Lion (Languedoc-Roussillon). PhD Thesis, University of Perpignan, 199 pp.
- Certain, R. and Barusseau J.P., 2006, Conceptual modelling of straight sand bars morphodynamics for a microtidal beach (Gulf of Lions, France), ICCE 2006, San Diego.
- Dally W.R., Dean R.G., and Dalrymple R.A. , 1984. A model for breaker decay on beaches. In 19th Coastal Eng. Conf. Proc., pages 82-88. ASCE.
- De Vriend H.J., 1987, 2DH Mathematical Modelling of Morphological Evolutions in Shallow Water, Coastal Engineering ,11, pages 1-27
- De Vriend H.J. and Stive M.J.F., 1987, Quasi-3D Modelling of Nearshore Currents, Coastal Engineering ,11, pp. 565-601.
- Dibajnia M. and Watanabe A., 1992, Sheet flow under nonlinear waves and currents, Coastal Engineering, pp. 2015-2029.
- Hamm, L., Capobianco, M., Dette, H.H., Lechuga, A., Spanhoff, R., Stive, M.J.F, 2002, A summary of European experience with shore nourishment, Coastal Engineering, 47, 237-264.
- Larroudé Ph., Long-term simulation with 2DH and 3D models for nourishment on Mediterranean beaches, 5TH IAHR SYMPOSIUM ON RIVER, COASTAL AND ESTUARINE MORPHODYNAMICS , University of Twente, The Netherlands, (17-21 SEPTEMBER 2007)
- LNHE-Chatou, 2002, Telemac2d - modelisation system of Telemac, version 5.2 – user-validation manual, Technical report, edf-gdf
- LNHE-Chatou, 2002, Sisyphe - modelisation system of Telemac, version 5.2 – user-validation manual, Technical report, edf-gdf
- LNHE-Chatou, 2002, Artemis - modelisation system of Telemac, version 5.2 – user-validation manual, Technical report, edf-gdf
- Longuet Higgins M..S., 1970, Longshore currents generated by obliquely incident sea waves, Journal of geophysical research, vol 75, n°33, pp. 60778-60801
- Payo A. , Baquerizo A. & Losada M.A. (2004) Uncertainty assessment of long term shoreline prediction, *Coastal Eng.*, vol. 2, pp. 2087-2096, ASCE, J. McKee Smith Ed
- Svendsen I.A. 1984, Mass flux and undertow in the surf zone, *Coastal . Eng.* , 8, pp. 347-365.

KEYWORDS – CSt07

Abstract acceptance number 68

YEARLY SIMULATION WITH A COMPLET NON LINEAR 2DH MODEL
FOR NOURISHMENT STRATEGIES ON MEDITERRANEAN BEACHES

1st Author: Larroudé Philippe

large scale features

nearshore region

morphomogical evolution

Sediment transport

Nourishment

numerical simulation 2DH and Multi1DH model